

**BENCH TESTING OF  
INDUSTRIAL FLUID  
LUBRICATION  
AND WEAR PROPERTIES  
USED IN MACHINERY  
APPLICATIONS**

**GEORGE E. TOTTEN • LAVERN D. WEDEVEN  
JAMES R. DICKEY • MICHAEL ANDERSON**

**EDITORS**

STP 1404



**STP 1404**

***Bench Testing of Industrial Fluid  
Lubrication and Wear Properties  
Used in Machinery Applications***

*George E. Totten, Lavern D. Wedeven, James R. Dickey, and  
Michael Anderson, editors*

ASTM Stock Number: STP1404



ASTM  
PO Box C700  
100 Barr Harbor Drive  
West Conshohocken, PA, 19428-2959

Printed in the U. S. A.

## Library of Congress Cataloging-in-Publication Data

Bench testing of industrial fluid lubrication and wear properties used in machinery applications / George E. Totten . . . [et al.], editors.

p. cm.—(STP; 1404)

“ASTM stock number: STP1404.”

Includes bibliographical references and index.

ISBN 0-8031-2867-3

1. Lubrication and lubricants—Testing—Congresses. I. Totten, George E. II. ASTM special technical publication; 1404.

TJ1077 .B43 2001

621.8'9—dc21

2001022358

Copyright © 2001 AMERICAN SOCIETY FOR TESTING AND MATERIALS, West Conshohocken, PA. All rights reserved. This material may not be reproduced or copied, in whole or in part, in any printed, mechanical, electronic, film, or other distribution and storage media, without the written consent of the publisher.

### Photocopy Rights

**Authorization to photocopy items for internal, personal, or education classroom use, or the internal, personal, or educational classroom use of specific clients, is granted by the American Society for Testing and Materials (ASTM) provided that the appropriate fee is paid to the Copyright Clearance Center, 222 Rosewood Drive, Danvers, MA 01923; Tel: 978-750-8400; online: <http://www.copyright.com/>.**

### Peer Review Policy

Each paper published in this volume was evaluated by two peer reviewers and at least one editor. The authors addressed all of the reviewers' comments to the satisfaction of both the technical editor(s) and the ASTM Committee on Publications.

To make technical information available as quickly as possible, the peer-reviewed papers in this publication were prepared “camera-ready” as submitted by the authors.

The quality of the papers in this publication reflects not only the obvious efforts of the authors and the technical editor(s), but also the work of the peer reviewers. In keeping with longstanding publication practices, ASTM maintains the anonymity of the peer reviewers. The ASTM Committee on Publications acknowledges with appreciation their dedication and contribution of time and effort on behalf of ASTM.

# Foreword

This publication, *Bench Testing of Industrial Fluid Lubrication and Wear Properties Used in Machinery Applications*, contains papers presented at the Symposium on Bench Testing of the Lubrication and Wear Properties of Industrial Fluids Used in Machinery Application held in Seattle, Washington in 26–27 June 2000. ASTM Committee D02 on Petroleum Products and Lubricants and its Subcommittee D02.L0 on Industrial Lubricants sponsored the symposium. George E. Totten, Union Carbide Corporation, Lavern D. Wedeven, Wedeven Associates Inc., James R. Dickey, Lubricants Consultants, and Michael Anderson, Falex Corporation, presided as co-chairmen and are co-editors of the resulting publication.

# Contents

<b>Overview</b>	<b>vii</b>
<b>SESSION I: PROBLEMS OF BENCH TESTING—CORRELATION WITH INDUSTRIAL EQUIPMENT</b>	
<b>On The Reasons That Make Bench Tests Unreliable—K. MIZUHARA AND M. TOMIMOTO</b>	<b>3</b>
<b>Limitations of Bench Testing for Gear Lubricants—B.-R. HOEHN, K. MICHAELIS, AND A. DOLESCHEL</b>	<b>15</b>
<b>Use of Bench Tests to Evaluate Water-Glycol Hydraulic Fluid Lubrication— G. E. TOTTEN, R. J. BISHOP, JR., AND L. XIE</b>	<b>33</b>
<b>SESSION II: BENCH TESTS AND TEST DEVELOPMENT—A</b>	
<b>The Luleå Ball and Disc Apparatus—J. LORD, U. JONSSON, R. LARSSON, O. MARKLUND, E. ERIKSSON, AND Ö. UUSITALO</b>	<b>53</b>
<b>A Spiral Orbit Rolling Contact Tribometer—E. KINGSBURY AND S. PEPPER</b>	<b>68</b>
<b>M-ROCLE Diesel and Biodiesel Fuel Lubricity Bench Test—J. W. MUNSON AND P. B. HERTZ</b>	<b>81</b>
<b>SESSION III: BENCH TESTS AND TEST DEVELOPMENT—B</b>	
<b>Assessment of the Tribological Function of Lubricants for Sheet Metal Forming— J. FILZEK AND P. GROCHE</b>	<b>97</b>
<b>Determination of Gear and Bearing Material Scuffing Limits Using High-Speed Disc Machines—R. W. SNIDLE, H. P. EVANS, AND M. P. ALANOU</b>	<b>109</b>
<b>Effects of Friction Modifiers on Wear Mechanism of Some Steels Under Boundary Lubrication Conditions—H. SO AND C. C. HU</b>	<b>125</b>
<b>Testing Extreme Pressure and Anti-Wear Performance of Crankcase and Gearbox Lubricants—A. F. ALLISTON-GREINER, A. G. PLINT, AND M. A. PLINT</b>	<b>140</b>

<b>Tribological Testing of Lubricants and Materials for the System “Piston Ring/Cylinder Liner” Outside of Engines—M. WOYDT AND N. KELLING</b>	153
<b>Aircraft Hydraulic Pump Tests with Advanced Fire-Resistant Hydraulic Fluids—S. K. SHARMA, C. E. SNYDER, JR., AND L. J. GSCHWENDER</b>	168
<b>A New Device for Traction Measurement on Ice—J. XIAO, H. LIANG, R. CRISENBERRY, AND M. COOK</b>	185

#### SESSION IV: ANALYSIS

<b>Influence of Test Parameters on Tribological Results—Synthesis from Round Robin Tests—M. WOYDT</b>	199
<b>Identification of Boundary Friction Coefficient Under Mixed Lubrication in Block-on-Ring Friction Tester with Aid of Partial EHL Analysis—S. TANAKA, T. NAKAHARA, K. KYOGOKU, AND S. MOMOZONO</b>	210
<b>Investigation of Frictional Properties of Lubricants at Transient EHD-Conditions—B.-O. ÅHRSTRÖM</b>	221
<b>Bench Test Determinations of Wear Modes to Classify Morphological Attributes of Wear Debris—B. J. ROYLANCE, T. P. SPERRING, AND T. G. BARRACLOUGH</b>	235 <sup>s</sup>
<b>A New Look at an Old Idea: The Torque Curve Revisited—K. M. HELMETAG</b>	258
<b>Evaluation of Fretting Wear Under Oscillating Normal Force—M. Z. HUQ AND J.-P. CELIS</b>	267
<b>The Use of Tribological Aspect Numbers in Bench Test Selection—A Review Update—M. ANDERSON</b>	283
<b>Corrosive Wear Testing of Metals in Seawater—T. KAWAZOE AND A. URA</b>	296

#### SESSION V: MODELING AND SIMULATION

<b>Simulation of Tribological Performance of Coatings for Automotive Piston Ring and Timing Chain in Bench Testing—C. GAO, N. GITIS, N. NGUYEN, AND M. VINOGRADOV</b>	309
<b>Tribology Testing for Load Carrying Capacity of Aircraft Propulsion System Lubricating Oils—L. D. WEDEVERN AND E. HILLE</b>	318
<b>Author Index</b>	333
<b>Subject Index</b>	335

# Overview

---

Bench tests are commonly used to evaluate the lubrication and wear properties of industrial fluids when used in various types of machinery. In some cases, custom-made equipment and test configurations have been developed to evaluate lubrication and wear of specific wear contacts in a particular machine. Unfortunately, bench tests are often used without any validation of the lubrication and wear properties obtained in the machinery being modeled. Such testing strategies are worse than no tests at all. Therefore, there is a great need in the lubricants industry to address this long-standing and increasingly important problem.

To address this problem, ASTM Committee D2 on Petroleum Products and Lubricants, along with its subcommittee D02.L0 on Industrial Lubricants, held a Symposium on Bench Testing of the Lubrication and Wear Properties of Industrial Fluids Used in Machinery Applications in Seattle, Washington on June 26–27, 2000. The objective of this conference was to provide a forum on the selection of bench tests and testing conditions to model lubrication and wear properties of fluids used in various industrial machines and components such as: compressors, pumps, chain drives, transmissions, bearings, and others.

This book is a collection of the papers presented at this event, all of which address various aspects of bench tests selection, limitations, along with lubrication and wear simulations. The topics discussed at the symposium were:

## **Problems of Bench Testing—Correlation with Industrial Equipment**

The three (3) papers in this section discuss different problems associated with bench test selection, particularly as the test results correlate with equipment lubrication. Some suggestions to address equipment lubrication correlation problems are: selection of appropriate test conditions; development of custom-made test equipment and the use of lubrication and wear simulations to identify appropriate test conditions.

## **Bench Tests and Test Development**

The ten (10) papers in this section describe the application of traditional tests, such as four-ball tests, to model hydraulic pump wear and lubricant additive evaluation and the development of new tests and testing protocol. In summary, this section shows that it is possible with proper design considerations, which are discussed here, and model validations to successfully apply bench tests in lubrication and wear analysis.

## **Analysis**

In this section, eight (8) papers address a wide range of methodologies for evaluation of bench test results. These include: examination of experimental test parameters, detection of boundary and EHD lubrication transitions, wear mode identification by debris analysis, the utility of tribological aspect numbers and others.

### **Modeling and Simulation**

The two papers (2) in this section outline the value and necessity of experimental simulation of tribological performance to properly evaluate machinery lubrication and wear problems. In many cases, the methodologies outlined here offer the preferred approach and illustrate the need for continued development of guides and standards that serve as a vital aid to the analyst.

In summary, although bench tests have been used from the beginning of tribological experience, there is a substantial and important need for the continued development of testing and analysis methodologies and related standards. However, in the meantime, this text will serve as a valuable reference for those in the field of lubricant analysis and wear.

*George E. Totten, Ph.D.*

Union Carbide Corporation  
Tarrytown, New York  
Symposium Chairman and Editor

*Lavern D. Wedeven, Ph.D.*

Wedeven Associates Inc.  
Edgemont, Pennsylvania  
Symposium Chairman and Editor

*Michael Anderson*

Falex Corporation  
Sugar Grove, Illinois  
Symposium Chairman and Editor

*James R. Dickey*

Lubricants Consultants  
Basking Ridge, New Jersey  
Symposium Chairman and Editor

**SESSION I: Problems of Bench Testing—  
Correlation With Industrial Equipment**

Kazuyuki Mizuhara<sup>1</sup> and Makoto Tomimoto<sup>2</sup>

## On The Reasons That Make Bench Tests Unreliable

---

**Reference:** Mizuhara, K. and Tomimoto, M., “On The Reasons That Make Bench Tests Unreliable,” *Bench Testing of Industrial Fluid Lubrication and Wear Properties Used in Machinery Applications, ASTM STP 1404*, G. E. Totten, L. D. Wedeven, J. R. Dickey, and M. Anderson, Eds., American Society for Testing and Materials, West Conshohocken, PA, 2001.

**Abstract:** It is well known that the wear rates of materials evaluated in bench testers are fairly reproducible. However, the performance of the materials obtained in bench tests and practical uses were sometimes completely different from each other. This paper discusses the reasons for such discrepancies observed in hydraulic pump testing in terms of the test conditions and the response of the fluid to them. By analyzing the test condition that reproduced the pump wear in bench tests, it is suggested that at lower temperatures and pressures, the behavior of the fluid at higher temperatures and pressures could be reproduced. Then it is concluded that applying the estimated load and sliding velocities in actual pump to bench tests that use different contact configuration may cause the erratic results. It is also concluded that estimating the phenomena governing the performance in an actual pump is one of the keys to conducting useful bench tests. The factors that affect the test results and the usefulness and limits of the bench tests are also discussed.

**Keywords:** bench testing, performance, film parameters, temperatures

---

<sup>1</sup> Mechanical Engineering Laboratory, 1-2 Namiki, Ibaraki, 305-8654, Japan.

<sup>2</sup> Nihon Pall Ltd., 46 Kasuminosato, Ami, Inashiki, Ibaraki, Japan.

### Introduction

There are many well classified ways to evaluate the tribological performance of the fluids [1]. The pump tests are regarded as the most reliable but costly. On the other hand, bench tests (model tests) are cheaper and suitable for fundamental research on friction and wear but unreliable for predicting the actual pump wear. The advantage of the bench tests in terms of technical value is the capability of giving the response of the fluids to each tribological system parameter such as velocity, load, and configuration. The many efforts however, have been made to improve the accuracy of predicting pump test results by bench tests, by further investigating the fluids performance by bench test seem unsatisfactory. Since the tribological performance depends on so many system parameters, it is almost impossible to predict the pump test results by means of a few aspects of the fluids evaluated by bench tests. In this paper, the reasons why attempts to predict pump test results by bench tests are unsatisfactory will be discussed.

### Parameters that Affect the Tribo-Test Results

The Stribeck curve (Figure 1) is widely used to distinguish the lubrication regimes [1]. This curve is based on the concept that fluid film thickness represents the solid separation and under complete separation, the viscosity of the fluid controls the friction thus friction increases with velocity or viscosity. This regime is called hydrodynamic lubrication. At lower viscosity or velocity, the fluid film is not thick enough to completely separate the two solid surfaces and start to allow partial contact of the solids. This regime is the mixed or partial EHD lubrication regime, in which surface roughness and the elastic modulus of the solid have considerable effect. Below that regime, two solids contact most of the time and called boundary lubrication regime. It is widely used but the values of the abscissa are

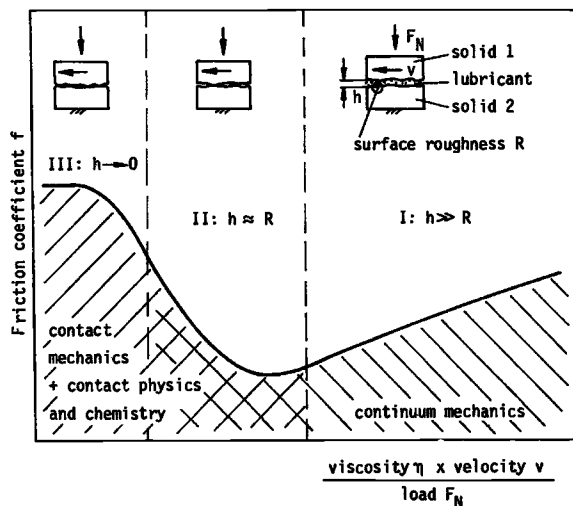


Figure 1 Stribeck curve and lubrication regimes [1]

meaningless at mixed or boundary lubrication regime, where most of the wear takes place. To better describe the mixed or boundary lubrication regime, the film parameter ( $\lambda$ ) which is the ratio of surface roughness and fluid film thickness, has some advantage, since it includes some ideas on the surface contact which might be controlling the wear [2]. It is well known that  $\lambda$  value is very effective in describing the transition of lubrication regime and predicting the fatigue life of the rolling elements [3]. Film parameter seems to have clearer physical image on the contact, however, those values themselves are again not so meaningful. The problems that  $\lambda$  values involve are not only the difficulty in calculating the fluid film thickness accurately [4] but also in calculating the roughness, since the nature of the roughness has large effect in practice and it is not clear what kind of roughness parameter should be used. It was successful for the rolling application where most of the surface asperities are flattened under high contact pressure. However in pumps application, as well known in piston ring application, running in or the surface texture change during the operation will be the key to achieve the long life [5]. Then more detailed discussion on the nature of the roughness is necessary.

Note that the fluids are not only forming the oil film but also forming the reaction films on the surface. These parameters are evaluating the physical part of the function. Anyway, assuming that these parameters can be used to describe the lubrication regime, then load, velocity, fluid viscosity and surface roughness are the parameters that control the lubrication regime. Since the fluid viscosity strongly depends on its temperatures, we should add temperature. Then let's see how these test parameters affect the tribo-system.

### **Load**

The effect of the load on tribo-system is the simplest of all. Increasing the load decreases both the film parameter and the Stribeck parameter thus drives the system towards the boundary lubrication regime.

### **Velocity**

The effects of velocity are somewhat complicated. At first glance, the film parameters or Stribeck parameter are increased. However, if the friction coefficient is the same, it generates more heat which is proportional to the multiple of the friction force and velocity. As mentioned above the fluid viscosity is sensitive to its temperature, then temperature increase may result in extensive viscosity drop that overwhelm the direct effect of the velocity, and results in reduction of these parameters. In a word, velocity may drive the system to either ways toward the hydrodynamic and boundary lubrication. It should be noted that even in the region where increased velocity reduces the friction, as

shown in Figure 2, friction does not reduce inverse proportionally with the velocity, then temperatures always increase with velocity.

### Surface Roughness

Surface roughness decreases the film parameters; however, it doesn't affect it at all if the fluid film thickness is large enough. Below the film parameter of 3, it is said that solid-solid contact begins to be involved. Increasing the solid contacts may cause more friction, heat and wear. However in the EHD or mixed lubrication regime, it is reported that the surface lay affects the EHD film thickness, and the topographic nature of the surface is important.

### Temperatures

As mentioned above, increasing the temperature reduces the fluid viscosity then film parameters. Fluid temperatures can be controlled externally however, the system always generates the friction force, then heats, that increase the temperature especially at the contact. In the hydrodynamic lubrication regime, increased temperature will reduce the friction and may eliminate further increase of the temperatures. On the other hand, in mixed lubrication regime, reduced viscosity enhances the solid contacts that increase the heat generation. Sometimes, it will drive the system towards the boundary lubrication regime and seizure. To prevent this catastrophic process, the additives are used.

The additive behavior is very tricky since the response of the additives depend

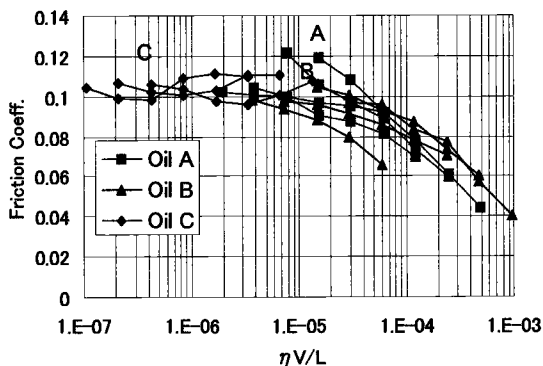


Figure 2 Stribeck curve obtained for a few fluids in a block on ring type tester [9].

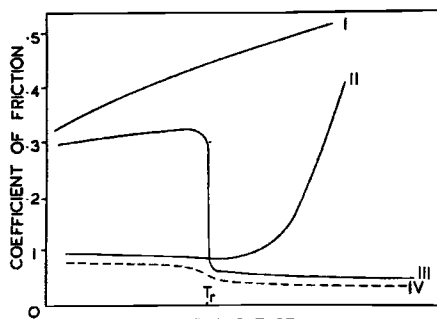


Figure 3 Frictional behavior of various lubricants as a function of temperatures. I, paraffin oil; II, fatty acid; III, E.P. lubricant which reacts with surface at temperature  $T_r$  ; IV, mixture of E.P. lubricant and fatty acid [6].

on the nature of the additives, however if these additives are effective it could be simplified and described as a function of temperature shown in Figure 3 [6]. Effect of oiliness additives disappears over certain temperatures and that of E.P. additives increases with increasing temperatures. So some fluids actually show better performance at higher temperature or severer conditions than mild conditions.

The most advantageous point of the bench test over pump test is its capability of revealing the fluids behaviors as a function of each parameter. In other words, it can characterize the total fluid performance in detail. It is a tribologist's dream that we can predict the pump test results based on the total description of the fluid performance. However, it must be time and cost consuming and useless to characterize hundreds of fluids in detail, since most of them, but the best one will not be used.

### How to Select the Test Parameters

The time and cost to totally describe the fluid performance must be more than that of pump tests. So, even for bench tests, test conditions must be selected. Then how? Hogmark et al. recommended to use the closest possible sliding condition that is resemblance to the actual field case [7]. It is better to start with something but nothing. However, they also suggested that the test should reproduce the wear mechanisms of the field case and should reproduce the temperature level of the test material. It means that you should use different sliding condition than actual machine if these two points are not satisfied in bench tests, which always happens.

Recently Takesue et al. [8] reported that by fitting the expected temperature increases, bench tests using actual vanes reproduced the fluids rankings in pump tests. The test conditions they employed are higher load and lower velocity than actual pump because of the tester's incapability of running at the same load and velocity. Their suggestion is basically to use the closest possible sliding condition while adjusting the PV values or temperature increase.

Table. 1 - *Tested Fluids*

Code	Description of Oils	Viscosity mm <sup>2</sup> /s		Specific gravity Kg/m <sup>3</sup>	Pressure viscosity coeff.(typical) GPa <sup>-1</sup>
		at 313K	at 373K		
A	Anti Wear type	32	5.7	870	21.2
B	Water Glycol	51	9.8	1058	5.14
C	Oil-in-Water	0.77	0.7	992	1.14
D	Water-in-Oil	77.7	14.2	920	*5.14
E	Phosphate Ester	41.6	5.1	1150	22.6
F	Polyol Ester	41.3	8.4	970	14.1

\* Assumed value, the other values are from references.

Those suggestions are reasonable, since the pump test results are definitely affected by the lubricant additives, then additives must be taking an important role. And given that the additives behavior on surface is described by the temperatures as shown in Figure 2, then temperatures must be one of the key parameters.

However, these suggestions seem to contradict one of our earlier works [9]. Table 1 shows the properties of fluids and Table 2 shows the test conditions. As shown in Table 2 the test conditions that we found the best reproducibility was a combination of a low sliding velocity and a low load (see Table 2). The velocity was only one hundredth of that in actual pumps, which gives only a limited temperature increase. As shown in Figure 4 the frictional behavior of the fluid that has a lot of EP additives (Oil C) depend on the temperatures. From this Figure, it is judged that at the best fit condition, the EP additives in oil C do not perform well. It is reasonable, however the test condition itself looks too far away from the conditions in actual pumps.

The success in reproducing the pumps performance, apparently based on the calibration process, importance of which had been stressed repeatedly [10]. So, it is reasonable to assume that the best

Table 2 - Bench Wear Test Conditions

Load N	Speed m/s	LV value Nm/s	Comment
66.15	0.037	2.4	Best fit
132.3	0.073	9.7	
246.6	0.147	36.2	
529.2	0.294	155.5	
66.15	0.294	19.4	
132.3	0.588	77.7	
246.6	1.175	310.9	
529.2	2.350	1243.7	Oil B only

\* ASTM D2882 [9]

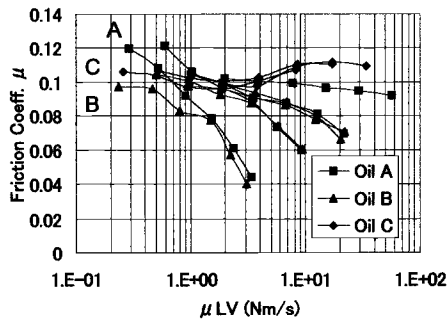


Figure 4 Frictional behavior of fluids as a function of power consumed at the contact.

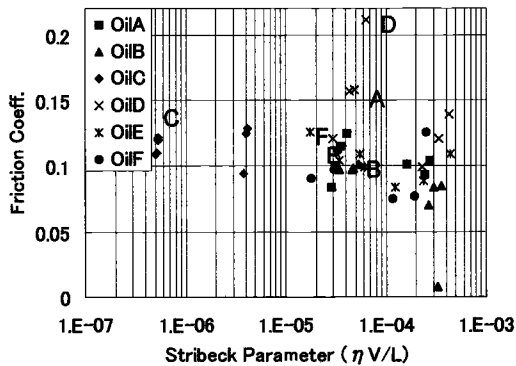


Figure 5 Frictional behavior of fluids as a function of Stribeck parameter.

fit condition is reproducing the fluid's behavior in a vane pump even if it is far from the closest possible test condition. Then it must be interesting to evaluate the sliding condition by several parameters.

Figure 5 and 6 show the friction and wear behavior of fluids as a function of Stribeck parameter, respectively. The characters A-F marked in the Figure suggest the results obtained at the best fit condition for each fluid. As shown in Figure 5, the chosen test conditions are mostly in boundary lubrication regime, where the Stribeck parameter is not that useful. However, a general trend that is higher the parameters the lower the wear rates, can be seen in Figure 6. Also, it is clear that the best fit condition is one of the severest in terms of the Stribeck parameter.

Figures 7 and 8 show the friction and wear behavior of fluids as function of the film parameter  $\lambda$  respectively. To calculate the fluid film thickness, the lubrication regimes are evaluated by using the viscosity parameter ( $gl$ ) and elasticity parameter

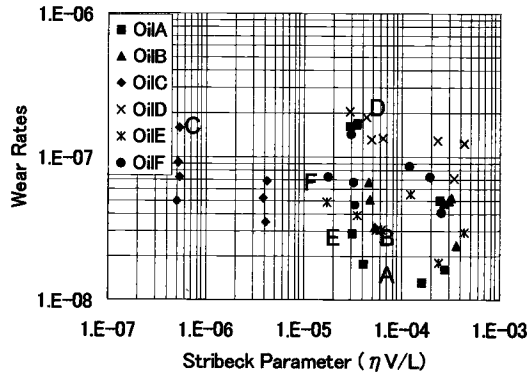


Figure 6 Wear rates of fluids as a function of Stribeck parameter.

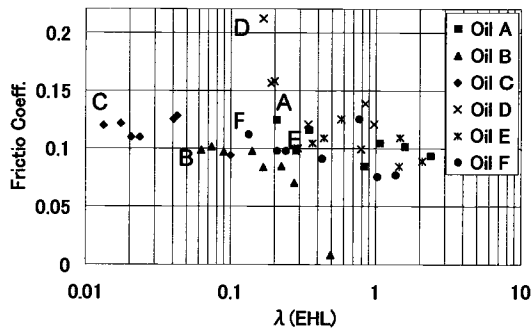


Figure 7 Frictional behavior of fluids as a function of film parameter.

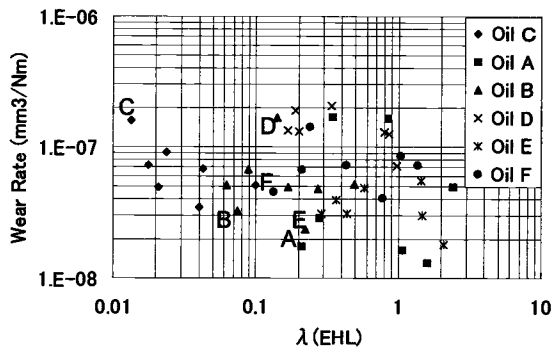


Figure 8 Wear rates of fluids as a function of film parameter.

(g3)[11]. Figure 9 shows the positions of tested conditions and the lubrication regimes proposed by Hooke [12]. The ovals in the Figure show the lubrication regime at the vane tip of a straight vane type vane pump, using the mineral oil analyzed by Nakahara et al. [13]. From this Figure the pressure viscosity coefficient of the oil is in effect both in vane pump and in bench test.

As can be seen in Figures 7 and 8, the data those were aligned on almost the same Stribeck parameter begins to spread and some correlation becomes evident. For example, frictions of oil B and D reduces with increasing  $\lambda$  values. However for wear, correlation is not clear for oils B and D but C that decreases with increasing  $\lambda$  values. It should be noted that the recommended condition is the severest in terms of the  $\lambda$  value, which represents the solid- solid contact. Then in terms of solid-solid contact, the best fit condition is the most severe.

Figures 10 and 11 show the friction and wear behavior of fluids as function of consumed power at the contact or temperature increase at the contact. As can be seen in Figure 10 and 11, with this parameter, the best correlations are found. Friction of most of the fluid decrease with increasing  $\mu LV$  value, showing that the additives are in action. In case of wear, the correlation is not as clear as that of friction, however two trends are observable. Wear rates of Oil A, B, E and F increases with increasing power. In contrast, the wear rate of oil C reduces with increasing  $\mu LV$  value. Among

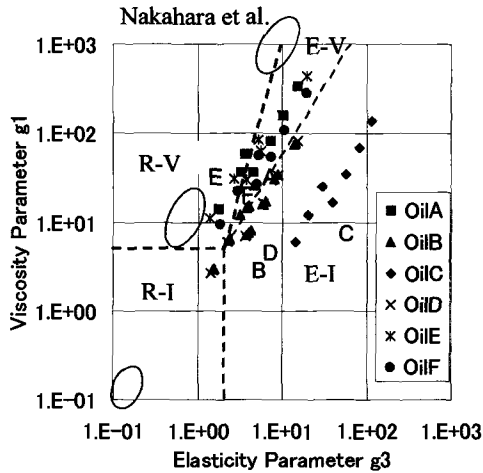


Figure 9 Regime of lubrication for cylindrical Herzian contact [12, 13].

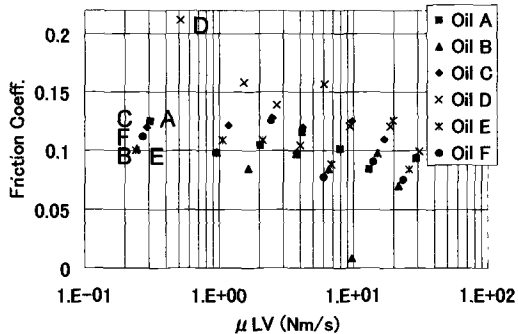


Figure 10 Frictional behavior of fluids as a function of power consumed at the contact.

these test conditions, only the condition that will cause the lowest temperature increase ranked the oil C as the worst.

Increase in fluid temperatures are less than 10K at the best fit condition and the fluids temperatures themselves are also much lower than that of pump tests. Then in terms of temperatures, the best-fit condition is the mildest.

As shown in Figure 9, at the best-fit condition, the lubrication regime is in EHL and the severity of the contact is one of the severest in terms of the extensiveness of the contact. However the contact pressure and temperatures are quite different from the pumps.

There are several temperatures that affect the lubrication capability. Surface temperatures of the test pieces, fluid temperatures, temperatures at the asperity contact. Lee et al. [14] investigated the seizure phenomena based on the physisorption behavior of lubricants and suggested that the seizure occurs at critical temperatures at the asperity contact that depends on hydrostatic pressure. According to the CTP theory, the maximum temperature in asperity contact controls the adsorbate concentration thus overrule the seizure. While the bulk fluid temperatures control the oil film thickness and film parameter then amount of solid solid contact, the temperatures at the asperity contact control the seizure at the asperity contact.

In case of the best fit condition, the contact pressures are the order of 10-100MPa [9] while that of actual pumps is around 1GPa [13]. Then critical temperature for tester is estimated to be 100-120°C lower than that of actual pump. Also the contact length of the tester is longer than that of actual pump, which will cause higher maximum temperatures at the contact in bench tests if the same sliding conditions are applied. This must be the reason why even at low fluid temperatures, each fluids show some correlation with the  $\mu$ LV value and the oil C shown typical E.P. additive behavior as described in Figure 3.

This will also explain why Takesue could rank the fluids properly at high temperatures. They had been using the actual vane and higher load that will increase the critical temperature.

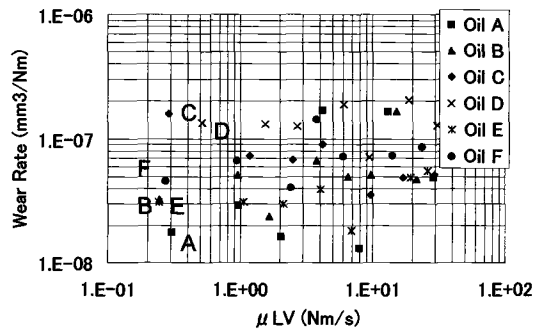


Figure 11 Wear rates of fluids as a function of power consumed at the contact.

**Strategy of Bench Testing**

Figure 12 shows the schematics of pump tests and bench tests. First of all we should keep in mind that both the hydraulic pump and bench testers are black boxes. Then it have to be sure that these two boxes are the same before we apply the estimated sliding condition in pump to bench test. Otherwise we must go through the calibration process to adjust the test results [10].

In calibration process, unless the structures in the black boxes are totally understood, we should concentrate on correlating the parameter such as wear amount but load or velocities even if those look unrealistic. It is difficult to apply the condition that seems far away from the actual pump. However, it should be done, since that is the way calibration supposed to be. As shown in this paper, the tribological process is not controlled by the apparent sliding conditions but the phenomena at the contact. If the same black box is used, then the same test condition could be applied, but if not, the test conditions should be different to each other to adjust the phenomena at the contact. Then what is most difference between the pump and tester? The answer in terms of tribological aspect will be the contact configuration. This explains the reason why we found an unrealistic test condition [9] whereas Takesue et al. could simulate the vane pump by applying similar sliding that resemble to the pump to the tester that uses actual vanes[8].

This sounds somewhat encouraging and also discouraging, since using the vane on disk type tester, simulating conditions for wear of vane and cam ring could be found easily. The process to find the test condition we suggested [9] will not be that cumbersome [15]. However if the wear in other part of the vane pump becomes the issue, we have to survey the other test conditions or use the tester that has the similar contact configurations.

Now we can suggest that the primary suspect for unreliableness is setting the test condition to apparent sliding conditions without using the same test configuration.

The reasons why this happens so frequently is the prejudice that the friction and wear are functions of the test conditions such as load and speed. In

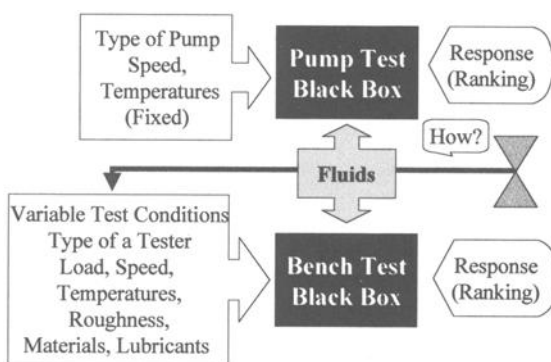


Figure 12 Calibrating pump test and bench tests.

many papers, experiments are conducted by using a specific contact geometry and the data are shown as a function of each parameter. The tendency of fluids response to each parameter can be fairly general but the performance at fixed velocity or load are not the same if the system is different. So, even making an extensive wear map using one contact configuration will not be sufficient.

However using the similar configuration will simplify the process correlating the pump tests and bench tests. Further research based on this concept will be necessary.

The other case that will cause the mismatch in test results is setting the test condition to the severest values i.e. highest speed, load and temperatures in the system, even if those do not happen simultaneously at the contact. These conditions give an advantage to the fluids that include a lot of additives, which is the typical pattern of the mismatch.

Finally it should be pointed out that reduced velocities are common for successful ranking of the fluids [8, 9, 16]. As discussed above, once some metallic contact occurs, higher velocities cause higher temperature increase and may results in catastrophic breakdown. So, lower velocity may be preferable to avoiding the instability and scatter of test results.

## Conclusions

The reasons why the bench test is unreliable are investigated by analyzing the unrealistic test condition in a block on ring tester that successfully simulated the wear in a vane pump. The followings conclusions are offered:

1. Friction and wear phenomena are not dependent on the apparent conditions but the conditions at contact.
2. Similarity in test configurations is necessary to apply the closest possible test conditions to actual pumps.
3. The power consumed at the contact, or temperature increase, is the best parameter to analyze the fluid behavior.
4. The film parameter has some advantage over the Stribeck parameter in the EHL regime.

## References

- [1] Czichos, H., "Tribology" *Tribology series 1, Elsevier*, 1978 pp.131.
- [2] Czichos H., Habich, K. H., "Mixed Lubrication and Lubricated Wear", *Proc. 11th Leeds-Lyon Symposium on Tribology*, 1985, pp.135-147.
- [3] Skurka, J. C., "Elastohydrodynamic Lubrication of Roller Bearings," *Journal of*

- Lubrication Technology, Trans. ASME*, Vol. 92, 1970, pp. 281.
- [4] Cann, P., Ioannides, E., Jacobson, B. and Lubrecht, A. A., "The Lambda Ratio – a Critical Re-examination," *Wear*, Vol. 175, 1994, pp. 177-188.
- [5] Dong, W. P., and Stout, K. J., "An Integrated Approach to the Characterization of Surface Wear I: Qualitative Characterization", *Wear*, Vol. 181-183, 1995, pp. 700-716.
- [6] Bowden, F. P. and Tabor, D., "The Friction and Lubrication of Solids", *Clarendon Press, Oxford*, 1986, pp. 239.
- [7] Hogmark, S. and Jacobson, S., "Hints and Guidelines for Tribotesting and Evaluation", *Lubrication Engineering*, Vol. 48, No. 5, 1992, pp. 401-409.
- [8] Takesue, M., "Methods to Evaluate the Practical Tribological Performance of Sliding Parts in Machines" *Ph D. Theses, University of Kyusyu*, 1999.
- [9] Mizuhara, K., Tsuya, Y., "Investigation of a Method for Evaluating Fire-Resistant Hydraulic Fluids by means of an Oil Testing Machine," *Tribology International*, Vol. 25, No. 1, 1992, pp 37-43.
- [10] Totten, G. E., and Bishop, R. J., "Evaluation of vickers V-104 and 20VQ5 Vane Pumps For ASTM D-2882 Wear Tests Using Water-Grycol Hydraulic Fluids", *Tribology of Hydraulic Pump Testing, ASTM STP-1310*, Totten, G. E., Kling, G. H. and Smolenski, D. J. Eds., American Society for Testing and Materials, 1997, pp. 118-128.
- [11] Johnson, K.L., "Regimes of Elastohydrodynamic Lubrication," *Journal of Mechanical Engineering Science*, Vol. 12, No. 1, 1970, pp. 9-16.
- [12] Hooke, C. J., "The Elastohydrodynamic Lubrication of Heavily Loaded Contacts," *Journal of Mechanical Engineering Science*, Vol. 19, No. 4, 1977, pp. 149-156.
- [13] Nakahara, T., Jung, J. Y. and Kyoungoku, K., "Lubrication Modes Between Vane Tip and Camring in Oil Hydraulic Vane Pumps," *Japanese Journal of Mechanical Engineerings*, B, Vol. 56, No. 521, 1990, pp. 79-87.
- [14] Lee, S. C., and Chen, H., "Experimental Validation of Critical Temperature-Pressure Theory of Scuffing," *Tribology Transactions*, Vol. 37, No. 3, 1995, pp. 738-742.
- [15] Totten, G. E., Bishop, R. J. and Kling, G. H., "Correlation of Water-Glycol Hydraulic Fluid Performance by ASTM D-2882 Versus Various Bench Tests," *Proceedings of the JSLE International Tribology Conference*, Yokohama, 1995, pp. 921-926.
- [16] Perez, J. M., Hansen, R. C. and Klaus, E. E., "Comparative Evaluation of Several Hydraulic Fluids in Operational Equipment, A Full-Scale Pump Stand Test and the Four-Ball Wear Tester. Part II. Phosphate Esters, Glycols and Mineral Oils." *Journal of STLE*, Vol. 46, No. 4, 1990, pp. 249-255.

Bernd-Robert Hoehn,<sup>1</sup> Klaus Michaelis,<sup>2</sup> and Andreas Doleschel<sup>3</sup>

## Limitations of Bench Testing for Gear Lubricants

---

**Reference:** Hoehn, B.-R., Michaelis, K., and Doleschel, A., “Limitations of Bench Testing for Gear Lubricants,” *Bench Testing of Industrial Fluid Lubrication and Wear Properties Used in Machinery Applications, ASTM STP 1404*, G. E. Totten, L. D. Wedeven, J. R. Dickey, and M. Anderson, Eds., American Society for Testing and Materials, West Conshohocken, PA, 2001.

**Abstract:** Base oil type, viscosity, and additive packages of gear lubricants influence gear failures as wear, scuffing, micropitting and pitting as well as power loss and efficiency. Numerous test methods have been developed to quantify these influences.

Different test equipment like a gear test rig, a twin disk machine and the Shell four ball tester are shown and discussed. Results of lubricants in these bench tests on scuffing, pitting and friction behaviour are shown and compared to each other and to gear performance.

It can be summarized that poor correlation has to be stated for the bench tests with 100% sliding rate. For the twin disk simulation poor correlation was found for scuffing results, good relative but poor absolute correlation for pitting results and both good relative and absolute correlation for the frictional behavior. From these investigations it has to be concluded that bench test results applied to gears have to be regarded very critically and can only be interpreted correctly with excellent experimental background and experience.

**Keywords:** Bench testing, gears, lubrication, scuffing, pitting, friction

---

<sup>1</sup>Professor, Gear Research Centre FZG, Technische Universitaet Muenchen, D-85747 Garching, Germany

<sup>2</sup>Research group Manager, Gear Research Centre FZG, Technische Universitaet Muenchen, D-85747 Garching, Germany

<sup>3</sup>Research Scientist, Gear Research Centre FZG, Technische Universitaet Muenchen, D-85747 Garching, Germany

## Introduction

Base oil type, viscosity and additive packages of gear lubricants influence gear failures as wear, scuffing, micropitting and pitting as well as power loss and efficiency. Numerous test methods have been developed to quantify these influences. Bench tests using simple and already available test specimens have the advantage of low cost, often short test times and small oil samples, and are therefore often used in the development of gear lubricants. But do the results of these tests correlate with gear performance?

## General Considerations on Test Strategies

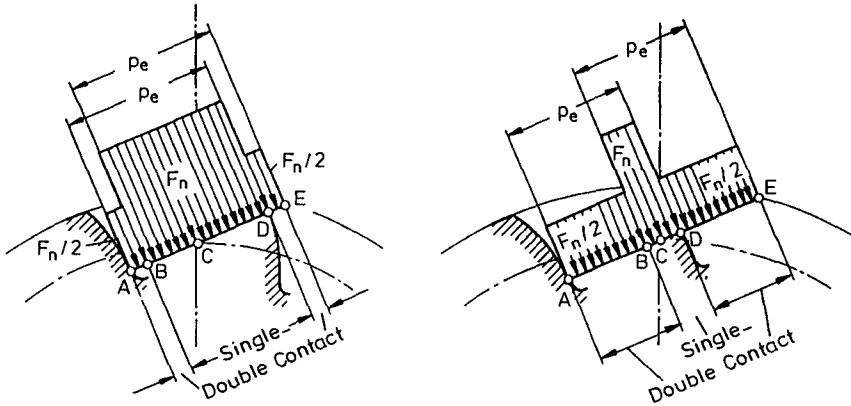
The best test configuration for full comparability is the actual gearbox under typical operating conditions. For industrial gear applications this is always too expensive and for automotive gear applications it is mostly too time-consuming.

The second best are test procedures using defined test gears with high reproducibility in geometry, heat treatment and surface finish being exposed to exaggerated operating conditions in order to reduce test time. Parameters which are modified compared to actual operating conditions have to be chosen very carefully for best simulation.

Because of cheap and quick testing a whole variety of bench tests was developed, in many cases only with marginal simulation of the operating conditions in a gear mesh.

### *Kinematic and Operating Conditions in Gears*

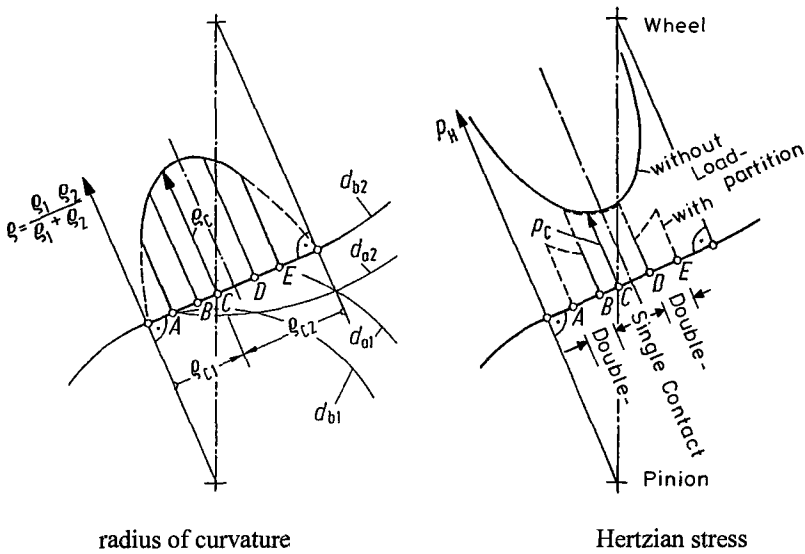
Along the path of contact gears are exposed to varying speed and load conditions. In the simplest case of a spur gear and disregarding dynamic effects, the local load varies between single and double tooth contact (Figure 1). Together with the local radius of curvature a distribution of the Hertzian stress along the path of contact can be derived (Figure 2). From the basic law of gear kinematics (Figure 3) follows that only on the pitch circle pure rolling is found. In all other points on the path of contact rolling and sliding at different proportions is present at the same time (Figure 4) [1]. The rolling speed  $v_r$  defined as the sum of the surface velocities of pinion and gear in each contact point, equal to the double value of the entraining velocity, is the governing parameter for lubricant film formation. The difference of the two surface velocities, the sliding speed  $v_s$ , is responsible for local shear forces, power loss and flash temperature. As the mesh moves on, the contact points on both partners travel out of the engagement zone. Conditions of 100% sliding, as in journal bearings, cannot be found in any point along the path of contact of gears. Figure 5 summarizes a characteristic parameter distribution of Hertzian stress  $p_c$ , rolling  $v_r$  and sliding  $v_s$  speed, slip rate  $s$  and flash temperature  $\vartheta_{fa}$  along the path of contact of a typical gear design.



profile contact ratio:  $\epsilon_\alpha = 1,1$

$\epsilon_\alpha = 1,8$

**Figure 1: Nominal Gear Tooth Load**



radius of curvature

Hertzian stress

**Figure 2: Radius of Curvature and Hertzian Stress along the Path of Contact**

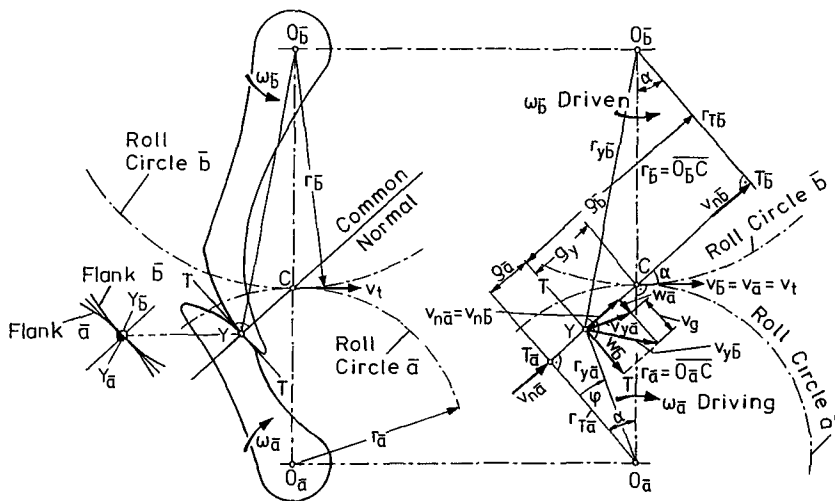


Figure 3: Basic Law of Gear Kinematics

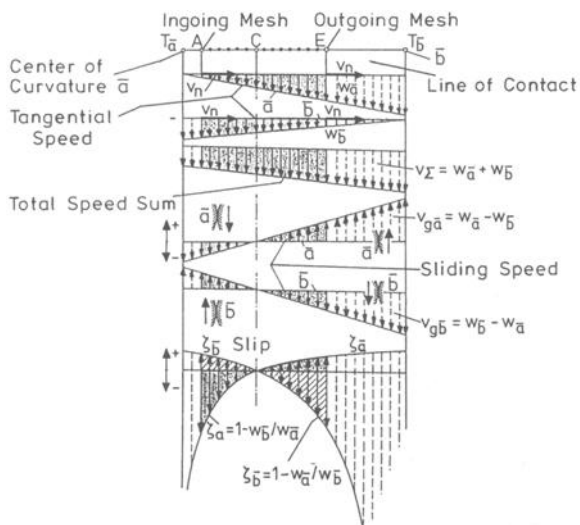


Figure 4: Local Speed Conditions along the Path of Contact

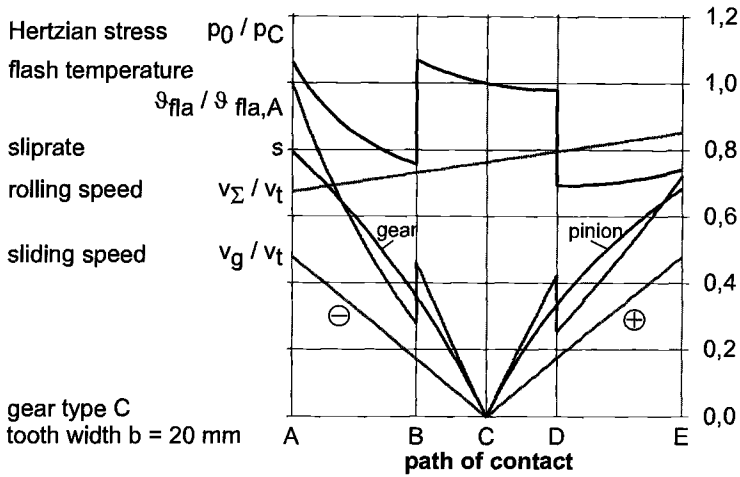


Figure 5: Characteristic Parameter Distribution along the Path of Contact

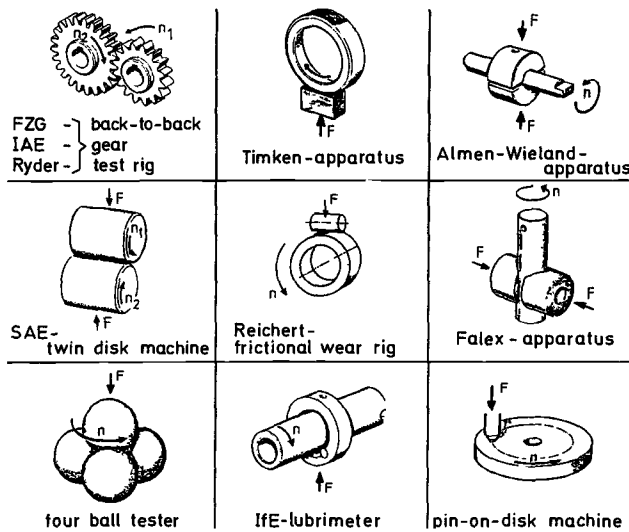


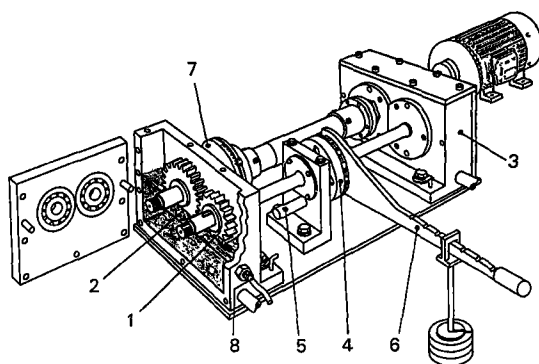
Figure 6: Principles of Gear Oil Testing Machines

### Test Configurations

Figure 6 shows examples of different test configurations which are on the market [2, 3, 4]. It can be differentiated between three categories:

- methods using test gears (FZG, IAE, Ryder)
- methods simulating one point on the path of contact (twin disk and roller tests)
- bench test methods with one partner standing still and the other sliding at 100% slip rate (four ball, Timken, pin-on-disk etc.)

*Gear Test Rig* - Investigations with test gear configurations are often performed on back-to-back gear test rigs. The FZG gear test rig (see Figure 7) [5, 6] is worldwide used for standard investigations of slow speed wear, scuffing, micropitting and pitting performance of gear lubricants. Centre distance is  $a = 91.5$  mm. Test and slave gears are connected by two shafts. One shaft is divided in two parts where a static torque is applied. Being set to rotation the test pinion drives the test gear and the loop is closed with the slave gear driving the slave pinion. The external motor has only to compensate for the power loss in the system. Thus high power can be transmitted through the test gears (some 300 kW) with a small driving engine of some 10 kW.



- |               |                           |
|---------------|---------------------------|
| 1 Test Pinion | 5 Locking Pin             |
| 2 Test Wheel  | 6 Load Lever and Weights  |
| 3 Slave Gear  | 7 Torque Measuring Clutch |
| 4 Load Clutch | 8 Temperature Sensor      |

**Figure 7:** FZG Back-to-Back Gear Test Rig

For good reproducibility of the test, test gear manufacturing has to be controlled very closely with respect to material, heat treatment and macro and micro geometry. Test gear geometry can be chosen for best simulation of the desired failure mode, avoiding not desired failure modes at the operating conditions.

The typical operating range of the rig is for Hertzian stress  $p_C$  up to  $1800 \text{ N/mm}^2$ , for pitch line velocity  $v_t = 8.3$  or  $16.6 \text{ m/s}$  and for oil temperature  $\vartheta_{oil}$  between  $60$  and  $120 \text{ }^\circ\text{C}$ . This covers the range of many industrial and automotive case carburized gear applications.

*Twin Disk Machine* - Twin disk or roller machines, like Amsler, Plint, or FZG with variable or fixed ratio of the sliding speed of the mating disks are able to simulate the kinematic conditions of one point on the path of contact of a gear. Figure 8 shows the FZG twin disk machine as an example [7]. The two disks are individually driven at different speeds between  $0$  and  $3500 \text{ rpm}$ . The normal load is applied by a spring mechanism and can be measured with strain gages at the supporting spring. The frictional force in the contact can be directly measured at the load cell. Test disk diameter is  $80 \text{ mm}$ . Disks are normally made from case carburized steel and ground after hardening.

Typical parameters of the rig are for Hertzian stress at line contact conditions  $p_H$  up to  $1500 \text{ N/mm}^2$ , for rolling velocity  $v_s$  up to  $16 \text{ m/s}$ , for slip rate  $s$  up to  $50\%$  and oil temperature  $\vartheta_{oil}$  between  $60$  and  $120 \text{ }^\circ\text{C}$ .

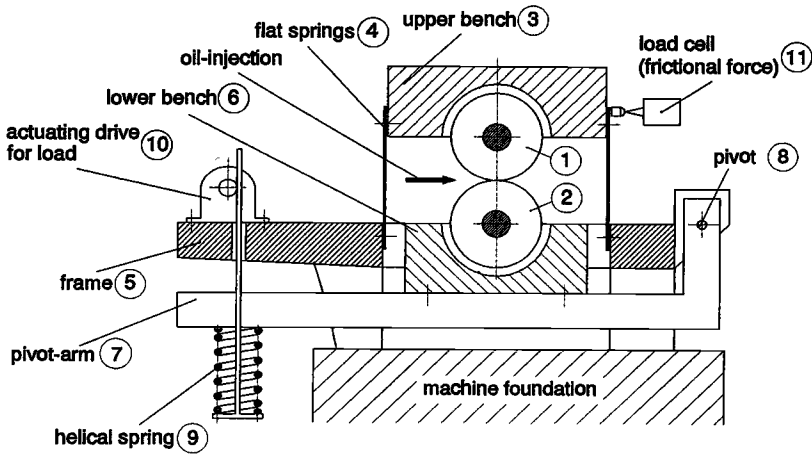


Figure 8: FZG Twin Disk Machine

Roller test rigs, as e.g. the roller test bench [8] of Zahnradfabrik Friedrichshafen (ZF) often use a fixed ratio of the slip rate of some 24%. Hertzian stress for line contact conditions can be as high as  $p_H = 3500 \text{ N/mm}^2$ , rolling speed  $v_z$  lies in the range of  $v_z = 8 \text{ m/s}$ .

The operating conditions of twin disk and roller machines cover the typical parameters of case carburized gears in industrial and automotive applications.

*Bench Test Machines* - As an example of a frequently used bench test machine the Shell Four Ball Tester is described (Figure 9) [9]. The upper rotating ball (4) is fixed to the drive shaft (2) with the taper connection holder, the lower three balls are fixed in cup (7) which can axially be loaded over the lever arm and weights. Test specimen are specially controlled balls from anti-friction bearings of diameter  $d = 12,7 \text{ mm}$  (1/2") made from the hardened bearing steel.

Typical parameters of the rig are for Hertzian stress at point contact conditions  $p_H$  up to  $7200 \text{ N/mm}^2$ , for rolling and sliding velocity  $v_z = v_g = 0.54 \text{ m/s}$ , for slip rate  $s = 100\%$  and oil temperature  $\vartheta_{oil} = 40 \text{ }^\circ\text{C}$ .

The Hertzian stress in this test lies way above gear contact stress, the speed is very low and the 100% slip conditions do not occur in a gear contact.

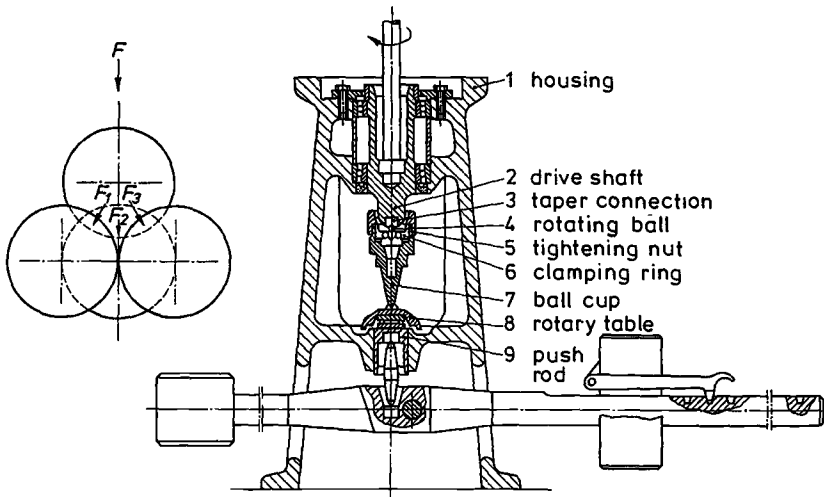
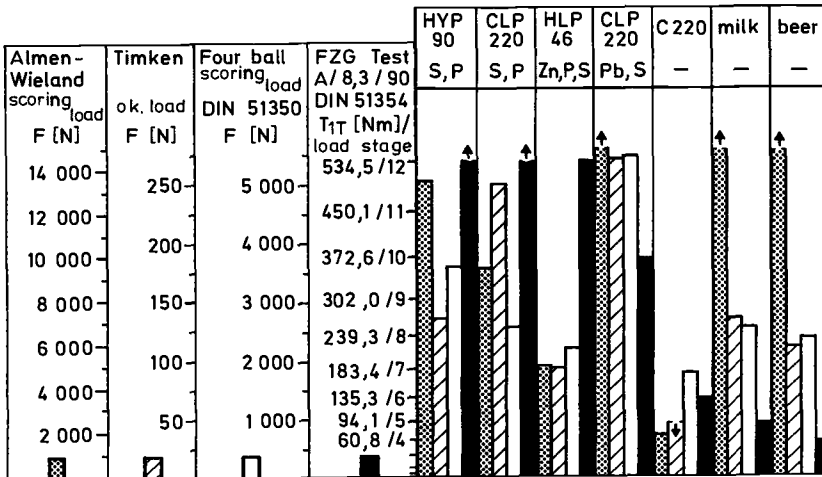


Figure 9: Shell Four Ball Tester

**Comparative Results in Bench and Gear Testers**

*Scuffing Investigations*

Different lubricants for different applications were tested according to different test methods (Figure 10) [10]. The following test lubricants were chosen in the order of their expected scuffing capacity: hypoid gear oil SAE 90 with sulphur-phosphorus additive of API GL 4 performance, industrial gear oil ISO VG 220 with sulphur-phosphorus additive API GL 3 performance, EP hydraulic oil ISO VG 46 with Zinc-di-thio-phosphate additive, industrial gear oil ISO VG 220 with lead naphtenate additive, industrial gear oil ISO VG 220 without EP additives, and, as extremes, milk and beer. Scuffing performance for these lubricants was evaluated in bench tests using the Almen-Wieland [11] rig, which is frequently used in Germany, in the Timken test [12] and the Four Ball [9] test, which are often required values in gear oil specifications and in comparison in the FZG test using gears as test specimen. The scuffing results in the Almen-Wieland test of milk and beer are higher than the results of the hypoid oil and EP industrial gear oils. The scuffing results in the Timken and the Four Ball test of milk and beer are in the same range as for the hypoid oil, higher than the hydraulic oil, and much higher than the non-EP industrial gear oil. Only the gear test method FZG shows adequate results for these gear oils, where the hypoid oil and the GL 3 industrial gear oil cannot be differentiated with this test procedure. Today more advanced test methods on the FZG gear test rig are available to determine the scuffing properties of lubricants up to the level of API GL 5 [13].



**Figure 10:** Scuffing Load Capacity Evaluated in Different Test Rigs

The scuffing capacity of different hypoid gear oils was investigated in a twin disk simulation as well as in a spur and a hypoid gear test (Figure 11) [14, 15]. Gear lubricants were two standard hypoid gear oils SAE 90 and SAE 75W80 with standard sulphur-phosphorus additive systems of API GL 4 level and one special lubricant with an addition of Molybdenum-di-sulphate to a standard hypoid gear oil SAE 80W90 with sulphur-phosphorus additive. The scuffing performance in the twin disk test of the MoS<sub>2</sub> containing lubricant was about three times higher than the scuffing capacity of the two standard hypoid oils. In the hypoid gear test the two standard hypoid oils could not be differentiated, the MoS<sub>2</sub> oil showed lower capacity. In the spur gear test the two standard hypoid oils could be differentiated and again the MoS<sub>2</sub> oil gave lower scuffing performance.

*Conclusion* - Simple bench tests with conditions of 100% sliding cannot be used to predict neither the absolute nor the relative scuffing capacity of gear oils. Even in a twin disk simulation with similar operating conditions compared to one point on the path of contact of a gear neither the absolute nor the relative scuffing performance of different gear oils is predicted correctly. Bench tests can only be used as batch or receipt control where the oil and additive type and concentration is known and assumed to be constant.

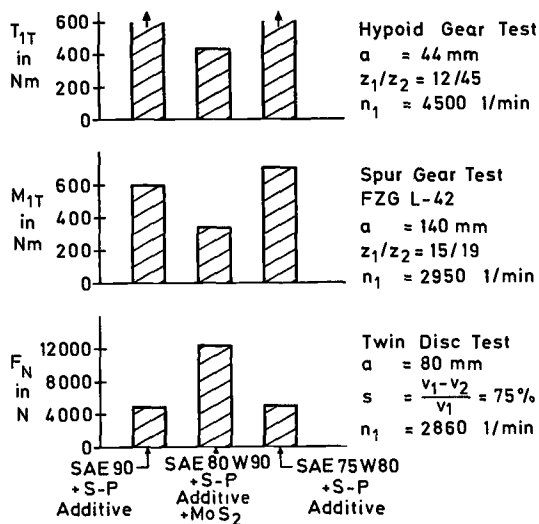


**Figure 11:** Scuffing Load Capacity in Gear and Twin Disk Testing

*Pitting Investigations*

The influence of lubricants with different frictional behavior on the pitting capacity of through hardened disks and gears was investigated [7]. A traction fluid ISO VG 32 with high coefficient of friction was investigated in comparison to a mineral oil ISO VG 100 with considerably lower coefficient of friction. Figure 12 shows the pitting life of disks at a Hertzian stress of  $p_H = 1300 \text{ N/mm}^2$ . Decisive operating parameters of the disk tests, as sum velocity  $v_\Sigma$  and film thickness  $h_{min}$ , were kept nearly constant for the two lubricants except for the coefficient of friction  $\mu$ . For 50% failure probability the pitting life of the mineral oil is 25 times higher as the pitting life of the traction fluid. Investigations with the same lubricants in through hardened gears of same material and heat treatment showed the same relative results with approximately 15 times higher pitting life of the mineral oil compared to the traction fluid (Figure 13). When the operating conditions of the disk tests are recalculated to the operating conditions of the gears, the disk results fit well into the SN-curve (stress-cycle) of the gear results. In this case also the absolute pitting capacity of disk and gear tests is comparable.

Comparative testing of case carburized rollers and gears determining the influence of case depth on pitting capacity [8, 16, 17] gave same or similar relative results (Figure 14). The absolute pitting capacity of the rollers, however, was found at almost double Hertzian contact stress for the rollers compared to the gears.

*Conclusion* - Pitting investigations of through hardened material showed good relative and absolute correlation in twin disk simulation and gear tests. Pitting investigations of case carburized materials gave good relative correlation but much higher absolute pitting capacity of the rollers compared to the gears.

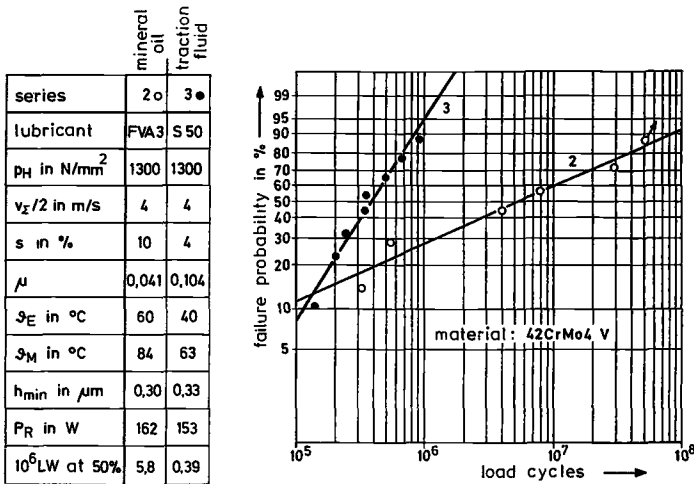


Figure 12: Pitting Life of Through Hardened Disks

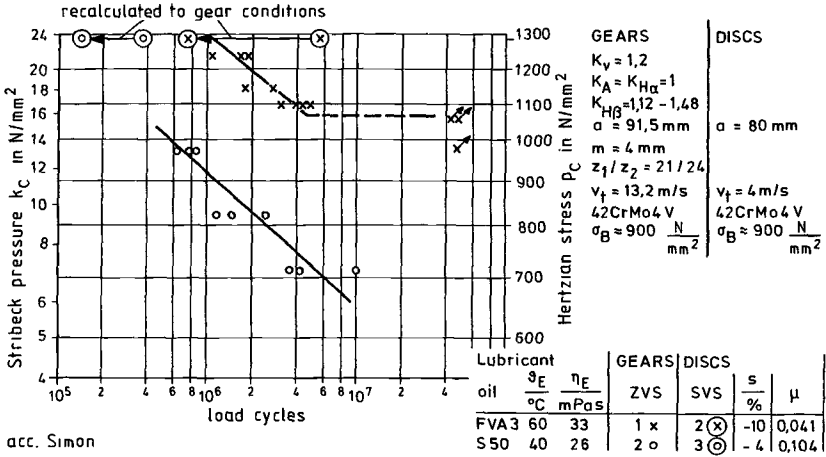


Figure 13: Pitting SN-Curves of Through Hardened Disks and Gears

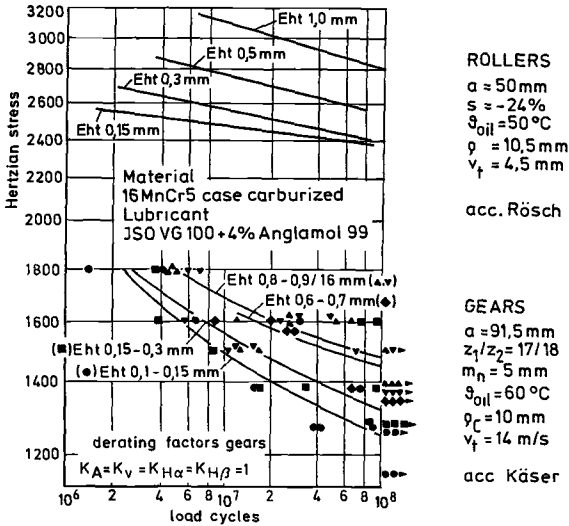
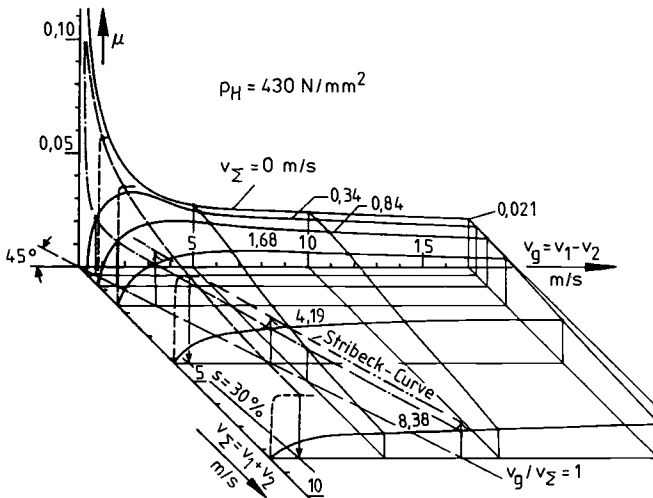


Figure 14: Pitting SN-Curves of Case Carburized Disks and Gears

*Frictional Behavior*

In simple bench tests with one partner standing still, meaning conditions of 100% sliding, the frictional heat from the non-moving partner can only be removed by conduction. In a gear as the mesh moves along the flanks of pinion and gear new contact points are formed continuously. The typical Stribeck curve of a journal bearing does not apply to gears. Figure 15 shows the field of the coefficient of friction for elastohydrodynamic lubrication as a function of rolling and sliding speed determined in a twin disk arrangement. The Stribeck curve can clearly be spotted as a singularity on the friction area [18].

For a mineral oil and a polyalphaolefin (PAO) the frictional behavior was determined in the twin disk machine and the back-to-back gear test rig [19]. Figure 16 shows the result of the twin disk investigation for the mineral oil, Figure 17 of the PAO as a function of rolling speed  $v_{\Sigma}$  and slip rate  $s$ . The typical steep increase from zero sliding to 10% sliding can be found for both lubricants, somewhat more gradual for the polyalphaolefin. For rolling speed  $v_{\Sigma}$  between 2 and 8 m/s the coefficient of friction for high sliding lies for the mineral oil between  $\mu = 0,040$  and  $0,060$ , for the PAO between  $\mu = 0,030$  and  $0,045$ . Figure 18 shows the mean value of the coefficient of friction along the path of contact from gear investigations for the same two lubricants. The coefficient of friction of the two lubricants lies in the same range in the twin disk and the gear investigations. Figure 19 shows the comparison for rolling speed  $v_{\Sigma} = 4$  m/s. A good correlation between gear and disk results can be found when using the disk results at a slip rate of  $s = 30\%$ .



**Figure 15:** Coefficient of Friction as a Function of Rolling and Sliding Speed

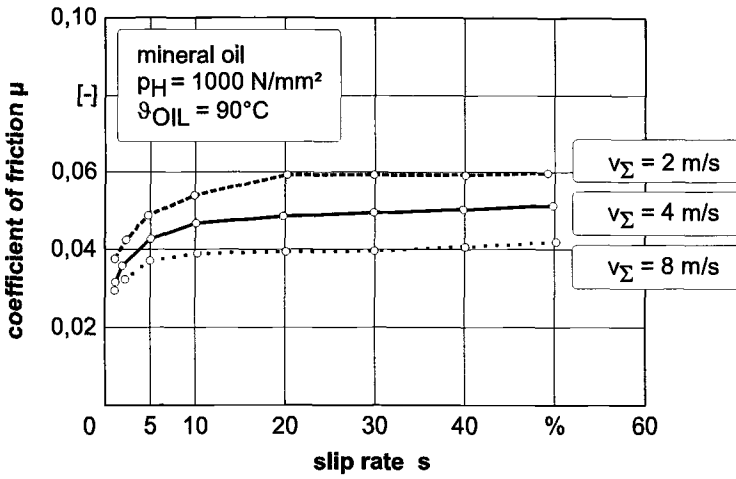


Figure 16: Coefficient of Friction of a Mineral Oil in the Twin Disk Test

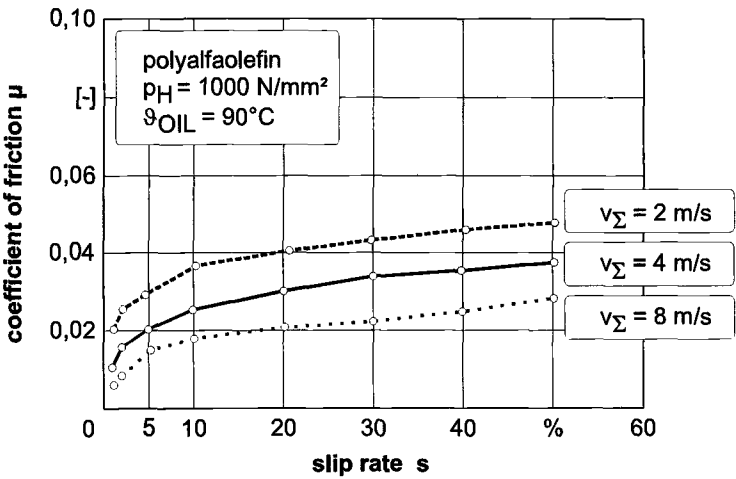
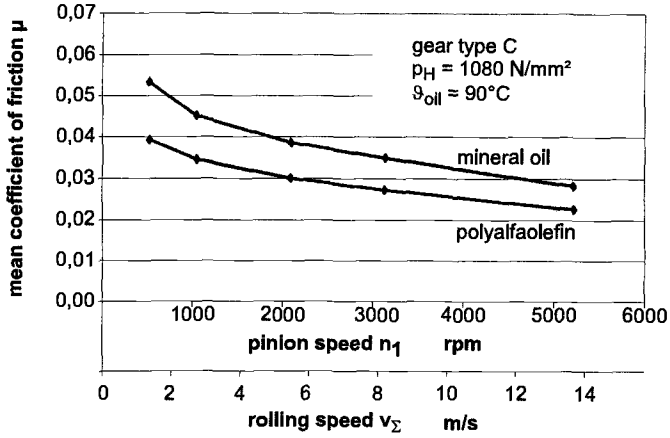
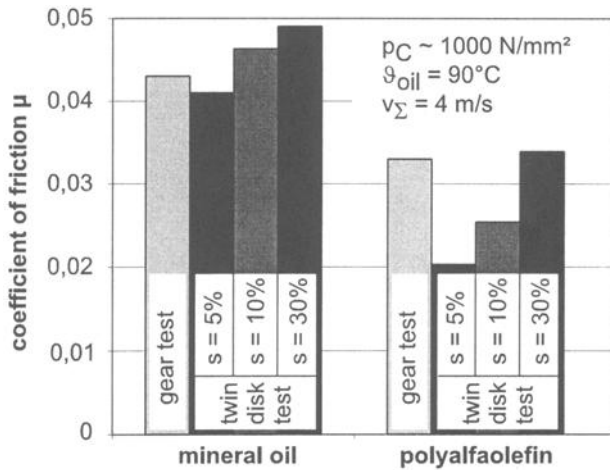


Figure 17: Coefficient of Friction of a Polyalfaolefin in the Twin Disk Test



**Figure 18:** Coefficient of Friction of a Mineral Oil and a Polyalfaolefin in the Gear Test



**Figure 19:** Comparison of Lubricant Frictional Properties in Disk and Gear Tests

*Conclusion* - Due to the kinematic conditions frictional behavior of lubricants evaluated in bench tests at 100% sliding rate can hardly be compared to gear results. Using twin disk arrangements simulating mean values of the sliding rate of gears the values of the coefficient of friction showed good relative and absolute correlation to gear results.

### Comparison of Bench Test and Gear Parameters

Simple bench tests often use totally different contact parameters than gears with respect to Hertzian stress and speed and are mainly run under 100% slip rate. Results from such test machines can hardly be correlated to gear results. These machines can well be used for batch control or receipt control when the type of oil, additive type and content are defined and have only to be controlled for adequate manufacturing. For the development of new lubricants or additives the results can be very misleading.

Even results from twin disk or roller tests simulating contact stress, rolling and sliding speed and temperature of one point along the path of contact of a gear, do not always correlate to gear results. This fact might be due to the fact that the gear mesh is a discontinuous process with teeth coming into contact and going out of contact. Each new tooth engagement requires new lubricating film formation with unfavourable local conditions of a scraping edge (Figure 20).

Good correlation with gear applications in practice can normally be found for gear test results. They are often costly and time consuming but reliable with relative and absolute correlation.

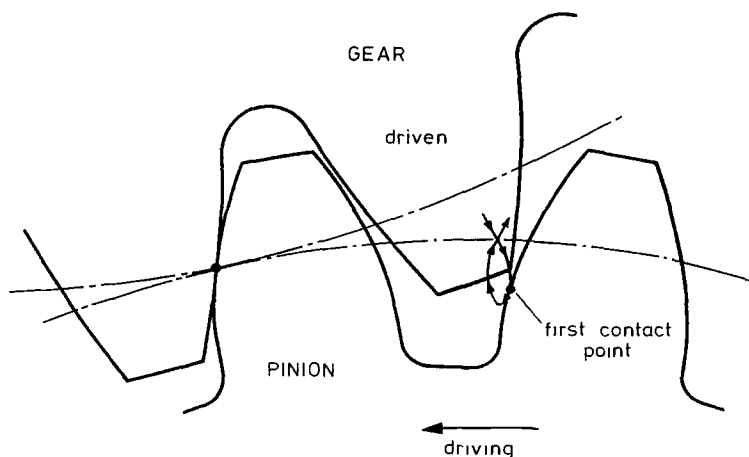


**Figure 20:** Scraping Edge at the Ingoing Gear Mesh

## Summary

Results of bench tests with 100% sliding rate, twin disk test simulating one point on the path of contact of a gear, and gear tests were compared for scuffing and pitting failures and coefficient of friction.

Poor correlation has to be stated for the bench tests with 100% sliding rate. For the twin disk simulation, poor correlation was found for scuffing results, good relative but poor absolute correlation for pitting results, and both good relative and absolute correlation for the frictional behavior.

From these investigations it has to be concluded that bench test results applied to gears have to be regarded very critically and can only be interpreted correctly with excellent experimental background and experience.

## References

- [1] Niemann, G., Winter, H.: „Maschinenelemente, Band II“ (Machine Elements). *Springer Berlin* 1985.
- [2] Winter, H., Michaelis, K.: „Scoring Load Capacity of Gears Lubricated with EP-Oils“. *Fall Technical Meeting Montreal Canada, Oct. 17 - 19, 1983*, AGMA Technical Paper No. P219.17.
- [3] Vogelpohl, G.: „Verschleiß von Maschinen und die Möglichkeiten seiner Verminderung mit Hilfe der auf Ölprüfgeräten gewonnenen Erkenntnisse“ (Wear in Machines and Possibilities of its Reduction by use of Characteristic Values from Lubricant Bench Tests) *Erdöl und Kohle, Ergas, Petrochemie* 14 (1961), Heft 10, S. 824-829.
- [4] Bartz, W.J.: „Über den Mißbrauch von Schmierstoffprüfgeräten“ (On the Misuse of Lubricant Bench Tests) *Mineralöltechnik* 14 (1970), S. 1-24.
- [5] ASTM D-5182-97e1: „Standard Test Method for Evaluating the Scuffing (Scoring) Load Capacity of Oils (FZG Visual Method)“.
- [6] CEC L-07-A-95: „FZG Gear Machine: Load Carrying Capacity Test for Transmission Lubricants“.
- [7] Simon, M.: „Messung von elasto-hydrodynamischen Parametern und ihre Auswirkung auf die Grübchentrugfähigkeit vergüteter Scheiben und Zahnräder.“ (Measurement of EHD Parameters and their Influence on Pitting Capacity of Through Hardened Disks and Gears). Dissertation TU München 1984.

- [8] Hoffmann, G., Lipp, K., Michaelis, K., Sonsino, C.M., Rice, J.A.: „Testing P/M Materials for High Loading Gear Applications“ *The International Journal of Powder Metallurgy*, Vol 35 (1999), p. 35-44.
- [9] ASTM D2596-97 „Standard Test Method for Measurement of Extreme-Pressure Properties of Lubricating Grease (Four-Ball Method)“
- [10] Wirtz, H.: „Schmierstoffe und anwendungsbezogene Schmierstoffprüfung“ (Lubricants and Practical Lubricant Testing). *Vortrag Technische Akademie Wuppertal*, Hubertusallee 18, 42117 Wuppertal, Mai 1980.
- [11] Hösl, W.: „Das Verhalten von  $\beta$ -Diketonen unter Bedingungen der Mischreibung“ (Behaviour of  $\beta$ -Diketones at Boundary Lubrication) Dissertation Universität Hannover, 1968
- [12] ASTM D2782-94(1996) „Standard Test Method for Measurement of Extreme-Pressure Properties of Lubricating Fluids (Timken Method)“
- [13] Höhn, B.-R., Oster, P., Michaelis, K.: „New Test Methods for the Evaluation of Wear, Scuffing and Pitting Capacity of Gear Lubricants“. *AGMA Technical Paper no. 98FTM8*.
- [14] Seitzinger, K., Richter, M.: „Grenzen und Möglichkeiten der FZG-Zahnrad-Verspannungs-Prüfmaschine, insbesondere zur Prüfung von Hypoidgetriebeölen“ (Limits and Possibilities of the FZG Back-to-back test rig - Testing of Hypoid Gear Oils) *Schmiertechnik und Tribologie* 18 (1971), S. 223 - 227, 19 (1972), S. 22 - 29, S. 58 - 60, S. 128 - 130, S. 145 - 148.
- [15] Winter, H., Michaelis, K.: „Scoring Load Capacity of EP-Oils in the FZG L-42 Test“ *Fuels and Lubricants Meeting Toronto*, Oct. 18-21, 1982, SAE Technical Paper Series 821183, S. 1 - 7.
- [16] Käser, W.: „Beitrag zur Grübchenbildung an gehärteten Zahnrädern. Einfluß von Härtetiefe und Schmierstoff auf die Flankentragfähigkeit“ (Pitting Load Capacity of Case Carburized Gears - Influence of Case Depth and Lubricant). Dissertation TU München 1977.
- [17] Rösch, H.: „Untersuchungen zur Wälzfestigkeit von Rollen - Einfluß von Werkstoff, Wärmebehandlung und Schlupf“ (Investigations on Pitting Load Capacity of Rollers - Influence of Material, Heat Treatment and Slip Rate). Dissertation TU München 1976.
- [18] Stössel, K.: „Reibungszahlen unter elasto-hydrodynamischen Bedingungen“ (Coefficient of friction for EHD Lubrication) Dissertation TU München 1971.
- [19] Höhn, B.-R.; Michaelis, K.: „Influence of Lubricants on Power Loss of Cylindrical Gears“ *48th Annual Meeting in Calgary, Alberta, Canada, May 17-20, 1993*. Tribology Transactions Volume 37 (1994) p. 161 - 167.

G. E. Totten,<sup>1</sup> R. J. Bishop, Jr.,<sup>1</sup> and L. Xie<sup>2</sup>

## Use of Bench Tests to Evaluate Water-Glycol Hydraulic Fluid Lubrication

---

**Reference:** Totten, G. E., Bishop, R. J., Jr., and Xie, L., “Use of Bench Tests to Evaluate Water-Glycol Hydraulic Fluid Lubrication,” *Bench Testing of Industrial Fluid Lubrication and Wear Properties Used in Machinery Applications, ASTM STP 1404*, G. E. Totten, L. D. Wedeven, J. R. Dickey, and M. Anderson, Eds., American Society for Testing and Materials, West Conshohocken, PA, 2001.

### Abstract:

The anti-wear lubrication performance of a series of hydraulic fluids was determined using various bench wear tests including: Four-Ball, Pin-on-V-Block Falex Wear Test, Timken Block-on-Ring, a recently developed cyclic contact stress (3-vane-on-ring) test and the ASTM D-2882 Vickers V-104C vane pump test. These bench tests were selected since they are used in the fluid power industry for fluid selection, qualification and performance troubleshooting. The results of this work showed that none of the bench tests evaluated provided any correlation with the wear rates obtained with the ASTM D-2882 pump test. Bench wear test correlations are possible only if the conditions of the wear test, such as wear contact geometry, loading, speeds, and materials reasonably model the specific wear contact of interest in the hydraulic pump. Even then, the general reliability of the bench testing conditions should first be validated by hydraulic pump testing.

**Keywords:** bench tests, pump tests, wear tests, wear

### Introduction

One method of evaluating the potential lubrication performance of a hydraulic fluid is to perform a test in the hydraulic pump (or motor) of interest. However, this is clearly impractical in view of the numerous pump manufacturers and models available. This problem may be further complicated since various pumps may be configured differently or manufactured with different material pairs for the wear contact. This problem could be greatly simplified with the use of one, or at least a limited number of “standard” hydraulic pump tests.

---

<sup>1</sup> Union Carbide Corporation, 771 Old Saw Mill River Road, Tarrytown, NY 10591.

<sup>2</sup> Solidworks Corporation, 300 Baker Avenue, Concord, MA 01742.

One standard test, ASTM D-2882, has been developed for this use. This test is conducted for 100 hours with a Vickers V-104C vane pump using a 5 gal (19.9 liter) reservoir at 65°C, 13.8 MPa (2000 psi), 1200 rpm, and an 8 gal/min (30.3 liter/min) cartridge. The German specification, DIN 51389, is similar except that the test is conducted for 250 hours, at 50°C, 10.3 MPa (1500 psi), and at 1500 rpm. Recently, the American automotive industry has issued a hydraulic fluid testing specification also incorporating the Vickers V-104C vane pump [1].

Although the Vickers V-104C vane pump has wide acceptance, and has served the industry well historically, it does suffer from a number of disadvantages, such as relatively high cost per test and relatively long test durations, which may preclude its use for such applications as quality control testing and general fluid development, as well as used fluid performance troubleshooting. Therefore, it would be desirable to develop a faster, lower cost "bench test" as a viable alternative to routine pump testing.

An important distinction exists between bench testing and results obtained with actual industrial machinery and components. Usually the goal of bench testing is to either rank a property or to relate the wear obtained to a single tribological condition. Often, it is not the primary goal to obtain a direct correlation between machinery and bench test wear.

In this paper, the "bench test" performance results of a number of experimental hydraulic fluids relative to the results obtained for the same fluids using ASTM D-2882 will be reported. This will be followed by a discussion of the results with respect to lubrication fundamental concepts and prior published work. Finally, general recommendations will be offered for consideration for future hydraulic pump and "bench test" development.

## Discussion

### A. Attempted Bench Test Correlations

1. *ASTM D-2882 Test Results*- The pump tests were conducted according to ASTM D-2882 with the following modifications:

- A one-gallon reservoir was used. (ASTM D-2882 calls for at least a five-gallon reservoir.)
- Instead of solvent flushing, as required by ASTM D-2882, the pump was dismantled, the heat exchanger and recirculation hoses were removed and cleaned individually and thoroughly to eliminate any possibility of system contamination.

Five experimental fluids representing a wide range of total wear on vanes + ring were evaluated. These fluids included four experimental water-glycol hydraulic fluids. Pump failure was not obtained with any of these fluids. Where sufficient quantities of fluid were available, the pump tests were run in duplicate. The results obtained are shown in Table 1. The fluids selected show 1-3 orders of magnitude difference in wear rates and that the results are reasonably reproducible. It should be noted that the interlaboratory wear rates obtained for the ASTM D-2882 pump test are often highly

variable, although individual laboratories may obtain much more repeatable results.

For this work, various additional testing procedures, outlined in Reference 21, were used which provided excellent test repeatability as shown by the duplicate data in Table 1. This is typical of what the additional precautions have provided over many years of experience with the ASTM D-2882 test with water-glycol hydraulic fluids. However, there is considerable concern, among many in the hydraulic fluid industry, that the ASTM D-2882 pump test results themselves may be either incorrect or misleading.

To address this problem, Union Carbide Corporation at Tarrytown, New York has conducted considerable research in an effort to obtain repeatable and reproducible results with the ASTM D-2882 test when applied to water-glycol fluid studies. The results of the necessary test improvements are summarized in Reference 21. When these improvements are applied, excellent test results have been obtained over the last 20 years, although a detailed statistical study has not been performed. However, an indication of the test repeatability, at least with duplicate analyses, is provided with the results shown in Table 1.

Table 1 - *ASTM D-2882 Pump Test Results*

Fluid ID No.	Fluid Type <sup>b</sup>	Wear (mg) <sup>a</sup>		
		Trial 1	Trial 2	Average
1	WG	220	110	165
2	WG	16	6	11
3	WG	10	50	30
4	WG	2300	1860	2080

<sup>(a)</sup> The combined weight loss of the ring plus the vanes in 100 hours.

<sup>(b)</sup> WG is a water-glycol hydraulic fluid.

2. *Bench Testing Protocol* - While it is true that conditions for a particular bench test may be selected, by varying contact materials, load, speeds and geometry, to achieve correlation with wear at a specific location in a pump, most often this is not done. Instead, it is more typical to encounter a specific standard test requirement without regard for the potential that there may be no correlation at all with the machinery wear being modeled.

In this work, a number of commonly encountered standard bench test procedures were evaluated. It is not uncommon for these tests to be used as alternatives for the ASTM D-2882 pump test. If these tests are used as alternatives to ASTM D-2882, it would be expected that the wear obtained should correlate with the pump test wear results. This is the objective of this study, to determine if such a correlation exists.

A further point must be made with respect to the actual bench test results reported here. The bench tests used were not selected as part of a R&D effort to identify a particular bench test which would provide the best pump test wear correlation. Instead, as often happens, the tests conducted were performed at the specific request of various customers. Therefore, one of the objectives of this work was to illustrate the viability of conducting, or possibly misapplying specific bench tests, without the necessary prior

validation work with the machinery wear condition of interest.

3. *Four-Ball Test Results* - The Four-Ball Test is one of the most frequently encountered tests in fluid lubrication. It is currently used as a performance criteria for purchasing specifications for hydraulic fluids and for wear characterization of used fluids.

The Four-Ball Test is conducted by mounting 4 balls, three balls are fixed in the bottom assembly and the top ball is rotated at a constant rpm speed and applied load. This test was conducted according to ASTM D-4172 with an applied load of 40 kg (88 lb.) and a rotational speed of 1200 rpm. The test was conducted for one hour and the wear scars measured. This test was modified to run at a lower temperature, 23-47°C, for the duration of the test to minimize any loss of the components of the water-glycol fluid formulation which would have occurred at the normal starting test temperature of 75°C.

The test results, which are summarized in Table 2, showed that while the wear scar was generally reproducible, there was essentially no correlation with the ASTM D-2882 pump test results.

Table 2 - *ASTM D-2882 Correlation  
With The Four-Ball Wear Scar Results (ASTM D-4172)*

<b>Fluid ID</b>	<b>Wear Scar (mm)</b>			<b>D-2882</b>
	<b>Trial 1</b>	<b>Trial 2</b>	<b>Average</b>	<b>Wear (mg)</b>
1	0.73	0.79	0.76	165
2	0.58	0.58	0.58	11
3	0.78	0.71	0.74	30
4	0.72	-	0.72	2080

A modification of the Four-Ball Test was reported earlier where the bottom three balls were replaced with rollers, was used to characterize polyol ester, phosphate ester and water-glycol hydraulic fluids[2]. This work showed that these tests gave erratic results, especially for water-glycol hydraulic fluids.

Perez [3] developed a "sequential" Four-ball test which was reported to provide an excellent correlation with the Sperry-Vickers 35VQ vane pump test [4] for mineral oil, phosphate ester and water-glycol hydraulic fluids. This modified test was not available for the test comparison of the fluids used in this study.

4. *Falex Pin-on-V-Block Test* - Another widely used lubrication anti-wear evaluation is the Falex Pin-on-V-Block Test. The work discussed here was conducted according to ASTM D-2670.

Wear may be recorded as the number teeth on the instrument ratchet mechanism advanced over the duration of the test, weight loss or wear scar. For this work, the number of teeth advanced and weight loss was evaluated. The results are shown in Table 3. (Weight loss data will be described subsequently.)

Table 3 - *Falex Pin-On-V-Block Test Correlation with ASTM D-2882*

<b>Fluid ID</b>	<b>Falex Unheated No. Of Teeth</b>	<b>Falex Weight Loss (mg)</b>	<b>D-2882 Wear (mg)</b>
1	18,9 (13.5)	0.0251	163
2	24,30 (27)	0.045	11
3	43,56 (49.5)	0.0601	30
4	122		2080

One of the greatest disadvantages with these bench tests is that it is not possible to control the reservoir temperature [6]. Significant temperature rise may occur increasing the potential for loss of critical formulation components such as, water and amines used for corrosion protection and which affect anti-wear properties. Test method D-2670 calls for a starting test temperature of  $24^{\circ} \pm 3^{\circ}\text{C}$  ( $75 \pm 10^{\circ}\text{F}$ ). However, without external temperature control, it is impossible to maintain a test temperature required to prevent volatilization of some of the components such as water. The effect of temperature on wear of water-glycol fluids using the Pin-on-Vee Block Test was not evaluated. This problem must be considered in future work.

The Falex anti-wear test using the Pin-on-V-block test configuration was modified to provide a more conforming journal contact as shown in Figure 1. Along with the journal contact with a conforming surface, the test system was modified to provide reservoir temperature control and filtration. This system was designated the "Gamma-Falex Test" and has been reported to successfully model the ASTM D-2882 test when used for water-containing hydraulic fluids, e.g., water-glycol and high water base fluids [5,6,7,8] Unfortunately, due to limited test fluid volumes, this test variation could not be evaluated for this work.

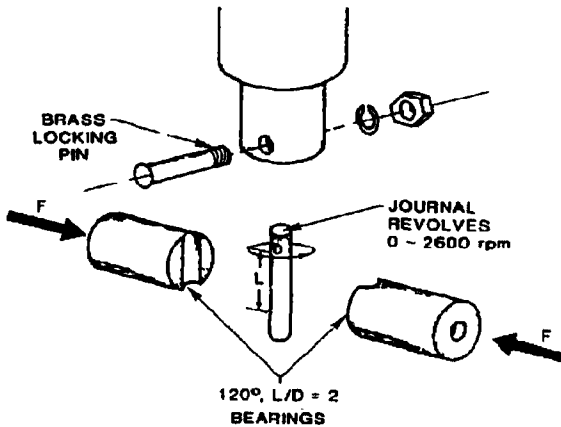


Figure 1 - Illustration of the wear contact configuration for the Gamma-Falex Test.

5. *Timken Test Correlation with ASTM D-2882* - The Timken EP Test utilizes a Block-on-Ring wear contact. Test method D-2782 is not an anti-wear test, but an EP test as measured by load carrying capacity. However, this is a test that has been required by some users in the past. Therefore, the test was evaluated as part of this study. The wear of four hydraulic fluids shown in (Table 1) were evaluated. The fluids used for this work were selected to represent fluids of similar composition but significantly different ASTM D-2882 wear results. The test comparison is provided in (Table 4), which shows essentially no correlation with the wear results obtained by ASTM D-2882.

It is important to note that only the single test condition reported for test method D-2782 was evaluated here. Furthermore, a potentially more interesting correlation with load carrying capacity was not performed either. These results show the problem of selecting a single set of test conditions and expecting wear correlation with industrial machinery (or even another standard test). Mizuhara has shown in his work that if the loading and speed are varied using the Timken Test Machine that it is possible to identify a set of test conditions that will yield the desired machine wear condition [15].

Table 4 - Comparison of Timken EP Test Results with ASTM D-2882<sup>a</sup>

Fluid ID	Timken EP OK Load	Test (kg) Failure Load	D-2882 (mg)
1	18	21	165
2	18	21	11
3	15	18	30
4	15	18	2080

<sup>a</sup> Experimental work performed by UEC Engineers and Consultants, Inc., Pittsburgh, PA.

6. *Testing of Anhydrous Hydraulic Fluids* - All of the testing results reported above were conducted using aqueous hydraulic fluids. Use of the bench tests above may produce significant temperature rises when confined to a small reservoir due to the friction produced in the system. If the temperature rise is sufficient, there may be significant fluid component losses, such as water, due to evaporation. This may produce significant problems with the test results, since the results obtained would not be reflective of the proper fluid chemistry.

To evaluate this as the reason for non-correlation of bench test results and ASTM D-2882 wear, a limited number of different anhydrous hydraulic fluids were evaluated using test method D-4172. The results are summarized in (Table 5). As observed previously for the aqueous hydraulic fluids, there was no correlation between the Four-Ball Test and ASTM D-2882 test results for the anhydrous hydraulic fluids.

Table 5 - *Comparison of Four-Ball Test Results for Anhydrous Hydraulic Fluids with ASTM D-2882 Test Results*

Fluid	ASTM D-4172-94 4-Ball Anti-Wear Scar (mm @40 kgf, 1 h, 75°C ±2)	ASTM D-2882 Anti-Wear Vane Pump (mg)
A	0.22	3.1
B	0.22	4.1
C	0.18	2.4
D	0.21	6.0

These results show the inadvisability of simply selecting a bench test and conducting the experimental work under a set of "standard" conditions. For a bench test to be properly applied, the appropriate load and contact speed condition for the bench test being used must be identified that will properly rank the various hydraulic fluids with respect to wear properties and failure mechanism of the machine, in this case a Vickers V-104CC hydraulic pump. To conduct such a test with a single set of un-validated conditions is no different than the proverbial "shot in the dark".

7. *Other Bench Tests* - In the above discussion, a "standard" bench test was used to model expected hydraulic pump wear and to be used as a replacements for hydraulic pump testing. In some cases, bench tests have been either specially modified or even custom designed to model pump wear. Selected examples will be provided here.

a. *University of Aachen Sliding Wear Bench Test* - A specially designed bench test was developed by Jacobs, et. al. to examine the effect of sliding wear that occurs in hydraulic pumps with different material pairs [17]. This machine is schematically illustrated in (Figure 2).

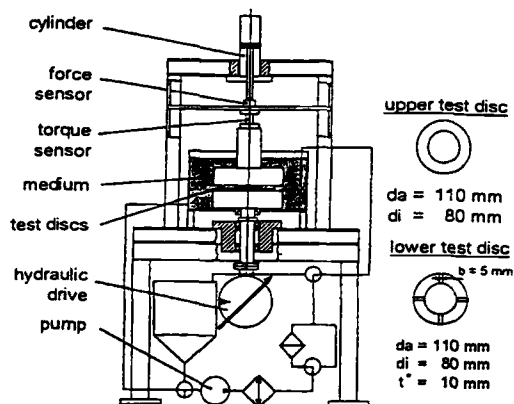


Figure 2 - Aachen mixed friction sliding wear machine.

b. *University of Leeds Testing Machine* - Priest, et.al., have also reported a bench test that is illustrated in (Figure 3) to model the sliding wear contact in the V-104C vane pump [18]. A schematic comparison of the wear contacts in the bench and V-104C vane pump is illustrated in (Figures 4 and 5), respectively. Excellent correlation between the bench and vane pump tests has been reported [18]

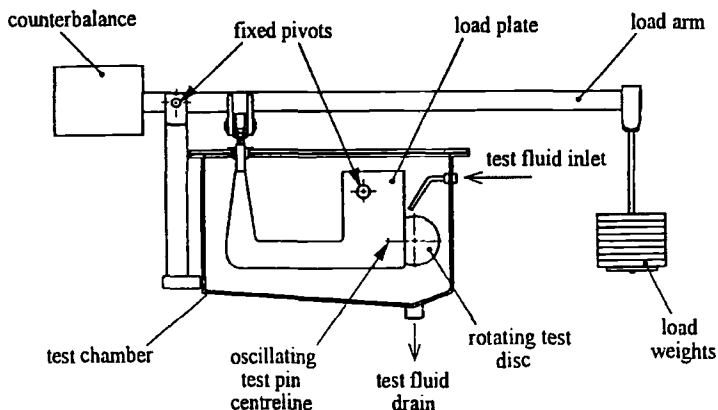


Figure 3 - University of Leeds Test Machine.

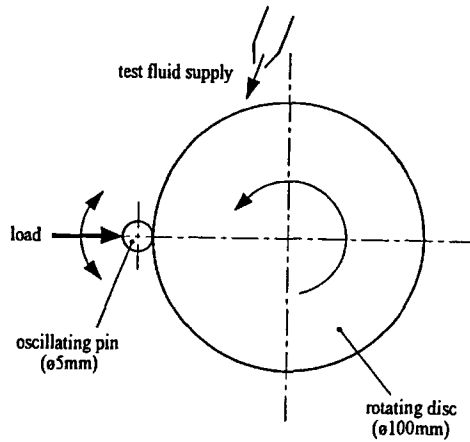


Figure 4 - Wear Contact for the University of Leeds Test Machine.

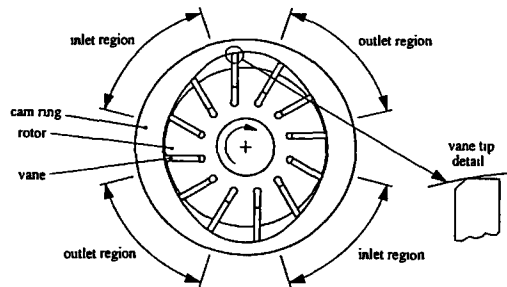


Figure 5 - Wear contact for the Vickers V-104C vane pump.

*c. Cameron-Plint Wear Test Apparatus* - The effect of metallurgy on sliding wear using various hydraulic fluids for aerospace applications has been performed using the Cameron-Plint wear testing apparatus shown in (Figure 6) [19]. In this test, the sliding motion of an upper cylinder on a lower plate surface is controlled by a variable speed motor.

*d. Unisteel Rolling Fatigue Machine* - Another bench test that has been used to model hydraulic fluid wear is the Unisteel Rolling Fatigue Machine shown in (Figure 7). In this test, a flat ring forms the upper part of a thrust bearing which contains the cage, half of the balls and one race from a production thrust bearing assembly [20].

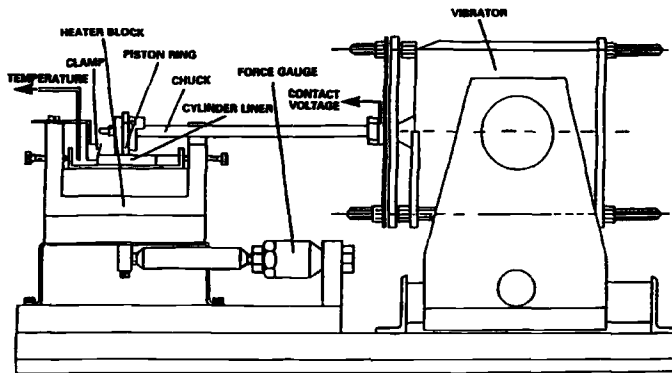


Figure 6 - Cameron-Plint Wear Test Machine.

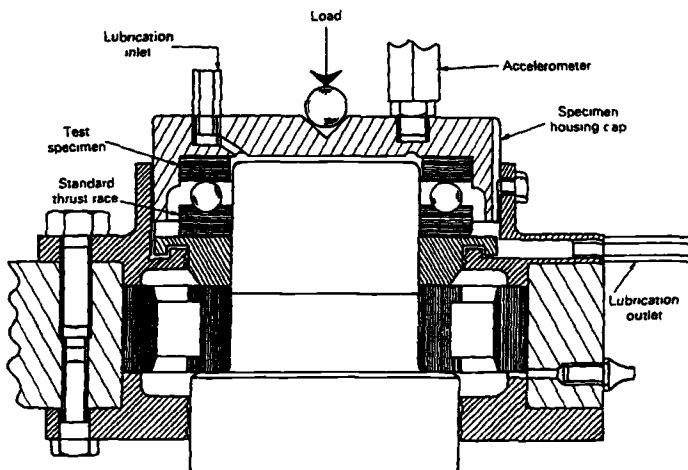


Figure 7 - Unisteel Rolling Fatigue Machine.

## B. Fundamental Principles of Lubrication

1. *Stribeck-Hersey Curve* - Hydraulic fluid lubrication may occur by one of at least four wear mechanisms; hydrodynamic, elastohydrodynamic (EHD), mixed film and boundary lubrication. The particular mechanism encountered is dependent on the film viscosity, velocity and applied load as illustrated in (Figure 8) [12]. Hydrodynamic lubrication is characterized by a relatively thick film thickness, typically  $>300$  nm, which is substantially greater than the asperity contacts of the wear surface. EHD lubrication is characterized by thin film lubrication. Although the lubrication films are only approximately 30 nm thick, they are greater than the asperity contacts. Film thickness for

boundary lubrication, typically approximately 3 nm, are less than the height of the asperity contacts. Mixed film lubrication occurs at the transition from EHD to boundary lubrication.

Ideally, hydraulic pumps operate in the hydrodynamic lubrication regime [11]. Under these conditions, the lubricating capability of the fluid is primarily dependent on the fluid film viscosity. However, it isn't possible to assure hydrodynamic lubrication under all operating conditions. For example, start-up conditions, oscillating motion, etc. can all create contact speeds insufficient to support hydrodynamic lubrication. Thus, a hydraulic fluid must exhibit some high load (mixed EHD) anti-wear characteristics.

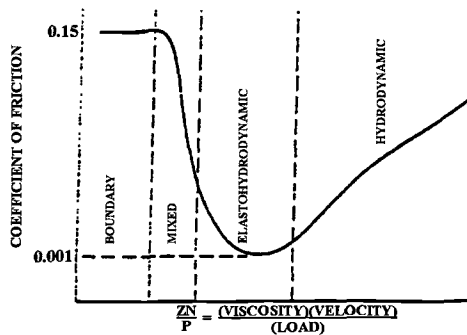


Figure 8 - Illustration of lubrication wear regimes using the Stribeck-Hersey curve.

2. Performance Map Characterization - It is possible to construct “performance maps” to identify EHD, mixed film and boundary lubrication properties of a hydraulic fluid [12]. A typical performance map is illustrated in (Figure 9).

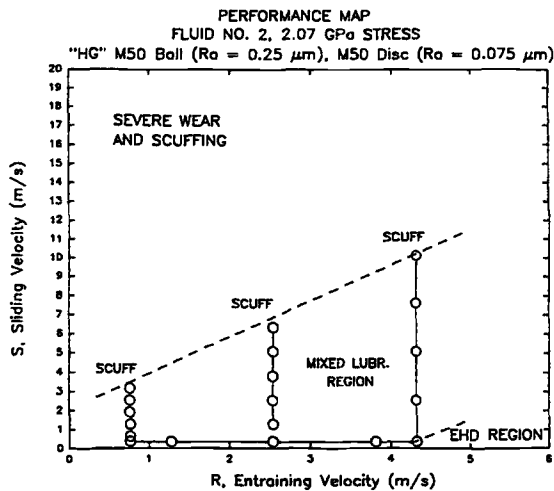


Figure 9 - Illustration of a typical performance map for a hydraulic fluid.

As Figure 9 shows, performance maps are constructed in terms of rolling (entraining) speeds (R) and sliding speeds (S). This is important since the generation of an EHD film is primarily a function of the entraining velocity (R) in the inlet region of the Hertzian contact. In this region, lubricating film generation is primarily a function of the physical properties (viscosity, pressure-viscosity coefficient, etc.) of the hydraulic fluid. The sliding speed (S) determines the shear strain within the high pressure Hertzian contact region. This region is important with respect to heat generation, surface film formation, wear and scuffing within the tribo-contact. The magnitude of the degree of surface interaction achieved, as a result of thin EHD films, influence the chemical properties of the fluid, e.g. adsorbed films, chemical reaction films, tribo-chemical reactions, and thermal/oxidative stability.

A correlation between the Ryder Gear Test, Four-Ball anti-wear test and their predictive placement on a performance map has been made [12]. As (Figure 9) shows, the lubrication results of the test represent just one point on the overall performance map and perhaps this point may be outside of the *range* required for the various lubricated surfaces in a particular hydraulic pump design. In fact this is a deficiency of conducting bench tests relative to the varying lubrication requirements in a machine, such as a hydraulic pump.

One possible goal for the future could be the establishment of performance maps with points identified for specific wear contact in different pumps. Such a performance map or maps may then provide a boundary of actual wear conditions for different types of wear surfaces such as vane-on-ring wear for different vane pumps or piston slipper-end plate wear etc. One of the limitations of this particular work is that it does not generally model long-term fatigue wear such as that encountered with rolling element bearings. This would require a different test protocol not reviewed here.

3. *Wear Contact Geometry* - The contact geometry of a tribo-contact should also be considered. There are typically three characteristic types. These are: a line contact (such as a roller-on-disk), an area contact (such as a flat surface-on-disk), and a point contact (such as ball-on-disk). All of these represent uniquely different lubrication problems and ideally the contact geometry of the tribo-contact should reasonably model the actual system being studied [10]. Some common test types are shown in (Figure 10) [9].



Figure 10 - Illustration of the tribo-contact conformity of various commonly used bench tests.

It is recommended that the contact geometry of the bench test selected reasonably model the actual system [9, 16]. Recently, Voitik has recommended the use of "Tribological Aspect Numbers (TAN)" to quantitatively and systematically characterize a wear contact [13]. Tribological aspect numbers quantify:

- Contact velocity characteristics
- Contact area characteristics
- Contact pressure characteristics
- Entry angle characteristics

Although the calculation of tribological aspect numbers will not be described here, various values listed by Voitik for some of the bench tests reported here are summarized in Table 6 [13]. Clearly, none of the test configurations exhibit the same "TAN" as the vane-on-disk which models the vane-on-ring of the vane pump. Also different "TAN's" would be expected for bearing lubrication, cylinder in bore, etc. encountered in other pump designs. (Table 7) provides "TAN" values for various wear contacts in a hydraulic pump. Perhaps better bench tests would be selected if a greater number of bench test "TAN" values were available to aid in the selection of test conditions. The use of "TAN's" are revealed in greater detail elsewhere in this book[13].

Table 6 – *Comparison of Tribological Aspect Numbers of Various Bench Test Configurations*

<u>TAN</u>	<u>Contact Geometry</u>
1418	Timken
1317	Four-Ball
1419	Vane-on-Disk
1519	Pin-on-Disk
1318	Ball-on-Disk
3229	FZG Test

Table 7 - *Wear Aspects of Significant Parts and Sub-Assemblies for a Hydraulic Pump*

Description	Material	TAN No.			
		A	B	C	D
Cylinder barrel bushing	Brass	3	4	2	9
Cylinder control surface	Brass	2	7	2	1
Valve plate	Nitrided steel	2	7	2	1
Piston	Nitrided steel	3	4	3	8
Slipper shoe	Brass	3	6	3	1
Swash plate	Nod. Cast iron GGG-60	2	5	3	1
Sliding plate	Nitrided steel	2	5	3	1
Saddle bearings	Brass	2	5	3	1
Retainer ball	Nitrided steel	2	4	3	9
Retainer plate	Tool steel	2	4	3	9
Drive shaft	Steel. induction hardened	2	5	3	0
Cylinder roller bearing	Steel. Hardened	2	4	3	9
Shaft seal	FKM/PTFE	2	4	3	1
Seals	BUNA-N/FKM	2	6	3	0
Control piston	Tool steel. induction hardened	2	5	3	1
Piston housing	Cast iron GGG-40	2	5	3	1
Slide stone	Steel. Hardened	2	5	3	1
Control-valve housing	Cast iron GGG-40	3	5	2	8
Control-valve spool	Tool steel	3	5	2	8

### C. Bench Test Considerations

In addition to modeling the actual wear mechanism in the hydraulic pump, a successful bench test should [11]:

- Reproduce the wear mechanisms in the application of interest.
- Reproduce the temperature level of the material during normal wear.

Although accelerated tests may rate lubricants in the correct order (which did not occur in this work), the magnitude of the difference between the fluids studied may not be proportional with actual field experience [16].

If a bench test is to model field experience, it should [16]:

- Provide reasonable reproducibility.

- The results obtained must have some degree of correlation with results observed in actual service.

Although the bench tests discussed here were reasonably reproducible, they provided poor, if any, correlation with hydraulic pump results. By this criteria, none of the tests evaluated were suitable models of hydraulic performance.

It is also important to recognize the various forms of wear that may occur in pump operation. Some of these include [11]:

- Abrasive Wear
- Adhesive Wear
- Cavitation Erosion Wear
- Corrosion Wear

In the bench testing of hydraulic fluids under atmospheric pressure, it is difficult to model exactly the fluid pressure conditions encountered in hydraulic pumps. Thus, the potential for wear by cavitation may not be observed. Similarly, corrosive processes often take many hours, days or even months to occur in actual operation. They simply will not have time to occur under the accelerated conditions of the bench test. Furthermore, the promotion of the accelerated wear conditions may actually be accompanied by a change in the wear mechanism, for example, from abrasive to adhesive failure.

Mizuhara and Tsuya have studied the ability of a Block-on-Ring Test (ASTM D 2714-68) to model three different hydraulic pump tests (vane, gear and piston). The hydraulic fluids studied were: anti-wear oil, water-glycol, oil-in-water emulsion, water-in-oil emulsion, phosphate ester and polyol ester. The conclusions from this study were [15]:

- It was necessary to evaluate the fluids under a wide range of conditions.
- Load-carrying capacity has nothing to do with the anti-wear properties of the hydraulic fluids evaluated.
- Accelerated tests usually provide the wrong results.
- Materials for the actual test pieces must be similar to the actual machine.
- To successfully evaluate the wear characteristics of hydraulic fluids, a wear test in a hydraulic pump must be conducted.

The following test strategy was recommended for the use of laboratory wear testing machines:

1. Rank hydraulic fluids according to hydraulic pump tests.
2. Evaluate hydraulic fluids in a wear testing machine under a wide variety of conditions. Sliding pairs should be constructed of materials similar to those of the tribo-contact in the hydraulic pumps of interest.
3. Determine the testing condition that provides the proper fluid ranking according to hydraulic pump tests.

4. If the proper testing conditions are not found, expand the test variables.
5. Repeat procedure 3, if inadequate correlations are obtained, change the wear testing apparatus.

These conclusions, while cumbersome, are reasonable in view of the tribological principles reviewed above.

Ludema has stated that "the best approach to wear modeling is to develop an organized way to accumulate empirical results from tests that simulate practical systems and build models from those data". [14]. Clearly, if such a database were available, it would greatly facilitate correlation of standard wear test results to those obtained with hydraulic pumps under widely varying wear conditions.

### Conclusions

An unsuccessful attempt was made to correlate the wear test results of various standardized bench tests with ASTM D-2882, a Vickers V-104CC vane pump test. The bench tests included: Four-Ball (ASTM D-4172), Falex Pin-on-V-Block (ASTM D-2670), and Timken ASTM D-2782. In no case, did the bench tests successfully predict the wear rankings of the ASTM D-2882 Pump Test. This paper concludes that little or no correlation exists between the bench tests and conditions evaluated and ASTM D-2882 pump tests. While this may be true, it should be noted that ASTM has not been able to develop a Precision and Bias statement for ASTM D-2882 even after many years of testing. With that in mind, there exists a need to identify other bench tests that might better correlate with pump tests, such as, ASTM D-2882.

Analysis of the problem using fundamental principles of lubrication suggest that the poor correlations are probably reasonable because: the actual loading, rolling and sliding speeds, contact geometry and materials were not adequately considered. These data clearly show that it is inappropriate to simply select a bench test without careful consideration of the test conditions; including material pairs, loading, speed, etc. Bench tests are potentially useful starting points for hydraulic pump fluid lubrication studies, but they can not be indiscriminately applied. Therefore, it is further recommended that the findings previously reported by Mizuhara be rigorously applied [18]. (see Section C)

On the basis of this work and other related published work, hydraulic pump testing is recommended as the preferred method of evaluating hydraulic fluids, unless careful fundamental tribological studies are used. Otherwise, the data obtained are either erroneous or misleading predictors of pump wear.

Work continues within ASTM D.02.L Subcommittee to develop a bench test; "Cyclic Stress Vane Test", a vane-on-ring test configuration, which shows promise as a potential bench test model of a vane pump wear test. However, the work on this procedure is not yet complete.

### References

- [1] Steiger, J., "AAMA 524 Part 2: Anti-Wear Hydraulic Oils", *American Automobile Manufacturers Association*, January 31, 1995.

- [2] Korycki, J. and Wislicki, B., "Criteria the Lubricating Properties of Synthetic Fluids", *Proceedings of the Conference on Synthetic Lubrication*, A. Zakar, 1989, pp. 213-219.
- [3] Perez, J. M., Hanson, R. C. and Klaus, E. E., *Lubrication Engineering*, 46, (1990), pp. 249-255.
- [4] Sperry-Vickers "Pump Test Procedure for Evaluation of Anti-wear Hydraulic Fluids for Mobile Systems", Form M-2952-S.
- [5] Chu, J. and Tessmann R. K., *The FRH Journal*, 1, 1980, pp. 15-20.
- [6] Inoue, R., *The FRH Journal*, 3, 1982, pp. 45-49.
- [7] Inoue, R., *The BFPR Journal*, 16, 1983, pp. 445-453.
- [8] Tessmann, R. K., and Hong, T., *SAE Technical Paper Series*, Paper Number 932438, 1993.
- [9] Hogmark, S. and Jacobson, S., *Lubrication Engineering*, 48, 1992, pp. 569-579.
- [10] Maamouri, M., Masson, J. F., and Marchand, N. J., *Journal of Material Engineering Performance*, 3, 1994, pp. 527-539.
- [11] Silva, G., *SAE Transactions.*, 99, 1990, pp.635-652.
- [12] Wedeven, L., Totten, G. E. and Bishop R. J., *SAE Technical Paper Series*, Paper Number 941752, 1994.
- [13] Voitik, R. M., "Realizing Bench Test Solutions to Field Tribology Problems Utilizing Tribological Aspect Numbers", *Tribology - Wear Test Selection for Design and Application*, A. W. Ruff and R. G. Bayer, ASTM STP 1199, 1993, pp. 45-59.
- [14] Ludema, K. C., "Cultural Impediments for Practical Wear Modeling of Wear Rates", *Tribological Modeling for Mechanical Designers*, K. C. Ludema and R. G. Mayer, ASTM STP 1105, 1991, pp. 180-185.
- [15] Mizuhara, K. and Tsuya, Y., *Proceedings of the Japanese Society of Lubrication Engineering International Tribology Conference*, 1985, Tokyo, Japan, pp. 853-858.
- [16] Robinson, G. H., Thomson, R. F. and Webbere, F. J., *SAE Transactions.*, 67, 1959, pp.569-579.

- [17] Jacobs, G., Backe, W., Busch, C. and Kett, R., "A Survey on Actual Research Work in the Field of Fluid Power", IFAS-Aachen, Germany, Paper Presented at 1995 STLE National Meeting, Chicago, IL.
- [18] Priest, M., March, C. N. and Cox, P. V., "A New Test Method for Determining the Anti-wear Properties of Hydraulic Fluids", *Tribology of Hydraulic Pump Testing, ASTM STP 1310*, G. E. Totten, G. H. Kling and D. M. Smolenski, American Society for Testing and Materials, Philadelphia, PA, 1995.
- [19] Lacey, P. I., Naegeli, D. W. and Wright, B. R., "Tribological Properties of Fire-Resistant, Non-Flammable and Petroleum-Based Hydraulic Fluids", *Tribology of Hydraulic Pump Testing, ASTM STP 1310*, G. E. Totten, G. H. Kling and D.M. Smolenski, American Society for Testing and Materials, Philadelphia, PA, 1995.
- [20] Kenny, P. and Yardley, E. D., "The Use of Unisteel Rolling Fatigue Machines to Compare the Lubricating Properties of Fire-Resistant Fluids", *Wear*, 20, 1972, pp. 105-121.
- [21] Totten, G. E., Bishop, R. J., and Webster, G. M., "Water-Glycol hydraulic Fluid Evaluation by ASTM D-2882: Significant Contributors to Erroneous Results", *SAE Technical Paper Series*, Paper Number 961740, August, 1996.

## **SESSION II: Bench Tests and Test Development—A**

John Lord,<sup>1</sup> Ulf Jonsson,<sup>1</sup> Roland Larsson,<sup>1</sup> Olov Marklund,<sup>2</sup> Erland Eriksson,<sup>1</sup> and Östen Uusitalo<sup>1</sup>

## The Luleå Ball and Disc Apparatus

---

**Reference:** Lord, J., Jonsson, U., Larsson, R., Marklund, O., Eriksson, E., and Uusitalo, Ö., “The Luleå Ball and Disc Apparatus,” *Bench Testing of Industrial Fluid Lubrication and Wear Properties Used in Machinery Applications, ASTM STP 1404*, G. E. Totten, L. D. Wedeven, J. R. Dickey, and M. Anderson, Eds., American Society for Testing and Materials, West Conshohocken, PA, 2001.

**Abstract:** The ability to measure lubricant film thickness in elastohydrodynamic point contacts was greatly improved when the method of interferometry was introduced in the late 1960s. Constant refinements of the technique have made it possible to measure the thickness of thin films with an accuracy of a few nanometers. In order to further develop the technique and provide a tool for advanced lubricant experiments, a Ball and Disc Apparatus was developed. The aim was to accomplish an apparatus with an “open architecture” for easy expansion and the ability to use several sub-methods for film thickness determination.

The combination of suitable computer programming, electronics, mechanics, optics and fluid dynamics made it a complex task since several individuals had to merge their ideas into one design where the result had to be satisfying in all aspects. Even though the apparatus is under constant development, the basics are the same: a mainly computer controlled apparatus able to measure film thicknesses with high accuracy down to zero, friction force from zero to 120 N, contact loads from zero to 140 N (solely dependent on the disc used), running speeds, apart from static, from at least  $1 \times 10^{-3}$  to 4 m/s and producing detailed digital interferograms directly onto the computer’s hard drive for analysis.

Analyzing images is itself a tedious and sometimes difficult task if the appropriate tools are not available. However, a multi-channel method was also developed concurrently which does not depend on the usual colorimetric calibration problems, but rather on a trichromatic light source. This method of determining film thicknesses reduces the time spent to a few seconds per image captured during operation.

**Keywords:** elastohydrodynamic, EHL, interferometry, film thickness, ball and disc, lubricant, image analysis

---

<sup>1</sup>Division of Machine Elements,

<sup>2</sup>Division of Industrial Electronics

Luleå University of Technology

SE-971 87 Luleå, Sweden

## Introduction

The first successful attempts to measure the lubricant film thickness in an elastohydrodynamic point contact using interferometry were made in the mid-60s by Cameron and Gohar [1]. Since then advances have made it possible to refine the technique quite drastically in parts of the method such as electronics, optics and computer science etc.

Several research groups with a special interest in elastohydrodynamics have successfully developed experimental equipment to measure film thickness. The techniques used are basically the same but differ somewhat as for the particular hardware and software solutions.

The Division of Machine Elements, Luleå University of Technology, where the presented apparatus has been developed, has a long tradition of this type of work. Collaboration with the University's Division of Industrial Electronics has made it possible to enhance the measurement technique even further.

Interferometry has been increasingly used in EHL investigations since the late 60s. An important step forward came in the beginning of the 90s when Johnston et al. [2] introduced the spectrometer with white light interferometry for evaluation of constructive interference which made it possible to determine the film thickness with nanometer accuracy. The spacer-layer technique, developed by Westlake et al. [3], was a further refinement and made it possible to measure films with virtually zero thickness.

The next important step was taken by Gustafsson et al. [4] when they presented their image analysis method for detailed evaluation of coloured interferograms. This method made it possible to obtain film thickness maps with a spatial resolution of at least 500 by 700 data points and a film thickness resolution of a few nanometers. The original image analysis method was then further developed in order to avoid the need for calibration. Both methods are described below. The methods have been applied in several different investigations, e.g., [5-9].

The advanced image analysis method made it necessary to develop the mechanics and optics further, with data acquisition and control fully computerized.

## The Apparatus

The apparatus may be split into a number of units (see Fig. 1) including the control and data acquisition electronics and pneumatic control unit for applying load to the contact, as well as the actual ball and disc unit where the measurements are made and the computer where everything is controlled. Other units are the light source, temperature control equipment and video monitor.

### *Hardware*

The Ball and Disc unit is the physical structure where the ball is forced against the disc, thus producing an elastohydrodynamical contact (Fig. 2). It is made mainly of stainless steel and aluminum and holds the ball, disc, microscope and various transducers.

A base plate, made of thick stainless steel, is used as the foundation. The microscope is mounted on top of a column and adjusted by a coordinate table in order to view the ball and disc contact zone.

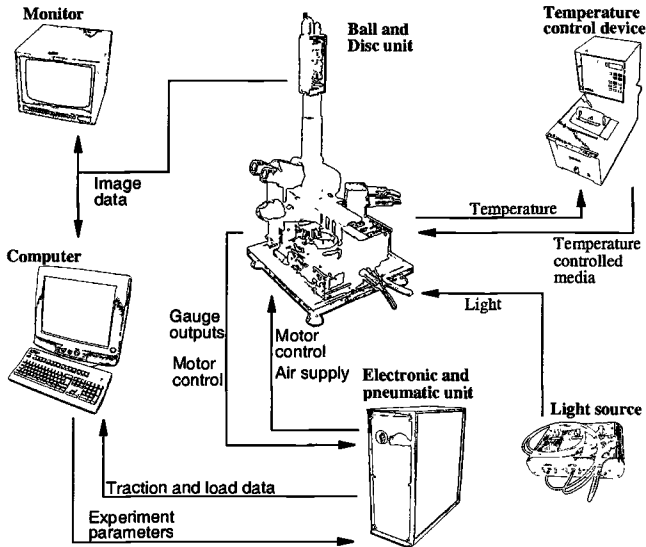


FIG. 1 Schematic layout of the Ball and Disc measurement system.

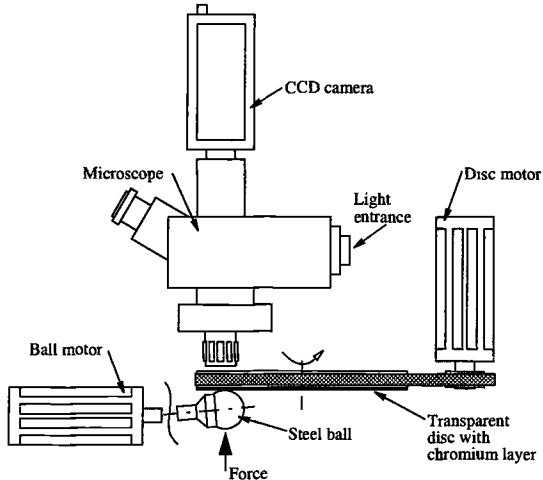


FIG. 2 Schematic drawing of the Ball and Disc unit including microscope and camera.

The ball is mounted with a screw through a hole in the ball on a hardened steel shaft which is precision machined with a lapped seat to keep the ball centered at all times while it is rotating (Fig. 3). The shaft, supported by three precision roller bearings, is driven by a motor via a flexible driving belt. The ball rotates within a lubricant bath. During rotation the ball drags lubricant into the contact.

The design of the disc holder, Fig. 3, has developed from being a shaft through the disc

center to one which holds the disc at its circumference. The disc holder is rigidly built and has a precision machined surface. The motor which drives the disc, is mounted on the disc holder.

The disc support bearing, gear and disc are all mounted at the side of the unit where the ball applies pressure. This means that it is not possible for any of these components to fall out of their place and cause damage. This design also keeps the amount of unnecessary fittings to a minimum.

A pneumatic system is used to load the ball onto the disc. This requires an air supply of approximately 8 bar. A precision valve reduces this pressure to the required level. A mechanical manometer provides direct pressure readings and a pressure gauge connected to a data acquisition board allows air pressure to be logged. Loading of the ball against the disc is accomplished with the use of a pressurized cylinder and force piston.

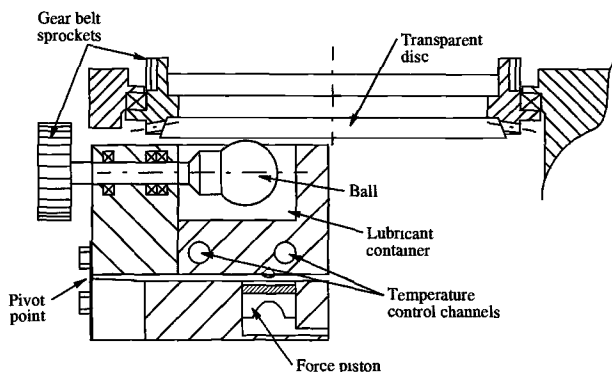


FIG. 3 Schematic drawing illustrating a cut out side view of the apparatus parts close to the contact.

The Ball and Disc Apparatus may also be used to measure traction forces during experiments, since the disc holder is designed to be able to rotate around a pivot point. This is also the reason for mounting the disc motor directly on the disc holder so it does not conflict with these measurements. Rotation of the disc holder is prohibited by a linkage to which a load cell is mounted. Both positive and negative forces applied to the load cell can be measured. See Fig. 4.

In order to avoid any hysteresis effects conflicting with the traction readings, the load cell linkage is mounted rigidly. An overload device with preloaded springs in both compressive and tensile directions prevents damage to the loadcell if it is stressed beyond its working capabilities which may happen unintentionally during an experiment.

### Software

There are three different tasks which have to be done by the computer software. These can be separated into: control of the rig, data acquisition and evaluation of measured data. The measured data include the images or interferograms captured during an experiment as well as operating parameters. These three tasks do not have to be done separately, but at this time, enhancements are being made continuously to all parts and such a solution is desirable. Partial or complete integration may be done later.

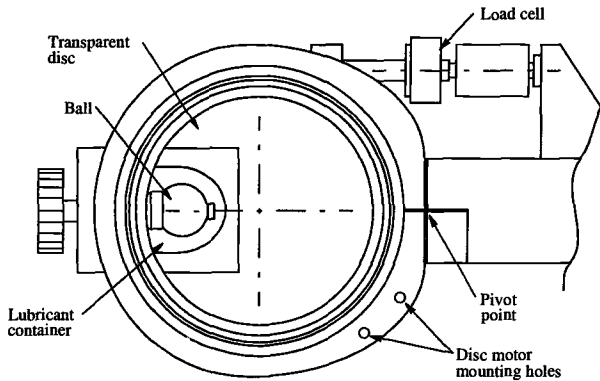


FIG. 4 Schematic drawing illustrating a top view of the apparatus parts close to the contact.

It is possible to use many different types of programming languages to develop control functions for the rig but factors like ease of development and modifications, possibilities to communicate with hardware, the speed of the final control program, are important when deciding which to use.

“Low-level” languages are quite easy and fast to use and produce efficient programs when only one or two parameters need to be controlled or acquired, especially when the available I/O ports on the PC are to be used. However, when many variables are going to be measured and controlled the obvious choice is to use a programming environment which is specifically developed for this kind of purpose. Such environment can also provide simple interface to data acquisition boards with an appropriate number of channels and sample frequencies.

National Instruments’ LabView<sup>®</sup> belongs to the latter category of programming languages and offers the opportunity to program freely within an environment and access input variables for data acquisition or output via motion control boards.

LabView uses a graphical programming interface. Hardware is easily accessed via the same interface using small programs specifically built for that purpose. This makes program development and addition of extra hardware features very easy which is of great interest when, for example, one off experiments are to be made which require an additional input channel. The programming environment, also allows the user interface to be developed at the same time using simple graphical commands. Designing an easy to use interface, however, is a more difficult task!

For the Ball and Disc Apparatus, a LabView application has been developed to both control parameters such as speed and slide-to-roll ratio of the ball/disc as well as for data acquisition, e.g. image capture.

The software used to evaluate the experimental results in the form of captured images of the interference pattern is not as critical as the controlling software as the evaluation does not need to be carried out as a real-time process. The importance here lies in ease of implementing mathematical models and how digital images can be processed. Matlab<sup>®</sup>

from Mathworks is a program for general computational problems and offers the features which are needed.

### *Electronics*

The electronics may be divided into a controlling part and a data acquisition part. The controlling part also requires some user input in the form of, for example, rolling speed, slide-to-roll ratio etc. which is then maintained by the controller. The acquisition parts are devices which capture the information required for the evaluation, e.g. load cell for friction force and images from the frame grabber.

A motion control board is mounted in the computer. This board is software controlled and its analog output channels are connected to two servo controllers. The servo controllers take their input from the motion control board and in turn ensure the speed of the ball and disc synchronous servo motors. The speed is controlled by a dual loop system. The inner loop consists of a commercial servosystem with a matched motor, whilst the outer loop is controlled by a DSP based 4 channel motion control board that is supported by LabView. The servo controllers are programmed with the motor's operating specifications and it is possible to set different maximum speed or torque depending on conditions. The servo motors are capable of 6000 rpm and 1 Nm torque and have built in thermistors in order to trigger an automatic shutdown if operating temperatures are exceeded.

The output from the rig are acquired by a camera for the interferograms and by a load-cell for the friction force. The camera is a standard 8-bit RGB CCD camera having both digital and analog output. The analog output is coupled to a high performance video recorder and a colour monitor. The video recorder is only used to store extensive testing sequences and to visually inspect unusual occurrences. The digital output from the CCD is connected to a frame grabber board mounted inside the computer and the images are then stored on the computer hard drive. Each image is stored in a separate file and other information related to that, and other images are also written in a file.

The load cell measures the friction force via its internal strain gage and has an output current proportional to applied force. This current is then converted to a voltage which is filtered and amplified in order to fit the range of the data acquisition board. A pressure transducer which measures the air pressure within the pneumatic system used to load the ball onto the disc is connected in the same way as the load cell.

### *Control*

Operator control is mainly done via a graphical interface in a Windows environment. The only adjustment which has to be done manually is the adjustment of the air pressure pneumatic valve in order to set the ball load.

The user interface for the control of experimental parameters is shown in Fig. 5. Via this interface the operator initially sets the "roll radius" which is the distance between the centre of the disc and the centre of the contact point. This is necessary since it determines the ratio of the ball- and disc speeds needed to achieve a certain slide-to-roll ratio. The speed and slide-to-roll ratio may be set by keyboard input or mouse pointer. The scales determining the maximum values of parameters such as speed, friction force etc. can be altered at any time in order to limit the maximum value or to increase the apparent resolution.

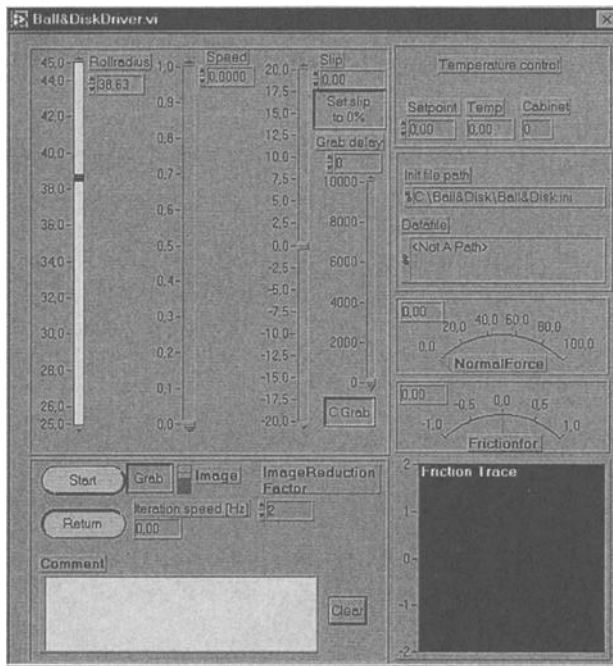


FIG. 5 *User interface during experiment.*

### Interferogram Evaluation Techniques

When optical interferometry was introduced in elasto-hydrodynamic film thickness measurements, images acquired using ordinary camera on photographic film were used. These pictures were then evaluated manually either by counting fringes or by using color matching when the illuminating light was white or by counting high intensity fringes when using a monochromatic light source.

Image analysis offers better accuracy and higher sensitivity than manual evaluation of film. New methods are continuously being developed but the first method applied to ball and disc measurements was developed at Luleå University of Technology in 1994 [4].

The first image analysis technique for the automatic evaluation of interferograms used a calibration image where the geometry was assumed to be known (spherical ball). In this way a calibration table could be constructed with values of hue, saturation and intensity, which are then used to determine film thickness in experiment images. There are, however, some problems in using this method as shown by Lord et al. [9], principally that accuracy may be lost when measuring very thin lubricant films (less than 50 nm). In order to increase the accuracy and evaluation speed, Marklund [10] developed the multi channel method which is based on phase stepping using trichromatic light.

Both methods are described briefly below along with evaluation using a spectrograph according to Johnston et al. [2].

### *HSI Method*

The HSI (hue-saturation-intensity) color model for interferogram evaluation uses a white light source in the experiments. Firstly, a calibration table which couples the three HSI components to lubricant film thickness has to be constructed. This is done by creating a known spacing between the ball and the disc. If the ball is positioned with a zero load point contact with the disc, the spacing will be given from the spherical shape of the ball with zero film thickness at the contact centre. From this calibration image it is possible to compute the calibration table. This calibration table is in the form of a parametric curve in the three-dimensional HSI space, with  $h$  as parameter.

Secondly, dynamic scenes, i.e. images of the contact at a certain load, speed, temperature etc., are recorded. The film thickness can then be obtained using a lookup procedure, i.e. comparing the measured HSI values to the calibration table values.

Much care has to be taken during the calibration phase since it is the quality of the calibration table that determines the absolute accuracy of the final measurements. If, for example, a small gap remains between the ball and the disc, the calibration table will be displaced and absolute film thickness measurements will be impossible. On the other hand, if the ball is loaded on the disc with too high a load, the ball and disc surfaces will be deformed and the gap will not have the expected shape. It is also very important to have smooth undamaged ball and disc surfaces.

The use of a spacer layer, which is briefly described later on, should not introduce any problems as long as the layer has a uniform and constant thickness.

### *Multi Channel Method*

A variant of the traditional temporal phase stepping can be achieved by varying the wavelength of a monochromatic light source by using, for example, a tunable laser diode [11]. In the EHL application, a custom made light source with a given number of  $K$  fixed monochromatic channels are used instead since, in this case,  $K$  interferograms must be recorded simultaneously. The channels are given by

$$\lambda_k^{-1} = \phi_0 + (k - (K + 1)/2)\Delta\phi \quad , \quad k = 1, \dots, K \quad (1)$$

where  $\phi_0$  and  $\Delta\phi$  are two degrees of freedom. Spectral filters are used to discriminate the channels during recording.

The most convenient configuration uses  $K = 3$  with, for example, channel wavelengths of  $\lambda_1 = 617$  nm,  $\lambda_2 = 540$  nm and  $\lambda_3 = 480$  nm, which allows the use of a standard color CCD-camera as detector.

The intensity signals, R,G,B, have to be made independent of each other. This is normally not the case for standard color CCD cameras since the color channel sensitivity functions overlap, but initial calibration may be used to overcome this problem.

However, only approximate phase values can be extracted using linear combinations of the three recorded interferograms, and an iterative procedure must be applied to determine the correct values. This algorithm is described in detail in [10].

### *Spectrographic Method*

Both the multi channel and the HSI method are similar in that they evaluate the whole contact area. The spectrographic method does not.

The spectrograph is an optical device which separates an incident light beam into its component wavelengths and is placed between the microscope and the CCD camera. The incident light beams are captured via a slit in the end of the spectrograph which faces the contact. Thus the multi wavelength light information along the slit is transformed to a 2-dimensional image, seen by the camera, with wavelength and spatial length of the slit. The slit where the line image is captured has a length of 8.8 mm and a width of 50  $\mu\text{m}$ .

Using a broad spectrum white light source, several constructive and destructive interferences can be detected at every point along the length of the slit. This, and the knowledge of the absolute fringe number, are enough information to construct a film thickness graph over the line covered by the slit.

The major drawback with the spectrographic method is obviously that only a one dimensional film thickness profile can be generated which causes problem when the minimum film thickness is to be determined. Moreover, it has proved to be a reliable method due to the fact that a spectrograph interferogram provides much information over the length of the slit. By varying the width of the slit it is also possible to enhance the resolution to less than 1 nanometer.

### **Operational Practice and Limits**

The Ball and Disc Apparatus is made of relatively low cost standard components whilst maintaining capability. It also makes an upgrade to an easy task since the system does not have to be changed extensively.

Depending on the disc material, different maximum Hertzian pressures can be achieved. This limit is set by two factors; the available air pressure to control preload and the maximum stress that the discs can tolerate without fracture. With a system pressure of 8 bar, the highest attainable force applied onto the ball in contact with the disc is 140 N. A glass disc may be stressed up to about 0.6 GPa and a sapphire disc up to, at least, 1.5 GPa. In the case of traction experiments where a polished steel disc is used, the highest load will produce a pressure of about 1.3 GPa. This will not cause any damage to the steel disc but could damage the disc carrier bearing.

The maximum operating speed is restricted by the servomotor and the gearing used in transmitting the motion from the motor to the disc or to the ball. At the highest speed and with the gearing used in the present version, the maximum speed of the ball circumference is 4 m/s. Since the ball may be placed at virtually any radius on the disc, the rolling speed is also dependent on the maximum speed of the disc. However, if the rolling track radius is kept greater than 36 mm, this maximum speed restriction will not be violated. The maximum speed for pure rolling will decrease if the ball rolls at a smaller track radius. This is not generally a problem since at small track radii, the captured interferogram will be distorted to some extent due to a pronounced ball spin. The minimum speed is limited by the ability of the motors to produce a steady torque at low speeds and problems with motor commutation and encoder resolution. The present design has successfully been used down to rolling speeds of 1 mm/s without any effect on film formation and the practical minimum speed limit without changing the gearing from the motors is probably less than 0.5 mm/s.

It is advantageous if the rig is placed in an environment where the amount of dust and other types of air contamination are kept at a minimum. This is especially true when thin film measurements are to be carried out. Any particle accidentally falling between the disc

and the squeeze area on the disc holder will create a disturbance in the interference pattern.

## Experiments

A number of experiments carried out in the Ball and Disc Apparatus are described briefly below. Some of these experiments used the standard rig while some required extra equipment or unusual handling.

### *Film Thickness and Traction Measurements*

Obtaining film thickness measurements is, of course, the main purpose of the apparatus, but as already mentioned, traction measurement can also be made. When the objective is to measure film thickness, the normal disc material for moderate Hertzian pressures is glass. The disc is coated on the contact side with a semi-reflective layer of chromium in order to improve the visibility of interference fringes. With a disc and a single layer of semi-reflective coating it is presently possible to measure thicknesses down to approximately 30 nm depending on which method is used. If ultra thin film thicknesses, down to zero, are to be measured, a spacer layer is applied on top of the chromium. This additional layer, often of silica sputtered on the disc surface, introduces a transparent “gap” of known thickness. Constructive interference of visible light can thus occur even for zero lubricant film thickness. The addition of a spacer layer between the lubricant film and the chromium layer introduces additional problems since its thickness has to be known at the point of measurement. Depending on the quality of sputtering, it may not be uniformly distributed over the disc surface. Measurements will be sensitive to thickness variations in the silica layer which normally has a thickness of approximately 300 nm. Methods are presently being developed in order to reduce these problems.

Figure 6 shows a typical interferogram and the corresponding film thickness map obtained by using image analysis. The experiment was carried out with very smooth surfaces but well defined roughness can also be used in order to find how roughness influences film formation, Fig. 7.

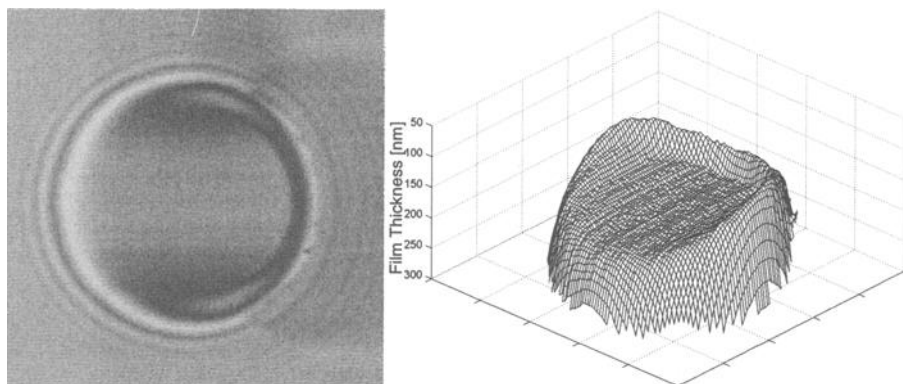


FIG. 6 *Interferogram (left) and the corresponding film thickness map (right). Smooth surfaces are used.*

Traction measurements are preferably made with a steel disc since it most closely resembles the materials used in normal applications. The traction measurement can,

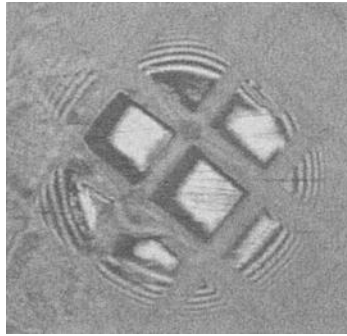


FIG. 7 *Interferogram with a roughness pattern sputtered on the ball surface.*

however, be made concurrently with film thickness measurements but may not always be within the scope of the experiment. Even though the disc holder is rigidly attached to the base plate, small deviations may occur when high loads are applied which introduces a small bias on the load cell output. Therefore the scaled output is corrected by calibrating at the specific load. A sample traction force result is shown in Fig. 8.

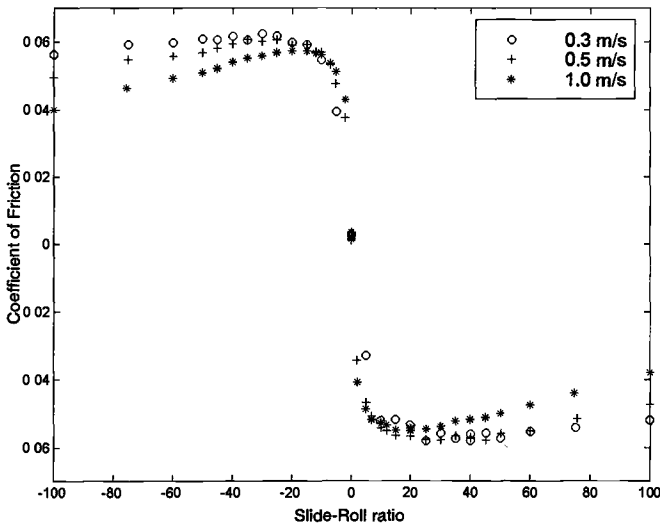


FIG. 8 *Sample of traction experiment results using DOP at 54 N load corresponding to 0.95 GPa Hertzian pressure at three different speeds.*

In the experimental results shown in Fig. 8, the slide-to-roll ratio has been set to zero followed by both positive and negative slide-to-roll ratios. When each extreme value (+100%/-100%) was reached, the slide-to-roll ratio was reset to zero and a friction reading was acquired again. This was to assure that no hysteresis was present.

*Liquid Lubricants* – Measuring the film thickness where a liquid is used as the lubricant is a fairly straight forward procedure. A small sample of the lubricant, about 20 ml, is required. The ball drags the lubricant up from the container into the contact. The amount can often be reduced without any risk of starvation of the contact depending on the lubricants viscosity and adhesion to the ball.

*Greases* – The physical properties of grease makes the measurement technique slightly different. Since lubricant replenishment is an important factor in grease lubricated contacts, different procedures are used depending on the objective of the experiments. Two major experiments are usually carried out in grease tests. The study of full film lubrication or the study of lubricant replenishment (the process itself or the film thickness decrease with time).

A study of grease lubrication is found in [8]. A high-speed camera was used in that experiment and it was thus possible to observe single soap thickener particles as they passed through the EHL contact, Fig. 9.

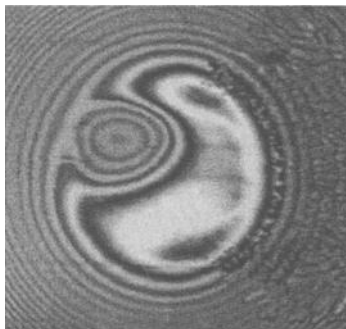


FIG. 9 Grease lubricated contact [8].

### *Odd Experiments*

While the main purpose of the Ball and Disc Apparatus is to measure film thicknesses in lubricated contacts, it is possible to use the apparatus for other tribological studies after some modifications. The image analysis software is not required in such tests but could be used separately for the evaluation (unwrapping) of other colour interferometric fringe patterns.

Two experiments with the ball and disc unit are described here.

*Measuring Electrical Properties of Lubricants* – In many industrial applications a lubricated bearing is exposed to an electric field, which may cause a current passage through the roller-race contact. This is seen for instance in electric motors, alternators and turbines. Bearing damage due to this current can in some cases, be eliminated or reduced by the use of insulated bearings. If this is not a real alternative, a conductive lubricant may be used.

The Ball and Disc Apparatus offers a possibility of measuring electrical resistance for an oil or grease. If the expected film thickness is sufficiently high, a glass disc with a semi-reflective chromium layer may be used. An electric circuit is created by applying contact brushes on the ball shaft end and on the disc holder. At the same time there must be an

electrically conducting path between the holder and the chromium layer on the disc. The chromium layer has a resistance in the order of 1 k $\Omega$  in series with the lubricated contact.

Since the film thickness, depending on operating conditions, is continuously monitored, it is possible to correlate the thickness with the lubricant resistance for the same situation. Care has to be taken to ensure that a full film exists.

Because the current contact area is not exactly the same as the hertzian contact area, it is not recommended to try to determine absolute resistivity values. Thus, the method may be most suitable for comparative studies, i.e. comparing lubricant resistivity values or studying the influence of lubricant parameters on lubricant resistivity.

Another interesting application of electrical resistance measurements in the Ball and Disc Apparatus is the possibility to measure the degree of direct contact between the ball and disc [12]. This enables studies of mixed lubrication which is an important and still relatively unexplored research field.

*Brake Pad Materials* – The ball and disc unit has also been used to study the contact between a brake pad and a disc. Eriksson et al. [13] used a Ball and Disc Apparatus to make in-situ observations of the contact patch between a part of a brake pad and a glass disc while measuring its friction force.

Instead of having a rotating ball, a stationary cylinder with a cut part of a brake pad was loaded against an uncoated glass disc to determine the contact behavior. It should, however, be noted that no film measurements were made with the use of the previously described interference pattern evaluation techniques.

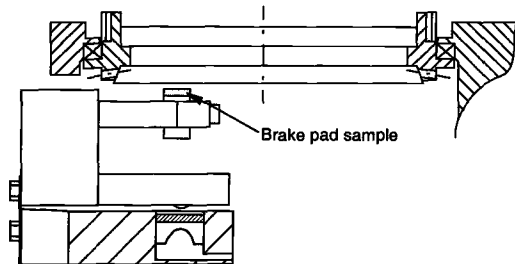


FIG. 10 Schematic drawing of the setup for brake pad material tests.

It was clearly seen how real contact regions grew, became worn and disappeared. It was also possible to see how the flow of wear particles were transported through the contact, between the real contact regions.

## Conclusions

The Ball and Disc apparatus has been developed as a platform for tribological measurements, especially interferometric measurements of the thickness of lubricant films in elastohydrodynamic lubrication. The unit can, as shown, be used for other experiments.

The apparatus has been designed in such a way that allows for continuous improvements and further development of all parts. The control, logging and analysis software has been developed using high-level user-friendly languages such as LabView and Matlab. These packages make it easy to add new features in the control, data acquisition and inter-

ferometric evaluation procedures.

The hardware is made of standard components as far as possible in order to keep development costs down and to make upgrading easier.

The apparatus is controlled from a computer and all measurement data are stored on the hard drive.

The Ball and Disc Apparatus is a very useful tool for tribological studies and is beginning to become a standard item in tribology laboratories.

## Acknowledgments

The authors wish to acknowledge the financial support of the Foundation for Strategic Research (JIG) and the Swedish Research Council for Engineering Sciences (TFR).

## References

- [1] Cameron, A. and Gohar R., "Theoretical and Experimental Studies of the Film in Lubricated Point Contact," *Proc. of the Royal Society*, London, Ser. A, 1966, pp. 520-536.
- [2] Johnston, G. J., Wayte, R. and Spikes, H. A., "The Measurement and Study of Very Thin Lubricant Films in Concentrated Contacts," *STLE Tribology Transactions*, Vol. 34, No. 2, 1991, pp. 187-194.
- [3] Westlake, F. J. and Cameron, A., "A Study of Ultra-Thin Lubricant Films Using an Optical Technique," *Proc. Instn Mech Engrs*, Vol. 182, Pt 3G, 1967-68, pp. 75-78.
- [4] Gustafsson, L., Höglund, E. and Marklund, O., "Measuring Lubricant Film Thickness With Image Analysis," *Proc. Instn. Mech. Engrs., part J: J. of Eng. Tribology*, Vol. 208, 1994, pp. 199-205.
- [5] Jolkin, A. and Larsson, R., "Film Thickness, Pressure Distribution and Traction in Sliding EHL Conjunctions," *Lubrication at the Frontier - The Role of the Interface and Surface Layers in the Thin Film and Boundary Regime*, *Tribology Series 36*, Elsevier, 1999, pp. 505-516.
- [6] Marklund, O. and Gustafsson, L., "Correction for Pressure Dependence of Refractive Index in Measurements of Lubricant Film Thickness With Image Analysis," *Proc. Instn. Mech. Engrs., Part J: J. of Engineering Tribology*, Vol. 213, No. J2, 1999, pp. 109-126.
- [7] Lord, J., Jolkin, A., Larsson, R. and Marklund, O., "A Hybrid Film Thickness Evaluation Scheme Based on Multi Channel Interferometry and Contact Mechanics," *ASME J. of Tribology*, Vol. 122, 2000, pp. 16-22.
- [8] Larsson, P.O., Larsson, R., Jolkin, A. and Marklund, O., "Pressure Fluctuations as Grease Soaps Pass through an EHL Contact," Presented at Austrib'98, Brisbane, Australia, Dec. 1998., to be published in *Tribology International*.

- [9] Lord J., Marklund, O. and Larsson, R., "Multi Channel Interferometry for Measurement of the Thickness of Very Thin EHL Lubricant Films," Presented at the 26th Leeds-Lyon Symposium on Tribology, Leeds, United Kingdom, Sept. 1999.
- [10] Marklund, O., "Interferometric Measurements and Analysis with Applications in Elastohydrodynamic Lubrication," PhD thesis Luleå University of Technology, 1998:29.
- [11] Ishii, Y., Chen, J. and Murata, K., "Digital Phase-Measuring Interferometry with a Tunable Laser Diode," *Opt. Lett.*, Vol. 12, No. 4, 1987, pp. 233-235.
- [12] Spikes, H., Guangteng, G. and Olver, A.V., "Contact Resistance Measurements in Mixed Lubrication," presented at STLE/ASME Tribology Conference, Orlando, USA, Oct. 1999.
- [13] Eriksson, M., Lord, J. and Jacobson S., "Wear and Contact Conditions of Break Pads - Dynamical In-Situ Studies of Break Pad on Glass," Presented at 9th Nordic Symposium on Tribology, Nordtrib, 2000.

Edward Kingsbury<sup>1</sup> and Stephen Pepper<sup>2</sup>

## A Spiral Orbit Rolling Contact Tribometer

---

**Reference:** Kingsbury, E. and Pepper, S., “A Spiral Orbit Rolling Contact Tribometer,” *Bench Testing of Industrial Fluid Lubrication and Wear Properties Used in Machinery Applications, ASTM STP 1404*, G. E. Totten, L. D. Wedeven, J. R. Dickey, and M. Anderson, Eds., American Society for Testing and Materials, West Conshohocken, PA, 2001.

**Abstract:** We describe a rolling contact tribometer exhibiting realistic, reproducible, quantifiable performance over a wide range of contact conditions. These conditions are variable to match a calculated severity integral for real ball bearing contacts. First-order kinematics in the tribometer are described by published ball bearing equations. The tribometer exhibits second-order mechanical contact effects found in real rolling contacts. It has elevated temperature, purged atmosphere, and vacuum capabilities. Results from the tribometer are shown to be directly applicable to a variety of situations in the real world.

**Keywords:** rolling contact tribometer, boundary lubrication, solid film lubrication, elasto-hydrodynamic lubrication, lubricant life, lubricant degradation, contact severity, friction coefficient, traction coefficient

### The Spiral Orbit Tribometer Bench Test

Tribological bench testing is done to get “quicker and cheaper” predictions of performance and life in lubricated machinery. Unfortunately, “better” is not always achieved, and bench test results often have little correspondence to rolling contact experience. One reason is that contact conditions in standard bench tests (pin-on-disk, four-ball, scuffing, pin-between-anvils, etc.) may be unrealistic, particularly for rolling contacts at low speed and high load, without hydrodynamic liftoff, common in ball bearings. The Spiral Orbit Tribometer (SOT) has been developed to evaluate lubricants subjected to rolling contact under a wide variety of conditions, but always with the goal of credible correspondence to conditions found in ball bearings. The SOT isolates a ball rolling between two plates; in effect, it is a single-ball thrust bearing without a separator, running under controlled lubrication, load, speed, and environment, and it produces results in accord with practical experience.

---

<sup>1</sup> Interesting Rolling Contact, Walpole, Massachusetts 02081

<sup>2</sup> NASA-Glenn Research Center, Cleveland, Ohio 44135

In particular, the SOT:

- Provides mean contact stress up to 3 GPa, environmental temperatures up to 150°C, ambient pressures from 760 to  $10^{-9}$  torr.
- Can distinguish boundary from elasto-hydrodynamic lubrication.
- Measures lubricant film formation, film health, and film destruction in the boundary, elasto-hydrodynamic, and solid lubrication regimes.
- Maintains its initial simple sphere-on-plane elastic contact geometry over a whole test. There is no wear as measured by weight loss or by profilometry.
- Uses plates and balls easily examined post-run, e.g. optical/electron microscopy, xps, profilometry, ftir, etc. Balls are cheap, plates can be easily refinished.
- Measures friction coefficient in boundary and solid lubrication.
- Measures traction coefficient in elasto-hydrodynamic lubrication.
- Measures lubricant degradation rate and degradation mechanism in boundary lubrication.
- Allows quantitative comparisons between boundary lubricant/bearing material combinations.
- Measures lubricant life in boundary and solid film lubrication.
- Allows quantitative predictions about the effects of variations in independent experimental parameters on lubricant life.

The SOT is a bench tester in the sense that a) it is a bench-top instrument, and b) it tests the ability of lubricants to survive the tribochemical and physical stress encountered in a rolling contact by ranking their lifetimes under well defined rolling conditions. One of its virtues is simplicity - the ball and flat plates are inexpensive test specimens whose geometry allows for easy post-test examination by optical or surface analytical chemical techniques that are more difficult for the curved surfaces of angular contact ball bearing races. In addition to its function as a bench tester for engineering evaluations, the SOT is also a true research instrument that may be used for basic research in contact mechanics, in fluid and solid film tribology, and in tribochemistry. The SOT will be described first, and then bench test results - specifically referring to the comparison of degradation rates of lubricants used in the vacuum of spacecraft - will be presented.

### *SOT Rolling Geometry*

A ball is loaded between a top plate and a bottom plate as shown in Fig. # 1. The bottom plate is stationary, the top plate rotates about a vertical axis, driving the ball. A guide plate locates the ball radially at the beginning of its first orbit. Once clear of the guide plate the ball rolls in an outward opening spiral track of small pitch, so that the ball contacts the guide plate again near the end of its first orbit before it can roll out from between the plates. The ball then rolls in a straight line along the guide plate back to its initial position and repeats the spiral orbit. During the straight-line motion along the guide and bottom plates (about 3% of the total orbit) the ball "rolls without slip" at both contacts; there is no gross sliding on either plate. However, at the top plate contact there is gross sliding. *This is the only gross sliding in the test*, and is called the "scrub". The guide plate is mounted on a transducer that measures the force required to make the

ball slip across the top plate. This repositioning force, normal to both the guide plate and the scrub track, divided into the load, gives a true sliding friction coefficient for solid or boundary lubrication, or traction coefficient for elastohydrodynamic lubrication. At all the ball-plate contacts during the scrub a pivoting angular velocity exists, just as it does in any real angular contact bearing (and in any pin-on-disk tribometer), but hysteretic boundary lubricated rolling/pivoting friction is directed along the track, is an order of magnitude smaller than sliding friction, and thus has no effect on the repositioning force measurement. Sliding friction coefficient is therefore independently measured during the scrub once each orbit. Outside the scrub there is rolling contact with pivot but without gross sliding at top and bottom plate contacts, again just as in any real angular contact bearing.

The SOT was conceived as a boundary lubrication tester, generally using microgram liquid lubricant charges applied on the ball, although larger fluid amounts, as well as solid lubricants, are possible. One of the plates is electrically isolated from ground so that any insulating film buildup (e.g. a friction polymer or an EHL film) can be detected by means of plate-to-ball-to-plate electrical resistance.

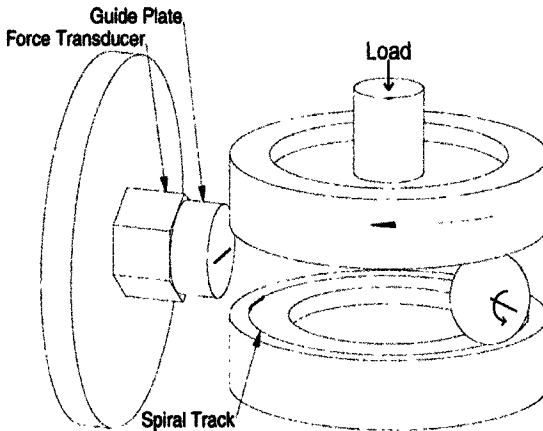


Fig. # 1. *Spiral Orbit Tribometer Geometry.*

### *Spiral Track*

The small pitch spiral is extremely robust over a wide range of load, speed, temperature and friction/traction; the SOT has never “lost a ball”. The spiral is not a centrifugal effect, instead it is the result of pivot-induced microcreep at the ball-plate contacts, treated in some detail in [1].

### Environment

The SOT was originally designed to operate in a turbo pumped ultrahigh vacuum chamber, achieving a pressure as low as  $10^{-9}$  torr with a low vapor pressure lubricant. This provided a good simulation of the vacuum environment experienced by mechanisms on spacecraft. A highly controlled environment also allows the use of *in-situ* chemical analytical probes such as residual gas analysis (RGA) and infrared spectroscopy to study gas, liquid and solid phase tribo-degradation in real time for basic research. In the model of the SOT designed for operation at ambient pressure, a simple enclosure allows operation in a purged environment, e.g. an inert gas, as well as open to the laboratory air.

### Bench Test to Real Bearing Correspondence: Contact Severity

The SOT is a true angular contact ball bearing (without a separator, but with the guide plate acting as a retainer of sorts to prevent the ball from falling out) whose first order kinematics can be written down by specializing in published bearing equations [2]. The five different SOT contacts (ball with the guide plate, top plate and bottom plate during the scrub, and ball with the bottom plate and top plate outside the scrub) have been analyzed in detail [3]. Results are thus directly applicable to real bearings. In particular, comparisons between contacts of different shapes (in the SOT the Hertz footprint is circular, while in angular contact bearings it is elliptical) can be made on the basis of *contact severity S*, which has been defined (by Kingsbury) as

$$S \equiv \mu \int_A p v_{pivot} \quad (1)$$

Here  $\mu$  is friction coefficient (measured for every scrub),  $p$  is local contact pressure,  $v_{pivot}$  is the local relative velocity within the Hertz contact region (produced by the pivoting angular velocity that is always present in any real bearing), and  $A$  is contact area. Thus  $S$  is the local shear stress-sliding velocity product integrated over the contact area, i.e. *S is the frictional energy deposited in the lubricant in the contact*. Numerical integration gives severity for an elliptical contact. In a circular SOT contact (footprint of radius  $a$ , carrying load  $L$ , at top plate rate  $\Omega$ ) the integral in closed form is:

$$S = \frac{3\pi}{16} \mu \Omega L a \quad (2)$$

Severity is important because it is the frictional energy loss into the lubricant that drives tribochemically-induced lubricant degradation and consumption. It is this consumption and disappearance of lubricant - by transformation into non-lubricating friction polymer or into gas phase products - that is responsible for lubrication failure in many systems. Of course temperature, rather than friction energy, could be considered as the driving force for chemical degradation, but temperature and energy are really the same thing, temperature being a measure of the average kinetic energy of a collection of molecules. A treatment of the way molecular kinetics increases chemical reaction rate is given in [4]. Thus direct friction measurements from the SOT (rather than a temperature derived from friction) flow naturally into severity calculations. Quantitative predictions of the levels and shape in a scrub gas burst, and of the dependence of lubricant life on contact stress [3,5,6] confirm the severity concept.

### Results for No Lubrication

Without any lubricant in a clean system in vacuum, friction coefficient is measured to be much greater than one, and plastic flow occurs at the ball / top plate contact (hardened steel) within a very few ball orbits [3].

### Results for Boundary Lubrication

#### *Representative Behavior*

The boundary lubrication regime is achieved by starting with clean plates and about  $50 \mu\text{g}$  of liquid lubricant on the ball. Then if the instrument is run at 100 rpm an EHL film will not be established, and the ball/plate interface is in solid/solid contact as indicated by low values of the electrical contact resistance. A typical coefficient of friction-ball orbit number chart is shown in Fig. # 2 for the indicated conditions, and is comparable to the usual "friction trace" – coefficient of friction as a function of time – as might be measured on a pin-on-disk tribometer. It is seen that the coefficient of friction is about 0.12 initially and is stable for thousands of ball orbits. The value of 0.12 is typical of boundary lubricated metal systems and indicates the presence of lubricant in the concentrated contact.

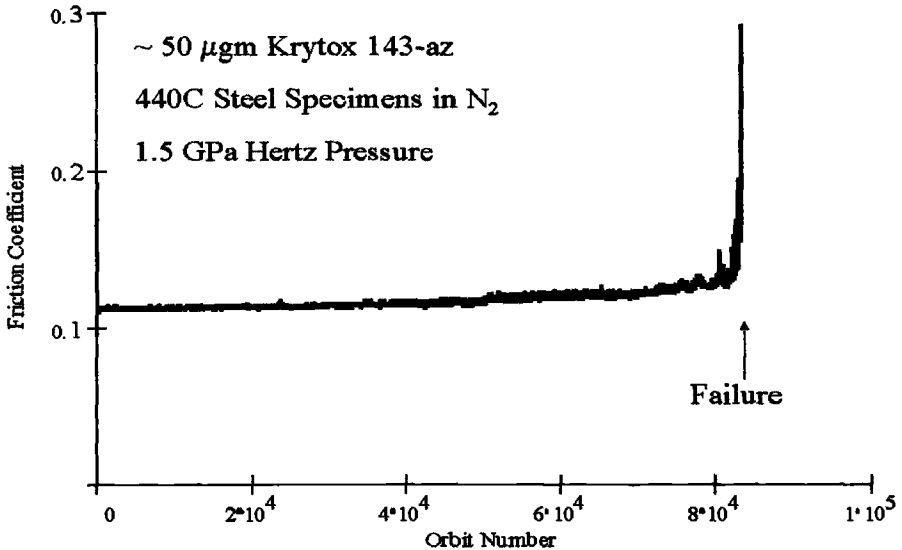


Fig. # 2. Typical friction history with a limited initial lubricant charge.

We emphasize the constancy and lack of scatter of the coefficients of friction measured at each of some 80,000 ball orbits (ball contacts on the guide plate). The

constancy and lack of scatter distinguishes the SOT from other tribometers in which the friction trace in the boundary lubrication regime can be very noisy. This desirable attribute is ascribed to the rolling aspect of the ball contact on the guide plate, which continually brings additional fresh lubricant into the sliding contact between the ball and the top plate. The other significant aspect of Fig. 2 is the sudden increase in the coefficient of friction at about 80,000 orbits, suggesting the absence of liquid lubricant. A post-test examination of the specimens with optical microscopy indeed showed friction polymer in the track, while infrared micro spectroscopy showed the absence of liquid lubricant on the ball and in the track. In fact, the lubricant was "used up" – tribochemically attacked at the steel specimens' surfaces to convert liquid to non-lubricating friction polymer and gas phase products. Operation in vacuum with a residual gas analyzer has confirmed the generation of these gas phase degradation products.

The key to achieving such a limited time friction trace is to restrict the initial lubricant charge to less than 100  $\mu\text{gm}$  which can usually be consumed in a reasonable test time. Also, a key to achieving *reproducible* test times is to pay scrupulous attention to preparation of clean specimen surfaces prior to lubrication and test. Cleanliness is important because adventitious surface impurities can act as lubricants and easily extend test times, thus masking the consumption rate of the lubricant deliberately applied.

Operating the SOT in the boundary mode allows a comparison of the consumption rates of different lubricants on the same bearing material or the consumption rates of a given lubricant on different bearing materials. Thus lubricants and bearing materials may both be ranked for their tribological compatibility in this instrument. And after all, this is what a bench tester is all about – a relatively inexpensive method for screening lubricants and bearing materials before committing to more expensive and time-consuming testing of the bearing and / or the mechanism itself. In the following section the results of such screening tests for liquid lubricants used in the space program are presented. The correspondence to full scale bearing tests is also indicated.

#### *Fomblin Z-25 on Different Metals*

The first research using the SOT was to study the effect of different bearing materials on the consumption rate of Fomblin Z-25 [7] in vacuum. This fluid has been widely used to lubricate instrument bearings on spacecraft. The results are of particular interest to the space community since there have been a number of reports (mostly anecdotal) of bearing failures by excessive friction polymer formation (referred to as "brown sugar") in 440C steel bearings lubricated by this fluid. Although most bearings are fabricated of 440C steel, other metals are sometimes chosen.

The results of the study are summarized in Fig. # 3, where the average number of ball orbits to failure are indicated for different plate materials. The ball was 440C steel in all cases, and the same lubricant charge was applied to the ball in each trial.

There is an evident correlation of higher lubricant consumption rate (shorter life) with increased chromium content. Chromium is thus implicated as a tribologically unfriendly element for Fomblin Z-25, in spite of the popularity of chromium based stainless steels. This well deserved popularity is due, of course, to corrosion resistance, not for any tribological reason. Indeed, chromium has a decidedly negative effect on the survival of tribologically-stressed Fomblin Z-25. The detailed tribochemistry underlying this effect of chromium remains to be understood.

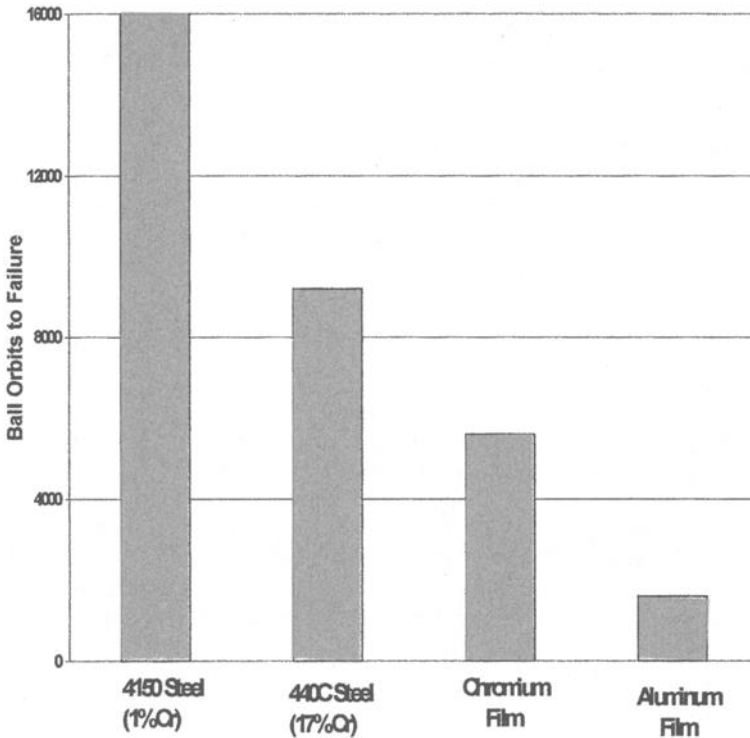


Fig. # 3. Lifetime of  $\sim 100 \mu\text{gm}$  of Fomblin Z-25 running on plates of different materials

Aluminum was included in the study, not because of its practicality as a bearing material, but because of a general understanding in the tribology community that the combination of Fomblin Z-25 and aluminum (or titanium) is highly destructive. This is confirmed by the results shown in Fig. # 3, where the consumption rate for aluminum-coated plates is an order of magnitude greater than that for 4150 steel.

### *Different Lubricants on 440C*

The material of choice for space-qualified instrument ball bearings continues to be 440C steel. 440C bearings have been lubricated by a variety of oils and greases. Four lubricants that have been widely used are Braycote 815Z, Fomblin Z-25 (the oil in Braycote 815Z), Krytox in any of its many viscosity grades and, most recently, Pennzane. The first three are hydrogen-free perfluoropolyalkyethers (PFPEs), while Pennzane is an oxygen-free pure hydrocarbon. It is of practical interest to determine the relative consumption rates of these lubricants on 440C steel.

The results of such a study [8] are given in Fig. # 4. The number of orbits to failure has been divided by the weight of the initial lubricant charge to provide a normalized lifetime for each trial of each lubricant. The error bars indicate that the degree of reproducibility achieved in these tests is entirely adequate to distinguish the different lubricants. Fomblin Z-25, a lubricant with a long history of service in the space program, exhibits the shortest life. Although Krytox 1443ac survives longer than Fomblin, Pennzane 2001A is clearly the lubricant that survives longest. It is bench test data such as this that has motivated consideration of Pennzane for use as a lubricant for instrument bearings in spacecraft.

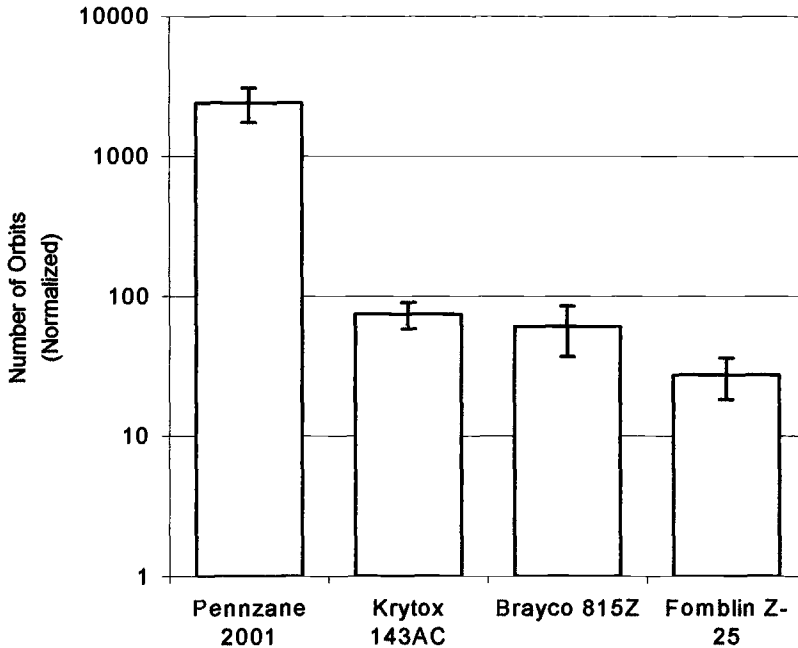


Fig. # 4. *Relative lifetimes of various space lubricants evaluated in the SOT*

*Correspondence to Full Scale Bearing Tests*

The criterion of success for a bench test is the correspondence of its results to the results from comparative tests on the full scale device the bench test is intended to simulate. In the case of the SOT comparative ranking of lubricants on 440C steel test specimens, one seeks a ranking of lifetimes of full scale 440C angular contact ball bearings lubricated with the same fluids. Such tests can be expensive and time-consuming. Fortunately, a program that evaluates different cleaning procedures on the lifetime of 440C steel ball bearings lubricated with just these fluids is underway [9]. As a byproduct of this still ongoing program, comparative lifetimes are now available for bearings lubricated with Braycote 815Z and Pennzane 2001A. The active lubricant in Braycote 815Z is Fomblin Z-25.

Results from this full scale bearing test program for the comparative lifetimes of 440C steel angular contact ball bearings lubricated with Braycote 815Z and Pennzane 2001A are shown in Fig. # 5. The bearings had been cleaned by a standard procedure prior to lubrication. Although one of the bearings lubricated with Pennzane is still running, it is clear that the bearings lubricated with Pennzane 2001A exhibit lifetimes at least an order of magnitude greater than the bearings lubricated with Braycote 815Z. Thus the results of comparative lubricant consumption rates obtained with the SOT bench tester correlate very well with the full scale tests. Such a successful correspondence is really the ultimate validation of the SOT as a bench tester.

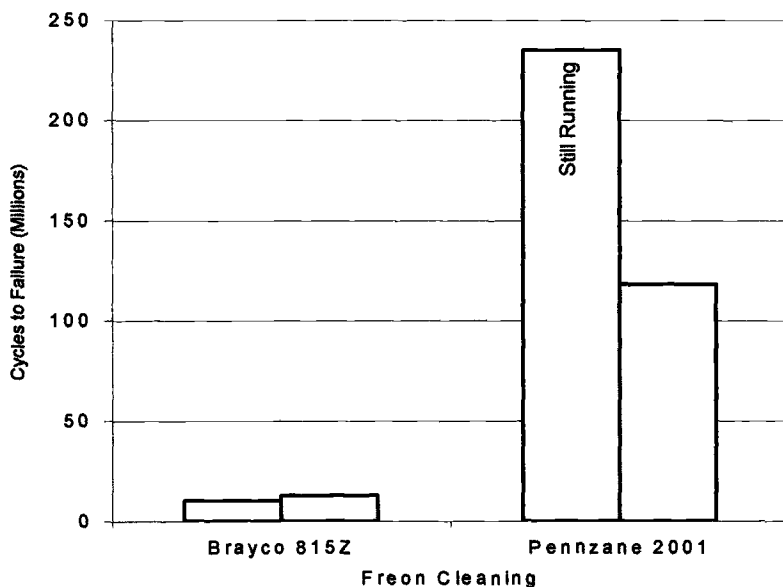


Fig. # 5. Life data from Lockheed Martin bearing test

### Results for Solid Lubrication

An experiment using the cover gas capability of the SOT confirms the well known sensitivity of the solid lubricant molybdenum disulphide ( $\text{MoS}_2$ ) to water vapor. Dry air was alternated with room air to obtain the data shown in Fig. # 6.

The test was conducted with a 1.27 cm ball and the system was purged with either dry air or air with a RH of 50%. These purge gases were switched while the system was running. It is evident that the friction is lower in dry air and higher in moist air, thus duplicating the expected classical behavior.

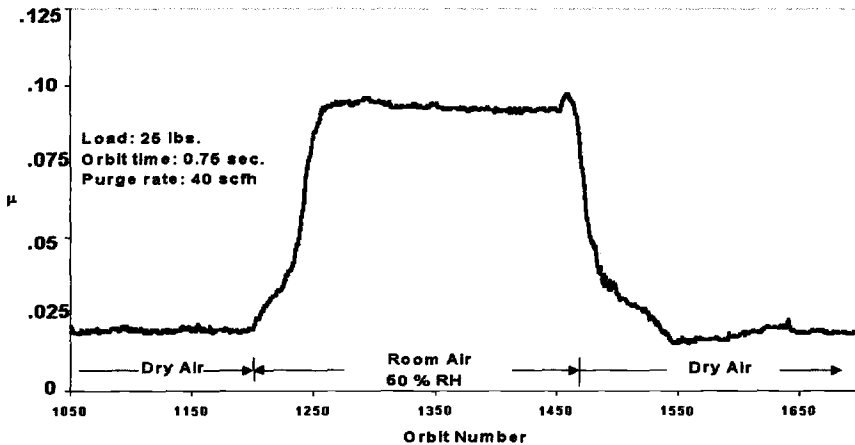


Fig. # 6.  $\text{MoS}_2$  friction in a purged environment.

A similar SOT test using graphite as the solid lubricant showed the opposite behavior; purge gas alternated between wet and dry changed the friction coefficient between low (wet) and high (dry), again confirming a classical tribological result.

This demonstrated capability of environmental control should be useful in assessing the sensitivity of liquid lubricant behavior to air, moisture, the absence of oxygen and even to such corrosive gases as diesel exhaust.

### Results for Hydrodynamic Lubrication

Sometimes it is unclear whether boundary or hydrodynamic lubrication should be expected in a slow rolling contact. The ability to measure contact resistance in the

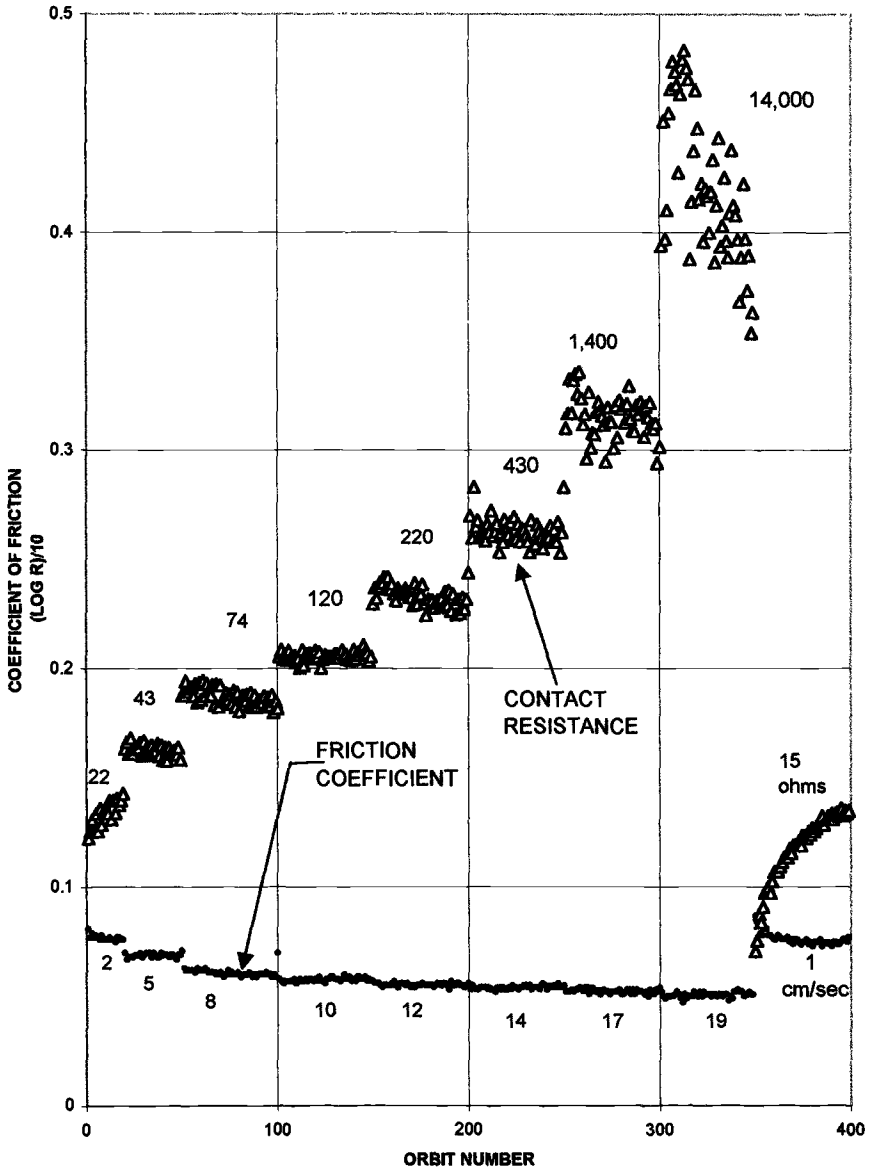


Fig. # 7 Boundary to elastohydrodynamic lubrication transition.

SOT can address this question. A SOT test with bulk synthetic hydrocarbon oil present in both meniscuses on the ball was run at increasing entrainment velocity (the average of the surface velocities which pull liquid lubricant into a rolling contact, an important parameter in EHL theory). The results are indicated in Fig. # 7, a plot of friction coefficient and (one tenth the log of) contact resistance against orbit number. During the first 20 orbits the entrainment velocity was 2 cm/sec; for the next 30 orbits it was increased to 5 cm/sec, then to 8, etc., as given by the numbers *under the friction curve*. For the last 50 orbits entrainment velocity was reduced to 1 cm/sec, half the original value. A gradual but small diminution in friction with increasing speed is seen, with a jump back to the original level in the final slow segment. The resistance curve shows jumps corresponding to the velocity steps. These jumps are much larger than they appear on the graph, which is a logarithmic representation. To make this clear, the average resistance in ohms for each segment is given *above the resistance curve*. There are 3 orders of magnitude change in resistance shown. A complete transition to megohm EHL resistance was not realized in this test owing to a top plate drive speed limitation of 150 rpm. Contact resistance reverts to a few ohms for the last slow segment. This reversible behavior is consistent with a partially penetrated hydrodynamic film changing its thickness with speed. But the slow buildup in resistance at a constant slow speed in the last 50 orbits is also consistent with solid friction polymer formed irreversibly from liquid lubricant accumulating on the track, as discussed in the boundary lubrication section.

### Summary

The SOT gives results consistent with known tribological behavior over a wide range of conditions. A quantitative theory exists to explain its basic operation. Results from the SOT have been presented for the relative lifetimes of popular lubricants for vacuum service. The results are in accord with recent full-scale bearing life tests with these lubricants. Taken together, these considerations go a long way towards removing general objections to tribological bench testing for rolling contacts. It seems reasonable that new information, quickly obtainable from the SOT, will be useful in designing new and difficult rolling applications, and also in getting fundamental information on boundary lubrication failure processes in rolling contact.

### References

- [1] Johnson, K. L., *Contact Mechanics*, Cambridge University Press 1985, Chapter 8.
- [2] Kingsbury, E. "Evaluation of the NASA Ball on Plate Tribometer as an Angular Contact Ball Bearing", *Proceedings of the 1997 International Rolling Element Bearing Symposium*, R. Price, Ed., Orlando, Florida, 1997.
- [3] Pepper, S. V., Kingsbury, E., and Ebihara, B., "A Rolling Element Tribometer for the Study of Liquid Lubricants in Vacuum", *NASA TP 3629*, October 1996.
- [4] Slater, J. C., *Introduction to Chemical Physics*, McGraw-Hill 1939, Chapter 4.

- [5] Jones, W. R. Jr., Jansen, M. J., Helmick, L. H., Nguyen, Q. N., Wheeler, D. W., and Boving, H. J., "The Effect of Stress and TiC Coated Balls on Lubricant Lifetimes using a Vacuum Ball-on-Plate Rolling Contact Tribometer", *NASA TM 1999-209055*, March 1999.
- [6] Kingsbury, E. "Influences on Polymer Formation Rate in Instrument Ball Bearings", *Tribology Transactions* v. 35, pp. 184-188, 1992.
- [7] Pepper, S. V. and Kingsbury E., "Destruction of Fomblin Z-25 by Different Materials", *Proceedings of the 1997 International Rolling Element Bearing Symposium*, R. Price, Ed., Orlando, Florida, 1997.
- [8] Jones, W. R. Jr., Pepper, S., Jansen, M., Nguyen, Q. N., Kingsbury, E., Lowenthal, S. H., and Predmore, R. E., "A New Apparatus to Evaluate Lubricants for Space Applications – The Spiral Orbit Tribometer (SOT)", *NASA/TM – 2000-209935*, March 2000.
- [9] Loewenthal, S. H., Jones, W. R. Jr., and Predmore, R. E., "Life of Pennzane and 815Z Lubricated Instrument Bearings Cleaned with Non-CFC Solvents", *NASA TM-1999-209392*, September, 1999.

Jason W. Munson<sup>1</sup> and P. Barry Hertz<sup>2</sup>

## M-ROCLE Diesel and Biodiesel Fuel Lubricity Bench Test

---

**Reference:** Munson, J. W. and Hertz, P. B., “M-ROCLE Diesel and Biodiesel Fuel Lubricity Bench Test,” *Bench Testing of Industrial Fluid Lubrication and Wear Properties Used in Machinery Applications, ASTM STP 1404*, G. E. Totten, L. D. Wedeven, J. R. Dickey, and M. Anderson, Eds., American Society for Testing and Materials, West Conshohocken, PA, 2001.

**Abstract:** Environmental concerns have prompted sulfur reductions in diesel fuels. These changes can decrease unadditized fuel lubricity, resulting in higher wear of diesel injection pumps and engines. Actual diesel pump and engine tests are costly, and existing diesel fuel lubricity bench tests appear to be failing to evaluate the fuel lubricity adequately. This has prompted the described development steps for the M-ROCLE bench test. It employs a crossed roller on cylinder geometry and computer data acquisition systems. The measured wear scar area stress is divided by the theoretical elastic Hertzian contact stress, and friction coefficient, to yield a dimensionless Lubricity Number (LN) indicating the lubricating property of the test fuel. Based on previous work and from correlation with HFRR test data, an LN > 1.0 was established as the pass value for a diesel fuel of sufficient lubricity. The overall coefficient of variation in published Lubricity Numbers, based on six individual test runs for some hundred fuels surveyed to date, was 5.3%. This is indicative of high precision in the M-ROCLE method.

**Keywords:** diesel fuel lubricity bench test, M-ROCLE, lubricity number, lubricity additives, biodiesel fuel, diesel injection pumps, friction, wear, lubrication

---

<sup>1</sup>Research Engineer, Mechanical Engineering Department, University of Saskatchewan, Saskatoon, SK Canada, S7N 5A9

<sup>2</sup>Professor of Mechanical Engineering, University of Saskatchewan, Saskatoon, SK Canada, S7N 5A9

## Introduction

Recent and proposed diesel engine emission legislation has prompted dramatic reductions in the sulfur content of diesel fuels. Hydrotreating to remove sulfur has also removed beneficial components and caused decreased diesel fuel lubricity. This has resulted in higher diesel injection pump and engine wear for inadequately additized fuels. The new ultra-low sulfur commercial diesel fuels will most certainly cause major diesel engine and injection pump damage if effective lubricity additives are not used. To insure that the lubricity additive has adequately increased the diesel fuel's lubricity, diesel engine, injection pump and lubricity bench tests must be employed.

Actual diesel engine and pump tests are expensive and time intensive. Existing diesel fuel lubricity bench tests have been reported as failing to evaluate the diesel fuel lubricity and additive effects [1, 2]. This has prompted the development of the Munson Roller on Cylinder Lubricity Evaluator (M-ROCLE) [3], which measures diesel fuel and biodiesel blended fuel lubricity in the laboratory with great precision. Several Canadian seasonal diesel fuels, commercial and industrial lubricity additives, as well as biodiesel lubricity additives have been tested on the M-ROCLE [4, 5]. Based on previous work and from correlation with HFRR test data, a minimum LN of 1.0 was established as the pass/fail value for a diesel fuel of sufficient lubricity.

## Original ROCLE Bench Test

Harvey, Goshawk, and Bubnick [6] first developed the original Roller on Cylinder Lubricity Evaluator (ROCLE) at the University of Saskatchewan in 1982. This was followed by adaptation for diesel fuel lubricity testing, by Galbraith and Hertz [7], in 1997. The original ROCLE machine is shown schematically below in Figure 1.

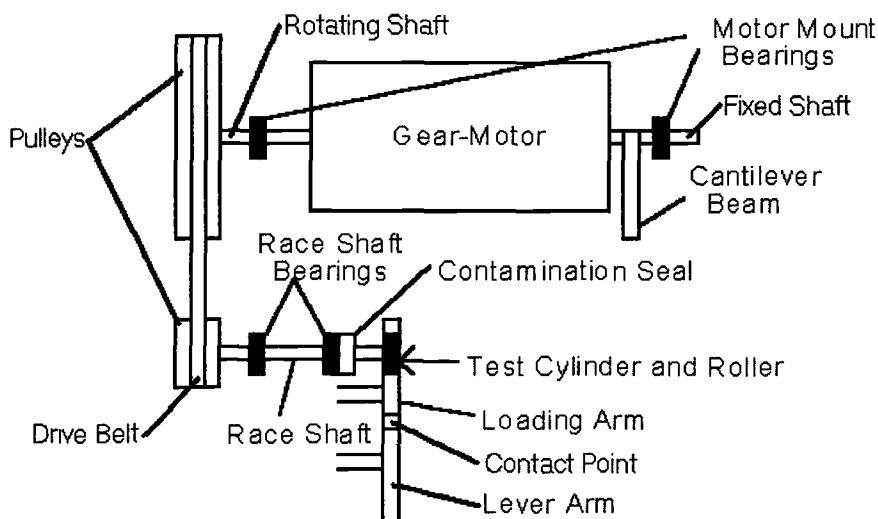


Figure 1: *Original ROCLE Configuration*

The original ROCLE incorporated a 2-arm loading system applying a vertical load of 25 N through a test roller to a rotating test race. The test specimens' axes were crossed, which resulted in high Hertzian point contact that developed into an elliptical wear scar bearing area. During the 1-minute test time, the roller produced wear against the race with the test fluid providing the lubrication. The initial wear rate was high as the freshly lubricated metal test specimens first came into contact. The wear rate decreased to a steady state level as boundary lubrication developed. The friction force was measured by sensing the motor reaction torque developed on the race shaft caused by the wearing of the two test specimens. The reaction torque flexed a cantilever beam with strain gages and a strip chart recorder plotted the proportional output voltage. Applying weights to a calibration arm simulated the reaction torque and this response was also plotted. Using the calibration strain factor and indicated reaction torque, the test fuel friction coefficient was calculated.

The wear scar area produced on the test roller was determined using an optical microscope and the area formula for an ellipse. The theoretical elastic Hertzian contact area (wear scar) shape was also elliptical. Using the wear scar area and the coefficient of friction, a dimensionless Lubricity Number (LN) [7] was calculated with Equation 2:

$$\sigma_{SS} = N_F / A_{SCAR} \quad (1)$$

where,

$\sigma_{SS}$  = steady state M-ROCLE contact stress,

$N_F$  = normal force,

$A_{SCAR}$  = wear scar area.

$$LN = \sigma_{SS} / \sigma_H \mu_{SS} \quad (2)$$

where,

LN = Lubricity Number, (LN>1.0 is required for sufficient diesel fuel lubricity)

$\sigma_H$  = Hertzian contact stress,

$\mu_{SS}$  = coefficient of friction of the test fuel.

The original ROCLE procedure did not employ control of room temperature or humidity. The apparatus, removable parts and the test specimens were all rigorously cleaned. The test specimens were stored in the test fuel [7] to prevent oxidation. The fuel reservoir had a capacity of 50 mL. An anti-foam rod was used to prevent the test fuel from developing foam as a result of air entrapment during the test.

### Loading System

The original loading system (Figure 2) included loading and lever arms. The loading arm held the test roller in place as it was forced against the test race. The original system was intended for much higher test loads [6] as when testing engine oils and gear lubricants. There were many design problems with this compound loading arm system.

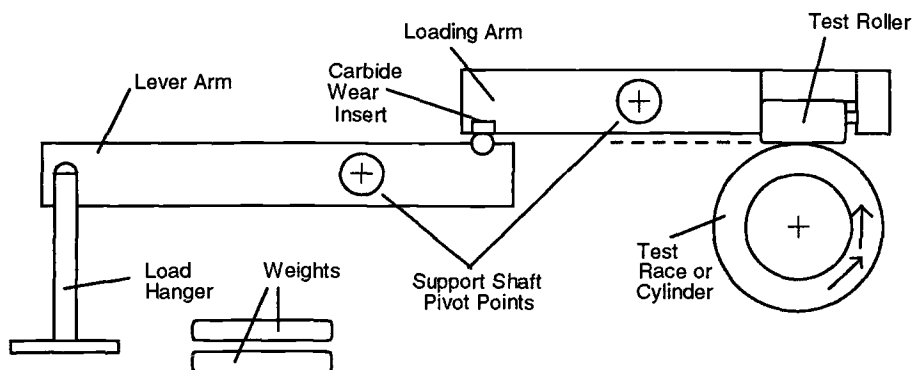


Figure 2: *Original ROCLE Loading Arm System*

### Loading Arm Redesign

The first loading arm problem involved the arm configuration. The tangent of the contact point of the test race and test roller did not intersect the loading arm pivot point. With the direction of rotation, the arm system acted as a self-activating brake that increased the vertical roller load as the friction increased. The level of self-energization would depend on the test fuel friction. When the fuel had good lubricity, the braking effect was smaller in comparison to when the fuel had poor lubricity.

The contact points between the two arms also caused problems. A carbide contact insert was originally installed to decrease the friction between the arms without using a lubricant. This carbide insert indicated wear and developed contact friction. The amount of inter-arm friction depended on the manner in which the arms were brought into contact.

The test roller mounting system allowed the tapered test roller to be mounted in either direction. This could change the position of the wear scar on the test roller, which would slightly change the contact diameter and resulted in inconsistencies in the position of wear scar relative to the roller. The upper arm surface that the test roller pressed against, when loaded, had become indented from roller contact and also caused inconsistent mountings.

A new single loading arm was designed to mitigate the problems of the original loading arms. The test roller-race contact tangent was changed to intersect the pivot point center of the loading arm to eliminate the frictional self-energization problem. The test roller would only have one possible mounting direction in order to control positioning. The 2-arm setup would be eliminated to decrease the chance of arm contact problems due to friction between the arms.

The new single loading arm had the test weight permanently mounted at the maximum allowable space restricted distance from the test roller position to decrease the effect of weight swing. Weight swing could cause abnormal wear scar elongation, laterally, along the minor axis. The greater the distance the weight was placed in relation to the contact point, the smaller the effect of any possible weight swing. The final constant test load of the loading arm at the contact point of the roller was 24.6 N. This load was used due to

actual fuel pump contact stresses between components that ranged from 552 MPa to 827 MPa [8], as well as the variable load work performed by Galbraith [7]. The 24.6 N load produces a Hertzian contact stress of 896 MPa, which is somewhat higher than actual pump contact stress.

### Reaction Torque

The fuel's coefficient of friction can have a significant effect on the fuel consumption of a diesel engine. The lower the friction coefficient of the diesel fuel was, other things remaining the same, the better the indicated fuel economy was [9]. The reaction torque produced by the ROCLE was recorded and quantified in order to calculate the coefficient of friction between the test roller and race using the test fuel as the lubricant. The reaction torque produced at the motor due to the friction between the test specimens had previously been displayed on a strip chart recorder plot as shown in Figure 3.

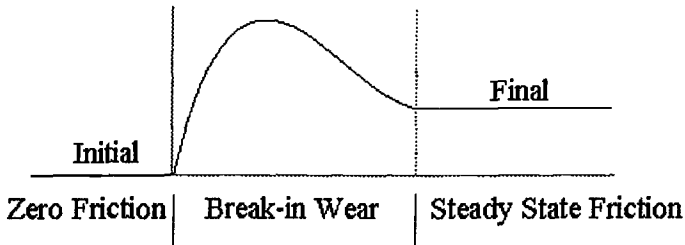


Figure 3: *Typical Fuel Test Reaction Torque vs. Time Plot*

This reaction torque was found to be the difference between the initial reaction torque (motor running without load) and the final reaction torque (motor running with load) after the initial break-in wear. It was assumed that the latter reaction torque line was constant, and the peaks and valleys were ignored. The number of plot paper divisions between them had originally measured the difference between the initial and final lines. The incomplete divisions were visually estimated. The approximation of divisions and the thickness of the lines could result in errors due to human subjectivity.

The original method of reaction torque calibration involved adding large weights (> 200 g) to the reaction torque calibration arm on the ROCLE. These large weights made for a straight reaction torque calibration line, but did not represent the small force area of interest in terms of the reaction torque produced during the fuel tests. In this research, weights (< 20 g) that represented the reaction torque range at the motor during a lubricity test were added to the reaction torque calibration arm. This resulted in more accurate calibration factors used to calculate the friction coefficient.

### Data Acquisition System Replacement

A new computer aided data acquisition system was incorporated for measuring the friction or reaction torque objectively. Significant amounts of noise were noticed when the computer data acquisition system was introduced. The entire data acquisition system

was grounded but some noise remained. This raised the concern that the low frequency was an alias of a higher frequency. Aliasing occurs when a frequency in the signal is larger than the sampling rate of the data acquisition system. The larger frequency would show as a mirror image in the frequency response. With the aid of custom software, it was found that the data acquisition software was aliasing the incoming signal. The best solution to the problem of aliasing, as well as to decrease the amount and amplitude of noise in the signal, was to develop a simple R-C (resistor-capacitor) circuit filter. The R-C filter was introduced into the circuit before the signal entered the board, which was also shielded. The R-C circuit was designed to filter out frequencies over 0.28 Hz. Due to the simple nature of the filter, friction torque frequencies above 0.28 Hz (up to 3 Hz) still remained but at much lower amplitudes than before.

**Original Cantilever Beam/Rod System**

The cantilever beam (Figure 4) was previously used to resist the reaction torque of the gear-motor and sense the reaction torque magnitude through strain gages on the beam. The strain gages were connected in a full Wheatstone bridge configuration. Each side of the cantilever beam had 2 strain gages. This direct-motor connected configuration was found to increase the amount of noise in the reaction torque signal. An off-motor cantilever beam configuration was implemented in the M-ROCLE design.

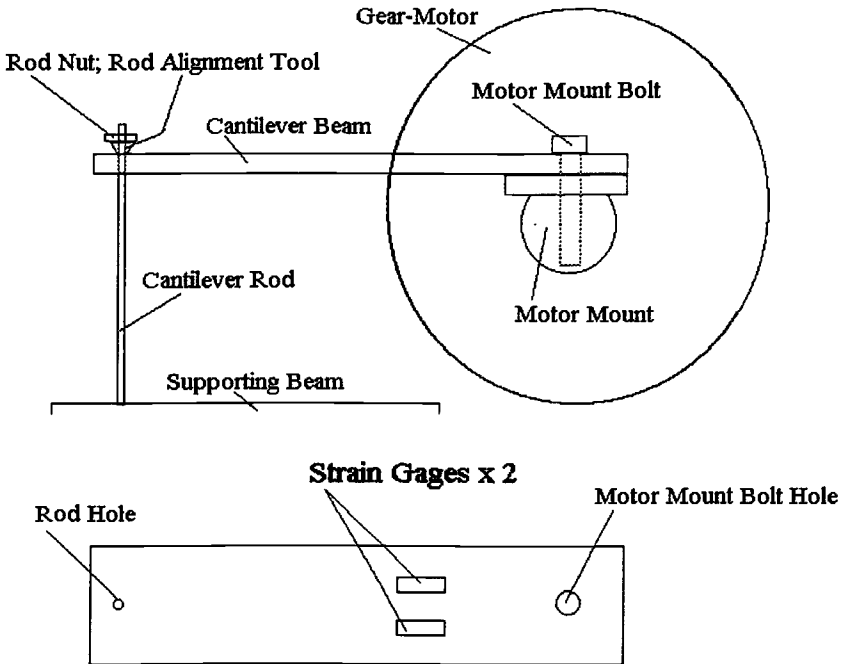


Figure 4: Original Cantilever Beam Configuration

### Beam and Configuration Redesign

The old cantilever beam was a simple rectangular bar, which had varying stress/strain from end to end. Figure 5 shows the new tapered cantilever beam that was designed for constant stress/strain across the strain gage zone with the beam sides tapered to intersect at the load point. The cantilever beam dimensions and the placement of the strain gages in the zone depended on the desired strain value, the strength of the beam, the allowable elastic deformation of the beam and coupling music wire, and the diameter of the motor mount connection. Music wire was found to have the greatest advantage as the reaction torque transfer medium in the off-motor beam mount configuration.

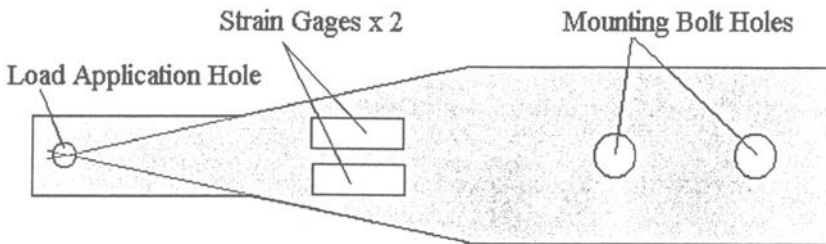


Figure 5: *New Tapered Cantilever Beam*

A necessary change to the system was to include a larger sheave diameter on the motor mount for the coupling music wire. The original motor mount shaft was too small to prevent plastic deformation of the music wire due to bending.

A larger drum diameter decreased the output signal strength. A circular aluminum bar was used to increase the sheave diameter. A thin groove was machined into the circumference of the drum to provide a constant diameter as the motor rotated and for music wire positioning. The cantilever beam was bolted in a remote vertical orientation, using angle iron, to the same table bed as the M-ROCLE. This new cantilever beam configuration reduced the amount of noise signal.

### Wear Scar Area Measurement

The resulting wear scar size depended on the ability of the fuel to lubricate the test roller and race interface. The original wear scar area measurement involved an optical microscope and application of the area formula for an ellipse. This method was subjective as to the length of each axis of the elliptical scar. Some scars were not perfect ellipses, resulting in inaccurate measurements. The new wear scar measurement method implemented image processing software and hardware. The wear scar areas were found with considerably less subjectivity and shape dependency.

### Lubricity Test Time Change

The original ROCLE procedure used a one-minute test time. Test time for wear scar development became a concern once the lateral movements of the loading arm and test race were controlled. The wear scars from very short test times seemed to be underdeveloped with feathery edging and imperfect elliptical shapes. To examine the effect of test time on wear scar shape, times of 1-, 2-, 2.5-, 3-, 4- and 5-minutes were first tried. After numerous specimens were tested in this manner, it was noticed that the 2.5- and 3-minute wear scars were nearly perfect ellipses with the 4- and 5-minute tests still essentially the same. Therefore, durations of only 2.5- and 3-minute test times were compared with the 3-minute tests, producing better wear scars.

### Room Temperature and Humidity Control

The original ROCLE tests were performed in a laboratory without individual room temperature and humidity control. Other fuel lubricity test procedures including the HFRR, SLBOCLE, and BOTD [8] maintained a test fuel temperature of either  $25\pm 1^\circ\text{C}$  (all) or  $60\pm 1^\circ\text{C}$  (HFRR). The room temperature is controlled at  $25^\circ\text{C}$  for the SLBOCLE but is not controlled for the HFRR [1]. The temperature within the environmental room was controlled at  $22\pm 1^\circ\text{C}$  for the M-ROCLE. The room was maintained at this temperature to assist in the control of the final  $25^\circ\text{C}$  test fuel temperature.

The SLBOCLE procedure maintained a room RH of 50% while the HFRR uses ambient room humidity [9]. The room humidity for the M-ROCLE was regulated at  $45\pm 5\%$  RH. The control of humidity was accomplished using a room humidifier and a portable dehumidifier to keep the humidity within this range. Other researchers [10] have observed effects on lubricity with variable humidity while others report no effects [11]. The room humidity and temperature were controlled with the M-ROCLE to completely remove the possibility of these influences.

### Fuel Reservoir Considerations

The fuel reservoir contained the test fuel during lubricity tests. The original test procedure included measurement of some test fuel temperatures but did not attempt to control the fuel temperature. The original ROCLE also used an anti-foam rod to control fuel foaming during the test. The rod was placed on the sidewalls of the fuel reservoir directly behind the rotating test race. This rod prevented air from becoming entrapped in the fuel as it re-entered the fuel reservoir after it rotated with the test race.

#### *Fuel Reservoir Changes -- Anti-Foam Rod*

The original fuel reservoir (Figure 6) was reexamined. The anti-foam rod was held in place sufficiently not to be pulled into the rotating test race. When doing foaming tests, it was noticed that more volume ahead of the test race in the reservoir resulted in a lower tendency to produce foam. It was also noticed when using the anti-foam rod that an amount of fuel would flow out of the reservoir along the rod.

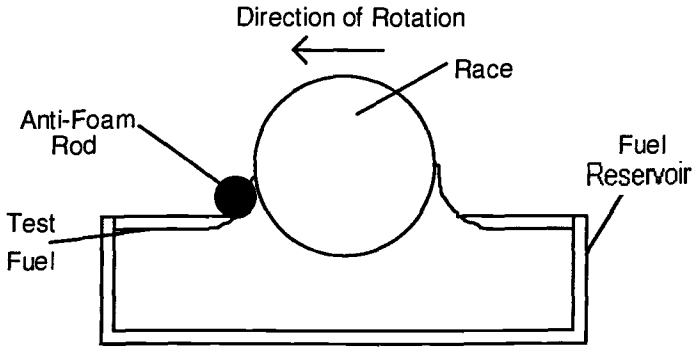


Figure 6: *Original Fuel Reservoir with Anti-Foam Rod*

A new fuel reservoir (Figure 7) was constructed that was longer than the original. A positive anti-foaming rod fixation was also introduced that did not allow the fuel to flow out of the reservoir. Notches were machined into the sidewalls of the reservoir that provided a counter-sinking of the top of the anti-foam rod. This helped both to contain the fuel and positively fix the wooden rod in place.

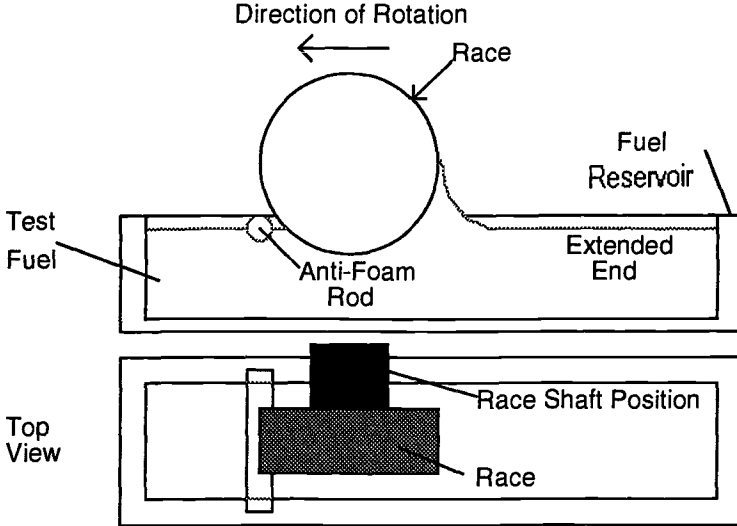


Figure 7: *Final Fuel Reservoir with Anti-Foam Rod*

**Specimen and ROCLE Cleaning Process**

The original cleaning process [7] of the ROCLE apparatus, accessories and test

specimens was changed slightly along with the chemicals used to clean these items. The test specimens (rollers and races) had been cleaned in an ultrasonic cleaner for 15 minutes in each of toluene and a 1-to-1 mixture of isopropyl alcohol and isooctane. The specimens were wiped dry with a lint-free cloth after the toluene wash. They were blown dry after the 1-to-1 mixture wash. The specimens were then rinsed with acetone and blown dry before being placed in the test fuel. These chemicals were used due to their high cleansing ability and relatively low toxicity when compared to other cleaners. It was noticed that test race and roller blemishing occurred during the wiping process and chemical stains sometimes appeared during the blow drying of the 1-to-1 mixture wash. The new cleaning procedure used the same first two steps with three chemicals but the specimens were transferred directly from one chemical to the next. The acetone rinse was still used but a lower evaporation residue acetone was substituted. The specimens were first dipped into a jar of the lower evaporation residue acetone then rinsed with fresh low evaporation residue acetone before being blown dry.

The revised accessory cleaning procedure and chemicals were the same as for the test specimen's new procedure except for two items. The fuel reservoir was too long to be completely covered with cleaning chemical, due to limitations in the ultrasonic cleaner size, therefore the reservoir was rotated 180° every 4 minutes and the duration of exposure was increased to a total of 16 minutes for each chemical.

The M-ROCLE apparatus cleaning procedure between different fuels included cleaning the exposed parts (entire loading arm and shaft cone and part of shaft) with the 1-to-1 isopropyl alcohol and isooctane mixture and a toothbrush. This was then rinsed with a higher residue acetone (< 10 ppm), then with low residue acetone, and blown dry.

The original ROCLE test procedure recommended disposable latex gloves that were rinsed of the talc powder with acetone. An acetone and toluene resistant neoprene glove was substituted and was cleaned after each test as well. The glove was cleaned with the 1- to-1 mixture followed by the higher residue acetone and rinsed with the lower residue acetone.

### **Loading Arm Hydraulic Release for Application to Test Race**

It was noticed by examination of the wear scars that the speed at which the test roller was lowered onto the test race made a difference in the scar shape and size. The higher the impact that the roller made with the test race, the larger the wear scar areas produced. The original method of manually load releasing, involving two loading arms, had less wear scar effect due to the 19-to-1 levering effect of the compound arms. However, with just one loading arm, the impact effect was much greater. A consistent hydraulic method for lowering motion and the release of the loading arm was developed. A small air cylinder, using fluid as the medium, was used to produce a lowering motion in which speed of the loading arm release could be easily controlled with a hydraulic flow control valve.

### **New M- ROCLE Bench Test**

A top view schematic of the M-ROCLE is provided in Figure 8. Test conditions for the M-ROCLE are given in Table 1. The M-ROCLE incorporated a single, fixed load,

loading arm in order to apply a vertical 24.6 N load through a test roller onto a rotating test race. The test roller and race were in a crossed axes configuration in order to produce a high contact stress and an elliptical wear scar.

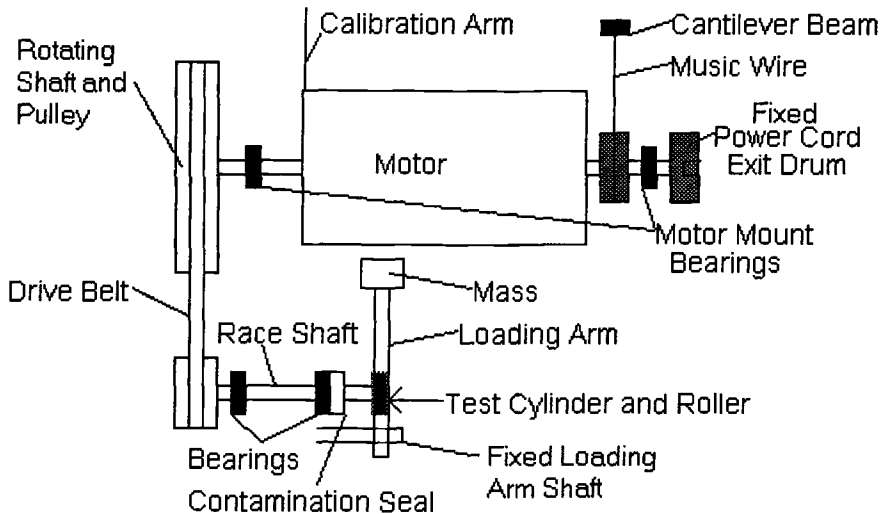


Figure 8: *New M-ROCLE Schematic*

Table 1: *M-ROCLE Test Conditions*

Test Fuel Volume	63±2 ml
Fuel Temperature	25±1.5°C
Room Temperature	22±1.0°C
Room Humidity	45±5% RH
Applied Load	24.6±0.5 N
Load Application Velocity	0.25 mm/sec.
Test Race Rotational Speed	600±10 rpm
Test Time	3.0±0.05 min.
Hertzian Contact Stress (Dry)	896 MPa
Test Race - Outer Diameter, Width	35.0 mm, 8.50 mm
Race, 4620 Steel, Rc 58-63, 22-28 RMS	(Falex F-S25)
Test Roller - Outer Diameters, Length	10.18, 10.74, 14.80 mm
Roller, Steel, Rc 55-60, ISO (µm) Ra 0.17	(Falex F15500)

During the test, the test roller rubbed against the race with the diesel fuel providing the lubrication. Initially, the wear rate was high when the 2 fuel-bathed metal test pieces first contact. The wear rate decreased to a steady-state equilibrium when boundary lubrication developed. This wear was characterized by the amount of friction force developed between the 2 test specimens. The friction force was obtained by measuring the reaction torque produced at the race. The cantilever beam was bolted vertically to a piece of angle iron, which was attached to the M-ROCLE machine table. The strain on the cantilever beam was recorded by a computer aided data acquisition system. Applying weights to the reaction torque calibration arm simulated the reaction torque and this reference was also recorded. This allowed the test strain signal output to be calibrated as a reaction torque value, from which the coefficient of friction was calculated.

The area of the wear scar produced on the roller specimen during the test was measured. The theoretical elastic shape of this contact area was elliptical. Using computer image processing software, the wear scar area was determined. With the wear scar area stress and the coefficient of friction, the Lubricity Number was calculated.

To obtain high statistical confidence in the results for a given fuel, six test runs were used in establishing a test protocol. If obvious specimen blemishes were detected in a particular test run, that run would be rejected. The statistical lubricity number for a given fuel was based on five or six separate tests. Previously published [3,4,5] evaluations of some hundred different diesel, biodiesel blends, and lubricity additive fuel combinations had produced a mean standard deviation in all M-ROCLE testing to date of some 5.3%.

The M-ROCLE test method introduced control of both the room temperature and humidity. The test fuel temperature was also controlled. The machine, removable parts and the test specimens were rigorously cleaned between tests. The cleaned specimens were stored in the test fuel until evaluation time [7] to prevent surface oxidation.

## Conclusions

The developmental steps of the new M-ROCLE lubricity bench test were described. These steps improved the reliability and decreased the subjectivity of diesel and biodiesel fuel lubricity evaluations compared to the previous ROCLE instrument. A crossed roller-on-cylinder geometry was still employed along with fuel storage of meticulously cleaned test specimens to prevent surface oxidation. The measured wear scar area stress was still divided by the theoretical elastic Hertzian contact stress, and friction coefficient, to yield a dimensionless Lubricity Number (LN) which indicated the lubricating property of the test fuel. Computer data acquisition systems for wear area and friction measurement were introduced along with numerous other machine modifications. Environmental control of laboratory test chamber temperature, humidity, and fuel temperature was implemented.

This modified instrument was better able to detect the effects of small additions of biodiesel and commercial lubricity additives. Based on previously published work and in correlation with HFRR test data, an LN of 1.0 was established as the pass/fail value for a diesel fuel of sufficient lubricity. The overall coefficient of variation for the M-ROCLE Lubricity Numbers, previously published for all fuels and additives surveyed to date, was 5.3%, which indicated high precision and good experimental repeatability.

## References

- [1] Lacey, P. and Howell, S., "Fuel Lubricity Reviewed," SAE Technical Paper 982567, 1998.
- [2] Cameron, F., "Lubricity of California Fuel," SAE Technical Paper 981362, 1998.
- [3] Munson, J.W., "Development of a Precision Diesel Fuel Lubricity Bench Test – The M-ROCLE," University of Saskatchewan, M.Sc. Thesis, 1999.
- [4] Munson, J. and Hertz, P.B., "Seasonal Diesel Fuel and Fuel Additive Survey Using the Munson ROCLE Bench Test," SAE Technical Paper 1999-01-3588, published in *Gasoline and Diesel Fuel: Performance and Additives*, (SAE SP-1479) pp 93-103, 1999.
- [5] Munson, J., Hertz, P.B., Dalai, A., and Reaney, M., "Lubricity Survey of Low-Level Biodiesel Fuel Additives Using the Munson ROCLE Bench Test," SAE Technical Paper 1999-01-3590, published in *Gasoline and Diesel Fuel: Performance and Additives*, (SAE SP-1479) pp 115-124, 1999.
- [6] Harvey, D., Goshawk, C., and Bubnick, R., "Design of a Tribological Bench Test for Energy Efficient Lubricants," M.E. 497 Design Project, Mechanical Engineering Department Report, University of Saskatchewan, 1983.
- [7] Galbraith, R.M. and Hertz, P.B., "The ROCLE Test for Diesel and Bio-Diesel Fuel Lubricity," SAE Technical Paper 972862, published in *Engine Oil Rheology and Tribology*, (SAE SP-1303) pp 61-66, 1997.
- [8] Voitik, R. and Ren, N., "Diesel Fuel Lubricity by Standard Four Ball Apparatus Utilizing Ball on Three Disks, BOTD," SAE Technical Paper 950247, 1995.
- [9] Hertz, P.B., "Winter 1997 Evaluation of Canola Methyl Ester and a Canola Oil Derivative obtained from Heated Seed as Lubricity Additives for Diesel Fuel," report prepared for Agriculture and Agri-Food Canada, November 1997.
- [10] Caprotti, R., "Harm Free Use of Diesel Additives," SAE Technical Paper 982569, 1998.
- [11] Mitchell, K., "The Lubricity of Winter Diesel Fuels," SAE Technical Paper 952370, 1995.

**SESSION III: Bench Tests and Test  
Development—B**

Jan Filzek<sup>1</sup> and Peter Groche<sup>1</sup>

## Assessment of the Tribological Function of Lubricants for Sheet Metal Forming

---

**Reference:** Filzek, J. and Groche, P., “Assessment of the Tribological Function of Lubricants for Sheet Metal Forming,” *Bench Testing of Industrial Fluid Lubrication and Wear Properties Used in Machinery Applications, ASTM STP 1404*, G. E. Totten, L. D. Wedeven, J. R. Dickey, and M. Anderson, Eds., American Society for Testing and Materials, West Conshohocken, PA, 2001.

**Abstract:** Tribology plays a significant role in enlarging the process limits and ensuring process stability as well as good quality of the forming parts in deep drawing. This paper focuses on assessing lubricant behavior and its influence on tribological conditions during the forming process. A basic condition for efficient usage of the potentials offered by lubrication is the availability of test methods allowing fast and safe evaluation of products. Two specific test stands for sheet metal processing are presented in this paper. These test stands are based on the strip drawing principle. Using these model tests, the capability of a lubricant can be tested under all relevant conditions and its suitability for certain applications can be determined. The experimental results of several tested lubricants will be shown. Subsequently, the results are verified with deep drawing tests of real forming parts.

**Keywords:** sheet metal forming, deep drawing, tribology, friction, wear, lubrication

### Introduction

In the automobile industry the demand for low vehicle weight has increased during the past years. In particular the area of sheet metal forming aims at this by the processing of larger and multiple-function integrated components, a higher material utilization and the application of high strength steel [1]. Thus, the requirements on the manufacturing process become even more extensive and complex. Nevertheless, the process limits with the sheet metal forming have to be enlarged. In addition, the stability of the forming process has to be optimized. In this connection the tribological conditions during the forming process are of great importance [2].

---

<sup>1</sup> Dipl.-Ing. and Prof. Dr.-Ing. Dipl.-Wirtsch.-Ing., Institute for Production Engineering and Forming Machines, Darmstadt University of Technology, Petersenstrasse 30, D-64287 Darmstadt, Germany.

**Forming Process**

The task of the sheet metal processing industry is to produce complex function integrated components with special properties from a flat blank. Therefore, the elementary forming processes like stretch drawing and deep drawing play an important role. In both cases the tool normally consists of a punch, a die and a blank holder (Figure 1).

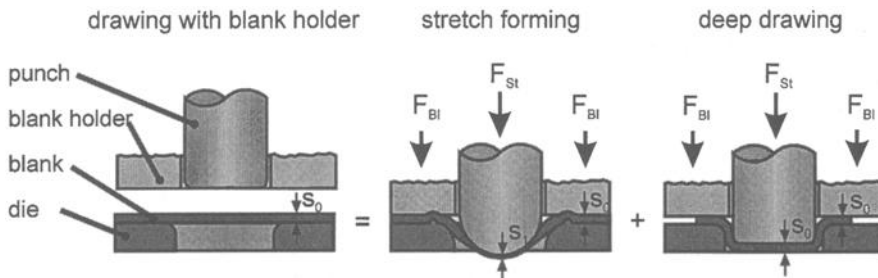


Figure 1 - Deep Drawing and Stretch Forming in the Sheet Metal Forming Process [3]

In the stretch drawing process the blank holder prevents the blank from sliding into the die. As a result, the blank is subjected to biaxial tensile stress during penetration of the punch. Thus, the sheet metal thickness is reduced. Deep drawing, in contrast, is a process of combined tensile and compression stress. The blank is formed under tangential compressive stress and radial tensile stress without intending to alter the thickness of the sheet metal.

In special cases, the two types of forming are applied in a temporal succession. The forming operation starts with a stretch drawing process in which the wall thickness of the stretched blank is reduced and the bottom of the drawn part is formed. In the following deep drawing process the blank holder force is reduced, so that the blank material flows over the rounded sections of the die without generating wrinkles.

However, when drawing complex body panels for a passenger car, stretch drawing and deep drawing are applied simultaneously. The tool geometry is designed such a way, that due to the punch impact, the blank slides from the blank holder area into the die. As mentioned before, the blank holder is used only to prevent the formation of wrinkles. In certain tool areas however, the amount of stretching should be increased. By using a locking bead and beading rods or by applying a sufficiently high blank holder force, the blank holder acts as a brake on the blank to slow down flow of material.

**Tribology**

The process limits with the deep drawing are determined by the boundary conditions dominant in the forming zone. These depend on a variety of mutually influenced parameters. Among, the most important process parameters are tool material, sheet metal material and its surface [4] as well as lubrication. Depending on the tribological system, completely different friction conditions can be active under identical stress conditions. An essential property in the sheet metal forming process is the high value of surface to

volume ratio. This causes extended contact areas with high tribological load. As already proved, the frictional share in the total forming force increases proportionally with increasing drawing ratio [5]. Thus, the maximum drawing ratio decreases with rising component size [6], so that tribological conditions become more and more the process limiting variable. Apart from the material properties, numerous studies have already analyzed tribology as a substantial influencing factor [7].

During forming operations, sliding friction conditions with lubrication occur. In describing friction in sheet metal forming, usually the coefficient of friction is used which is expressed as friction force divided by normal force. At lower sliding velocities, dry friction conditions could apply; this means that die and blank are primarily separated by the boundary layers of a molecular order of magnitude, whereby solid body friction is also possible on a submicroscopic scale. The workpiece slides on lubricating films of molecular magnitude (i. e. on these boundary layers). With insufficient lubrication, the boundary layers may break up locally and weld joints may develop. With an increase of sliding velocity and quantity of lubricant, portions of the interface are supported by hydrodynamic fluid lubrication (boundary or mixed friction). The thickness of the lubricating film increases, but the lubrication gap still remains smaller than the total of the surface roughness of both die and blank. With further increase in the sliding velocity and with enough lubricant, complete hydrodynamic friction can be achieved in which the lubricant film becomes thicker than the sum of the surface roughness of both forming part and die. This condition, however, cannot be obtained in practical metal forming operations. The greatest influence of sliding velocity, normal stress and lubricant viscosity occurs in the area of mixed friction. In this case, the blank must contain the lubricant as long as possible in the contact area during the sliding action. Depending on the component geometry, it could be necessary to increase the friction in certain tool areas for controlling the material flow. In most of the tool areas, however, low friction between sheet metal and tool must be achieved to guarantee that high strains are obtained without tearing the sheet metal.

Friction always also results in undesirable complex wear mechanisms at the contact surfaces between die and workpiece. Especially under high contact stress conditions and low lubrication, adhesion and abrasion occur, causing the forming operation to fail, requiring the tool to be refinished. The task of lubrication is to reduce friction and to minimize wear. Lubricants are required to develop a cohesive pressure and temperature-resistant lubrication film which separates the surfaces of blank and tool. In practice the application of appropriate die materials, together with process-optimized lubricants, can result in high drawing ratios and reduce the wear of forming dies significantly.

### **Developed Test Stands**

Both for technical and economic reasons it is not possible to investigate the tribological characteristics in an actual process. Instead, simulation in a model test considering the characteristics of the forming process has proven reasonably. Therefore, suitable model tests must be developed, which enable the direct measurement of the friction. To examine the influence of individual parameters, it must be possible to vary them separately. Considering the special characteristics of the forming process, those tests must reproduce the tribological system relevant for the respective forming process.

With this aim the measuring location must be accessible and has to provide reproducible results of measurement, which are transferable to the real process. The precision and transferability of the results to the actual process depend on the test principle used.

Several studies provide good overview on the usual principles in sheet metal working [8]. They can be divided according to DIN 50322 into different categories including modeled workpieces, certain tool sections (Figure 2) and general tests [9]. Substantial result is that the request after instrumentation accessibility contradicts with transferability on the real process. For the selection of a test principle a suitable compromise between all requests must be found.

To quantitatively model the tribology, systems are generally used which represent a certain tool section. For example, the tribological contact between tool and sheet metal can be simulated by moving a tool with a normal force linearly [10] or rotationally [11] over a fixed sheet metal. However, one-sided tool contacts do not consider the tensile stress in the blank which is important for smoothing effects of the sheet metal topography [12].

Thus, strip drawing tests are developed by pulling the sheet metal through a fixed tool. To judge the locally varying tribological characteristics at certain specific areas, those tests reproduce different individual tool sections (Figure 2).

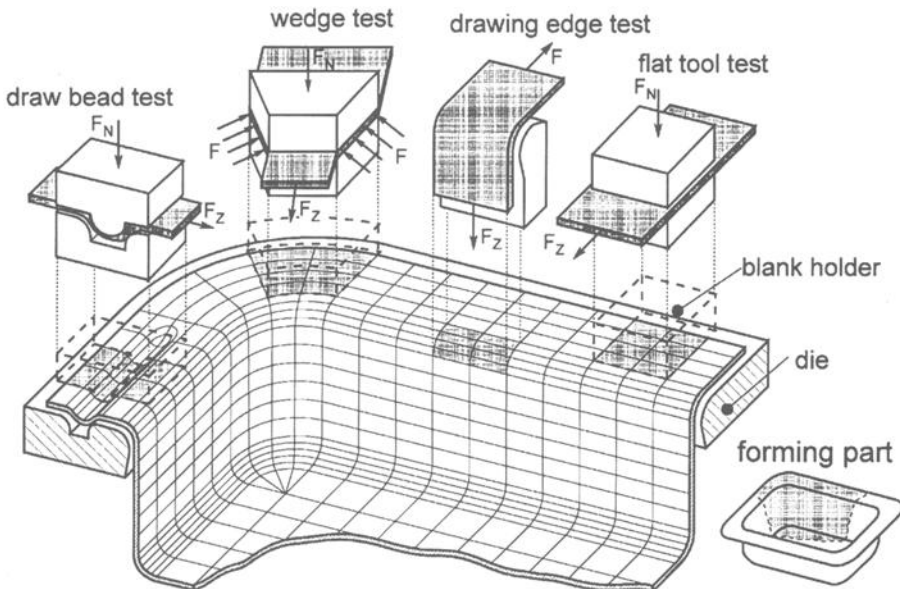


Figure 2 - Versions of Strip Drawing Tests Reproducing Different Tool Sections [13]

Using those test principles, frictional forces can be measured directly. Additionally, they offer a good reproducibility, a large consistence with the tribological conditions and these tests offer the possibility of varying the parameters individually and directly.

The Institute for Production Engineering and Forming Machines has developed specific test stands based on the principle of strip drawing. The first test stand enables single strip drawing tests for the measurement of frictional forces directly at the tools (Figure 3). This test stand renders different test configurations and tool sizes that enable the modeling of special areas of the actual tools in production. The strip drawing test with flat tools reproduces the tribological system blank holder-sheet metal-die, whereas the test with a drawing edge simulates the area of the radius of the drawing die. In addition, a strip drawing test with a draw bead may also be conducted.

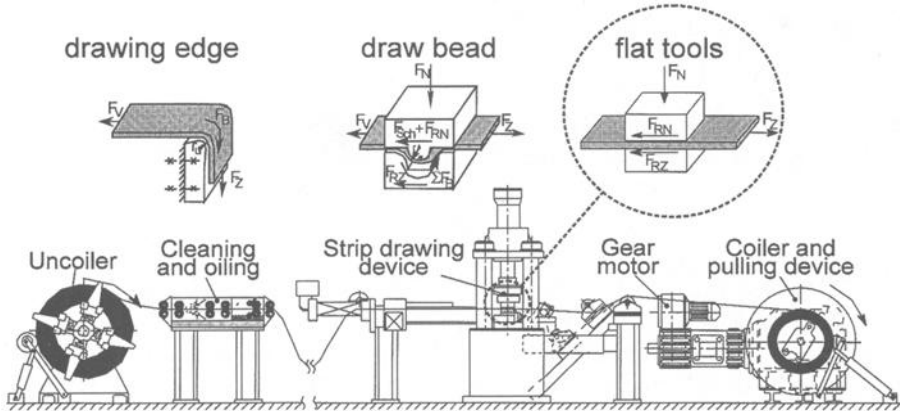


Figure 3 - Friction Test Stand

The sheet metal material is handled directly from the coil. The 100 mm broad strip passes through a combined cleaning and oiling module, in which the corrosion protection oil applied in the rolling mill is down-washed and the lubricant to be examined is applied.

The prepared sheet metal material then passes into the tool stored on dynamometers. The frictional force, the normal force and the total drawing force are measured and encoded as well as the sliding velocity. The measured data are analyzed using PC software.

For lubrication tests, the strip drawing test with flat tools is carried out as standard procedure. For each lubricant being tested, both contact normal stress and sliding velocity are varied systematically with all other conditions kept constant. Then, a plot of the friction coefficient  $\mu$  as a function of contact stress and sliding velocity is performed. Additionally, stick-slip effects may be marked. Thus, a comparison of lubricant performance is made possible on the basis of different criteria like maximum attainable contact stress, level of the friction coefficients and beginning of stick-slip.

Not only the quality but also the amount of lubricant applied to the sheet metal is of major importance. Therefore, the lubrication system of the test stand was optimized for varying the lubricant amount exactly. Using this testing procedure, the influence of lubricant quantity on the forming process can be investigated [14].

The second test stand is based on the same principle of strip drawing. In this case, however, the test stand is used to conduct an intermitting strip drawing test which enables a test of about 50.000 strokes under certain stress conditions. For simulation of high contact stress conditions, the tool geometry of this test stand reproduces the tool area die / blank holder and the following drawing edge [15]. The long-time test is realized using a cam driven crank lever with pneumatically acting clamping jaws. This procedure is similar to the real deep drawing process where new material is transported continuously into the forming zone. This test has been developed for investigation of the wear behavior of tools [16] and the galling behavior of sheet coatings with respect to the influence of different lubrication systems.

### Experimental Results

Five different, typical lubricants of the German sheet metal processing industry were investigated and compared on the friction test stand. For verification of the model test, the results were correlated to the forming capacity of two model workpieces using these lubricants.

#### *Frictional Investigations*

For frictional investigations, five typical lubricants with different viscosities were selected from the automotive industry. The test matrix contains a low viscosity slushing oil, two Prelubes with low drawing properties, a low viscosity drawing oil and a special high viscosity drawing oil for complex forming operations (Table 1).

Table 1 - Investigated Lubricants

Test indication	Description	Viscosity at 40°C
Lub A	Slushing oil	36 mm <sup>2</sup> /s
Lub B	Prelube	53 mm <sup>2</sup> /s
Lub C	Prelube	83 mm <sup>2</sup> /s
Lub D	Drawing oil	120 mm <sup>2</sup> /s
Lub E	Special drawing oil	420 mm <sup>2</sup> /s

All lubricants were tested on the same electrolytically alloy galvanized sheet material with the tool material being a globular gray cast iron GGG 60, which is often used in the German automobile industry. A lubricant amount of 2 g/m<sup>2</sup> was kept constant during all tests.

In Figure 4 the friction coefficient  $\mu$  is plotted as a function of contact stress for all five lubricants. These tests were performed at a sliding velocity of 50 mm/s. For all lubricants, the friction coefficient decreases slightly with higher loads. The plotted curves are limited by the normal loads, which are too high for sliding friction. Above this limit, the strip adheres to the tool and tears. Besides the frictional coefficient, this limit is very important for the forming process, and it is indicated as the maximum attainable contact stress.

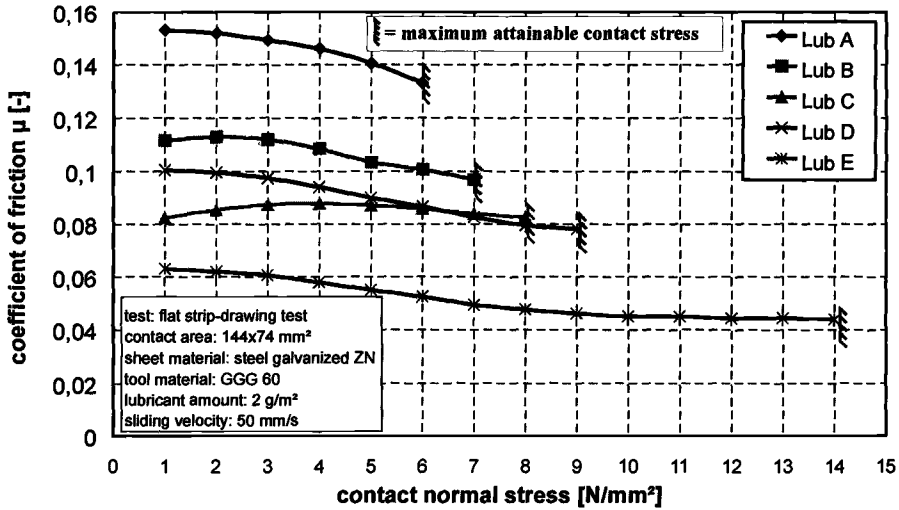


Figure 4 – Friction Result for Different Lubricants

The influence of the viscosity is obvious. The higher the viscosity of the tested lubricant, the lower is the friction. In addition, the tribological system reaches higher contact stresses under sliding conditions. Compared with the slushing oil, frictional forces can be halved by using the special deep drawing lubricant E of high viscosity. Furthermore, the system reaches more than the double maximum contact stress.

Lubricant C deviates slightly from the other lubricants. Compared to lubricant D, lower friction is achieved at low contact pressures. This turns at high surface pressures. Friction is little higher and the tests attain a lower maximum contact stress than lubricant D. Obviously, the frictional behavior of the two lubricants depends on the contact pressure conditions.

For all lubricants, there is mixed friction. While the major part of the contact area slides on a lubricating film of molecular magnitude, higher lubricant viscosity increases hydrodynamic lubrication. With higher viscosity a greater part of the interface is supported by hydrodynamic fluid lubrication, so that the total friction force is reduced.

For using the results of those model tests, it is necessary to know to which extent these tests reproduce the frictional conditions of an actual process. Therefore, the results must be compared with drawing results of actual formed parts.

### Model Forming Parts

Also actual formed parts may be used for evaluation of tribological properties. By creating performance flowcharts with crack boundaries or measuring the maximum attainable drawing depth, conclusions on the friction performance can be made. Thus, a frictional ranking of the lubricants can be obtained. In these investigations, a rotationally symmetric cup and a drawing workpiece (pedal pot) were selected because it is known they fail due to high friction under the blank holder (Figure 5).

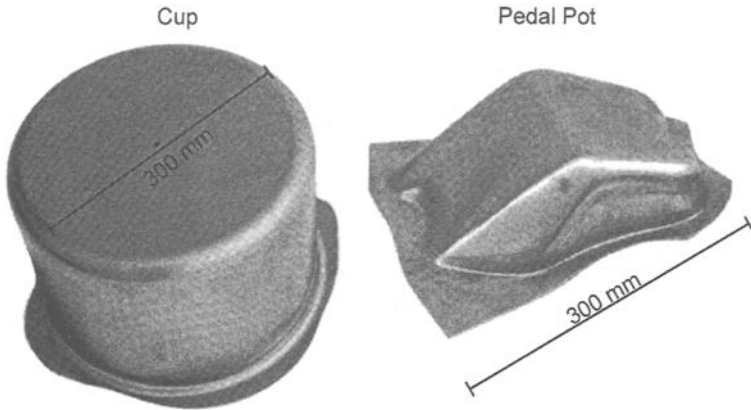


Figure 5 – Selected Forming Parts

To receive accurate results, the cup should be as large as possible. With increasing cup diameter, the forming ratio increases linearly, while the proportion of the friction increases exponentially in a squared relationship. Thus, a drawing tool with a punch diameter of 300 mm and a blank diameter of 600 mm was chosen. To examine the influence of drawing velocity, punch rates of 4 and 40 mm/s were investigated. In Figure 6 the drawing depths for the different lubricants at which first cracks occur, are shown.

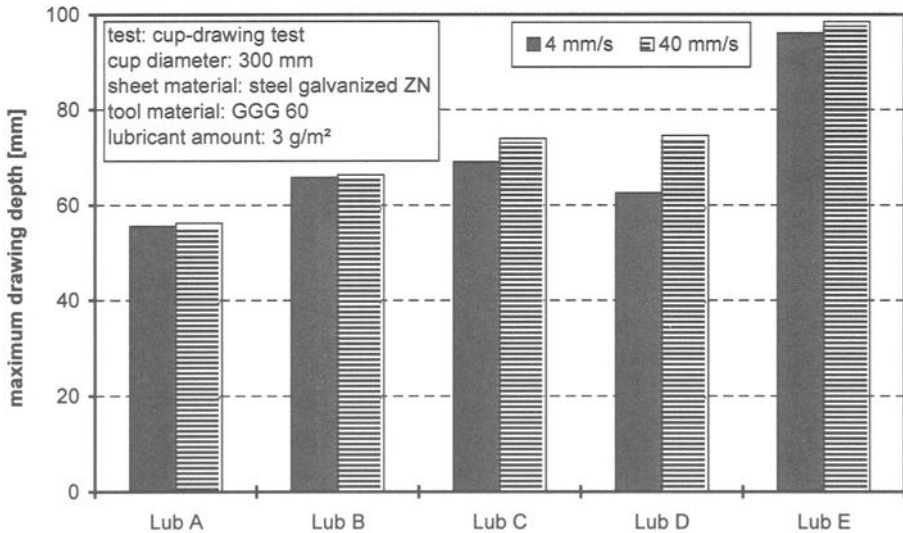


Figure 6 – Drawing Depth for Different Drawing Velocities

All trials demonstrate the influence of the viscosity. The higher the viscosity of the tested lubricant, the higher is the attainable drawing depth of the cup. This is due to the fact that, in conformity with the friction tests, a high viscosity results in low friction

under the blank holder supporting material flow. Thus, the blank material flows more easily over the drawing edge of the die. The total force is reduced and the process limit is achieved at higher drawing depths. Consequently, application of a higher viscosity lubricant enlarges the process limits and enables more complex geometries to be processed. Also the influence of the drawing velocity is to be detected clearly, the trial with lubricant D at 4 mm/s may only vary slightly.

A second test series was executed with an actual component, the pedal pot. In contrast to the cup a performance flowchart was created. Therefore, the blank holder forces must be determined, when the forming part does not tear and when no wrinkles occur under the blank holder. Between these two boundaries, workpieces can be produced without failure.

For this test, a series of drawing experiments was conducted with the five lubricants on 5 different blank sizes. The drawing depth of the workpiece of 75 mm was kept constant in all tests. The ratio of the flat blank area and the cross section of the workpiece is indicated as related drawing ratio  $\beta^*$ . With increasing drawing ratio, the forming stress grows, so that the workpiece tends to fail earlier. By increasing the blank holder force incrementally the crack and wrinkle limits can be identified for each lubricant. The performance flowchart of each lubricant is constructed by plotting both boundaries over the drawing ratio. The results of the lubricants A, C and E are presented in Figure 7.

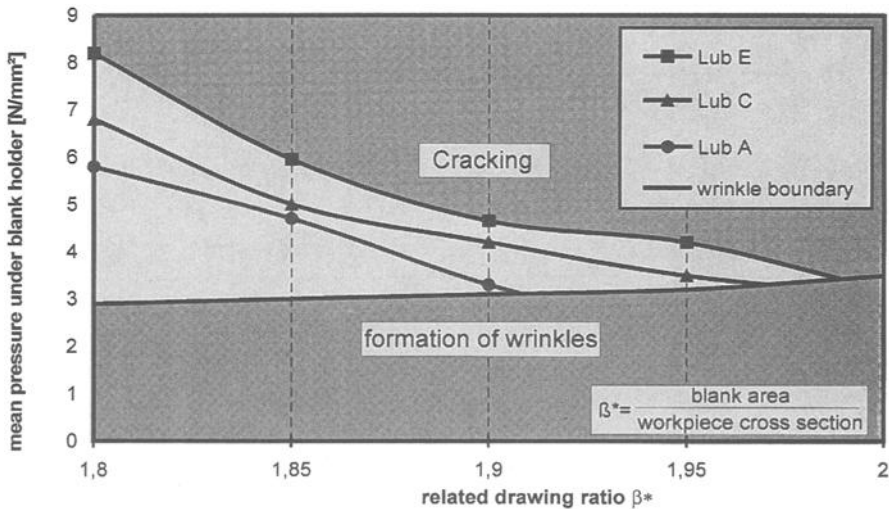


Figure 7 – Performance Flowchart Drawing a Real Component

Obviously, the limiting surface pressure under blank holder for workpiece cracking is reduced for all lubricants with increasing drawing ratio. This is due to the fact that the deformed metal volume rises with higher drawing ratio and the forming share becomes increases as the limiting factor. Hence, the required force increases and the workpiece cracks at a lower surface pressure. The wrinkle boundary does not depend on the

lubricant. Below a surface pressure of approx. 3 N/mm<sup>2</sup>, wrinkles occurred with all lubricants.

Also, the influence of lubrication can be seen in Figure 7. First of all, regarding a certain drawing ratio, the workpiece starts cracking at higher surface pressures with increasing viscosity. Thus, being able to apply a higher blank holder load, the geometrical precision of the forming process can be improved. Furthermore the process limits are wider. This contributes to a higher process stability, because the process is less sensitive to disturbances.

At higher drawing ratios, the difference between lubricants is lower, because the frictional share in the total force is reduced. Nevertheless, using a lubricant with higher viscosity at a certain blank holder load, the maximum drawing ratio increases. This results in higher attainable drawing depths, which corresponds with the results of the drawing cup.

#### *Comparison and Verification*

The results of both test series are compared in Table 2 to those of the strip drawing tests. The friction results are represented by use of mean friction coefficient (from 1 to 6 N/mm<sup>2</sup>) and the maximum attainable contact stress. From cup drawing test, the drawing depth is taken and from the pedal pot tests the maximum surface pressure under the blank holder at a related drawing ratio of 1.85 is used.

Table 2 – *Comparison of Experimental Results*

lubricant	strip drawing		pedal pot	cup
	mean friction coefficient [-]	maximum contact stress [N/mm <sup>2</sup> ]	maximum contact pressure [N/mm <sup>2</sup> ]	maximum drawing depth [mm]
Lub A	0.146	6.0	4.7	57
Lub B	0.108	7.0	4.9	66
Lub C	0.086	8.5	5.0	74
Lub D	0.095	9.0	5.5	75
Lub E	0.059	14.0	5.9	98

The results of lubricant E are used as a reference and set to 100%. The remaining results were referred to this result as shown in Figure 8. The friction coefficient should be as low as possible for a favorable assessment of a lubricant, the remaining sizes as high as possible. In order to increase the clarity, the reciprocal value of the coefficient of friction was represented. Thus, a lubricant is favorable at high reciprocal values.

For maximum attainable contact normal stress, the same ranking of the lubricants results as for the cup and the pedal pot. The ranking of the coefficient of friction deviates slightly with the lubricants C and D. Taking the results of cup and pedal pot as a reference, coefficients of correlation of the strip drawing results are calculated to this reference. The correlation of the maximum attainable contact stress amounts to 0.98 respectively 0.90, the friction coefficient amounts to 0.98 respectively 0.89. This is due

to the lower viscosity lubricant C which produces very low friction in the strip drawing test at low loads, which contradicts to the drawing result of both forming parts. However, the frictional behavior at high loads is more important for cracking criteria, and at high load the friction of this lubricant is worse. This fact is completed by a lower achieved contact stress. When correlating frictional results directly with process limits of actual forming process, the frictional behavior at high loads should be preferred, especially the maximum attainable contact stress.

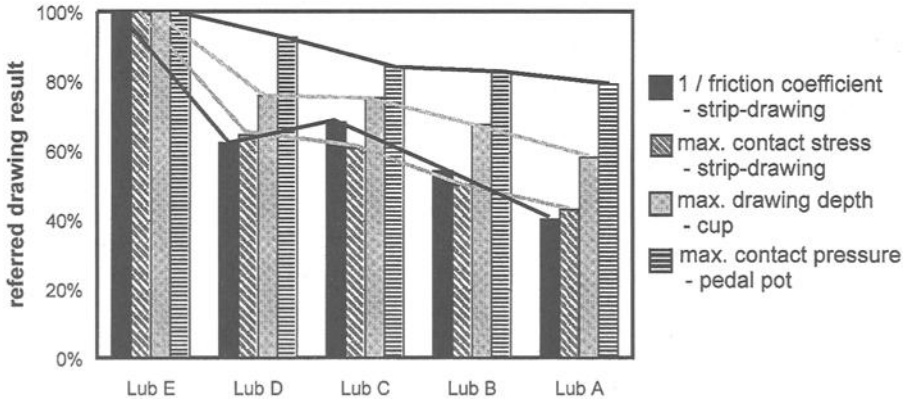


Figure 8 – Comparison of Friction Test and Drawing Tests of Real Forming Parts

Nevertheless, both criteria of the strip drawing test correlate well with the results of the model workpieces. This result and further experiences prove that the strip drawing test is suitable for illustrating friction conditions in complex tools.

Due to the good transferability of the strip drawing results on actual forming processes, this friction test was taken as the testing guideline of the VDA (Federation of the German Automobile Industry) for Prelubes. In this guideline, it is specified that the performance of new Prelube candidates in this testing procedure well be used to compare with results of already existing lubricants.

**Summary**

A test stand was described, which simulates the tribological system appearing in sheet metal forming processes. A number of typical lubricants used in the German automobile industry were investigated and compared. The results were verified subsequently with drawing results of two forming parts.

Both criteria from the strip drawing test correlate well with the drawing results of the model forming parts. This indicates that the strip drawing test is suitable for simulating friction conditions in complex deep drawing tools.

Using this testing procedure, the capability of lubricants for sheet metal forming can be tested under all relevant conditions and their suitability for certain applications can be estimated.

**References**

- [1] Nakawaga, T., "Recent Development in Auto-Body Panel Forming Technology," *Annals of the CIRP*, STC-F Keynote paper, 1994.
- [2] Staeves, J., and Filzek, J., "Surface Qualification in the Sheet Metal Domain," *Proceedings She Met*, 1998.
- [3] *Schuler – Metal Forming Handbook*, Springer-Verlag Berlin Heidelberg 1998.
- [4] Filzek, J., and Schmoeckel, D., "Function-oriented Surface Parameters for Sheet Metal Forming," *Proceedings 6<sup>th</sup> ICTP*, Volume 3, 1999, pp. 2169-2174.
- [5] Siebel, E., and Mertlik, H., "Friction Conditions in Deep Drawing," (German), *Report of European Research Association for Sheet Metal Forming*, Germany, 1953, pp. 245-250.
- [6] Withhüser, K.-P., "Investigation of Test Methods for Assessing the Tribological Conditions in Deep Drawing," (German), Ph.D. thesis, University of Hannover, Germany, 1980, pp. 18-23.
- [7] Wilson, W.R.D., "Tribology in Sheet Metal Forming," *Proceedings 1<sup>st</sup> ICTMP*, 1997, pp. 1-8.
- [8] Schey, J. A., "The Applicability of Tribotesters to Sheet Metal Working," IDDRG Work Group Meeting, Colmar, 1995.
- [9] Staeves, J., "Assessment of Sheet Topography with Regard to Friction During Forming Process," (German), Ph.D. thesis, Darmstadt University of Technology, Germany, Shaker-Verlag Aachen, Band 41, 1998.
- [10] Heide van der, E., and Huis in 't Veld, A. J., "A New Test Method for Ranking Sheet Metal Forging Lubricants," *Proceedings 1<sup>st</sup> ICTMP*, 1997, pp. 104-107.
- [11] Emmens, W. C., "Tribology of Flat Contacts and its Application in Deep Drawing," Ph.D. thesis, University of Twente, The Netherlands, 1997.
- [12] Bay, N., and Wanheim, T., "Real Area of Contact and Friction Stress at High pressure Sliding Contact," *Wear*, 1976, pp. 201-209.
- [13] Netsch, Th., "Method for Determination of Friction Models for Sheet Metal Forming," (German), Ph.D. thesis, Darmstadt University of Technology, Germany, Shaker-Verlag Aachen, Band 27, 1995.
- [14] Staeves, J., and Schmoeckel, D., "Determination of the Minimum Quantity of Lubricant for Sheet Metal Forming," *Proceedings 1<sup>st</sup> ICTMP*, 1997, pp. 340-345.
- [15] Hortig, D., and Schmoeckel, D., "Analysis of Local Loads on the Draw Die Profile with Regard to Wear Using the FEM and Experimental Investigations," *Proceedings She Met*, 1999, pp. 193-202.
- [16] Schulz, A., Stock, H.-R., Mayr, P., Staeves, J., and Schmoeckel, D., "Deposition and Investigation of TiN PVD Coatings on Cast Steel Forming Tools," *Surface and Coatings Technology*, 1997, pp. 446-450.

R. W. Snidle,<sup>1</sup> H. P. Evans,<sup>1</sup> and M. P. Alanou<sup>1</sup>

## **Determination of Gear and Bearing Material Scuffing Limits Using High-Speed Disk Machines**

---

**Reference:** Snidle, R. W., Evans, H. P., and Alanou, M. P., “**Determination of Gear and Bearing Material Scuffing Limits Using High-Speed Disk Machines,**” *Bench Testing of Industrial Fluid Lubrication and Wear Properties Used in Machinery Applications, ASTM STP 1404*, G. E. Totten, L. D. Wedeven, J. R. Dickey, and M. Anderson, Eds., American Society for Testing and Materials, West Conshohocken, PA, 2001.

**Abstract:** The paper describes the design of disk machines which are used to simulate the contact and scuffing conditions in high-speed aerospace gears and rolling contact bearings. In ground gears the surface finish of the teeth is predominantly in the direction perpendicular to that in which rolling and sliding takes place, and in order to reproduce this configuration in disk tests it is necessary to axially grind the specimens. This has been achieved using a novel grinding/generating process which also gives a self-aligning crowned geometry, thus avoiding spurious edge effects. In the case of rolling element bearings, surface finish is generally of a much higher quality with finish predominantly in the rolling direction. The disk machine developed for simulation of this type of contact therefore uses honed/polished surfaces. Results obtained from the disk machines are shown corresponding to typical high-speed/high-temperature conditions found in aerospace practice.

**Keywords:** gears, rolling element bearings, scuffing, lubricant testing

### **Introduction**

The performance of gears and rolling element bearings is often limited by scuffing, defined as localized surface damage caused by solid-phase welding [1]. Scuffing is a form of surface distress associated with breakdown of the lubrication mechanism, which in components operating at moderate to high speeds is elastohydrodynamic lubrication (EHL). The occurrence of scuffing is a serious tribological problem since it can lead to rapid wear and complete deterioration of the surfaces involved. This form of surface failure can occur at any stage in the life of machinery and the inability, as yet, to fully understand the mechanism of scuffing and predict its occurrence on the basis of a theoretical model is an obstacle to further development of gearing and bearings, particularly for demanding applications such as high-speed, high-temperature transmissions used in aero gas turbines, for example. There is therefore a clear need for test methods which can be used to evaluate scuffing limits for particular combinations of materials,

---

<sup>1</sup>School of Engineering, Cardiff University, Cardiff CF2 3TA, UK

lubricants and surface treatments under conditions which simulate, as closely as possible, the real operation of gears and bearings. The use of actual gears and large bearings is relatively expensive and disk tests are often used as a cheaper alternative. Disk rigs can be used to simulate the rolling/sliding kinematics of gear tooth contacts at any particular instant during the meshing cycle, but a specific criticism made of conventional tests of this type in which the disks are prepared by circumferential grinding is that the orientation of the resulting grinding marks does not correspond to the situation in the majority of gears where rolling and sliding takes place at right angles to the finish. A further complication of cylindrical disks is the effect of edges and the difficulty of arranging a uniform distribution of load across the elastic contact. This leads to scatter in the scuffing loads.

These issues have been addressed in a program of work at Cardiff University where a special high-speed disk machine has been designed in which the disks are effectively axially finished and crowned to give a truly self-aligning contact with finish in the correct direction. Scuffing tests have been carried out to cover the range of operating conditions present in very high-speed aerospace gears and bearings using both case-carburized and nitrided steels with gas turbine engine oil as the lubricant. The performance of conventionally ground surfaces has also been compared with superfinished disks and this shows a typical doubling of the scuffing load capacity when the surface finish is improved in this way. The same arrangement is also being used in a developed version of the principle as a fatigue rig for determination of micropitting wear limits of different steels and finishes including diamond-like coatings.

### **High-Speed Disk Machine for Gear Tooth Contact Simulation**

The two-disk machine was designed and built with the aim of simulating gas turbine engine gearing conditions, in terms of contact stress, sliding and rolling speeds, and oil temperature as closely as possible. An illustration of the test head of the machine is shown in Figure 1. The disks are 76.2 mm diameter and 10 mm wide and are driven from a power recirculating gearbox. The ratio of the speeds of the two shafts may be pre-set from unity (pure rolling) up to a value of almost five. In the work reported here the ratio of the speeds was 4.24 which gives a slide/roll ratio (defined as the ratio of the relative sliding speed to the mean entraining velocity at the contact) of 1.24. One shaft is supported on fixed bearings and the second shaft is mounted in a swinging yoke. Load is applied to the contact between the disks by means of a push rod and hydraulic cylinder acting on this yoke and the load is monitored by an electronic load cell placed between the ram and push rod. Both disks are "crowned" with a transverse radius of curvature of 304.8 mm so that the dry (Hertzian) contact between the disks is an ellipse of aspect ratio of about 4:1 with its major axis parallel to the axes of the disks. The maximum load that is normally applied to the contact in scuffing experiments is 4150 N which produces a corresponding maximum Hertzian contact pressure of 1.7 GPa. At this load the major and minor axes of the contact ellipse are 4.3 mm and 1.1 mm, respectively. This leaves a margin of about 3 mm on either side of the contact to allow for development of the load capacity up to a contact pressure of 2 GPa in micropitting experiments. The maximum speed of the machine is 12,000 rpm on the faster disk.

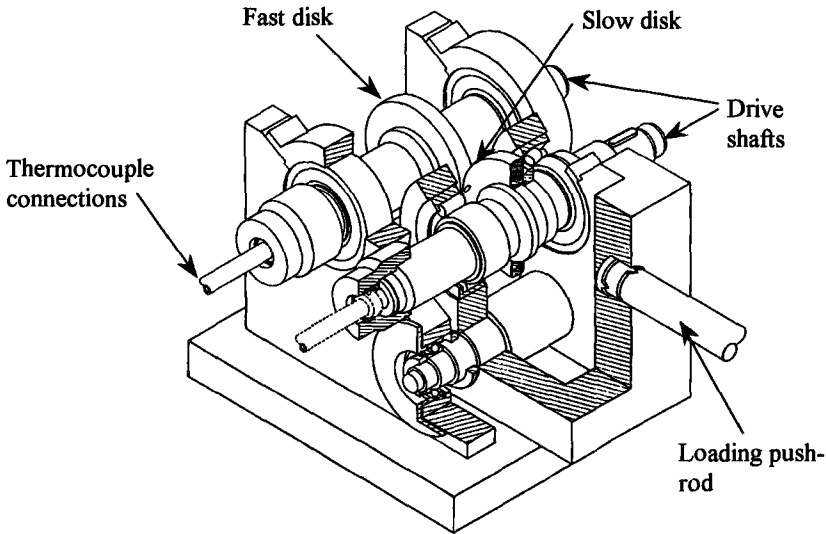


Figure 1 – Test head of disk machine

**The Test Disks**

The disks are typically of alloy steel to the specification shown in Table 1 which is a steel commonly used in gas turbine gearing (nitriding steel has also been tested).

Table 1 - Typical composition of steel used for the test disks

Element	C	Si	Mn	P	S	Ni	Cr	Mo
%	0.16	0.23	0.40	0.01	0.006	4.05	1.20	0.25

After initial machining the disks are case-carburized, hardened and tempered in accordance with the gas turbine engine manufacturer's specification. This involves a final sub-zero quench and tempering at 250 °C. The hardness of the surfaces of the disks is typically 640 Vickers hardness No. (HV10). Following heat treatment the bores of the disks are finished by internal grinding, and then pressed and clamped on to the removable test shafts of the disk machine. A sample of ground disks may be "etch inspected" as a check for possible grinding burns. Several pairs of shafts are available so that a batch of disks can be mounted upon the test shafts for finishing. Final grinding of the working surfaces of the disks is carried out on the test shafts, and this ensures accurately concentric running of the disks in the test head at high speeds.

The disks are finished in a specially devised grinding rig as illustrated in Figure 2. The abrasive wheel is diamond dressed to the form of an internal cone. This arrangement generates the desired crown on the disks (which prevents unpredictable edge effects when

the disks are in contact) and also gives grinding marks in an approximately axial direction. The orientation of the finish on the disks is therefore transverse to that of rolling/sliding which is the situation in conventional involute gears. The magnitude of the crowning radius is determined by the angle to which the abrasive wheel is dressed and the setting height of the axis of the disk relative to that of the abrasive wheel. The crown radius is checked by taking an axial profile of the disk using an accurately calibrated profilometer. Typical axial and circumferential profiles from a disk prepared in this way are shown in Figure 3 (a) and (b), respectively. By using abrasive wheels to the same specification as used in the finishing of the gears of interest it is possible to reproduce the finish of the target gears in terms of the roughness average (Ra) value. The ground disks used in our work are typically finished to an Ra of  $0.4 \mu\text{m} \pm 0.05 \mu\text{m}$  (cut-off=0.25 mm).

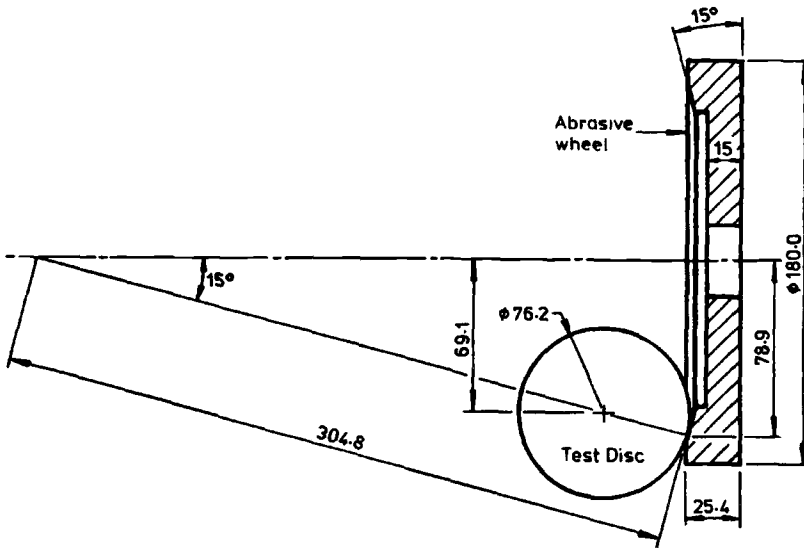


Figure 2 - Arrangement for grinding the test disks (dimensions in mm)

After finishing in this way a batch of ground disks may be further processed by polishing or hard coating in order to investigate ways of improving scuffing resistance of a given steel/oil combination. A technique that has been found particularly beneficial is superfinishing using a mild abrasive process. In this method the disks are immersed in a vibrating bath containing water, abrasive powder and small zinc "chips". After several hours of this treatment the disks take on an almost mirror finish. A typical circumferential profile from a disk which has been polished in this way is also shown, for comparison, in Figure 3 (c). It should be noted that this profile and the profile from the ground disk are shown at the same magnification. Axial traces from polished disks showed that polishing produced no significant effect on the crown radius or overall dimensions. Gears have also been superfinished using this process which produces no significant reduction in the accuracy of the tooth profile (approximately  $2 \mu\text{m}$  is removed from the surface) and gives a marked increase in pitting endurance [2].

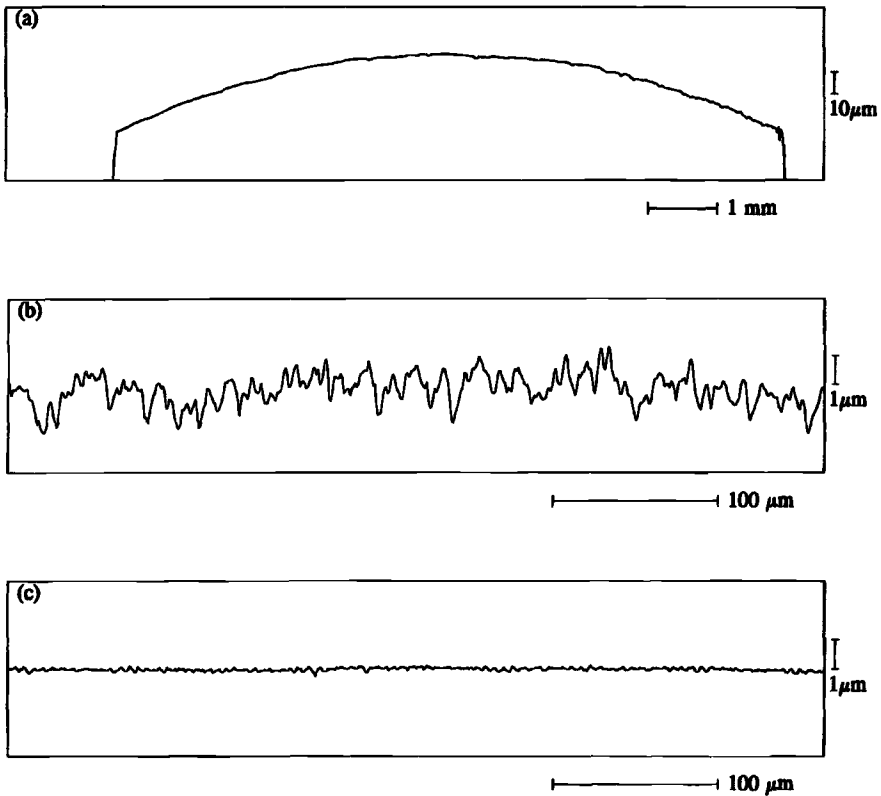


Figure 3 – Surface profile of the test disks. (a) and (b) axial and circumferential profiles, respectively, of ground disk; (c) circumferential profile of superfinished disk.

The test disks are provided with embedded thermocouple junctions mounted in small copper ferules which are then pressed into small holes 3 mm below the working surfaces on the center of the running track. This ensures a good mechanical anchorage and thermal contact between the thermocouple and disk. Connections to the thermocouples are made through shafts (shown in Figure 1) and silver-graphite slip rings. The bulk temperatures of both disks are continuously recorded.

Tangential frictional traction due to sliding between the disks is measured by means of a torque dynamometer mounted in the drive shaft of the slower moving disk shaft. This device measures the friction of the bearings supporting the slower disk in addition to the frictional traction. The bearing and slip ring friction component of the measurement is carefully calibrated as a function of load and speed by rolling the two disks together with the drive to the fast disk disconnected. The bearing/slip ring friction recorded in this case may then be assumed to be twice that for the slow shaft bearings since the support bearings

for the two shafts are identical. The total shaft friction is continuously recorded during the test.

A recent development of the disk rig involves complete computer control of its operation together with fully automated data acquisition. This allows programming of a standard loading sequence, for example, and automatic detection of scuffing from the friction torque together with rapid unloading to prevent undue damage to the surfaces which can then be possibly re-used after grinding.

### Typical Results

Scuffing is provoked in the tests by running the disks at constant speed and increasing the load between them at 3 minute intervals according to a loading sequence in which the maximum Hertzian contact pressure is increased in steps of 0.1 GPa, starting at a value of 0.6 GPa and proceeding to a maximum value of 1.7 GPa or until scuffing is detected. The lubricant used in all the tests conducted so far is Mobiljet II, a synthetic gas turbine engine oil with a nominal viscosity of 5 cSt at 100 °C. In the majority of tests the oil is heated and supplied to the test disks at a temperature of 100 °C. Oil is circulated through the test head with the disks rotating in contact at a light load until the temperatures of both disks stabilize. The first load stage of the standard sequence is applied and held constant for 3 minutes. The load is then increased and the process repeated. A typical record of the progress of the final stages of a scuffing test is shown in Figure 4. This shows that after an increase in the load there is a corresponding increase in friction and the temperatures of both disks (it should be noted that the pen positions of the recorder are offset and changes to each trace start at the time that the load increment is applied). At light loads the temperature of the slower disk is higher than that of the fast disk, but at heavier loads the faster disk achieves the higher temperature.

A further feature of the tests is that at lower loads an increase of load produces a rapid rise in both friction and temperature which then level off to a steady value. At the higher load stages, however, there is a tendency for the friction and bulk temperatures of the disks to rise and then fall back to lower values. This is attributed to a "running in" effect during which, it is suggested, the surface conditions improve, so reducing friction and the generation of heat.

The process of gradually increasing load eventually leads to scuffing failure which causes an unmistakable sharp rise in friction accompanied by corresponding rapid increases in the temperatures of both disks as shown in Figure 4. At this stage the load is quickly released and the test stopped. The bulk temperature of both disks then falls rapidly. The test illustrated was run with a medium sliding speed of 16 m/s and entraining speed of 13 m/s. Scuffing occurred approximately 35 seconds after application of the eighth load stage (1850 N, maximum Hertzian pressure of 1.3 GPa). Circumferential profilometer traces from the disks used in this test are shown in Figure 5. Both traces are from the faster disk. Trace (a) was taken from the disk before the test was run and trace (b) was taken from an un-scuffed part of the running track after the test was completed. These two profiles show the significant modification to the surface caused by the running in effect. For each load stage the friction force is calculated by taking the mean friction force as shown on the recordings and adding a correction for bearing friction as described above.

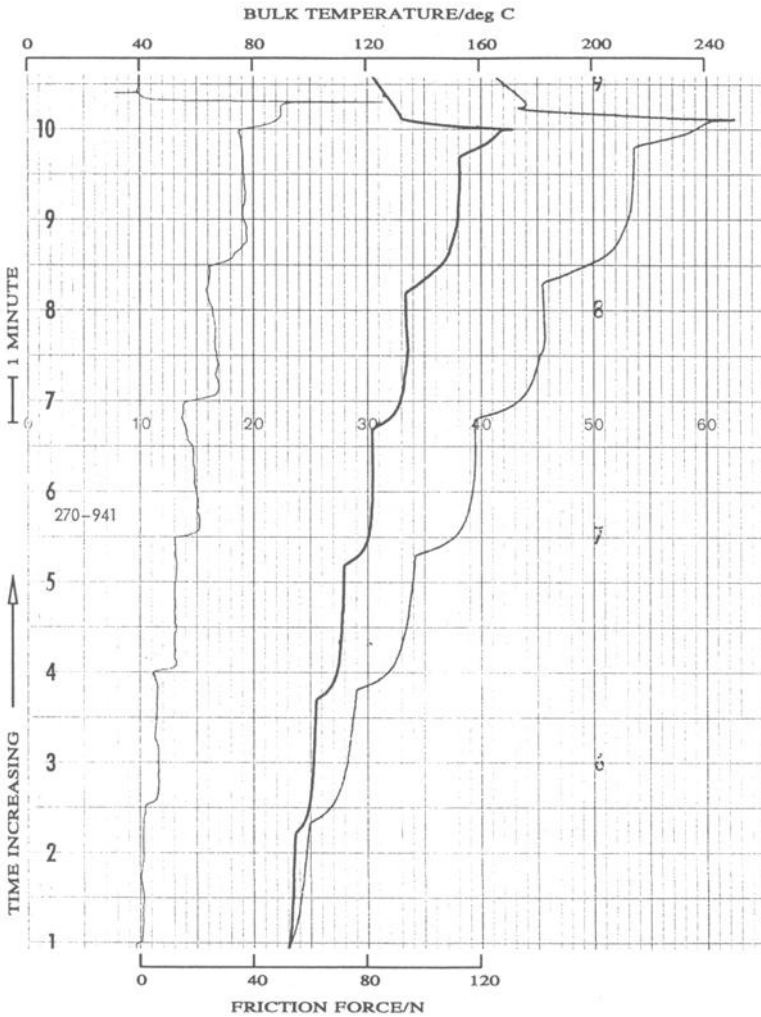


Figure 4 - Record of final stages of a scuffing test with ground surfaces. The friction trace is on the left; disk bulk temperatures (slow and fast) are on the right.

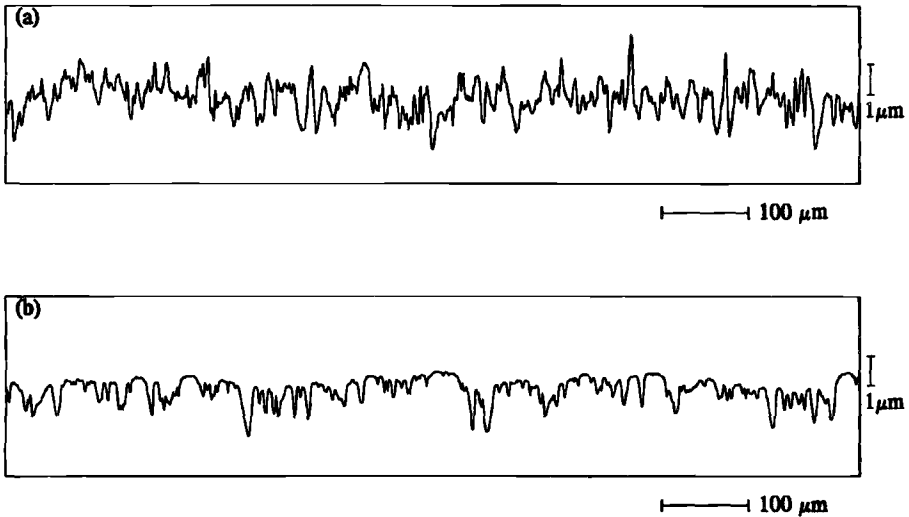


Figure 5 - Surface profiles from a ground disk used in a scuffing test. (a) un-run surface of fast disk; (b) run-in but un-scuffed part of fast disk.

Tests have also been carried out with superfinished disks. The test record shown in Figure 6 was also carried out at a sliding speed of 16 m/s. Scuffing occurred in this test at the 4150 N load stage, which is four load stages higher than the corresponding test with ground surfaces. The behavior of both friction and bulk temperature is similar to that with ground surfaces, but the temperatures and friction are much lower throughout the test. At the same load the friction with superfinished surfaces is less than half that for ground surfaces. Circumferential profilometer traces from the superfinished surfaces are shown in Figure 7. These profiles show little evidence of surface changes as a result of running. Because of the relatively high vertical magnification of these profiles the underlying long wavelength structure of the surface is evident. The significantly lower temperatures generated with superfinished disks are associated with reduced friction as measured directly. Some detailed results of tests carried out using this rig are given in references [3-5]. The effect of superfinishing of gears on frictional losses has also been investigated [6] where it is found that superfinishing can reduce frictional power by up to about 30%.

### High-Speed Ball Thrust Bearing Simulation Rig

This rig, which is also a two disk arrangement, was designed for determination of scuffing P-V (product of maximum Hertzian contact pressure in MPa and relative sliding speed in m/s) limits. The layout of the rig is shown in Figure 8. The smaller roller (40 mm diameter) simulates the ball and the larger roller (100 mm diameter) represents the raceway component. In order to provide a nominal point contact between the rollers the larger specimen is crowned with a radius of 150 mm. The resulting radii of relative curvature at the contact are therefore 14.29 mm in the rolling direction and 150 mm in the transverse

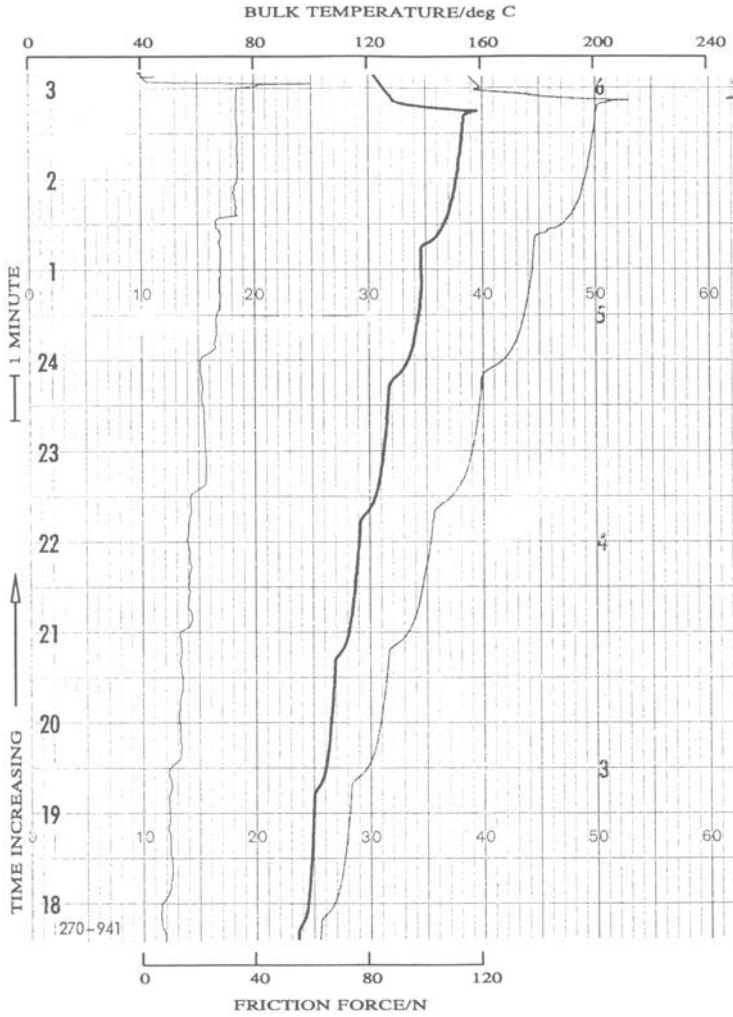


Figure 6 - Record of final stages of a scuffing test with superfinished surfaces. The friction trace is on the left; disk bulk temperatures (slow and fast) are on the right.

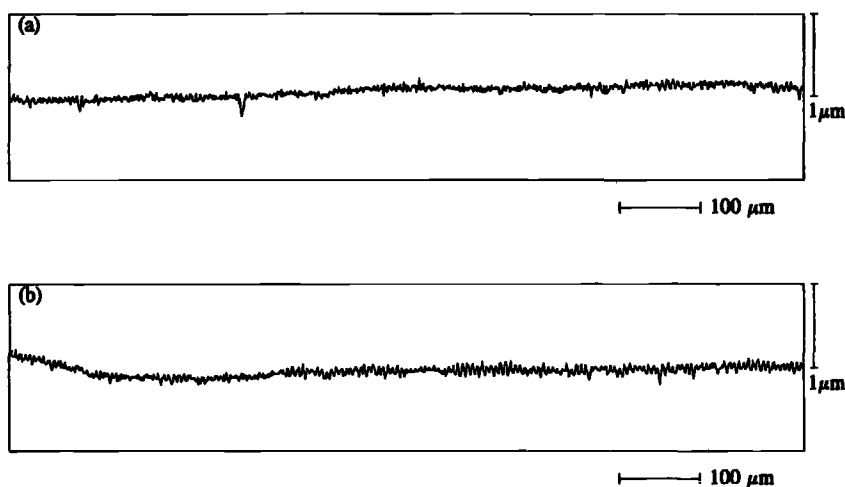


Figure 7 - Surface profiles from a superfinished disk used in a scuffing test. (a) un-run surface of fast disk; (b) run-in but un-scuffed part of fast disk.

(axial) direction which gives an equivalent Hertzian contact having axes in the ratio of approximately five, with rolling in the direction of the minor axis of the contact as in a ball bearing. At a Hertzian dry contact pressure of 2.0 GPa the contact semi-dimensions are predicted to be approximately 2.4 mm in the axial direction and 0.5 mm in the rolling direction. To ensure precise rotation of the test rollers at high speeds they were designed with integral shafts with the working surfaces and bearing locations finish ground on dead centers. The smaller of the two rollers was made sufficiently wide to accommodate two separate test tracks and provision was made in its bearing housing to offset it axially relative to the crowned roller. This allows two tests to be carried out on the small roller. Only one test per crowned roller was possible. In the series of tests carried out in this work the rollers were of M50 bearing steel manufactured and finished to aerospace bearing specification. The smaller roller was provided with drilled holes for location of embedded thermocouples which were connected to signal processing hardware via slip rings. The larger roller was not provided with embedded thermocouples but its surface temperature was measured using a thermocouple trailing on its running track. The rollers are gear-connected in the ratio 1.62 so that the ratio of their surface speeds is 4.04. This gives a slide/roll ratio at the contact of 1.21. The rollers are driven by a variable speed motor capable of speeds of up to 9000 rpm. The larger roller runs directly on needle roller bearings and the smaller roller runs on double-row spherical roller bearings. The rollers are connected to the drive gears via flexible couplings as shown in Figure 8.

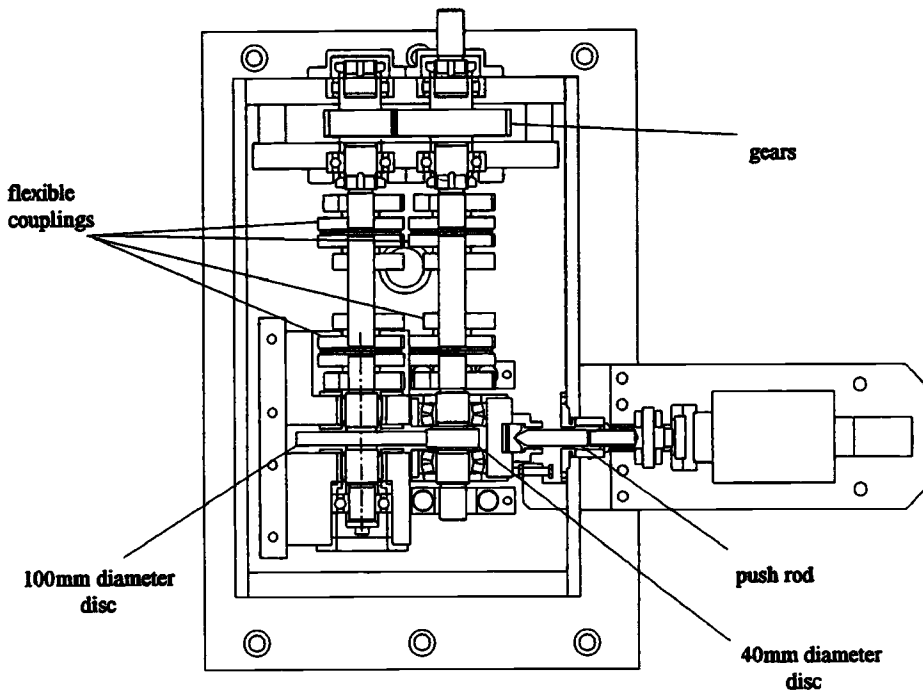


Figure 8 - *Layout of high-speed ball thrust bearing simulation rig*

The bearings supporting the shaft of the smaller roller are mounted in a housing that is free to swing so as to bring the rollers into contact. Load is applied through this housing to the contact by a hydraulic ram via a pressure control valve. The maximum load applied is 5.5 kN which gives a maximum Hertzian pressure of 2.1 GPa at the contact. Under conditions of scuffing failure a quick-release valve can be operated to rapidly unload the rollers. The test oil (Mobiljet 2) is supplied from a heated tank and pumped through a steel mesh filter rated at 1  $\mu\text{m}$ . In the tests carried out the oil temperature was 80  $^{\circ}\text{C}$ . Data from the rig may be continuously recorded for later processing. The quantities recorded are motor speed, contact load, roller temperature and motor torque. The latter quantity is regarded as an approximate, qualitative measure of friction at the contact since it is simply a measure of motor current and does not take account of bearing and other losses. Development of this rig will include a torque transducer in the shaft of the lower speed roller for measurement of contact friction.

Results of a typical test using this rig are shown in Figure 9. The figure shows the progress of a test run at a very high sliding speed of 30 m/s. Following an increase in load a corresponding rise can be seen in the temperature of both rollers. The temperature of the larger, faster roller is higher than that of the smaller, slower roller and this was the case in all tests carried out so far. The difference in the temperatures increases at the higher loads. The friction trace is treated as a qualitative indicator only as stated above, but there is a

clear increase in the mean friction force as the load is increased. The sequence of increasing loads continues until scuffing is detected, which in this test was shortly after the application of the fourteenth load stage corresponding to a maximum Hertzian pressure of 1.8 GPa.

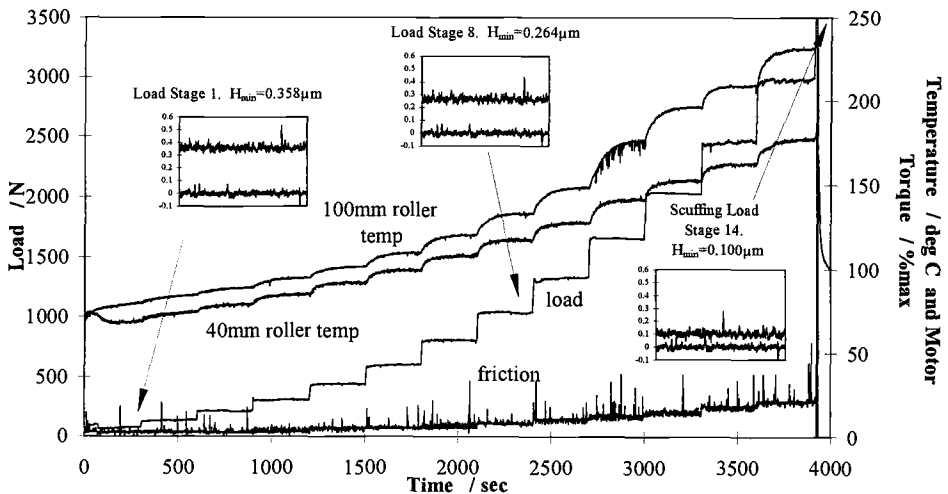


Figure 9 - Results of scuffing test showing variation of load, roller temperatures and indication of friction together with illustration of surface profiles from the two rollers separated by predicted EHL film thickness at three stages of the test. Sliding speed 30 m/s.

The occurrence of scuffing is easily detected by a sudden increase in vibration and noise from the rollers, and when this occurs the contact is rapidly unloaded so as to preserve as much of the run but un-scuffed surface of the rollers as possible for subsequent examination. Scuffing can be confirmed by visual examination of the rollers after the rig has stopped. At load stages 1, 8 and 14 (the stage at which scuffing occurred) profile traces from the two surfaces actually used in the test are shown with their mean lines separated by the predicted EHL film thickness as predicted by the elliptical contact formula of Chittenden et al. [7] It is striking to note that the scuffing stage corresponds to the case in which the highest peaks on the two surfaces begin to interfere. At lower load (lower temperature) stages the surfaces are well separated. Axial profile traces of the scuffed components from a test at a lower sliding speed of 20 m/s are shown in Figure 10.

The extent of damage is related to the rapidity with which the load is removed following initial failure, but the traces confirm the typical behavior of scuffing in which there is both loss and transfer of material with a tendency for the slower surface (40 mm diameter roller) to have a net loss of metal and the faster surface a net gain. The thrust bearing simulation rig has only recently been brought into operation, but results obtained so far suggest that the concept of limiting P-V as a design criterion is of limited value. Scuffing tends to take place at an almost constant value of the load in spite of higher temperatures at the higher

sliding and rolling speeds. Calculated values of minimum film thickness (just prior to scuffing) over a range of sliding speeds from 10 m/s to 30 m/s are almost constant and correspond to a value at which some surface interaction would be expected based on measured roughness. These results are reported in detail in a recent paper [8].

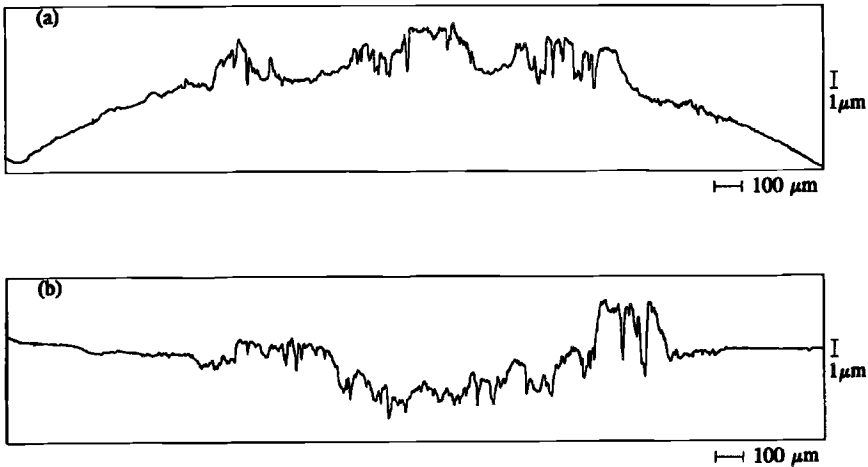


Figure 10 - Axial profiles of surfaces from scuffed disks. (a) 100 mm diameter roller; (b) 40 mm diameter roller. Note that profiles are shown to the same scale.

## Discussion and Conclusion

The main advantage of disk machines as a means of predicting the behavior of heavily loaded lubricated contacts found in gears and rolling element bearings is the simplicity and relatively low cost of the test specimens. A common criticism of conventional disk tests, aimed at simulation of gears, in which the specimens are circumferentially ground, however, is that the direction of the surface finish is incorrect. This problem has been addressed by devising a special grinding arrangement which gives the correct axial finish. The process is a true generating action which produces accurately circular parts and has the added advantage of giving a crowned surface which overcomes the problem of edge effects which are unquantifiable in cylindrical disks if perfect alignment cannot be achieved in practice. The results shown here demonstrate the clear way in which scuffing is detected by an unmistakable sharp rise in friction. It is therefore possible to determine the precise conditions, in terms of load, friction and specimen temperature, at which scuffing occurred. A significant improvement in scuffing performance can be achieved as a result of superfinishing of the surfaces.

A comparison of the performance of ground and superfinished surfaces is shown in Figure 11. The figure shows results for three sets of disks. The first set were of carburized steel, conventionally ground to  $0.4 \mu\text{m Ra}$ ; the second set were of the same steel but

superfinished to approximately  $0.05\mu\text{m Ra}$ ; and the third set were of M50 bearing steel honed and polished to simulate bearing balls and raceways with  $\text{Ra}$  of  $0.010\ \mu\text{m}$  to  $0.015\ \mu\text{m}$ . The first two sets were tested in the high speed disk machine under otherwise identical conditions and the third set in the bearing simulation rig. The most striking aspect of the M50 results is the virtual constancy of the scuffing load over the range of sliding speeds considered. This tendency is also shown by the superfinished, carburized disks. The ground disks show a more drooping characteristic. The P-V values at scuffing for the three sets are shown in Figure 12. This parameter is seen to vary over a considerable range for the polished surfaces which is contrary to the constant value that is implied when this parameter is proposed as a criterion to avoid scuffing.

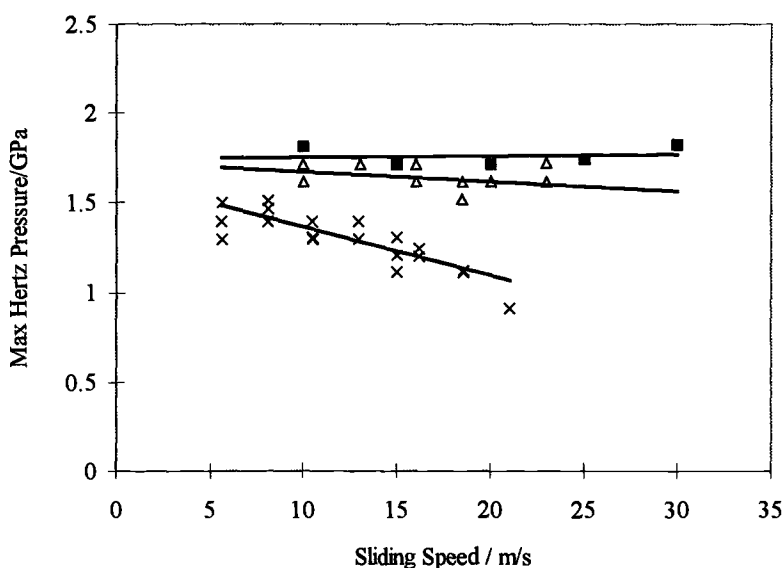


Figure 11 - Collected experimental results, maximum contact pressure at scuffing versus sliding speed.  $\times$  rough ground gear steel rollers;  $\Delta$  superfinished gear steel rollers;  $\blacksquare$  M50 bearing steel rollers.

The calculated values of minimum EHL film thickness just prior to scuffing in the M50 tests showed remarkable constancy (in the range  $0.100\ \mu\text{m}$  to  $0.109\ \mu\text{m}$ ). This observation lends support to the idea of calculated EHL film thickness in relation to roughness as a criterion for scuffing. However, this criterion does not appear to be relevant to the much rougher surfaces representative of gears. In the ground surface tests the predicted film at scuffing was considerably smaller than the roughness and there was considerable evidence of beneficial surface modification or “running in” during the earlier, lightly loaded stages of the tests. This effect was completely absent in the work on polished surfaces in which profiles from the run (but unscuffed) surfaces were indistinguishable from the freshly prepared surfaces. This apparent difference in EHL film forming and scuffing behavior of

rough and relatively smooth surfaces clearly warrants further investigation on the basis of a thorough understanding of the elastohydrodynamics of real engineering surfaces. Some progress is being made in analyzing this regime of lubrication under true engineering conditions [9].

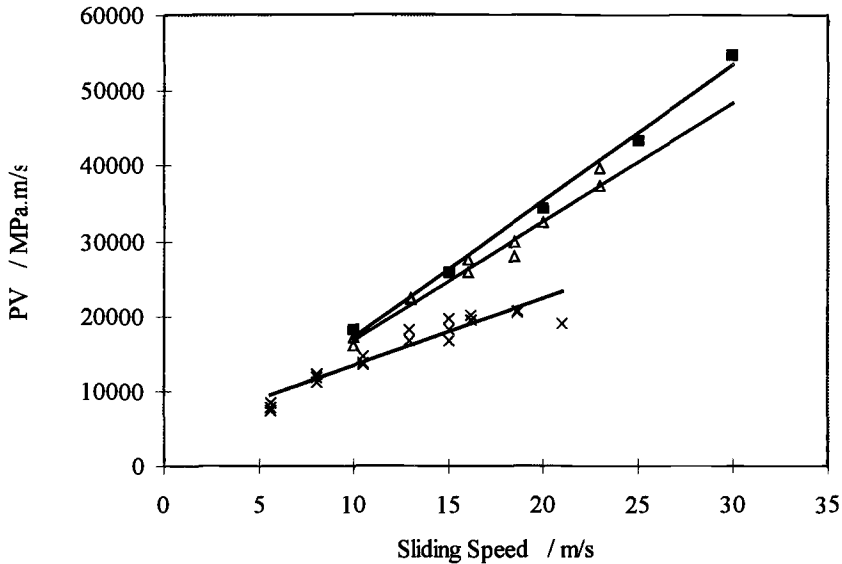


Figure 12 - Experimental results, PV versus sliding speed.  $\times$  rough ground gear steel rollers;  $\Delta$  superfinished gear steel rollers;  $\blacksquare$  M50 bearing steel.

## References

- [1] O.E.C.D., *Glossary of Terms and Definitions in the Field of Friction, Wear and Lubrication*, 1969, pp. 52-53.
- [2] Krantz, T.L., Alanou, M.P., Evans, H.P. and Snidle, R.W., "Surface Fatigue Lives of Case-Carburized Gears with an Improved Surface Finish," paper submitted to ASME for publication in *Journal of Tribology*, 2000.
- [3] Patching, M.J., Kweh, C.C., Evans, H.P. and Snidle, R.W., "Conditions for Scuffing Failure of Ground and Superfinished Steel Discs at High Sliding Speeds Using a Gas Turbine Engine Oil," *Trans ASME Jn. of Tribology* Vol. 117, 1995, pp. 482-489.
- [4] Patching, M.J., *The Effect of Surface Roughness on the Microelastohydrodynamic Lubrication and Scuffing Performance of Aerospace Gear Tooth Contacts*, PhD thesis, University of Wales, 1994.
- [5] Snidle, R.W. and Evans, H.P., "The Effect of Superfinishing on the Performance of Gear Tooth Contacts," Paper presented at a seminar on *Aerospace Transmissions*

- Technology Into the 21st Century*, ZF Friedrichshafen AG, Germany. IMechE, London, 1995.
- [6] Britton, R. D., Elcoate, C. D., Alanou, M. P., Evans, H. P. and Snidle, R. W., "Effect of Surface Finish on Gear Tooth Friction," *Trans ASME Jn. of Tribology*, Vol. 122, 2000, pp. 354-360.
- [7] Chittenden, R. J., Dowson, D., Dunn, J. F. and Taylor, C. M., "A Theoretical Analysis of the Isothermal Elastohydrodynamic Lubrication of Concentrated Contacts," *Proc. R. Soc. Lond.*, Vol. A397, 1985, pp. 245-269, 271-294.
- [8] Martin, M.J., Alanou, M.P., Evans, H.P., Snidle, R.W., Kawamura, H. and Dodd, A., "Scuffing Performance of M50 Bearing Steel Lubricated with a Gas Turbine Engine Oil at High Sliding Speeds," Paper presented at *STLE Annual Meeting*, May 2000
- [9] Elcoate, C. D., Evans, H. P., Hughes, T. G. and Snidle, R. W., "Thin Film, Time Dependent Micro-EHL Solutions with Real Surface Roughness," *Proc 25<sup>th</sup> Leeds/Lyon Symposium on Tribology*, Elsevier, Amsterdam, 1999, pp. 163-174.

Hon So<sup>1</sup> and Chih Chung Hu<sup>1</sup>

## Effects of Friction Modifiers on Wear Mechanism of Some Steels Under Boundary Lubrication Conditions

---

**Reference:** So, H. and Hu, C. C., “Effects of Friction Modifiers on Wear Mechanism of Some Steels Under Boundary Lubrication Conditions,” *Bench Testing of Industrial Fluid Lubrication and Wear Properties Used in Machinery Applications*, ASTM STP 1404, G. E. Totten, L. D. Wedeven, J. R. Dickey, and M. Anderson, Eds., American Society for Testing and Materials, West Conshohocken, PA, 2001.

**Abstract:** The effects of some commercial friction modifiers on antiwear performance of some steels were assessed experimentally under high contact pressures. The main compounds of the friction modifiers were, respectively, calcium carboxylate compound, organic molybdenum compound, phosphorous/sulfur (P/S) chemistry and polytetrafluoroethylene (PTFE). A ball-on-disk configuration was employed in the wear tests. The sliding speed of the disk on the stationary ball ranged from 0.785 m/s to 1.885 m/s and the applied load ranged from 39.2 N to 78.5 N. Bearing steel, high-carbon steel and medium-carbon steel were used to make the members of sliding pairs. The results show that only the additives that can produce chemical films on rubbing surfaces can reduce friction more effectively. Except PTFE, the other three additives have such an effect, but not as significant as claimed. Among these, P/S chemistry is the best, but this additive can cause excessive wear on rubbing surfaces in long-time use. Mo compound can provide a significant effect of antiwear on all three types of steel subjected to high contact pressures, while Ca compound has an antiwear effect only at comparably low pressures. Both Ca and Mo compounds cause wear on rubbing surfaces in a form of parallel deep grooves. PTFE neither improves antiwear performance, nor reduces friction on the rubbing surfaces of steel.

**Keywords:** Friction modifier; Boundary lubrication; Wear mechanism; High pressure

### Introduction

---

<sup>1</sup> Professor and Ph. D. student, respectively, Mechanical Engineering Department, National Taiwan University, Taipei, Taiwan 10660.

Friction modifiers (or friction reducers) have been used for many years in some lubrication systems. Some manufacturers claim that an addition of a friction modifier to a suitable fluid lubricant could reduce the coefficient of friction between two sliding metallic surfaces to a value as low as 0.01 when the sliding contact is in a boundary lubrication condition. Many investigators report that an addition of friction modifiers to engine and transmission oils could surely improve fuel efficiency and reduce power losses. In this regard, various types of friction modifiers have been developed to meet requirements of different applications. Examples found in industrial applications are the use of cams and followers, gear transmissions, metal forming processes, such as drawing of thin tube, sheet metal forming, and so on. In such applications, the sliding speeds of two contacting members may vary from 0.01 m/s to several meters per second. To avoid yielding occurring in contact members, contact pressures are always designed not to exceed the value of 1000 Mpa in accordance with the material used. Such a pressure is lower than that in an extreme-pressure test.

Papay [1] proposed a definition for friction modifier (or reducer) and presented a theory of friction modification. Many other researchers [2-5] confirmed that additions of molybdenum compounds to engine and gear oils could improve efficiency and reduce power losses. However, Arbabi and Eyre [4] found that an addition of molybdenum disulfide ( $\text{MoS}_2$ ) not only had little improvement in surface protection, but also increased in wear rate under some special conditions. On the contrary, Yamamoto and Gondo [5] found that both molybdenum dithiocarbamate and molybdenum dithiophosphate could reduce friction as well as wear of bearing steel oscillating against bearing steel. Hong and co-workers [6] found that the use of calcium and magnesium sulfonates as extreme-pressure (EP) additives in tapping and threading fluids could enhanced the efficiency. Muaki and co-workers [7], using active sulfur and calcium sulfonate as additives in paraffinic oils in a deep drawing process, found that both active sulfur and calcium sulfonate could improve formability, but only active sulfur had greater effect of lowering friction on ironing process. Gutman and Stotter [8], using polytetrafluoroethylene (PTFE) as an additive in engine oil, obtained the result of a reduction of up to 4 percent in fuel consumption.

From the point of view of mechanical engineers, it is always a problem to choose a suitable lubricant from a large variety of products, since the manufacturers claimed what they recommended was the most suitable one. However, the tested data they provided were based on standard tests that were different from the conditions in practice. Therefore, the purpose of this investigation is going to evaluate the effects of some typical commercial friction modifiers used in conditions similar to that in practice on friction as well as on antiwear performance of some steels. Moreover, the effect of a friction modifier can be defined as the ability to reduce friction in a sliding contact of metallic members.

**Experimental Method**

*Test Rig*

A multi-specimen friction test machine was used as the test rig. In this, the arrangement of a rotating disk sliding on a stationary ball was chosen (Figure 1). The sliding speed of the disk ranged from 0.785 m/s to 1.885 m/s. The normal load applied in a form of dead weights to the contact varied from 39.2 N to 78.5 N (4 kg - 8 kg). The oil temperature was kept at 25°C.

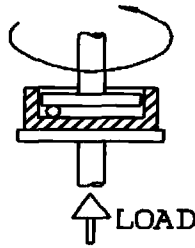


Figure 1– Schematic diagram of the ball-on-disk configuration.

*Specimens*

The ball specimens of 6.35-mm diameter were made from E52100 bearing steel and high-carbon steel equivalent to AISI 1095. The disk specimens of 34.5-mm diameter and 13-mm thick were made from E52100 bearing steel and medium-carbon steel equivalent to AISI 1050. The hardness numbers and center-line-average (CLA) surface roughness of the specimens are listed in Table 1.

Table 1 – Hardness and Surface Roughness of Specimens

	Bearing steel ball	Bearing steel disk	High-carbon steel ball	Medium-carbon steel disk
Vickers hardness	850	756	914	564
Surface roughness ( $\mu\text{m}$ )	0.28	0.043	0.39	0.042

*Lubricants and Additives*

Two paraffinic oils were respectively employed as the base oil in the tests, namely, MN and LN. Their specific gravities and viscosities are shown in Table 2.

Table 2 – Specific Gravities and Viscosities of Base Oils

Base oil	Viscosity (Pa s)		Specific gravity		Viscosity Index
	40°C	100°C	40°C	100°C	
LN	0.022	0.0039	0.858	0.810	102.7
MN	0.035	0.0057	0.862	0.814	109.6

Four different types of friction modifiers denoted by FM-1 to FM-4 were added to the base oils in specified weight percentage to form sample lubricants. The friction modifiers used in this study are commercial products and easily obtained from lubricant dealers. The lubricant identities and the main compositions of the friction modifiers are listed in Table 3.

Table 3 – Test Lubricants and Main Chemical Compositions of Friction Modifiers

Lubricant ID	Description (main compound of additives)	Main compositions of additives				
		Ca	N	P	S	Mo (wt%)
A	LN + 5 wt% FM-1 (calcium carboxylate compound)	4.6				
B	LN + 1 wt% FM-2 (organic molybdenum compound)		6.4	12.3	8.1	
C	LN + 1 wt% FM-3 (P/S chemistry)		3.1	6.1	6.4	
D	LN + 3 wt% FM-4 (colloidal PTFE)	Colloidal PTFE 0.1 - 1 $\mu$ m (exact composition unknown)				
E	MN + 5 wt% FM-1 (calcium carboxylate compound)	4.6				

### Test Procedures

The numbers of total sliding cycles for rubbing pairs in tests were preset to some specific values. Once the total sliding cycles reached a preset number, the test was finished and the wear scars on the specimens were measured and examined with a photomicroscope. Nine specific numbers of sliding cycles ranging from  $1 \times 10^4$  to  $8 \times 10^5$  were used in the present study.

### Results

To evaluation the antiwear effect of friction modifiers on different type of steel, three types of steel were selected to make three groups of sliding pairs. The types of

steel in each group were (1) bearing steel disk and bearing steel ball (BS/BS), (2) medium-carbon steel disk and bearing steel ball (MCS/BS), and (3) bearing steel disk and high-carbon steel ball (BS/HCS).

*Measurement of Wear Scars on Balls*

*Bearing Steel Against Bearing Steel* — By measuring wear scars on the ball specimens, found that not all the friction modifiers used in this study had antiwear effect. Figure 2 indicates that the wear scars grew with sliding distance. Compared with the results obtained by using plain base oil LN, the lubricant D containing FM-4 (PTFE) did not have antiwear performance. Among the four friction modifiers, organic molybdenum compound (FM-2) had a better antiwear effect at a sliding speed of 0.785 m/s. The result (Figure 2) also shows that the wear scar on a ball specimen would reach a limit size when the sliding pairs were lubricated with the lubricants A and B, respectively. At a higher sliding speed of 1.57 m/s, the sizes of wear scars decreased markedly, whichever one of friction modifier was used. By the theory of hydrodynamic lubrication, the load carrying capacity of sliding point contact induced by the fluid film is directly proportional to the sliding speed. At such a speed, the decrease in wear scar size was mainly caused by the hydrodynamic effect, by which a considerable part of the applied load was supported. Under such a condition, the lubricant A, containing calcium carboxylate compound had the best antiwear performance over the other three friction modifiers.

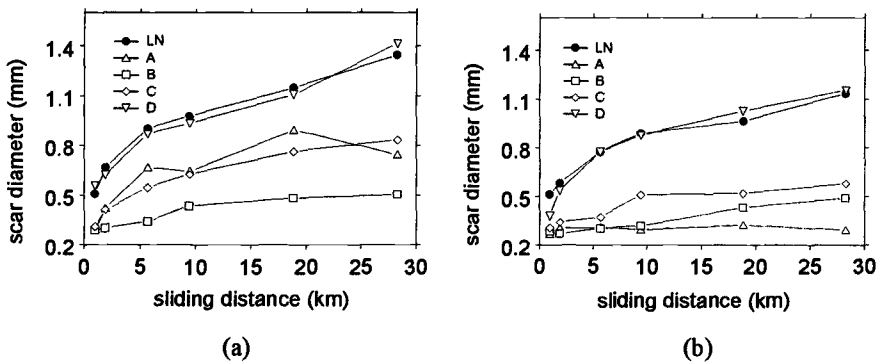


Figure 2 – Variation of scar size on balls with sliding distance for BS/BS subjected to an applied load of 58.9 N and sliding speeds of (a) 0.785 m/s and (b) 1.57 m/s.

*Sliding Members of Different Steel* — When the material of a sliding member was different from the other, the antiwear effect of friction modifiers on such a sliding pair was also different. Typical results are indicated in Figure 3. Among the three groups

of sliding pairs, the combination of medium-carbon steel disks and bearing steel balls yielded the best antiwear effect, whichever one of friction modifier was present. Among the four friction modifiers, FM-1 (Ca compound) and FM-2 (Mo compound) had better effects of antiwear performance.

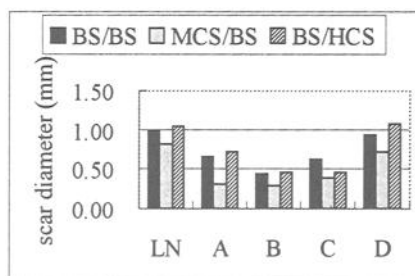


Figure 3 – Comparison of scar sizes on balls for the three groups of sliding pairs at a sliding speed of 0.785 m/s, a load of 58.5 N and a total sliding distance of 9.42 km.

#### Micrography of Wear Surfaces

Micrographic examination indicates that the appearances of wear scars on balls lubricated with base oil, LN and lubricant D were quite similar (Figure 4 (a)-(b)). The wear of the surfaces was caused by abrasion. While those on balls lubricated with lubricants A and B could be grouped into the same kind, except that the scar sizes were different. In Figure 4 (c)-(d) there are many wear grooves generating on the worn surfaces. By energy-dispersion of X-ray (EDX) analysis on such worn surfaces, calcium and molybdenum were found respectively (Figure 5). Obviously, some kinds of chemical film were produced on worn surfaces. Due to rubbing action, the film was broken to form wear grooves. In addition, while a groove was formed, some material in the steel matrix was peeled off to make a loss of material.

The appearance of worn surfaces lubricated with lubricant C indicates a different pattern as shown in Figure 4 (e). The surface looks clean and smooth in some conditions. By EDX analysis, there was no any other element but those of the steel itself on the worn surface. Therefore, there might be a layer of steel that reacted with some active elements of additive FM-3 (P/S chemistry) to form a chemical film. Such a film was scraped off by rubbing action as soon as it was formed.

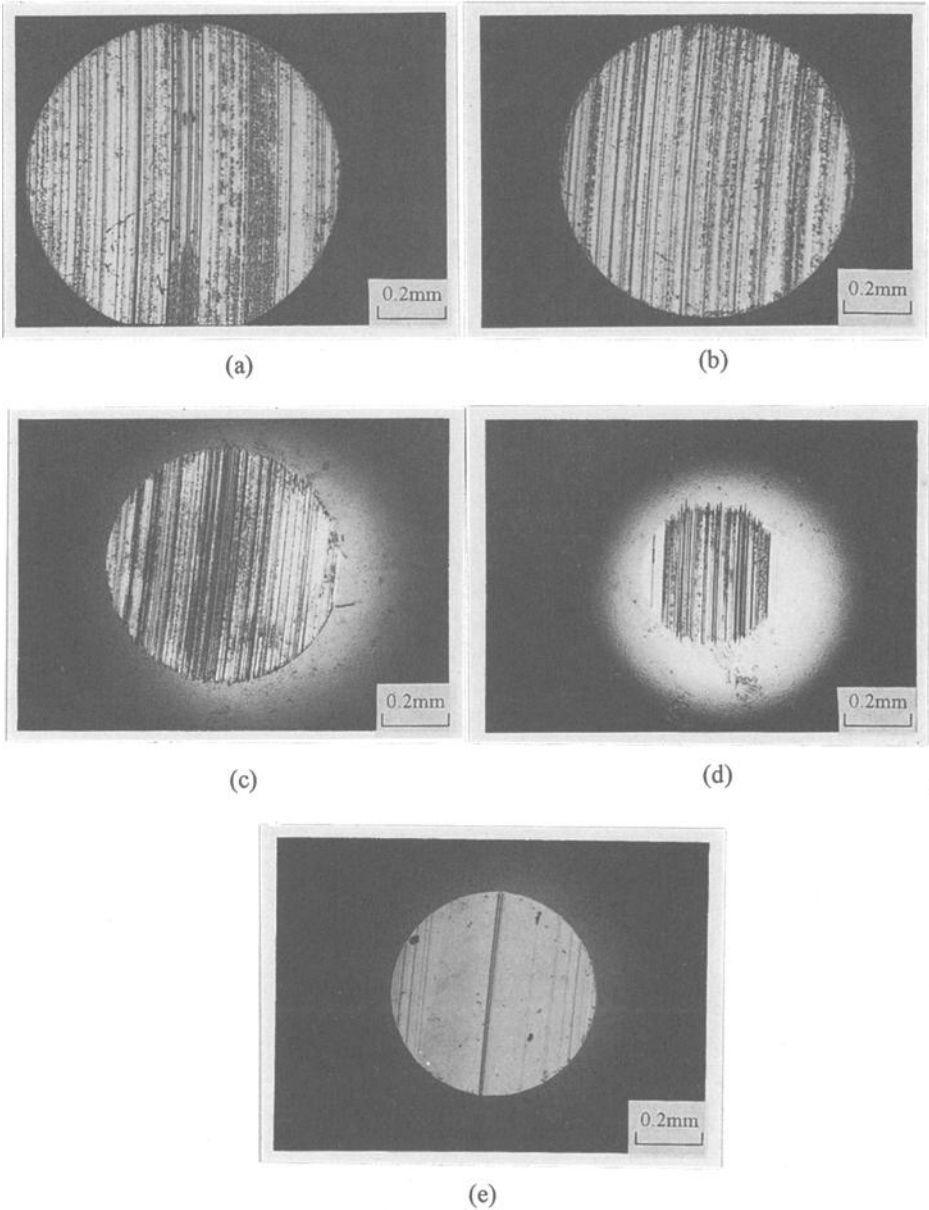


Figure 4 – *Appearances of wear scars on bearing steel balls sliding against bearing steel disks at a speed of 0.785 m/s and a total sliding distance of 9.42 km in the presence of (a) base oil LN, (b) lubricant D, (c) lubricant A, (d) lubricant B and (e) lubricant C.*

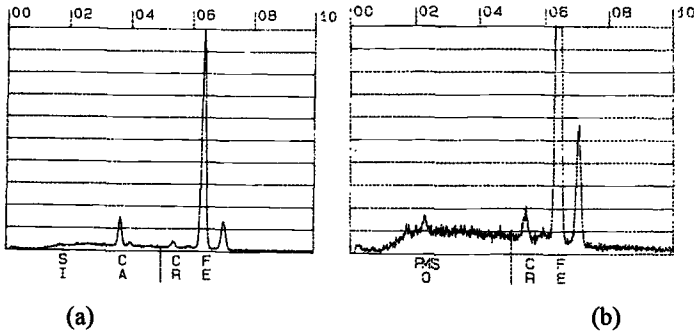


Figure 5 – Typical EDX spectra of wear surfaces on bearing steel balls lubricated with (a) lubricant A, and (b) lubricant B.

*Profile of Wear Surfaces on Disks*

The profile of wear surfaces can be measured with a profiling-type Proficorder. When base oil LN or lubricant D was used, the profile of wear surfaces on disks mainly depended on the type of steel in a sliding pair. Dominant wear loss was always contributed by the member of lower hardness. When the hardness of the two members was near the same, the smaller member lost more material than the bigger member did. Compared with the wear appearances of the contiguous balls shown in Figures 4, typical results for the profile of wear surfaces of the disks are shown in Figure 6. When a bearing steel disk slid against a high-carbon steel ball, little wear was found on the disks (Figure 6 (c)).

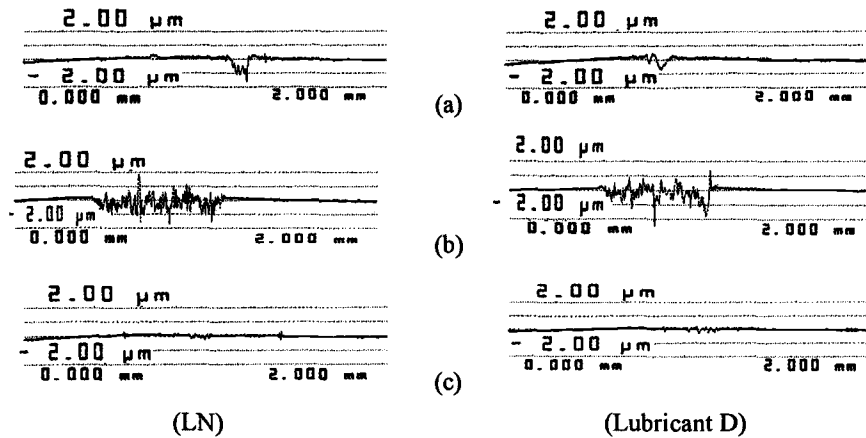


Figure 6 – Profile of wear surfaces of disks sliding against the balls shown in Figures 4 lubricated with LN and lubricant D, respectively for (a) BS/BS, (b) MCS/BS, (c) BS/HCS.

The wear patterns of the disk members lubricated with lubricants A and B were quite similar (Figure 7). When compared with Figure 6 (c) for the case of a bearing steel disks sliding on high-carbon steel balls, the wear on the disks was remarkable (Figure 7(c)).

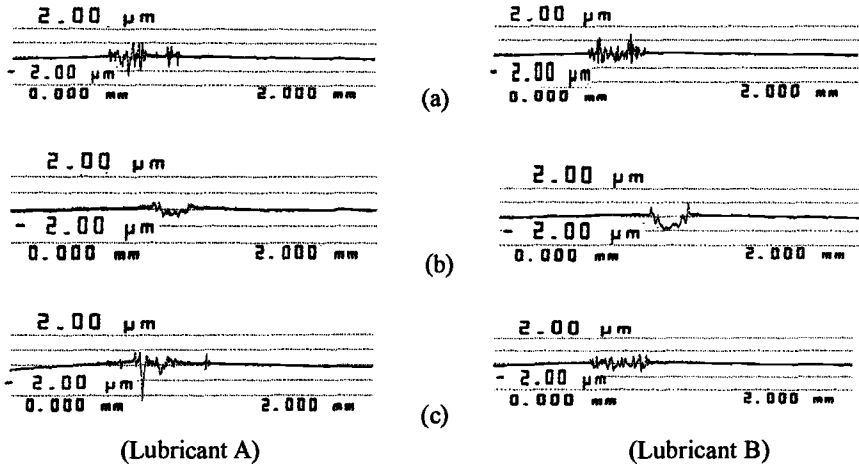


Figure 7 – Profile of worn surfaces of disks sliding against the balls shown in Figure 4 lubricated with lubricants A and B, respectively for (a) BS/BS, (b) MCS/BS, (c) BS/HCS.

The wear loss of disk members depended on the material of contiguous balls when lubricant C was used. For example, when both members of a sliding pair were made of bearing steel, the wear of the disk was mild (Figure 8) when compared with the ball (Figure 4(e)). On the other hand, when a bearing steel disk slid on a high-carbon steel ball, the bearing steel disk resulted in markedly wear.

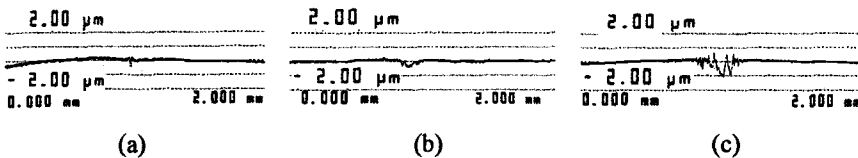


Figure 8 – Profile of worn surfaces of disks sliding against the balls shown in Figure 4 lubricated with lubricant C for (a) BS/BS, (b) MCS/BS and (c) BS/HCS.

*Coefficient of Friction*

*Sliding Members of the Same Material*—The use of friction modifiers could lower frictional force on sliding pairs made of bearing steel. Such an effect at low sliding speed is more significant than that at high speed. Especially, when using lubricant C,

the friction on the contact could be reduced to about half of the value from using the base oil LN alone. One exception was found by use of lubricant D, the coefficient of friction increased slightly. Such results are shown in Table 4. Because fluid film pressures can be generated in the sliding contact, this means that the hydrodynamic effect increases with increasing sliding speed. Consequently, friction can be reduced at higher speeds. As before, the use of lubricant D yielded the worst result. However, an addition of P/S chemistry can reduce friction effectively.

Table 4 – Coefficients of Friction on Sliding Contacts Lubricated with Various Lubricants

Lubricant	Sliding speed	
	0.785 m/s	1.57 m/s
LN	0.117-0.137	0.099-0.122
A	0.100-0.118	0.083
B	0.085	0.084
C	0.077	0.062
D	0.118-0.127	0.101-0.115

*Sliding Members of Different Materials*—The results show that when the members of a sliding pair were made of different type of steel, the effect of different friction modifier on reduction in friction was also different. Among the three groups of sliding pairs, the group combining medium-carbon steel disks and bearing steel balls had the lowest value of friction coefficient, while the group joining bearing steel disks and bearing steel balls had the highest value, whichever one of friction modifiers was used. On the other hand, among the friction modifiers used in this study, FM-2 (Mo compound) and FM-3 (P/S chemistry) had greater effects. One exception was found that the effect of FM-3 on the three groups of sliding pairs was nearly the same (Figure 9).

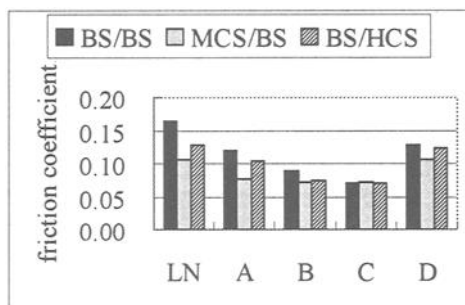


Figure 9 – Comparison of friction coefficients for sliding pairs of different steel lubricated with various lubricants at a sliding speed of 0.785 m/s and a load of 58.8 N.

**Discussion**

*Interaction of Hydrodynamic Effect with Friction Modifier*

The ball-on-disk configuration was employed in this study. This led to an unexpected result encountered in wear tests. Of which, the apparent contact pressure decreased as the size of wear scar increased with sliding distance. Consequently, a hydrodynamic effect was generated. To identify the hydrodynamic effect on friction and wear of bearing steel sliding on bearing steel, lubricant E containing FM-1 (Ca compound) was used in tests. The results (Figure 10) indicate that the size of wear scar as well as friction coefficient increases either with increasing applied load or with decreasing sliding speed. Either increase in sliding speed or decrease in applied load can enhance the hydrodynamic effect that can support a part of the applied load. Consequently, the size of wear scar and the coefficient of friction decreased correspondingly. Therefore, we can make a conclusion that the effects of friction modifiers should be more significant at lower sliding speeds.

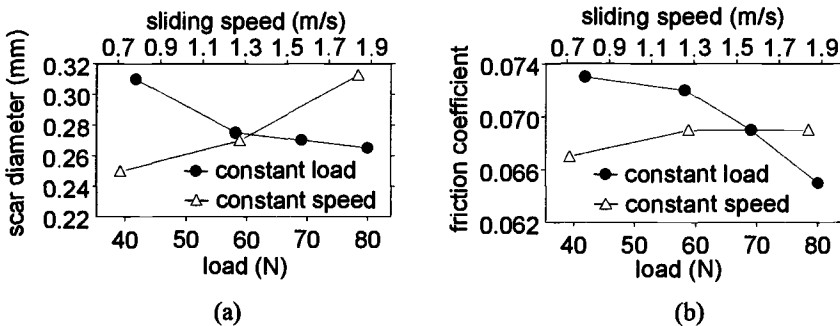


Figure 10 – The plots of (a) scar diameter and (b) friction coefficient against sliding speed (●, at a load of 58.9 N) and applied load (△, at a speed of 1.57 m/s), respectively when lubricant E was used for BS/BS.

*Effects of Chemical Film on Friction*

The EDX analysis (Figure 5) on wear surfaces confirms the formation of chemical films on rubbing surfaces when friction modifiers FM-1 (Ca compound) and FM-2 (Mo compound) were used. The existence of such chemical films may reduce the adhesive force between the two contiguous surfaces. The friction on the contact is therefore decreased.

When lubricant C was used in tests, it was difficult to obtain direct evidence to confirm the formation of chemical films on rubbing surfaces. However, indirect

evidence, such as the appearance of rubbing surfaces could confirm that as soon as a chemical film was produced, it was removed by following rubbing action. This means that the shear strength of such a film was low. Consequently, the friction on the contact could be reduced to further extent. On the contrary, because of failure in formation of any chemical film, the use of base oils and lubricant D remained in a high friction state. Moreover, the friction on the rubbing contact was not steady and fluctuated with sliding distance when these two lubricants were used. Compared with such a fluctuating condition, the friction on the sliding pairs lubricated with lubricants A, B or C was quite steady as shown in Figure 11.

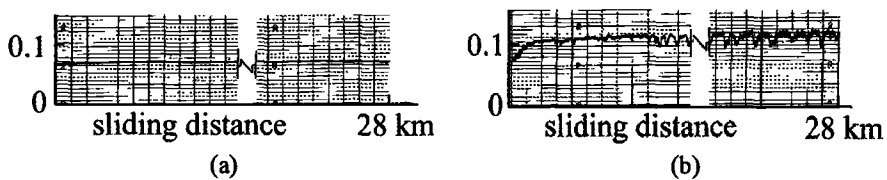


Figure 11 – Variation of friction coefficient with sliding distance for sliding pairs subjected to a load of 58.8 N and at a speed of 1.57 m/s lubricated with (a) lubricant B and (b) lubricant D.

#### *Effects of Chemical Film on Wear*

The antiwear performance of a friction modifier depends not only on the capability of forming any kind of film on rubbing surfaces, and also on the strengths of the film itself. In general, the strengths of a chemical film include the shear strength and the normal strength that is the ability of bearing a high contact pressure without cracking. By measuring wear scar sizes, one can obtain the rate of scar growth for a specific lubricant as that shown in Figure 2. When the scar growth rate is low in the first several thousand meter sliding distance, the antiwear performance of that lubricant is good at high contact pressure. FM-2 (Mo compound), for example, is the best among the four friction modifiers. Under a significant hydrodynamic effect, the antiwear performance of FM-1 (Ca compound) is the best. Obviously, the strengths of the chemical film produced in the presence of FM-2 is higher than that of FM-1. Therefore, the antiwear performance of FM-2 is better than that of FM-1. On the contrary, the strengths of the chemical film produced on the sliding surfaces lubricated with lubricant C is low enough to be removed easily. The scar growth rate is therefore the highest among these three lubricants.

#### *On types of steel*

The results show that the sizes of wear scars on the bearing steel balls were the

smallest when they were rubbed with medium-carbon steel disks. By inspecting the profile of the worn surfaces of the disks, the wear profile matched that of the contiguous balls, respectively. The contact roughly became a conforming one. Such a result was caused by the disks of lower hardness, which were easily worn down to match the profile of the contiguous balls. Under such a condition, the wear scars on the balls were the smallest among the three groups of sliding pairs.

### *Wear Mechanism*

When base oils and lubricant D were used, the loss of material from rubbing surfaces were mainly caused by directly plowing and cutting actions between rubbing surfaces. Such actions produced roughly worn surfaces. On the other hand, the addition of calcium carboxylate compound or active P/S chemistry in a base oil produced chemical reaction films that provided considerable protection against excessive wear from the matrix material. As soon as the films were scraped off by rubbing action, a new film formed immediately. It was found that the film produced with calcium carboxylate compound could grow and remain on the rubbing surfaces (Figure 5a), when the contact pressure decreased or the wear scar size increased. The wear mechanism of the rubbing surfaces in the presence of organic molybdenum compound is different from those mentioned above. The additive reacted with the ferrous matrix to produce a chemical film. Subjected to high contact pressures as well as tangential stresses, the film cracked along the sliding direction and then was plowed off. Consequently, deep grooves were produced on the rubbing surfaces. Deep grooves did not form at the same time, but, one by one. After the first groove appeared, the second groove could be produced after a certain sliding distance, and then the third, and so on. As the scar size grew bigger, the depth and the width of the grooves became smaller. It was found that in the presence of Mo compound the hydrodynamic effect provided little advantage to the growth of the wear scar size, but could delay the growth rate of scar size. Figure 12 indicates the scars of ball specimens at the sliding speeds of 0.785 m/s and 1.57 m/s, respectively. In the same sliding distance, the scar size is smaller at higher sliding speed.

### **Conclusions**

The experimental results obtained in the present study confirm that not all-commercial friction modifiers can have significant effects of reducing friction and wear on any type of steel under the prescribed test conditions. In addition, the combination in materials of a rubbing pair can affect the performance of a friction modifier. According to present results, some conclusions can be drawn.

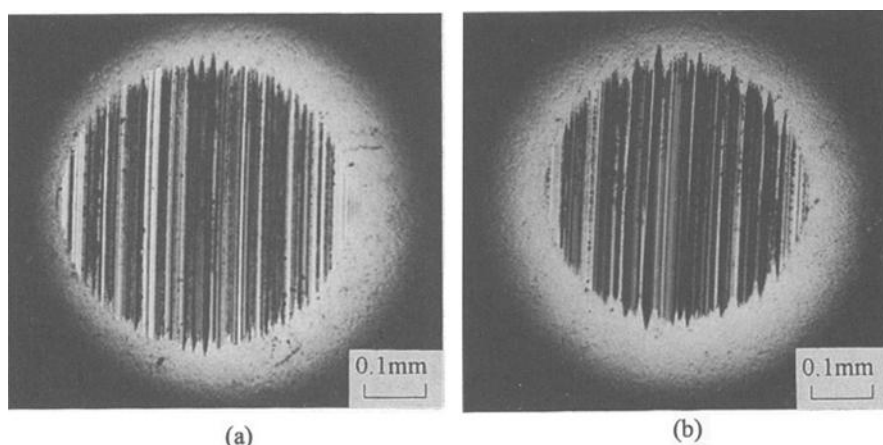


Figure 12 – *Appearances of wear scars on bearing steel balls sliding against bearing steel disks at the speeds of (a) 0.785 m/s and (b) 1.57 m/s, respectively, in a total sliding distance of 37.68 km in the presence of lubricant B.*

1. Antiwear performance of friction modifiers depends mainly upon the ability of bearing a high pressure as well as the shear strength of the chemical film that is produced on the rubbing surfaces. Among the friction modifiers used in this study that can generate chemical films, the organic molybdenum compound has the best antiwear performance over the others at low sliding speeds. However, this friction modifier does not have a significant performance of reduction in friction. Calcium carboxylate compound can produce a film on rubbing surfaces, but its normal strength is too low to support a high contact pressure. Therefore, the wear rate is high at slow sliding speeds.
2. P/S chemistry has an equal effect of lowering friction on the sliding pairs of different steel. However, in the presence of such an additive, wear of the rubbing pairs will be continuous as long as the rubbing action lasts, even though the contact pressure is not extremely high. Therefore, this additive is neither suitable for long-time use, nor suitable for machine members that have to maintain a high precision requirement in operation.
3. Under the conditions prescribed in this study, the use of FM-4 containing PTFE as an additive neither improves antiwear performance, nor reduces frictional force on rubbing surfaces of all sliding pairs used in this study.
4. The wear mechanism of the rubbing surfaces in the presence of organic molybdenum compound is different from those by using the other friction modifiers. The wear on the rubbing surfaces is mainly caused by formation of deep and long

grooves along the sliding direction. Hydrodynamic effect provides little advantage to limit the growth of scar size, but only delays the rate of wear scar growth.

### Acknowledgment

This work was sponsored by the National Science Council of the Republic of China under Contract NSC 86-2212-E-002-004.

### References

- [1] Papay, A. G., "Oil-Soluble Friction Reducers—Theory and Application," *ASLE, Lubrication Engineering*, Vol. 39, 1983, pp. 419-426.
- [2] Kubo, K., Shimakawa, Y., and Kibukawa, M., "The Effect of Gear Oil Viscosity and Friction Reducer Type on Transmission Efficiency," *Tribology International*, Vol. 19, 1986, pp. 312-317.
- [3] Pacholke, P. J., and Marshek, K. M., "Improved Worm Gear Performance with Colloidal Molybdenum Disulfide Containing Lubricants," *STLE, Lubrication Engineering*, Vol. 43, 1987, pp.623-628.
- [4] Arbabi, H., and Eyre, T. S., "Investigation into the Lubricating Effectiveness of Molybdenum Disulphide Dispersion in a Fully Formulated Oil," *Tribology International*, Vol. 19, 1986, pp. 87-91.
- [5] Yamamoto, Y., and Gondo, S., "Friction and Wear Characteristics of Molybdenum Dithiocarbamate and Molybdenum Dithiophosphate," *STLE, Tribology Transaction*, Vol. 32, 1989, pp. 351-357.
- [6] Hong, H., Riga, A. T., Cahoon, J. M., and Vinci, J. N., "Evaluation of Overbased Sulfonates as Extreme-Pressure Additives in Metalworking Fluids," *STLE, Lubrication Engineering*, Vol. 49, 1993, pp. 19-24.
- [7] Muraki, M., Tagawa, K., Ide, H., and Nakamura, T., "Frictional Behaviour of Lubricants during Deep Drawing and Ironing Processes for Zinc-Coated Steel Sheets," *Proceedings of Institution of Mechanical Engineers, Part J, Journal of Engineering Tribology*, Vol. 210, 1996, pp. 189-197.
- [8] Gutman, M., and Stottor, A., "The Influence of Oil Additives on Engine Friction and Fuel Consumption," *ASLE, Lubrication Engineering*, Vol. 41, 1985, pp. 150-154.

Alex F. Alliston-Greiner,<sup>1</sup> A. George Plint,<sup>1</sup> and Michael A. Plint<sup>1</sup>

## Testing Extreme Pressure and Anti-Wear Performance of Crankcase and Gearbox Lubricants

---

**Reference:** Alliston-Greiner, A. F., Plint, A. G., and Plint, M. A., “Testing Extreme Pressure and Anti-Wear Performance of Crankcase and Gearbox Lubricants,” *Bench Testing of Industrial Fluid Lubrication and Wear Properties Used in Machinery Applications, ASTM STP 1404*, G. E. Totten, L. D. Wedeven, J. R. Dickey, and M. Anderson, Eds., American Society for Testing and Materials, West Conshohocken, PA, 2001.

**Abstract:** When designing a bench test to model wear in lubricated contacts associated with engine and gearbox applications, considerations of scale are important. It is hazardous simply to attempt to define the “real life” conditions (load, speed, temperature, etc.) and glibly apply them to test pieces on a bench test machine. If large amounts of energy are being dissipated in small test specimens with supporting structures that do not allow the heat to escape, then it is clear that the specimens will become very hot. The bulk temperature may exceed what is experienced in practice, producing transitions in wear or frictional response. This paper outlines the relationship of wear and failure to energy dissipation in terms of two global parameters, Matveesky’s Friction Power Intensity and Plint’s Energy Pulse, and applies these to previously published data. It then shows how these can be used in the design of appropriately scaled, simple bench test procedures for the evaluation of lubricants for two practical EHD lubricated contacts (gears and cam/follower).

**Keywords:** friction power intensity, energy pulse, gear lubricant, crankcase lubricant, gears, EHD lubrication, failure of lubricated contacts, wear

### Introduction

A number of mechanisms depend for their successful operation on the transmission of force and power through elasto-hydrodynamic (EHD) contacts. These include all types of gearing, cam and follower mechanisms and rolling contact variable ratio transmissions.

All such contacts are subject to wear during their long-term operation and wear failures manifested by pitting, scuffing or scoring, smearing, transfer of material from one surface to another, and abrasion.

---

<sup>1</sup> Former Director of Tribology, Managing Director and President (deceased), respectively, Plint & Partners Limited, Old Station Business Park, Compton, Berks., RG20 6NB, UK.

The first of these mechanisms, pitting, is relatively well understood and is a consequence of cycles of sub-surface stress associated with the contact loading. Pitting can also occur in the absence of relative sliding and is the characteristic mode of failure of rolling element bearings. The other wear mechanisms are associated with the relative sliding of the surfaces in contact: none of them can take place without the expenditure of energy in the contact zone, mostly in the form of friction.

The anti-scuffing or load-carrying performance of a lubricant is obtained by introducing additives that only become active under "stressed" conditions. In general a hypoid gear oil will have both the extreme pressure type and anti-wear type additives whereas crankcase lubricants will be based on the multi-functional ZDDP anti-wear/anti-oxidant additive. The anti-wear additives react at lower temperatures than extreme pressure agents and ensure that the lubricant provides protection over a wide temperature range.

The test equipment and procedures developed for assessing these lubricants have always assumed that it is necessary to reproduce the highly stressed conditions of load and speed. A common feature of the procedures is that they in one way or another push the lubricated contact to a failure point and so claim to make a measurement of the "film rupture strength" or "load carrying capacity".

While this approach helps ensure that lubricants are "fit for purpose" from a quality assurance standpoint, they provide little insight into the specific strengths or weaknesses of competing formulations or offer much useful guidance on how they might be improved. Detailed observations of lubricant behavior are more easily obtained from simple laboratory rig tests (as opposed to gearbox, motored or fired engine tests) but the link with service life needs to be established. Indeed even industry-standard rig tests have been observed to correlate neither with engine performance nor with each other.

It appears self evident that the tendency for wear to occur should correlate with the intensity of energy dissipation in the contact zone. A properly designed EHD contact can, in the course of its working life, be the location for the expenditure of a vast amount of frictional energy, but with no ill effects. But it is also observed that a brief period of operation under conditions of excessive friction can lead to complete destruction of the working surfaces.

This paper outlines the relationship of wear and failure to energy dissipation and provides some guidance over the design of simple test procedures for the evaluation of two practical EHD lubricated contacts.

### **Wear Criteria: The Energy Pulse**

Plint [1] introduced the concept of the Energy Pulse ( $E_p$ ), which is the product of Matveesky's [2] Friction Power Intensity (FPI) and the contact transit time. Unlike the FPI, the Energy Pulse takes into account the length of time during which the material is subjected to frictional energy. The transit time is usually different for the two surfaces since, except in the case of the zero entrainment condition (when both surfaces are moving with equal velocity in opposite directions) their velocities are unequal.

$$E_p = \left[ \frac{\mu P v_t}{2 A} \right] J/mm^2$$

where  $\mu$  = friction coefficient,  
 $P$  = applied load, N  
 $v_s$  = relative sliding velocity, m/s  
 $A$  = area of contact, mm<sup>2</sup>  
 $t_t$  = transit time, s

The factor of 2 is based on the assumption that the energy generated in the contact zone is equally split between the two surfaces. Clearly this will not necessarily be true when the surfaces are at unequal temperatures. In practice, the slower moving surface will have the higher Energy Pulse.

Plint then observed that the  $E_p$  was analogous to the Archard Wear Law, but using the friction force  $\mu P$  rather than the applied load  $P$ . This seems logical since it is the rubbing process that is producing the wear, but it does assume that  $\mu$  can be measured for the contact under study.

$$\Delta V = kPv_s t_t \text{ mm}^3$$

where  $\Delta V$  is the volume of wear produced and  $k$  is a wear coefficient. Dividing by the contact area the depth of wear is obtained:

$$\delta = \left[ \frac{kPv_s t_t}{A} \right] \text{ mm}$$

Each Energy Pulse, therefore, can be regarded as an incremental contribution to wear or surface damage in the contact. The sum of the Energy Pulses can be used as a measure of the total wear and a predictor of wear patterns in rolling/sliding contacts.

*Defining the Energy Pulse*

For the generic rolling/sliding line contact in Figure 1 with contact length  $a$  mm and width  $b$  mm and  $v_2 > v_1$  the average FPI for the contact zone is:

$$Q_f = \mu P \frac{(v_2 - v_1)}{A}$$

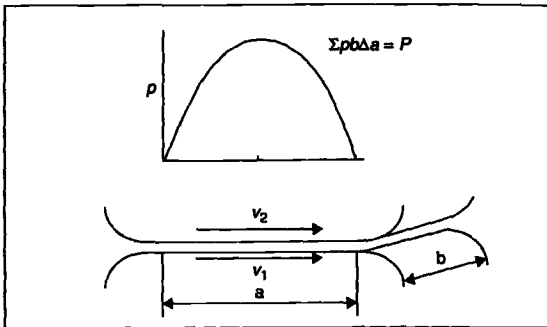


Fig. 1 -- Generic sliding/rolling Hertzian line contact

The transit times for the contact are  $t_t = (a/v_2) \cdot 10^{-3}$  for the upper body and  $(a/v_1) \cdot 10^{-3}$  for the lower body. The  $E_p$  for the two bodies are:

$$\text{upper body } E_p = \mu P \frac{(v_2 - v_1)}{2bv_2} \cdot 10^{-3}$$

$$\text{lower body } E_p = \mu P \frac{(v_2 - v_1)}{2bv_1} \cdot 10^{-3}$$

The  $E_p$  is independent, for a given applied load, of the load per unit width of contact. The smaller  $a$ , the greater FPI, but this is balanced by a reduction in the transit time. There are a number of other implications:

1. The energy pulse is always greater for the slower-moving surface than for the faster.
2. If  $v_1 = v_2$  (i.e. pure rolling) there is no energy pulse.
3. In any given mechanism under specified loading conditions, the level of the energy pulse is independent of running speed (it depends only on the sliding velocity).
4. If one surface is stationary relative to the point of contact, as in many tribology test machines, the energy pulse for that surface becomes infinite as the energy input is continuous.

#### *Expected Values of the Energy Pulse*

The Energy Pulse varies directly with the coefficient of friction in the contact. In gear and cam/follower contacts this cannot be measured directly. Merritt [3] suggests a value of  $\mu = 0.08$  as typical for spur gears, Bell and Colgan [4] assumed  $\mu = 0.10$  for a cam follower contact for their modelling purposes. They also studied boundary lubricated friction under a range of loads and speeds in the Plint TE 77 High Frequency Friction Machine and obtained values of  $\mu$  from 0.06 to 0.08.

Figure 2 shows the magnitude of the Energy Pulse (maximum reached in the contact cycle) for the standard gear testing machines (assuming  $\mu = 0.1$ ). At the maximum load the FZG machine imposes an  $E_p$  of  $0.0274 \text{ J/mm}^2$  that is lower than the other machines. It is well known that modern lubricants can pass FZG load stage 12 by a substantial margin, leading to the adoption of the Ryder configuration for more severe tests. An  $E_p$  level of  $0.0274 \text{ J/mm}^2$  would be sufficient to raise the temperature of a steel gear by about  $75^\circ\text{C}$  to a depth of 0.1 mm.

The figure also shows the  $E_p$  for the standard sliding test machines used for load carrying studies. Since the point of contact is stationary on one specimen, the energy input is continuous: there is no Energy Pulse. In these cases the FPI parameter must be considered and these are shown for the same contacts in Figure 3. The Gear and Cam/Follower rigs all have similar FPI levels, but the bench-scale rigs have a wide range of FPI. When it is considered that all this power is being dissipated into small test pieces, it is perhaps understandable that they give different rankings for lubricants when compared with the larger component test rigs.

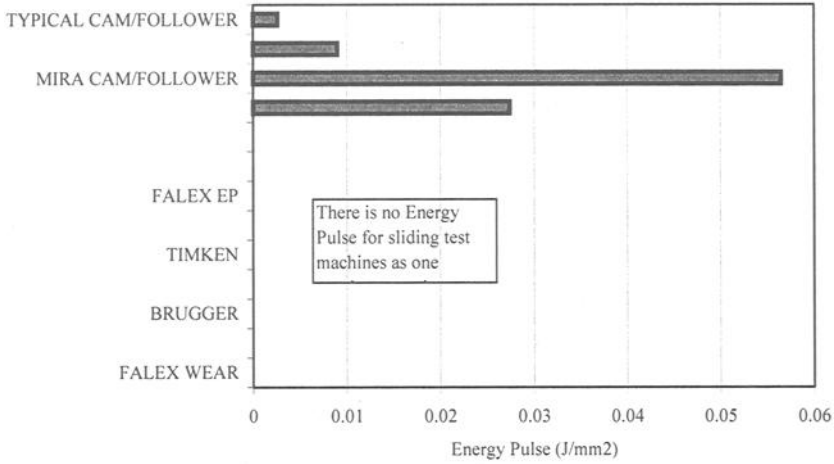


Fig.2 -- Energy Pulse parameter for common test machines

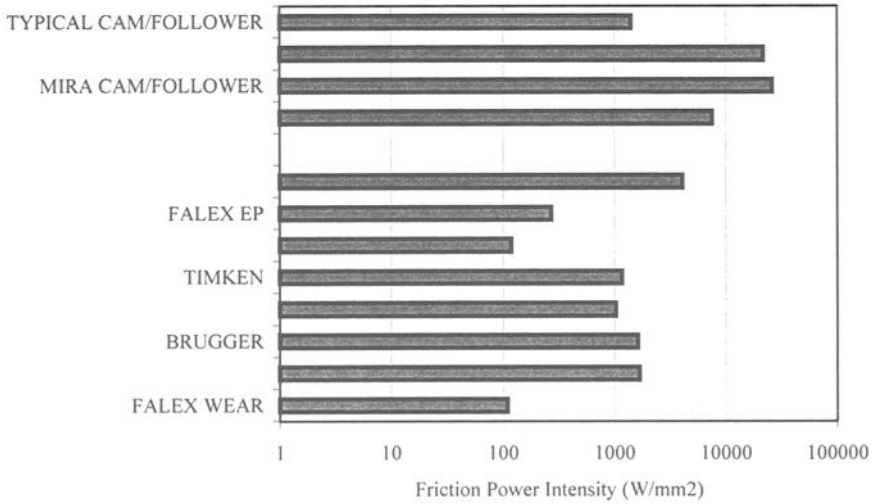


Fig.3 -- Friction Power Intensities for common test machines

In machine components there can be very high FPIs but because the contact durations are short, the Energy Pulse is low and hence the incremental damage is low. In simple sliding test machines there is no Energy Pulse as such: one specimen receives a continuous flow of energy and therefore the rate of damage will be correspondingly high. The Energy Pulse parameter can be used to define the severity of contacts both in the application and on the test machine.

What are the implications for lubricant screening tests? Two approaches suggest themselves: the first is to design a rig test to give the right level of  $E_P$  and therefore build up a picture of the wear and failure patterns. The second is to try and eliminate the  $E_P$  and concentrate on relating the wear or failure of the surfaces to specific temperatures: this latter case requires that the contact temperature is made an independent test variable.

**Tests Using The Energy Pulse**

*Cam and Follower Contact*

Bell and Colgan set out to find an explanation for the wear patterns commonly found in pivoted follower valve trains used in modern high-speed automotive engines. In these systems, wear is much more pronounced on the follower than the cam. The depth of wear along the path of contact of the follower was measured after running the engine at a camshaft speed of 1500 rpm for 100 hours.

Figure 4 shows such a wear pattern. It is clear that the most severe wear takes place at the ends of the path of contact, where the point of contact with the cam comes to rest and reverses its motion. There are secondary maxima, designated by  $R_1$  and  $R_2$ , which correspond to the positions of the point of contact during passage of the opening and closing ramps of the cam.

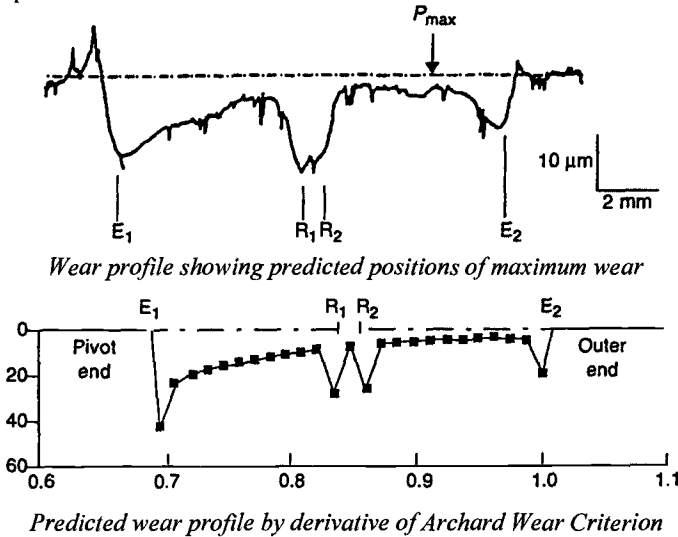


Fig. 4 -- Wear of finger follower after Bell and Colgan [4]

Bell and Colgan made a systematic study of various parameters that might be expected to correlate with this wear pattern, including:

1. Maximum Hertzian contact pressure.
2. Flash temperature rise, from the Blok equation.
3. Locations of minimum EHD oil film thickness.

None of these criteria gave a correct prediction of the observed wear pattern. They then attempted a correlation using a derivative of the Archard Wear criterion, expressed in the form:

$$\delta = \left[ \frac{k(h) P v_s t_f}{A} \right] \text{ mm}^3$$

where  $\delta$  is the depth of wear and  $k(h)$  is a wear coefficient, which is a function of materials and lubricant and of the calculated oil film thickness  $h$  in the contact. This expression is evidently identical to Plint's expression for the Energy Pulse, with  $k(h)$  substituted for  $\mu/2$ . It was assumed that  $k(h)$  would increase as film thickness diminished, the same trend as would be expected for  $\mu$ .

Figure 4 also shows the pattern of wear predicted for the follower using their criterion and a step-by-step computation, from which close agreement is apparent. This confirmed that maximum damage occurred not at the point of minimum film thickness (although the wear is also high at that point), but at the point of maximum contact dwell time (Energy Pulse in the terms of this paper).

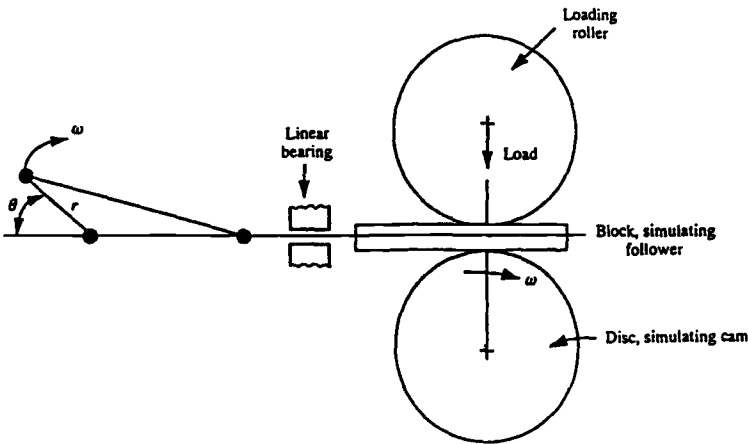


Fig. 5 -- Basic kinematic design of Shell reciprocating Amsler rig after Bell [5]

These conditions were then modeled by using a modified Amsler test device [5] in which a block was reciprocated against a driven roller (Figure 5). By adjusting the stroke of the block, the contact dwell time could be adjusted to give values similar to that of the cam/follower system. In this way a simple test generates the same type of wear patterns as the complex mechanical system and thus provides a more controlled and accessible test environment.

*Two Roller Contact (a Simulation of Gear Contact)*

Bell's model test on the reciprocating Amsler produced a cyclic Energy Pulse. The more traditional method of working in EHD lubrication is a two-roller machine. Here two disks can be run with a fixed ratio of sliding to rolling and therefore a fixed value of Energy Pulse. The failure of the rollers can be linked to a critical level of  $E_p$

Bell, Dyson and Hadley [6] carried out extensive experiments on rollers having a radius of 38.1 mm and a width of 11 mm, under conditions closely resembling those at the start of gear engagement. The rollers were of steel to specification BS En34, (a low carbon 2% nickel case hardening steel) hardened to 870 VPN. The lubricant was a solvent refined paraffinic oil without extreme pressure additives, viscosity SAE 100; such an oil would, of course, be expected to show substantially lower scuff resistance than a modern gear oil. These tests covered a wide range of variables:

- Rolling speeds: 0.24 to 11.25 m/s
- Sliding speeds: 0.48 to 4.00 m/s
- Loads: 232 to 1595 N/mm face width

Sufficient data are given to allow the value of the Energy Pulse to be calculated (Figure 6). The figure also shows which tests terminated in scuffing of the rollers and the correlation with the value of  $E_p$  is evident. The results are also plotted in order of diminishing Friction Power Intensity (Figure 7). Here there is a degree of correlation but the results are much more closely grouped and it would be difficult, on the basis of these tests, to specify a "safe" level of FPI .

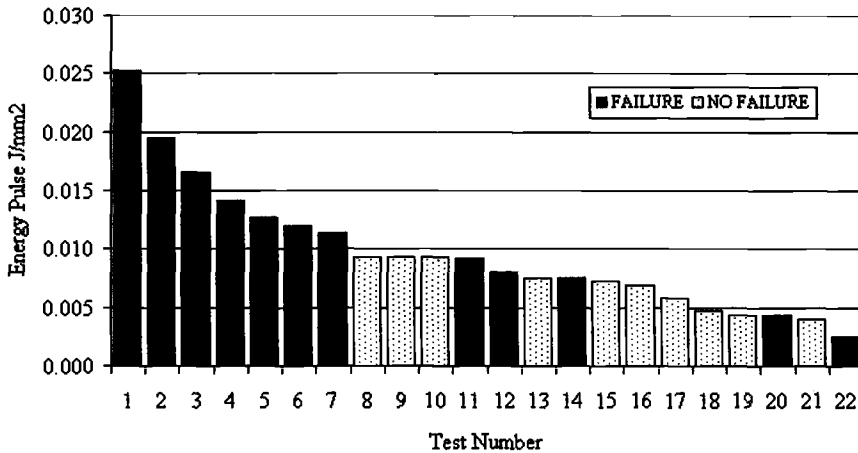


Fig. 6 -- Energy Pulse parameter for Bell, Dyson & Hadley's data

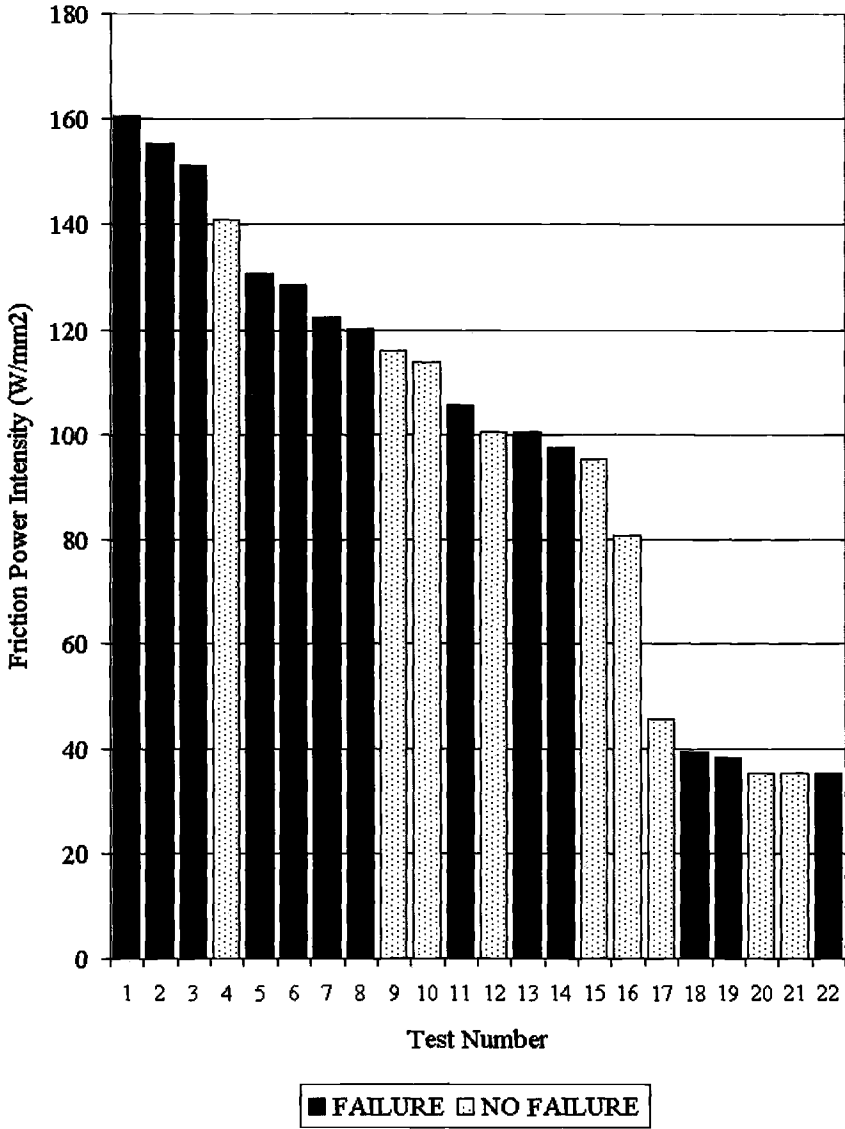


Fig. 7-- Friction Power Intensities for Bell, Dyson & Hadley's data

It appears from these tests that, for this combination of materials and lubricant, a value for  $E_p$  greater than  $0.01 \text{ J/mm}^2$  is sufficient to precipitate scuffing failure.

### Tests Eliminating The Energy Pulse

Eliminating the Energy Pulse and therefore running a test under isothermal conditions can move the focus of a test entirely on to the response of the lubricant chemistry to the contact temperature. In simple sliding machines (e.g. 4-Ball) and combined rolling/sliding contact machines (e.g. gear test) the temperature is out of the control of the experimenter [7].

The test geometry adopted is that of reciprocating sliding with short strokes. Sliding velocities are maintained at low levels in order to minimize frictional heating and, in the case of lubricated tests, to promote boundary lubrication. This reduction of frictional heating means that there can be independent control of contact temperature by external control of the bulk temperature. Mills and Cameron originally promoted these principles [8]. The reciprocating contact ensures that the dynamic interplay between film formation and film removal found in practice is being reproduced.

There are two main approaches to running tests under these minimal Energy Pulse conditions.

#### *Constant Temperature Tests*

Failure of the contact can be promoted, after a suitable running-in period, by increasing the contact loading until scuffing is reached. The scuffing failure point needs to be well characterized and this is the subject of some detailed discussion by Cooper and Moore [9]. In addition to a friction transition they emphasize the importance of surface analysis as a confirmation. The advantage of the reciprocating contact is that the specimens are small enough to make this task relatively easy.

Cooper and Moore present a very detailed range of tests where they establish failures in a reciprocating contact under the following conditions:

Ball:	6 mm diameter, AISI 52 100 bearing steel
Plate:	AISI 52 100 hardened to 780 kg/mm <sup>2</sup> , finished to 0.05 +/- 0.01 $\mu\text{m}$ $R_a$
Stroke:	15 mm
Frequency:	0.25 and 1.0 Hz
Load:	25 to 250 N in 25 N steps
Temperatures:	selected in the range 50°C to 260°C
Lubrication:	drip fed at a rate of 3 mL/hour

Measurements during the test are friction and contact potential (an indication of the degree of reduction in asperity contact). With the lubricant supplied continuously the transitions in friction and film formation could be related to the additive chemistry of the unoxidized lubricant sample. The small plate sample size again permits the chemical analysis of the reaction layers formed at different loads and temperatures and this means that a very detailed picture of the lubricant response can be obtained.

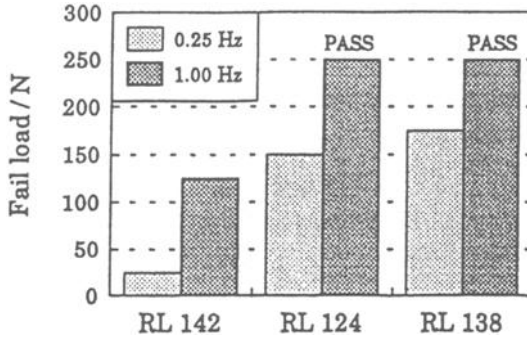


Fig. 8 -- Failure loads on the Plint TE 77 for TU3 reference oils after Cooper & Moore [9]

Under constant temperature conditions, a load was selected and the evolution of friction, contact potential and wear could be determined. The load was increased to the next value and similar results taken. Two scuffing failures were observed for crankcase lubricants and these were used successfully to correlate with known performance in the TU3 valve train test (Figure 8).

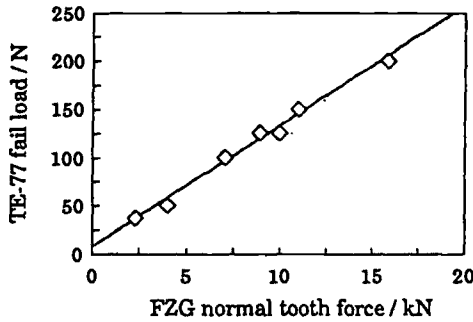


Fig. 9 -- Correlation between failure load conditions in FZG gear test and Plint TE 77 scuffing tests after Cooper & Moore [9]

They also studied hydraulic oils and found that the failure temperatures correlated very closely with the FZG failure load stage, Figure 9.

*Variable Temperature Tests*

Failure of the contact can be promoted, after a suitable running-in period, by increasing the contact temperature. The determination of the failure point also requires careful confirmation and this was characterized both by the friction and contact potential readings.

Alliston-Greiner [10] studied a range of crankcase and hypoid gear oils with known FZG failure load performance in a reciprocating contact:

Ball: 6 mm diameter, AISI 52 100 bearing steel  
 Plate: NSOH B 01 gauge plate, hardened to 60-65  $R_c$  finished to 0.2  $\mu\text{m } R_a$   
 Stroke: 15 mm  
 Frequency: 2.5 Hz  
 Load: 50 N for run-in then 250 N  
 Temperatures: ramped from 50°C to failure at 2°C/minute  
 Lubrication: drip fed at a rate of 10 mL/hour

After the running-in period the tests were run with a fixed load of 250 N. The failure point was determined as the first friction transition above a coefficient of  $\mu = 0.1$  accompanied by a collapse in the contact potential. Figure 10 shows a range of four oils of S-P chemistry with FZG pass stages of 9, 10, 11 and 12 exhibiting failure temperatures of 152, 157, 190 and 284°C, respectively.

Alliston-Greiner also used the technique to compare different chemistries, base stocks, and viscosities and to look at the effect of additive depletion. This kind of detailed information is not available from tests where the Energy Pulse is the controlling parameter.

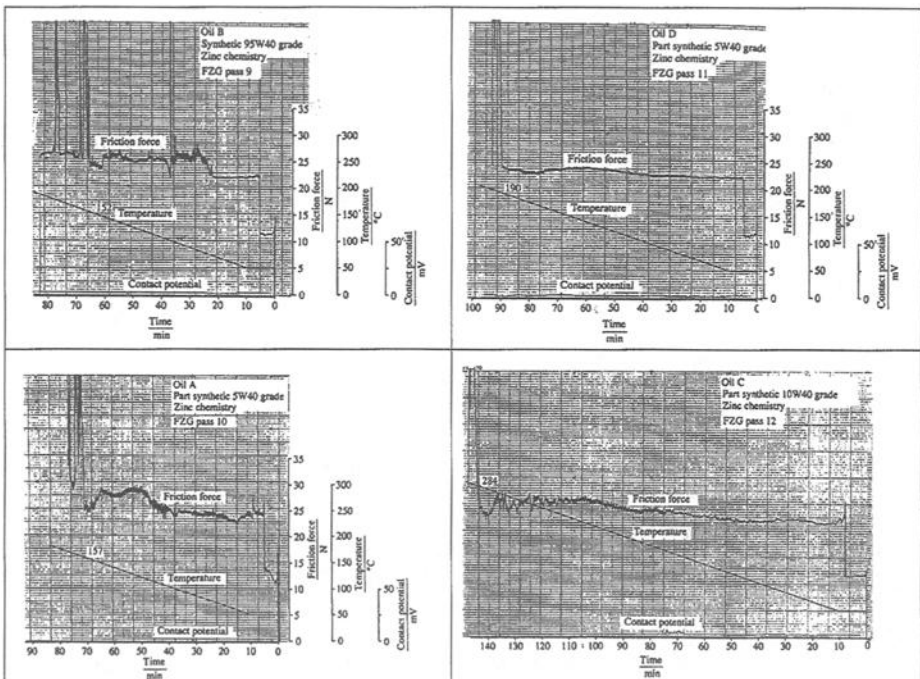


Fig. 10 -- Correlation between failure temperature (marked by sudden rise in friction force) and FZG gear test fail load stage on Plint TE 77 after Alliston-Greiner [10]

## Conclusion

This paper started with the assertion that wear in an EHD contact can only arise as a result of the expenditure of frictional energy in the contact.

There have been attempts to quantify this effect, of which the most widely known and successful has been the Archard Wear Criterion. The Friction Power Intensity of Matveesky has also been used as a measure of the rate at which frictional energy is generated in the contact, but this clearly needs to be multiplied by the duration of that energy input to give a meaningful indication of the true severity of the contact conditions. Plint's Energy Pulse, while analogous to the Archard Criterion, is logically preferable since it makes explicit reference to the frictional forces involved.

The use of the Energy Pulse then allows the experimenter to design tests to study the wear and failure of EHD lubricated contacts. There are two approaches, either to model the Energy Pulse using simplified sliding/rolling systems or to eliminate the Energy Pulse and study the effects of bulk temperature on failure. Combinations of these techniques have been demonstrated to give high levels of correlation with standard gear and cam/follower tests.

## References

- [1] Plint, M. A., "The Energy Pulse: A New Criterion and its Relevance to Wear in Gear Teeth and Automotive Engine Valve Trains," *Proceedings of the XI National Congress on Industrial Tribology, Delhi*, January 22-25, 1995, pp. 185-192.
- [2] Matveesky, R. M., "The Critical Temperature of Oil with Point and Line Contact Machines," *ASME Transactions*, Vol. 87, 1965, pp. 754ff.
- [3] Merritt, H. E., *Gear Engineering*, Pitman, London, 1971.
- [4] Bell, J. C., and Colgan, T. A., "Critical Physical Conditions in the Lubrication of Automotive Valve Train Systems," *Tribology International*, Vol. 24, No. 2, 1991, pp. 77-84.
- [5] Bell, J. C., "Reproducing the Kinematic Conditions for Automotive Valve Train Wear in a Laboratory Test Machine," *Proceedings of the Institution of Mechanical Engineers*, Vol. 210, 1995, pp. 135-144.
- [6] Bell, J. C., Dyson, A., and Hadley, J. W., "The Effects of Rolling and Sliding Speeds on the Scuffing of Lubricated Steel Discs," *ASLE Transactions*, Vol. 18, 1974, pp. 62-73.
- [7] Plint, A. G., "Machines and Methodologies for Wear Testing Extreme Pressure and Anti-Wear Properties of Lubricants," *Proceedings of the XI National Congress on Industrial Tribology, Delhi*, January 22-25, 1995, pp. 375-386.
- [8] Mills, T. N. and Cameron, A., "Basic Studies on Boundary, EP and Piston-Ring Lubrication Using a Special Apparatus," *ASLE Transactions*, Vol. 25, 1982, pp. 117-124.
- [9] Cooper, D. and Moore, A. J., "The Influence of Boundary Films on Lubricant Anti-Scuff Performance," *Leeds-Lyon Symposium, Lubricants and Lubrication*, 1994, pp. 617-633.
- [10] Alliston-Greiner, A. F., "Testing Extreme Pressure and Anti-Wear Performance of Gear Lubricant," *Proceedings of the Institution of Mechanical Engineers*, Vol. 205, 1991, pp. 89-101.

Mathias Woydt<sup>1</sup> and Norbert Kelling<sup>1</sup>

## **Tribological Testing of Lubricants and Materials for the System “Piston Ring/Cylinder Liner” Outside of Engines**

---

**Reference:** Woydt, M. and Kelling, N., “Tribological Testing of Lubricants and Materials for the System “Piston Ring/Cylinder Liner” Outside of Engines,” *Bench Testing of Industrial Fluid Lubrication and Wear Properties Used in Machinery Applications, ASTM STP 1404*, G. E. Totten, L. D. Wedeven, J. R. Dickey, and M. Anderson, Eds., American Society for Testing and Materials, West Conshohocken, PA, 2001.

### **Abstract:**

The test procedure for characterizing the tribological behavior of lubricants and materials for the system “piston ring/cylinder liner” outside of engines is now operational and validated. The test parameters presented in this paper ( $F_N = 50 \text{ N}$ ;  $v = 0,3 \text{ m/s}$ ,  $s = 24 \text{ km}$ ) may act only as an indicator and should be adopted to the tasks regarded. It allows the check prior expensive engine testing, if a tribo-material, tribo-couple or new lubricant will reach a satisfactory engine performance.

The introduction of piston ring segments and cylinder liner as specimen into the test rig as well as the volumetric wear determined by means of stylus profilometry represented a big step forward in order to increase the transferability of “tribo-tests” to engine tests on an acceptable level.

**Keywords:** tribology tests, wear, friction, lubrication, piston rings, cylinder liner, tribometer

### **Introduction**

The modification and substitution of materials and coatings as well as new formulated lubricants, and further development of surface morphologies through new machining processes that are used in mass production, incorporate an unknown intervention in the friction and wear properties of a well-understood tribosystem.

Today, the development times have been reduced to half, meaning that faults must be clarified ever more quickly. Further, the components are increasingly lighter and more compact, thus prolonging maintenance intervals and placing more demands on tribo-materials.

Prior to production and the field testing, the number of candidate tribomaterials and lubricants (tribomaterials “n” times tribomaterials “m” times lubricants “x”) have to be safely reduced to a reasonable number [1] of promising material pairings by using test

---

<sup>1</sup> Federal Institute for Materials Research and Testing (BAM), Dept. VIII.11, Unter den Eichen 87, D-12200 Berlin (Germany)

rigs to determine the functional behavior. Using 4 different piston rings times 5 liner materials times 3 lubricants gives quickly 60 possible tests, which can't be run due to cost and time limitations.

An engine test on the bench costs between 20,000 and 125,000 \$ depending on equipment, instrumentation, engine size and test duration. The application-oriented characterization of the friction and wear behavior of a material pairing or lubrication under mixed/boundary lubrication – for one tribometer presented in this paper – for the tribosystem “piston ring/cylinder liner” costs approximately 1,500 EURO, including test rig, samples, operation and wear evaluation. Additionally, the results are ready after 22,5 to 100 hours.

Basically, the runs in test rigs seeks to acquire knowledge about the level of the wear rate, coefficient of friction, wear mechanisms and influence of process parameters, which are difficult to collect from engine tests, but don't tend to substitute engine tests.

Saving money and time will only possible, if the results from the test rigs (Tribometers) can be transferred to the functional behavior in the application. The aim of this contribution is to illuminate the difference between earlier and current tribometers and the testing philosophies with respect to model the mixed/boundary tribology of piston ring/cylinder liners.

### **Mixed/boundary lubrication**

#### *Development of the test procedure*

Engine engineers always remain skeptic with respect to the characterization of the tribological behavior in the system “piston ring/cylinder liner” outside of engines. At the beginning eighties a so called small stroke monocylinder was designed and built in the frame of a research [2] project funded by the German Research Association for Combustion Engines (Forschungsvereinigung Verbrennungskraftmaschinen (FVV)), which simulated the operational conditions of the upper cylinder liner section. Up to ten piston rings were mounted on a piston dummy. The overall correlation between this monocylinder was not completely satisfactory, but the test rig was in the mid-nineties taken-over by an engine manufacturer and modified.

A similar test arrangement was developed and used by FORD [3] in the nineties only with one piston ring package.

The test matrix in the research [4] project “Improvement of the tribological limits of engineered ceramics for high-temperature tribology” funded by the German Federal Ministry of Research and Technology (BMFT, No. 03T0013A-C) mid eighties was so gigantic, that the automotive industry requested a tribological test procedure, because they don't intend to run engine tests with engineered ceramics exhibiting an unknown tribological behavior. During this project more than 600 test were run.

Continuous sliding and oscillating sliding are the two motion modes to simulate the tribological behavior of piston ring/cylinder liners. There exists today no consensus in the testing community, whether the continuous [4,5,6,7,8] sliding or the oscillating

[2,3,9,10,11,12] sliding leads to a greater transferability. Both motion modes operate under mixed/boundary lubrication.

Also for valve train [13] systems they exist a strong tendency and demand to perform tests in test machines and to reproduce the wear behavior.

#### *Evaluation of test parameters*

In principle, test parameters and conditions must be developed that correspond as much as possible with those in the practical application. This is in deviation to all standardized test procedures (ASTM, DIN, ISO, AFNOR,...), which prescribe fixed conditions and geometries.

The applicant therefore develops a comprehensive systems analysis according to DIN 50320 of the operation conditions of the tribosystem. A brief questionnaire on operating condition is published in [14]. This analysis usually shows considerable gaps with regard to knowledge of the tribosystems. But which valued parameters demanded by tribosystems during application, changing in time and quantity, are now relevant for the tests?

The following displays the strategy to identify the operating conditions for the most concerned section of the cylinder liner, the upper section, which operate under mixed/boundary conditions and in same case with a portion of dry friction.

#### *Sliding velocity*

The wear intensive region of the liner represents the upper section (top) with 5% to 10% of the stroke and can be identified by means of axial stylus profilometry of the regarded engines as average used ones. The so-called typical cases of 80% conduct for passenger car engines to a sliding velocity of  $\sim 0.3$  m/s.

#### *Normal force*

Both the normal force and the temperature will be adopted as static values according to the situation at the upper liner section. The combustion (ignition) pressure acting radially on the piston ring (over  $360^\circ$ ) will be converted into a normal force for the test sample (segment). Typically, the normal force lies between 30 N and 100 N.

#### *Temperature*

A temperature of  $170^\circ\text{C}$  is regarded to be representative for the oil film.

#### *Friction mode*

Boundary/mixed lubrication is the result using a parameter set of  $F_N = 50$  N,  $v = 0.3$  m/s and  $T = 170^\circ\text{C}$ , which is always confirmed from the values of the coefficients of friction. A normal force of  $F_N \geq 50$  N is more representative for diesel engines and  $F_N \leq 50$  N for gasoline engines.

#### *Ambient media*

The bath contains 500 ml of test fluid using a refill for each test, which is more than 10 times greater than that for oscillating tests. This volume is regarded necessary, because 22.5 hours and more of testing degrade the oil. The samples are completely immersed in the bath.

*Mounting situation*

In contrast to the oscillating tests, where the wear particles remain the tribo-contact, both tribo-elements (samples) are mounted in a way enabling wear particles to leave the tribo-contact. The wear particles are dispersed in the oil bath or sediment at the bottom.

*Test geometry*

Figure 1 displays the four today possible test geometries. A big step forward transferability represents the preparation of cylinder liner samples from engines, because they exhibit the metallurgy, microstructure and topography of honed liners as in engines. Additionally, the process to coat an inner surface (liner) determines the properties of any coatings. Overall, the liner samples contain, in an unknown manner, all influences of the production process. Customers [11,3,6,7,8] feel to be on the safe side using liner samples, even more costly.

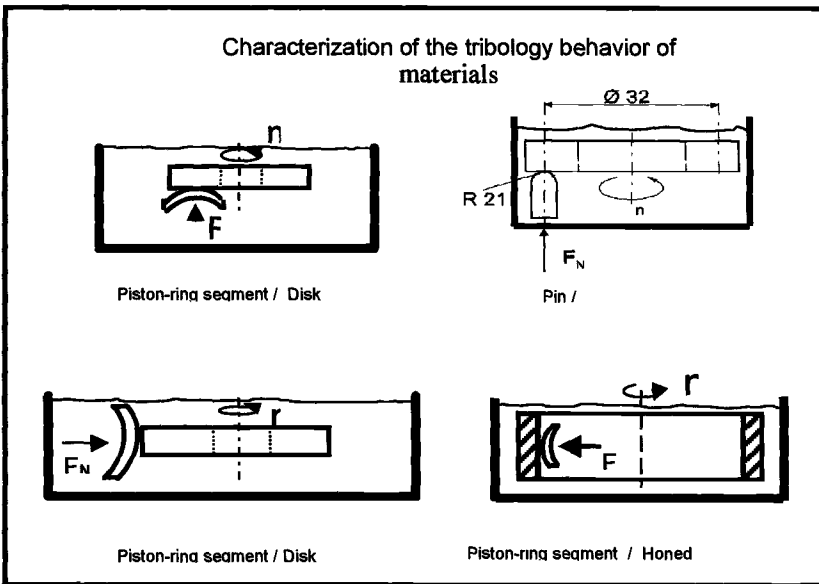


Figure 1: Compilation of possible test geometries

The other geometries using disks, balls and/or toroids were applied in cases, where for any kind of reason of time schedule no “components” are available. Engine manufacturers don’t tend to spend money in the processing of components, if the tribological behavior of a novel material or coating coming right out from research is unknown.

*Testing time shorting effect*

The test runs continuously at 0.3 m/s acting in the upper liner section. Assuming 100 mm of stroke and 5 % or 10 % related to the upper liner section so approximately 1m of

sliding gives 20 to 40 engine revolutions (four stroke). 24,000 m of total sliding represents 480,000 to 960,000 revolutions.

On the other hand, the wear scar diameter of the piston rings are between 0.5 mm and 6 mm in length. Assuming, that the samples of the piston ring run now continuously under the conditions of the upper liner section so approximately 1 m of sliding gives 167 to 2,000 engines revolutions.

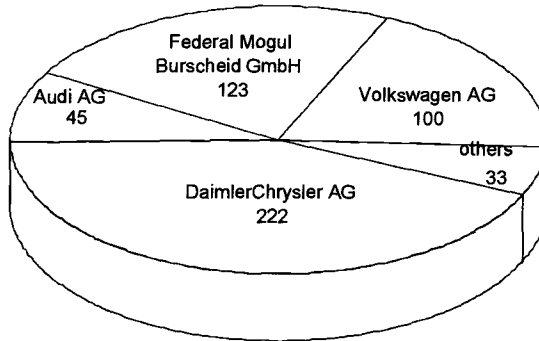
*Test fluids*

As is known from practice, that used oils increase wear rates. Fresh oils degrade more to the end of the drain intervals, so the use of used oils increase further the time shorting effect. Unfortunately, used oils are unspecified containing an unknown amount of particles and degradation products. For each run, the oil container is re-mixed. Customers deliver normally more used oils than needed for the test program and collected from “transporters” in city use, because the oils were “heavy” solicited and have avoided at least one drain interval.

Typically, to rate the wear behavior of materials, used oil are employed.

Table I: *Repartition of the number of tests performed for automotive customers*

**Distribution of customers for the characterization of the tribological behavior of material couples for the tribosystem "Piston-ring / Cylinder liner"**



(period 01/93 → 01/2000)

*Transferability*

This represents the key questions in tribotesting. The final [5,4] report (project referred above) from 1992 of Volkswagen AG stated, that the morphologies of the wear track and scars between tribotesting and engine runs were qualitatively comparable. Tribotesting enables a qualitative wear ranking (best and worst tribo-couples), but no quantitative relation exists between tribotesting and engine runs in that meaning, that a wear rate of “X” mm<sup>3</sup>/Nm correspond to “y” μm/h in piston ring wear. It was also recommended, to decrease the normal force from F<sub>N</sub>=100 N down to F<sub>N</sub>=50 N and to increase the

temperature from  $T=150\text{ }^{\circ}\text{C}$  to  $T=170\text{ }^{\circ}\text{C}$ . The addition of  $\text{HNO}_3/\text{H}_2\text{SO}_4$  to the used oil in order “destroy” the alkaline reserve is contra-productive.

Engine manufacturers and systems suppliers seem to answer in a positive manner the question of the transferability (see Table I), when they regularly sub-contract tribotests and/or purchase tribometers.

These test parameters usually characterize the tribological behavior in normal operation with warm engine. For cold start or dry run conditions and overheated engines, other parameters must be selected.

#### *Design of the test rig*

The test [15] rig (tribometer) consists of a vertically beared shaft where at the end of the shaft is mounted the rotating disk or liner (s. Figure 2). Stationary samples (ball, toroid, segment of a piston ring) are pressed via a dead weight against the disk. Using a cylinder liner, the loading device is turned by  $90^{\circ}$ . Both stationary and rotating sample are immersed in a temperature controlled oil container.

The friction torque, the normal force, the bath temperature and the total linear wear are continuously measured during each test.



*Figure 2: Cylinder liner segment and piston ring contact situation (left figure: samples in the oil bath container; right figure: Arrangement for adjusting the rotating sample)*

#### *Experimental procedure*

The piston ring material were combined in single tests with the liners and in some cases repeated test or tests with a longer distance were performed in order to be able to better

distinct between the tribo-couples. 24 km of sliding takes at 0.3 m/s 22 h 12 min of testing time. All samples were marked with an individual, durable identification number. The samples holder is mounted on a three screw fixture in order to adjust the perpendicular running of the test surface in respect to the rotating shaft.

*Standardized samples*

Balls, toroids and pins represent standardized samples with an accurate and defined geometry, so the geometry was never determined.

*Piston rings*

Customers deliver production type piston rings or individually produced piston rings, which were cut in segments of ~20 mm in length. The determination of the profile of a piston rings by means of stylus profilometry is recommended for passenger car rings exhibiting a wear rate  $k_v < 10^{-9} \text{ mm}^3/\text{Nm}$ , because the accuracy differs already on one piston ring considerably. Truck rings exhibit almost a better geometric accuracy.

*Cylinder liners*

Honed liners according to production specification or modified specifications guarantee a high transferability of the results. In order to detect wear rates  $k_v < 10^{-7} \text{ mm}^3/\text{Nm}$ , a smooth finishing in deviation to production specifications is necessary. The repeatability of roughnesses of production liners is inadequate for tribotesting, so the roughnesses  $R_a$  (C.L.A.),  $R_z$ ,  $R_{vk}$  and  $R_{pk}$  are measured on each liner prior testing.

**Tribological quantities**

The friction torque, the normal force, the bath temperature and the total linear wear are continuously measured during each test on paper recorder and computer.

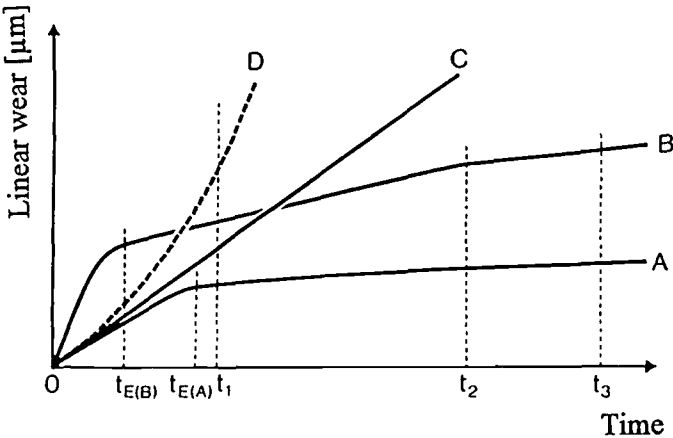


Figure 3: Possible evolution of wear length versus time of tribo-couples known from engine test<sup>16</sup>

### *Linear Wear*

The total linear wear length recorded by the inductive distance transducer contains the linear wear of stationary and rotating specimen, but normally <90% of the length is due to the overlap ration attributed to the stationary sample. After the tests, the repartition of the wear length is done by stylus profilometry and optical measurement of scar diameters. The evolution of the wear length versus time serves as indication, if

- a.) a running-in behavior (favorable) occurs,
- b.) at which geometric contact pressure the high-wear/low-wear transitions occurs and
- c.) after which distance was the coating worn-out.

It is also in engine [16] testing typical, that the wear rate vary with testing time (see Fig. 3). In consequence, any kind of test procedure must ensure, that the test time is long enough to reach steady-state. From the experience of more than 1,000 tests can be concluded, that 24,000 m is for 95% of the tribo-couples a representative sliding distance to overview the tribological behavior.

### *Wear volume*

The wear volume is the only final quantities enabling a comparison of the wear behavior, if different and changing geometry and sample dimension are used. The wear rate allows further a comparison, if different load and sliding distances were applied. The different couples are ranked by their wear rate and coefficient of friction at test end. In the case of running-in, the differential (stationary) wear rate (without running-in wear amount) has to be applied for ranking. In the case of a high-wear/low-wear transition in the tribo-test, the engineers have to verify, that the geometric pressure in the test result in greater than is his application.

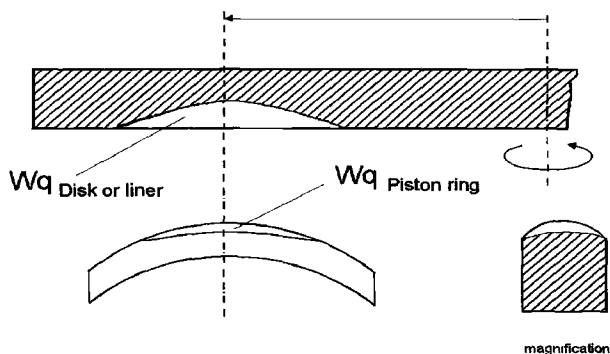


Figure 4: Schematic view of the stylus profilometry on piston ring and liner samples in order to evaluate the wear volume from planimetric wear  $Wq$  [ $\mu\text{m}^2$ ]

The planimetric wear of tracks on the disk  $W_q$  [ $\mu\text{m}^2$ ] or liner were measured at four positions by stylus profilometry in order to calculate with the circumferential diameter the volume and wear rate (see Figure 4). The stylus profile of the piston ring segment before and after test are compared in order to calculate the wear volume.

For engine application wear rates for any piston ring material should be smaller than  $k_v < 5 \times 10^{-8} \text{ mm}^3/\text{Nm}$  and for the liner materials smaller than  $k_v < 10^{-7} \text{ mm}^3/\text{Nm}$ .

*Statistical evaluation*

In tribological model testing (or pin-on-disc), tribo-couples ranked according to their wear volume differ in tribological behavior, if the wear rate are distinct by factors or in some cases one order of magnitude. From the point of view and a long experience, single test are sufficient, when the procedure and the samples it self are optimal.

In projects using materials with a comparable metallurgy leading to a small difference in the wear rates make triple or fivefold tests necessary. In such cases, the 95% deviation in the wear volume is  $\pm 30\%$  to  $\pm 50\%$ . Such standard deviations and much greater are known from engine testing [16].

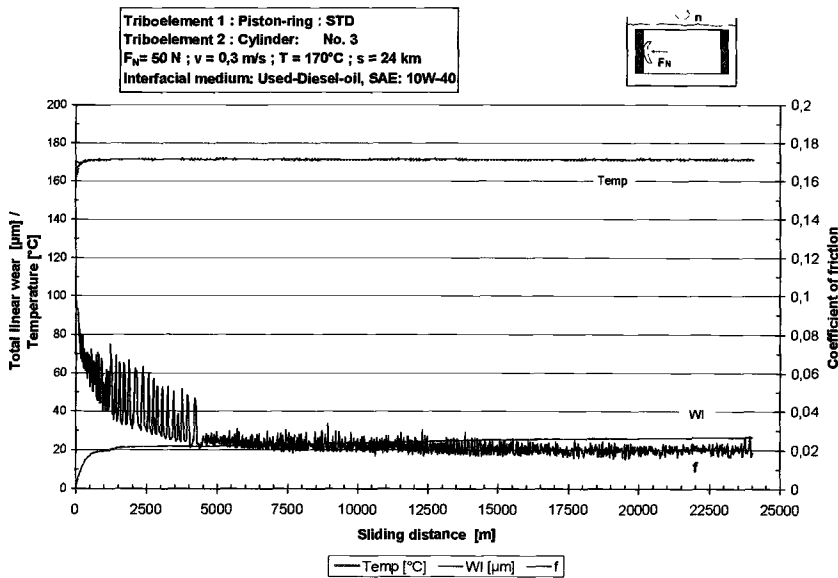


Figure 5: Tribological quantities as function of sliding distance under mixed/ boundary lubrication

**Area of applications**

Using the characterization of the tribological behavior of lubricants and materials for the system “piston ring/cylinder liner” outside of engines results and knowledge were

acquired and elaborated, which was impossible to achieve engine testing in view of the time schedule and cost budget for the following subjects:

- Influence of titanium [in 0.01 w.-% steps] and vanadium concentration in grey cast iron [6],
- Influence of thermal treatments on aluminium blocks,
- Influence of silicon content [up to 30%] associated with reduced grain sizes,
- Thermally sprayed coating in modified aluminium alloys,
- Influence of honing process parameters [6,17] ,
- Influence of different standard piston ring types,
- Wear resistant coatings for deficient lubrication [7,18],
- Biodegradable lubricants and additives,
- Influence of process parameters for laser nitriding [19] of aluminium,
- Coefficient of friction under boundary/mixed lubrication of materials interacting with different base fluids in additives and
- Bench marking of competitor's products.

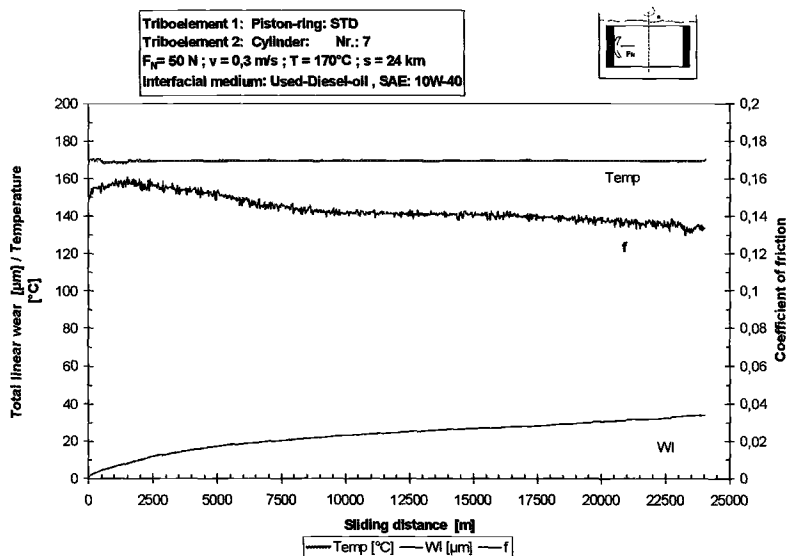


Figure 6: Tribological quantities as function of sliding distance under mixed/ boundary lubrication

### Test results

The key outcome is the time dependent evolution of the COF and the linear wear rate with the wear rates. Data basing is a further possibility in the case of a long experience with many results.

*Test diagrams*

Figure 5 displays a running-behavior already after a short distance, whereas the COF starts at ~0.1 and decreases down to ~0.02. No running-in behavior for both wear and friction exhibits the tribo-couple displayed in Figure 6, whereas in Figure 7 after a short distance a strong and desired high-wear/low-wear transition is visible, which don't influence the frictional behavior.

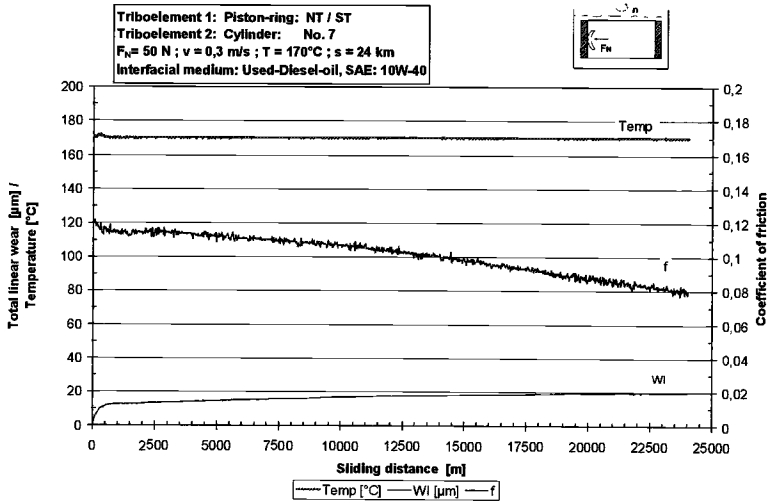


Figure 7: Tribological quantities as function of sliding distance under mixed/ boundary lubrication Figure

*Plot of results*

The plot of results and presentation almost depend on the subject regarded. Figure 8 and 9 plot the wear coefficient (rate) versus coefficient of friction at test end and display the influence of different oils. It is visible, that the polyalkyleneglycols (PAG-diol) result always in a lower COF under boundary/mixed lubrication and improve fuel-economy. The polyalkyleneglycols (PAG-diol) can compete as low-additivated fluids with fully formulated, synthetic hydrocarbon based oils. For the use in engines, the wear rates for piston rings must be lower than  $10^{-8} \text{ mm}^3/\text{Nm}$ .

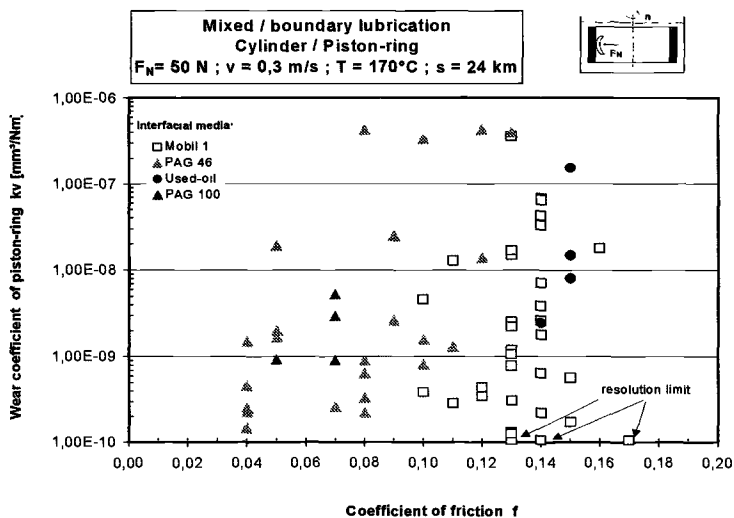


Figure 8: Summarizing plot of “Coefficient of friction at test end” versus “Wear rate for piston rings” of a set of tribo-couples in different media

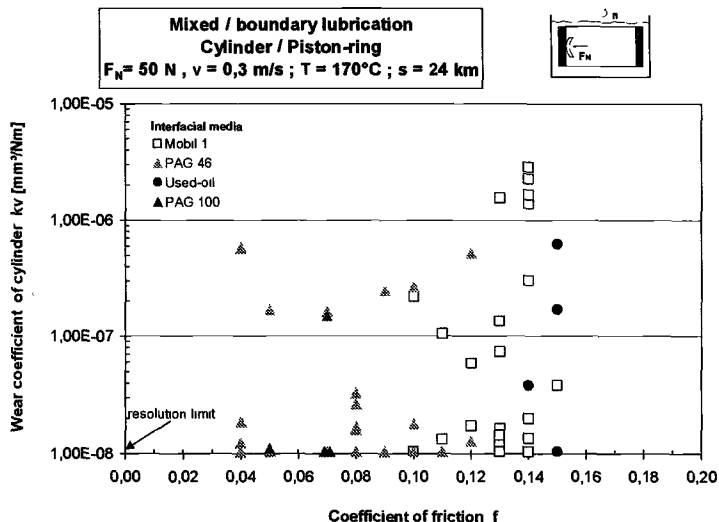


Figure 9: Summarizing plot of “Coefficient of friction at test end” versus “Wear rate for cylinder liners” of a set of tribo-couples in different media

### Summary

The test procedure for characterizing the tribological behavior of lubricants and materials for the system "piston ring/cylinder liner" outside of engines is now operational and validated. It allows the check prior expensive engine testing, if a tribo-material, tribo-couple or new lubricant will reach a satisfactory engine performance. The testing matrix can be reduced to promising candidate materials and to a reasonable number engine tests.

The introduction of piston ring segments and cylinder liner into the test rig represented a big step forward in order to increase the transferability of "tribo-tests" to engine tests on an acceptable level.

The test parameters presented in this paper may act only as an indicator and should be adopted to the tasks regarded.

### References

[1] Woydt, M.

*Living in a material world*, Testing Technology International, 1998, p. 170-174

[2] Broszeit, E., und H.-J. Schröder:

*Außermotorische Verschleißprüfung (Final report)*, Forschungsvereinigung Verbrennungskraftmaschinen, D-60498 Frankfurt, FVV-Nr. 314, Abschlußbericht, Heft 401, 1987

[3] Rao, V.D.N., D.M. Kabat, H.A. Cikanek, C.A. Fucinari and G. Wuest

*Material systems for cylinder bore applications – Plasma spray technology*  
SAE Technical Paper 970023

[4] Habig, K.-H., M. Langer, M. Woydt, J. Kadoori, N. Kelling, A. Huck und H. Hausner

*Steigerung der Einsatzgrenzen von keramischen Sonderwerkstoffen bei tribologischer Hochtemperaturbeanspruchung (Improvement of the tribological limits of engineered ceramics for high-temperature tribology)*

2. Symp. Materialforschung des BMFT 1991, Vol. III, p. 2027; ISBN 3-8249-0020-3

[5] Huck, H.

*Einsatz keramischer Spritz- und Massivsichten zum Verschleißschutz in brennraumnahen Motorbauteilen (Application of ceramic liners and thick coatings in the combustion chamber of engines)*

8. Int. Colloquium „Tribologie 2000“, Januar 1992, Esslingen, Volume 2, S. 15.6-1, ISBN 3-924813-28-0

- [6] Heller, A.  
*Einfluß von Gefüge- und Bearbeitungsparametern auf die tribologischen Eigenschaften von Zylinderlaufbahnen aus Grauguß (Influence of micro-structure and finishing on the tribological properties of liners in grey cast iron)*  
Diplomarbeit (Master of Engineering thesis), September 1995, Otto-von-Guericke-Universität Magdeburg, D-39016 Magdeburg (Germany)
- [7] Gasthuber, H., R. Gadow, J.-P. Krugers and M. Woydt  
*Verschleißschutzschichten für Systeme mit Mangelschmierung (Wear resistant coatings for systems under deficient lubrication)*  
BMBF-Project 3N3046 (German Federal Ministry of Education and Research),  
Poster at the Werkstoffwoche 1998 (Materials Week), Munich (Germany)
- [8] Barnickel, J., H.W. Bergmann und S. Reichstein  
*Aufbau und Eigenschaften von lasernitrierten Randschichten auf Aluminiumwerkstoffen (Structure and properties of laser nitrided aluminium surfaces)*  
Härterei-Technische-Mitteilungen, Vol. 53 (5), 1998, p. 337-342
- [9] Ye, A., H. S. Cheng and N. S. Chang:  
*Wear characteristics of nickel/silicon carbide composite coating in lubricated reciprocating contacts, Tribology Transactions, Vol. 39(3), 1996, p. 527-536*
- [10] Naylor, M.G.S.  
*Wear-resistant ceramic coatings, paper presented at the U.S. Department of Energy Annual Automotive Technology Development Contractor's Coordination Meeting, Dearborn, MI, October 22-25, 1990, publ. SAE P-243, pp. 273-281*
- [11] Zhang, Y., L. Yun and Z. Houjun  
*An experimental investigation into the wear of the cylinder liner-piston ring in engines*  
Tribotest Journal 2-3, March 1996, p. 281-288
- [12] Becker, E.P., and K.C. Ludema  
*A qualitative empirical model of cylinder bore wear*  
WEAR Vol. 225-229, 1999, p. 387-404
- [13] Roger, G.W. and J.C. Bell  
*Review and evaluation of lubricated wear in simulated valve train contact conditions*  
SAE paper 952473

[14] Woydt, M.

*Beschaffung innovativer Werkstoffe (Modern methods to retrieve innovative material solution, under review for L&E)*, Tribologie&Schmierungstechnik, 45. Jg., Heft 1, 1998, p.37-41

[15] Thiele, E.

*Verfahren zur Ermittlung der Funktionstauglichkeit von Schmierölen*  
Patent DE 196 44 029 A1, 07. Mai 1998

[16] Morsbach, M. and P. Jörren

*Praxisrelevante Verschleißermittlung an Kolbenring- und Zylinderlaufflächen*  
Motortechnische Zeitschrift, Vol. 52(3), 1991, p. 126-132

[17] Kloft, M. and R. Strich

*Verfahren zum Herstellen einer Gleitfläche auf einem metallischen Werkstück*  
Patent application DE 195 40 572 A1

[18] Gasthuber, H., R. Gadow, J.-P. Krugers and M. Woydt

*Verschleißschutzschichten für Systeme mit Mangelschmierung (Wear resistant coatings for systems under deficient lubrication)*

BMBF-Project 3N3046 (German Federal Ministry of Education and Research),  
Poster at the Werkstoffwoche 1998 (Materials Week), Munich (Germany)

[19] Barnickel, J., H.W. Bergmann und S. Reichstein

*Aufbau und Eigenschaften von lasernitrierten Randschichten auf Aluminiumwerkstoffen (Structure and properties of laser nitrided aluminium surfaces)*

Härterei-Technische-Mitteilungen, Vol. 53 (5), 1998, p. 337-342

Shashi K. Sharma,<sup>1</sup> Carl E. Snyder, Jr.,<sup>1</sup> and Lois J. Gschwender<sup>1</sup>

## Aircraft Hydraulic Pump Tests with Advanced Fire-Resistant Hydraulic Fluids

---

**Reference:** Sharma, S. K., Snyder, C. E., Jr., and Gschwender, L. J., "Aircraft Hydraulic Pump Tests with Advanced Fire-Resistant Hydraulic Fluids," *Bench Testing of Industrial Fluid Lubrication and Wear Properties Used in Machinery Applications*, ASTM STP 1404, G. E. Totten, L. D. Wedeven, J. R. Dickey, and M. Anderson, Eds., American Society for Testing and Materials, West Conshohocken, PA, 2001.

**Abstract:** During the development of the fire-resistant hydraulic fluids for DoD (Department of Defense) aircraft, candidate fluids were formulated and then characterized initially by various laboratory bench tests. Endurance pump tests were then conducted on the candidate fluids to validate their performance. Pump tests under accelerated conditions were conducted on three candidate fire-resistant hydraulic fluids and several candidate nonflammable hydraulic fluids, using pressure-compensated axial flow piston pumps and an instrumented, small-volume, closed-loop hydraulic test stand. Case-drain temperature and signal-noise on the pump outlet pressure and the case-drain flow provided better failure indicators than the case-drain flow. The fluids containing viscosity-index-improvers underwent large viscosity losses. No viscosity loss was observed for the fluids that did not contain the viscosity-index-improvers. Lower viscosity fluids performed as well as the higher viscosity fluids in these pump tests. However, the ball-bearing material and the heat treatment had a bigger impact on pump life. Use of an M-50 bearing in place of the AISI-52100 bearing doubled the pump life.

Based upon the laboratory screening tests and the validation pump tests, the best performing fire-resistant hydraulic fluid was recommended for use in the DoD aircraft. Performance of the recommended fluid was further demonstrated in successful aircraft flight tests. Only limited hydraulic system simulator and aircraft subsystem testing has been conducted on the best-performing nonflammable hydraulic fluid candidate to date, but the performance was acceptable.

**Keywords:** hydraulic pumps, hydraulic fluids, viscosity, bearings, polyalphaolefin, chlorotrifluoroethylene, nonflammable hydraulic fluid

---

<sup>1</sup> Air Force Research Laboratory, Materials Directorate, Wright-Patterson Air Force Base, OH.

## Introduction

During the development of the advanced fire-resistant and nonflammable aircraft hydraulic fluids [1, 2], various laboratory methods were used to assess their properties. These properties included viscosity, thermal and oxidative stability, flash point, flame propagation, shear stability, corrosion resistance, four-ball wear and others. Performance of the promising candidate fluids emerging out of the laboratory evaluations had to be validated in aircraft hydraulic components/systems. Full-scale hydraulic system simulator (Iron Bird) tests or flight tests could accomplish this but these are very expensive. Flight-tests without prior validation in aircraft components are considered high risk. A more practical, cost-effective approach is to conduct endurance hydraulic pump tests under carefully controlled conditions. The hydraulic pump in a system is generally considered to be the component most sensitive to most of the properties of a hydraulic fluid (e.g., viscosity, lubricity, vapor pressure, foaming, etc.). Long-term pump tests were conducted under realistic but severe conditions for the validation of the candidate formulations. The four ball wear tests were used to check the effectiveness of the antiwear additives. The pump tests were only conducted with the formulated fluids. Therefore, correlation between the performance of the base oils and the formulations, in the four ball wear tests and the pump tests could not be drawn. The failure modes observed during these pump tests and some important diagnostic features are discussed in this paper.

## Pump Tests

### *Test Stand*

The pump tests were conducted using a closed-loop test stand as shown in Figures 1 and 2. The test circuit consisted of a variable speed drive motor, a throttling valve, a heat exchanger, a reservoir, 5 $\mu$  filters, flow meters, pressure sensors, thermocouples and other safety and control devices. A computerized data acquisition and control system was used, and the test parameters were also continuously recorded on chart recorders. With the data acquisition and control system, tight shutdown limits could be input that allowed the test to shut down quickly without causing significant secondary wear. The system also provided the necessary safety aspects to allow the stand to be run 24 hours a day seven days per week. Most of the failed pump tests described later shut down automatically due to higher case drain temperature.

The throttling valve worked as a flow control device that also subjected the fluid to high shear. The working volume of the test loop was only about a gallon. Thus, a small volume of the fluid was subjected to high stress levels. While the reservoir was not in the test loop, it provided the makeup fluid when fluid samples were drawn or leakage occurred. Fluid samples drawn from the circuit during the tests were analyzed

to check the condition of the fluid. Between tests, a complete disassembly and cleaning of the test stand was performed to minimize cross-contamination.

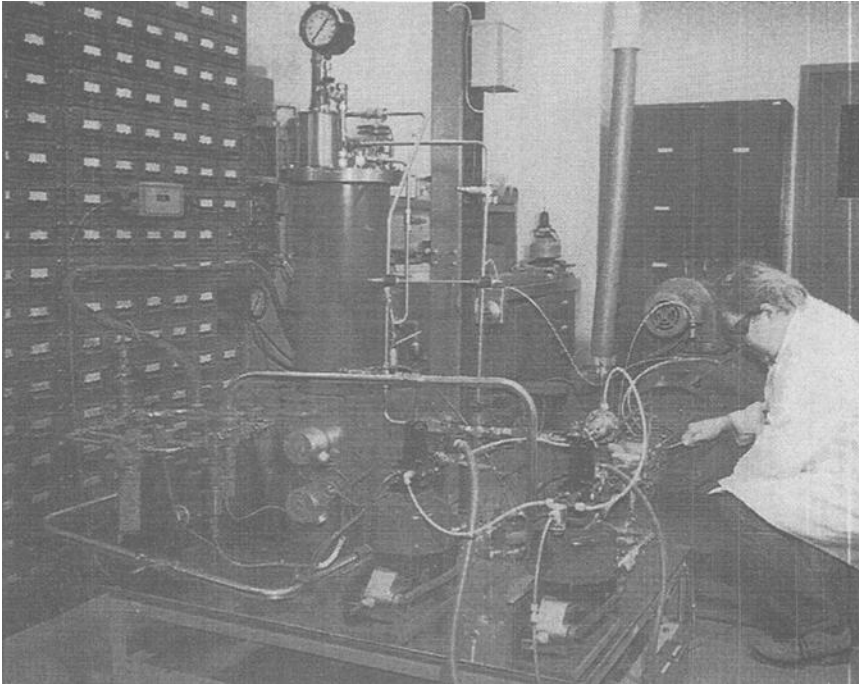


Figure 1. Pump Test Stand

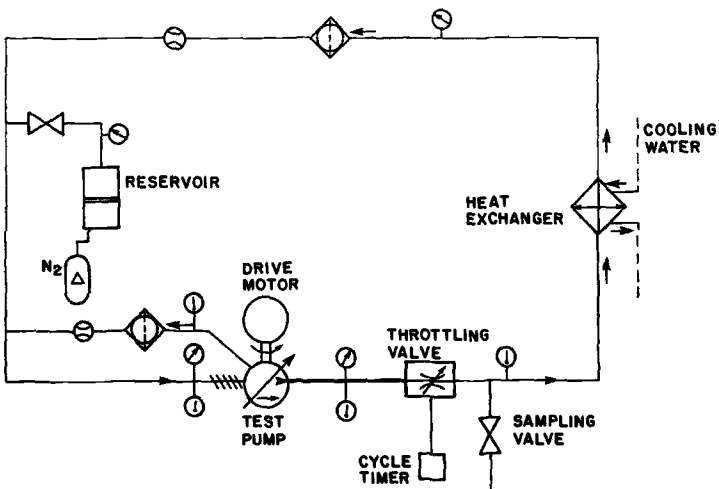


Figure 2. Schematic of the Pump Test Circuit

### *Test Pump*

Axial flow, pressure compensated hydraulic pumps, Vickers model PV3-075-15 (used in the F-16 Emergency Power Unit) were used in these tests. A new or rebuilt pump was used for each test. A partially disassembled pump is shown in Figure 3. A shaft/bearing assembly from another pump is also shown for clarity. The test pump was disassembled (see Figure 4) to photograph the critical wear surfaces, both before and after the test. An axial flow piston pump contains numerous wear interfaces that experience different lubrication regimes as listed in Table 1. The fluid/pump combination must perform well in boundary, mixed, and fluid film (elastohydrodynamic and hydrodynamic) lubrication. Pump parts were inspected after the test to assess the wear and cavitation damage.

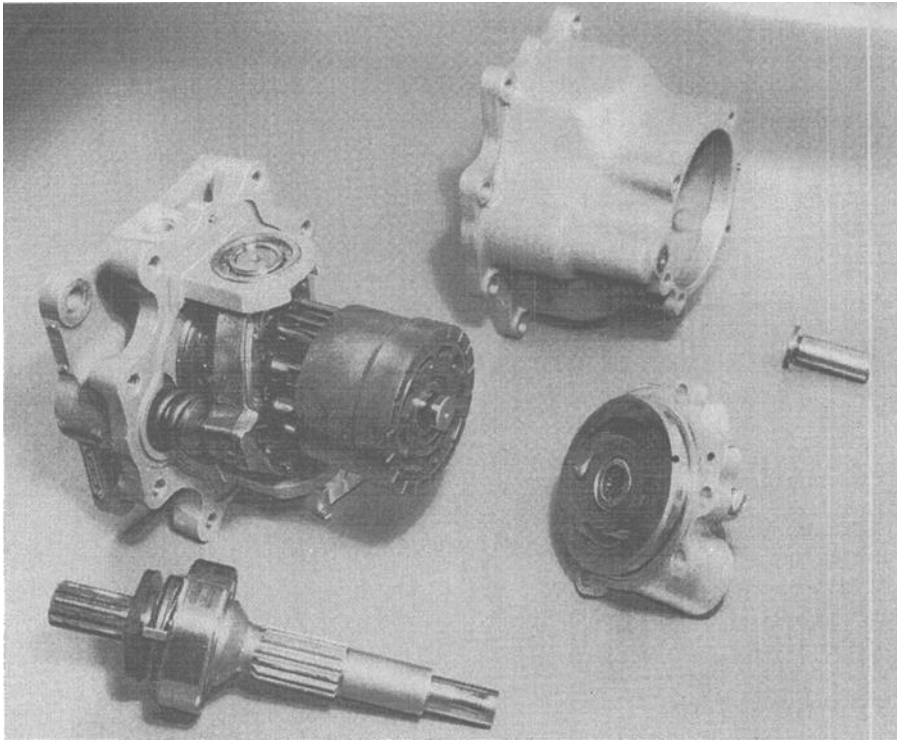


Figure 3. *Test Pump, Vickers Model PV3-075-15*

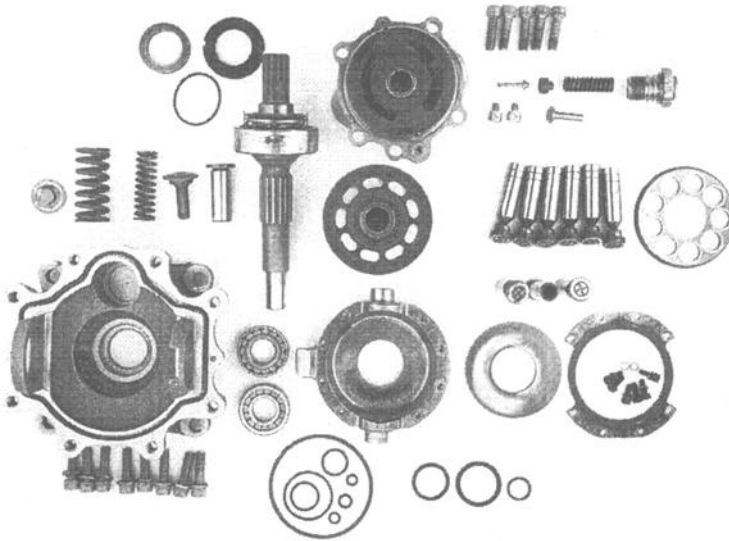


Figure 4. Disassembled Test Pump, Vickers Model PV3-075-15

Table 1. Lubrication Regimes in an Aircraft Hydraulic Pump

Interface	Lubrication Regime	
	Fluid Film Lubrication	Boundary Lubrication

Actuator Piston		X
Shaft and Cylinder Block Splines		X
Pintle Bearings		X

Following Rotating/Sliding Interfaces at Higher Speeds

Piston Shoe Ball Joint	X
Cylinder Block and Valve Plate Faces	X
Piston Shoe Faces and Bearing Plate	X
Pistons and Cylinder Bores	X
Hold Down Plate and Bearing Plate	X
Main Thrust Ball Bearing and Needle Bearing	X

Following Rotating/Sliding Interfaces at Slower Speeds

Piston Shoe Ball Joint	X
Cylinder Block and Valve Plate Faces	X
Piston Shoe Faces and Bearing Plate	X
Pistons and Cylinder Bores	X
Hold Down Plate and Bearing Plate	X
Main Thrust Ball Bearing and Needle Bearing	X

*Test Parameters*

The test parameters are listed in Table 2. The maximum fluid temperature in the circuit (usually case drain) was maintained close to the upper design limit of the pump and within the thermal stability limits for the fluid. The main output flow of the pump was cycled between ~12 gpm and ~3 gpm every minute to increase the severity of the tests. Due to the thermal inertia of the system, only the average fluid temperatures could be controlled. During the higher flow cycle (TVO - throttling valve open) the temperatures increased and during the lower flow cycle (TVC - throttling valve closed) the temperatures decreased. A total of ~10°F variation in temperature was typical between the two flow cycles (see Figure 5). Similar variations were present in the case drain flow and filter pressure drop.

Table 2. *Pump Test Parameters*

Pump Outlet Pressure	3000 psig
Pump Inlet Pressure	50-60 psig
Main Flow Rate (TVO)* (TVC)**	12 gpm (1 minute) 3 gpm (1 minute)
Speed	5000 rpm

\* TVO – Throttling Valve Open

\*\* TVC – Throttling Valve Closed

*Pump Test Results with Fire-Resistant Hydraulic Fluids*

Silhydrocarbon and PAO (polyalphaolefin) based fluids as described in Table 3 were used. The silhydrocarbon and PAO formulations also contained antiwear and antioxidant additives. A base line pump test with a mineral oil based hydraulic fluid, MIL-H-5606, was also conducted for comparison.

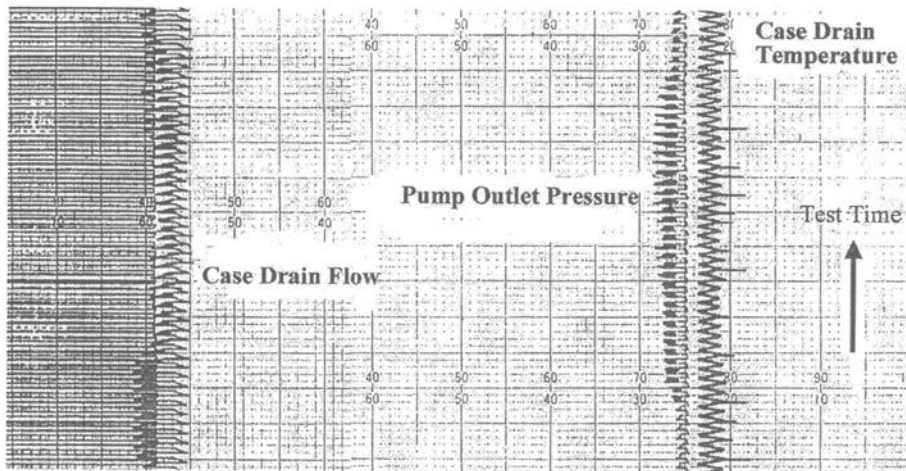


Figure 5. Typical Strip Chart Recording from Pump Test

Table 3. Endurance Pump Tests with MIL-H-5606 and Fire-Resistant Hydraulic Fluids

TEST NO.	DATE	FLUID	PUMP MODEL & S/N	Test Temp (°F)	HOURS
7	1/82-7/82	MLO-80-541 (MIL-H-5606)	VICKERS PV3-075-15 MX-352669	260-270	590
10	4/85-6/85	MLO-85-109 (PAO Dimer-Trimer Blend)	VICKERS PV3-075-15 MX-365345	245-255	500
11	7/85-9/85	MLO-85-255 (PAO Dimer-Trimer Blend)	VICKERS PV3-075-15 MX-363401	240-250	500
12	10/85-11/85	MLO-85-306 (PAO Dimer+PMMA* +Metal Deactivator)	VICKERS PV3-075-15 MX-364405	245-255	500
13	3/86-4/86	MLO-86-38 (Dimer-Trimer Blend + Metal Deactivator)	VICKERS PV3-075-15 MX-363403	245-255	500
21	12/87-1/88	MLO-87-430 Silahydrocarbon	VICKERS PV3-075-15 MX-439842	240-250	395
22	6/88-10/88	MLO-88-151 Silahydrocarbon	VICKERS PV3-075-15 MX-441304	240-250	506

\* polymethylmethacrylate VI improver

*Pump Tests with Silahydrocarbon Hydraulic Fluids-* Two pump tests were conducted with the silahydrocarbon based hydraulic fluid. In the first test, a piston/shoe assembly failed after 395 hours as shown in Figure 6. Failure of the piston/shoe led to secondary damage to other components such as the main bearing. The test was repeated with a new pump and successfully completed the 500 hours. The pump parts looked like new after the test.

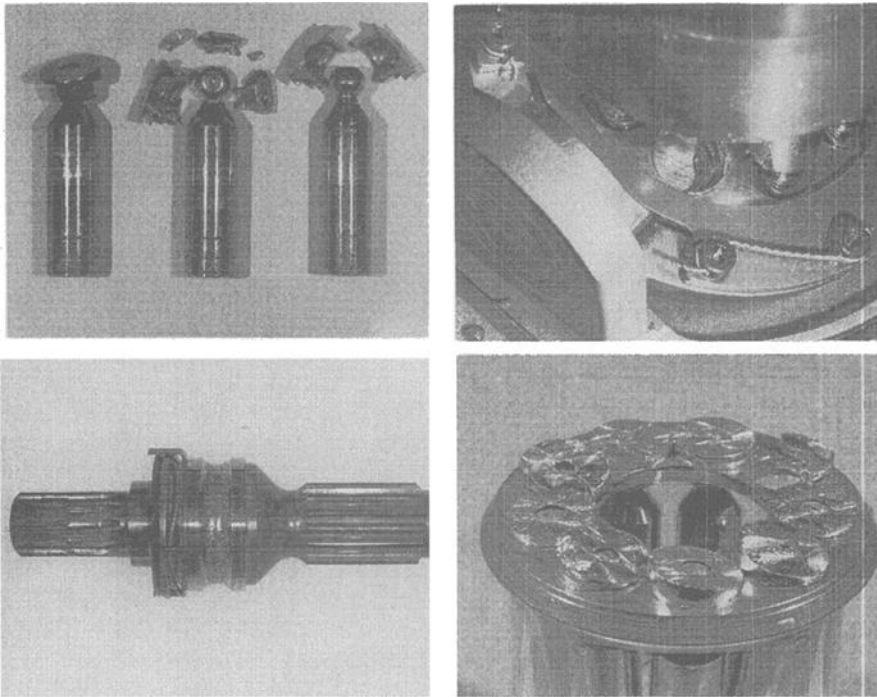
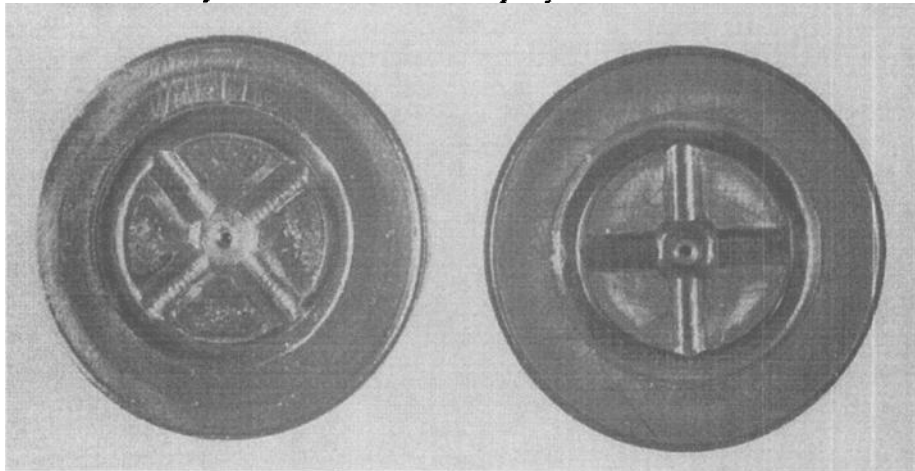


Figure 6. *Piston Shoe Failure in Pump Test 21*

*Pump Tests with Polyalphaolefin Hydraulic Fluids-* All pump tests with the candidate fluids successfully finished the scheduled 500 hours. There was only polishing wear observed on the wear surfaces. Slight darkening of the bronze parts was also observed when the test fluid did not contain the metal-deactivator, benzotriazole. The discoloring was strictly cosmetic and did not affect pump performance. Slightly more cavitation on the piston-shoe faces (see Figure 7) was observed for the VI (viscosity index) improver containing fluid.

The fluid viscosity dropped sharply during the tests for the VI-improved fluids (MIL-H-5606 and PAO dimer + VI improver), whereas there was no viscosity loss for the non-VI-improved fluids, as shown in Figure 8. During Test 7, an O-ring leaked

after 45 hours and new fluid was added to the test stand. This resulted in the increased viscosity as shown in Figure 8. Similarly, some of the fluid from the reservoir entered the test loop during the pump disassembly/inspection after 250 and 500 hours, resulting in slight increase in the test fluid viscosity. It is interesting to note that the sheared, reduced viscosity fluid did not adversely affect the pump performance, and perhaps an even lower viscosity fluid would have worked equally well.



a. *Piston Shoe from Pump Test 12 with PAO Dimer + VI Improver*

b. *Piston Shoe from Pump Test 13 with PAO Dimer + Trimer*

Figure 7. *Piston Shoes from Pump Tests with Fire-Resistant Hydraulic Fluids [1]*

Case drain flow is the internal fluid leakage across the cylinder-block/valve plate interface and around the pistons. An increase in case drain flow is generally attributed to pump wear. As shown in Figure 9, the case drain flow increased only for the VI-improver containing fluids. This is attributed to the reduction in the viscosity of these fluids and not to the pump wear. For Test 7 (with MIL-H-5606), the increase in viscosity after 45, 250 and 500 hours due to introduction of new fluid into the test loop resulted in a corresponding reduction in the case drain flow. Test 12 was run continuously for 500 hours without any mid-test stoppage, therefore no new fluid was introduced into the test loop. A continuous reduction in the viscosity and a corresponding increase in the case drain flow is observed for this test, as shown in Figure 10. The local fluctuations in the case drain flow are caused by the variation in the fluid temperature. If the fluid viscosity decreases with usage, using the case drain flow as a diagnostic parameter can be misleading. An increase in the case drain flow may simply be due to the reduced viscosity and not due to increased wear.

Based upon these pump tests and other considerations, the PAO dimer-trimer blend was recommended as a fire-resistant hydraulic fluid (later designated as MIL-PRF-87257) to replace the flammable MIL-H-5606.

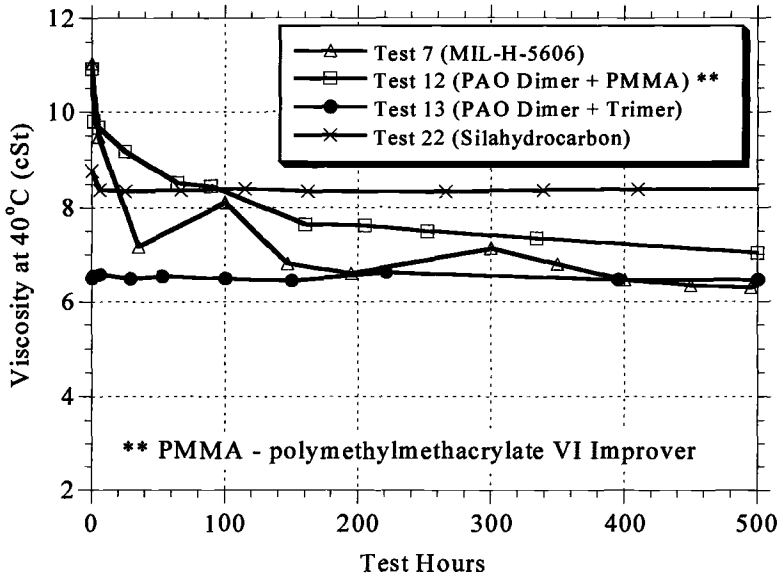


Figure 8. Viscosity of the Fluid Samples from Pump Tests with MIL-H-5606 and Fire-Resistant Hydraulic Fluids

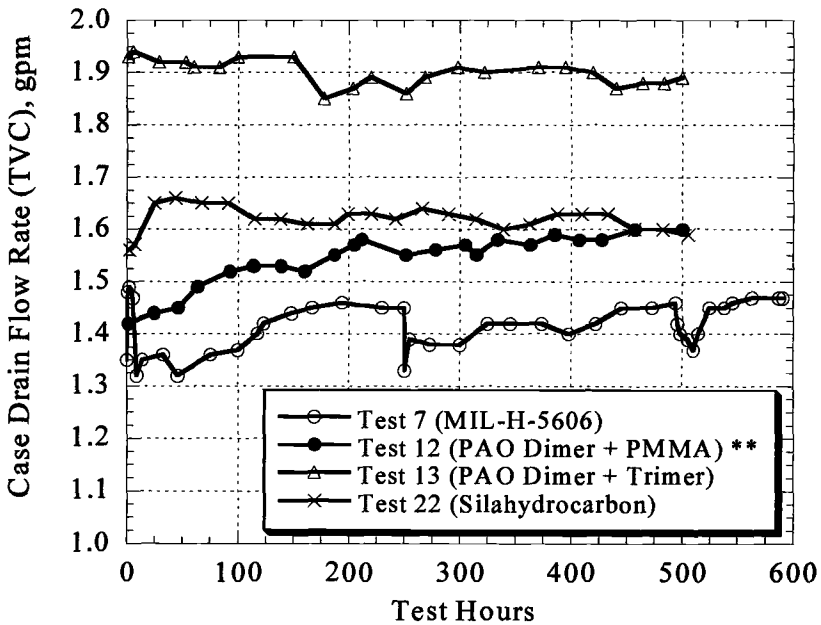


Figure 9. Case Drain Flow for Pump Tests with MIL-H-5606

*and Fire-Resistant Hydraulic Fluids*

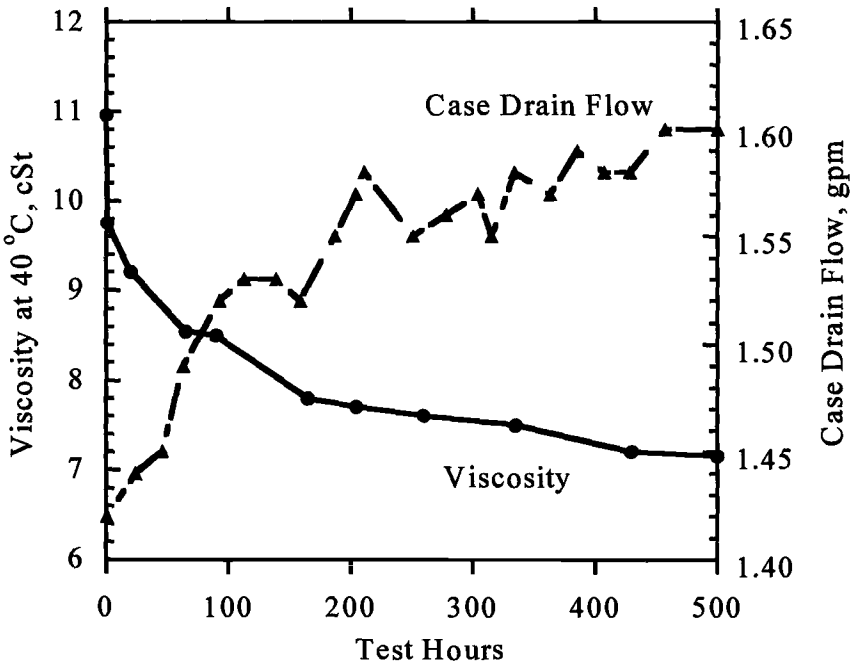


Figure 10. *Viscosity and Case Drain Flow for Pump Test 12 (PAO Dimer + VI improver Fluid)*

*Pump Test Results with Nonflammable Hydraulic Fluids*

Table 4 shows the pump tests conducted with the chlorotrifluoroethylene oligomer (CTFE) based nonflammable hydraulic fluids. A Vickers pump, model PV3-075-15 was used for most of the tests. However, for the higher temperature test (Test-32), a modified version of this pump (model PV3-075-37) was used. In PV3-075-37 pump, the shoes and cylinder block were made from tool steel in stead of bronze, and an M-50 bearing was used in place of the AISI-52100. It should be mentioned that the test pump PV3-075-15 was originally designed for the mineral oil (MIL-H-5606), and was not optimized for the CTFE fluid. More wear was observed in the CTFE pump tests, and is attributed to the different chemistry of the fluid. Different wear characteristics observed are discussed below.

Table 4. Endurance Pump Tests with Nonflammable CTFE Hydraulic Fluids

TEST NO.	DATE	FLUID	PUMP MODEL & S/N	TEMP (°F)	HOURS
8	10/82-3/83	MLO-82-150 (CTFE 3.1+BSN+3M)	VICKERS PV3-075-19 MX-357772	250-260	560
9	12/83-4/84	MLO-83-715 (CTFE)	VICKERS PV3-075-15 MX-355007	250-260	500
15	10/86-11/86	MLO-86-419 (CTFE 3.1+BSN+3M)	VICKERS PV3-075-15 MX-441306	250-260	470
20	10/87-11/87	MLO-87-426 (CTFE 3.1+BSBDA+3M)	VICKERS PV3-075-15 MX-441305	255-265	500
24	2/89-3/89	MLO-89-14 (CTFE 3.1+Zn+3M)	VICKERS PV3-075-15 MX-443030	235-245	500
25	4/89-5/89	MLO-89-129 (CTFE 3.1+BSN+3M)	VICKERS PV3-075-15 MX-444595	235-245	500
26	6/89	MLO-89-133 (CTFE 6.3+BSN+3M)	VICKERS PV3-075-15 MX-480358	240-250	332
27	8/89	MLO-89-227 (CTFE 27+BSN+3M)	VICKERS PV3-075-15 MX-352667	235-245	172
28	12/89-1/90	MLO-89-130 (CTFE 3.1+Zn+3M)	VICKERS PV3-075-15 MX-444581	240-250	286
29	2/90-4/90	MLO-89-130 (CTFE 3.1+Zn+3M)	VICKERS PV3-075-15 MX-480345	235-245	930
30	2/90-7/90	MLO-89-348 (CTFE 27+BSN+3M)	VICKERS PV3-075-15 MX-357772	235-245	353
32	3/91-4/91	MLO-90-631 (CTFE 3.1+Zn+3M)	VICKERS PV3-075-37 MX-503782	275 300 325 350	50 25 50 7

CTFE 3.1: chlorotrifluoroethylene base oil, 3.1 cSt at 100°F

CTFE 6.3: chlorotrifluoroethylene base oil, 6.3 cSt at 100°F

CTFE 27: chlorotrifluoroethylene base oil, 27 cSt at 100°F

BSN: barium dinonylnaphthalene sulfonate, anti-corrosion additive

BSBDA: anti-corrosion additive

ZN: zinc dinonylnaphthalene sulfonate, high temperature (350°F) anti-corrosion additive

3M antiwear additive

Wear of the main bearing (an angular contact ball bearing) was the primary wear-mode. In an earlier CTFE test (Test-8), the main bearing performed well for more than 500 hours, whereas in later tests it started to fail prematurely. Toward the latter part of the test, the pump became noisier, accompanied by an added signal noise on the pump outlet pressure and the case drain flow, as shown in Figure 5. Wear on the bearing races/balls can impart a wobbly motion to the cylinder block thereby inducing fluctuations on the pump outlet pressure and the case-drain flow signals. A combination of these two events (pump noise and signal fluctuations) constituted the onset of the main bearing failure. In most tests, the pump would still maintain its performance characteristics for a long time after the onset of bearing failure. This is shown in Figure 11 by the checked portion of the bars.

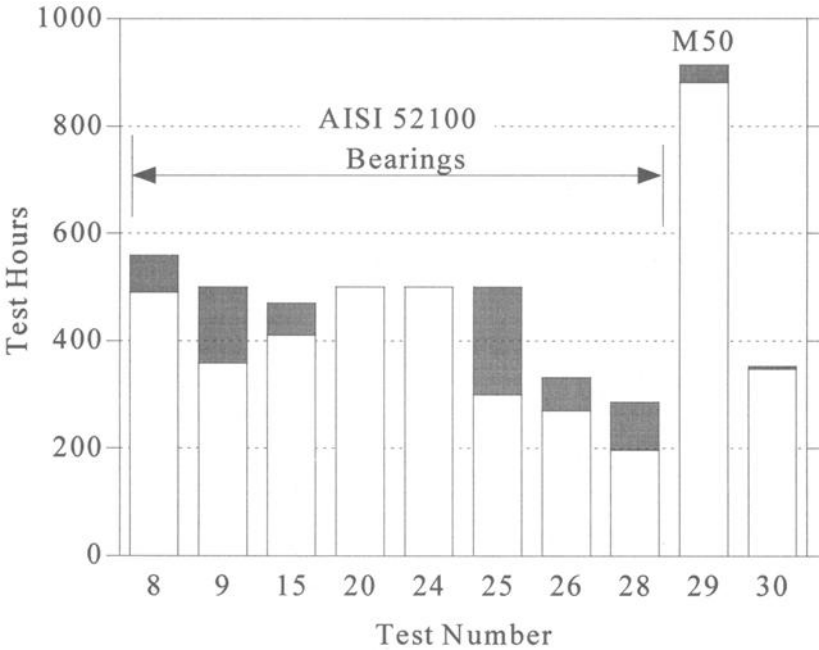
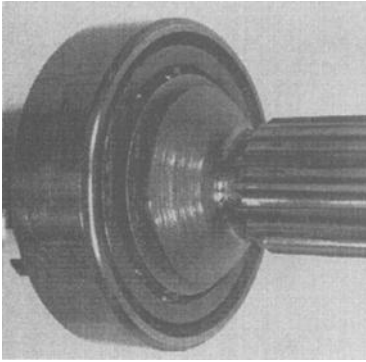
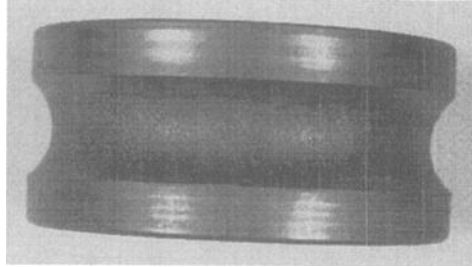


Figure 11. Onset of Bearing Failure in CTFE Pump Tests

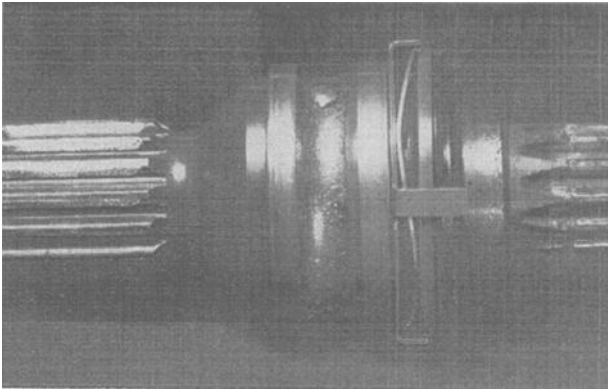
Two types of bearing wear were observed. In some of the tests, severe spalling of the races and balls was observed as shown in Figure 12b and Figure 12c. In other tests, there was no spalling but the races and the balls exhibited severe polishing wear and had lost their dimensional tolerances as shown in Figure 12d. The angular contact bearing used in this pump does not easily come apart with hand pressure when the bearing is in good condition as shown in Figure 12a. When the bearing has worn considerably (spalled or polishing wear), it comes apart easily.



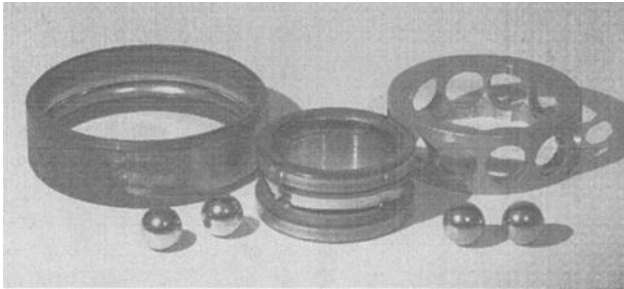
a. *After 500 Hr. Pump Test with Fire-Resistant Hydraulic Fluid. Bearing in Good Condition*



b. *After 470 Hr. Pump Test with CTFE-3.1+BSN+3M (Test 15) Severe Spalling on Inner Race*



c. *After 335 Hr. Pump Test with CTFE-6.3+BSN+3M (Test 26) Severe Spalling on Inner Race*



d. *After 500 Hr. Pump Test with CTFE-3.1+ZN+3M (Test 24) Polishing Wear on Races and Balls*

Figure 12. *Bearing Wear in Pump Tests*

The pressure-viscosity coefficient and the EHL (elastohydrodynamic lubrication) film forming capabilities of the CTFE fluid used in the tests until this time were less than its hydrocarbon counterparts (Figure 13). The base fluid used for these tests has a viscosity of 3.1 cSt at 100°F. Since the EHL film thickness for the VI improved fluids depends on their base oil properties [3], properties of the base oils were used in these calculations. Higher viscosity CTFE fluids (6.3 cSt and 27 cSt at 100°F) were formulated that would provide film thickness equivalent to the fluids that performed well in pump tests, such as MIL-H-5606 and the PAO fluids. Pump tests (Tests 26 and 27) with higher viscosity CTFE fluids were conducted. The bearings still failed prematurely, indicating that the improvements in the EHL film thickness imparted by the higher viscosity fluid were being masked by the chemical interactions between the fluid and the surfaces. The composite surface roughness of the bearing surfaces is ~7 micro-in, and based upon the calculated film thickness the bearings would be operating in partial or boundary lubrication regime. Under these severe lubrication conditions, the material properties of the bearing and the fluid play significant role in reducing the wear. While some bearing materials may perform well with one class of fluids, the same may fail prematurely with another chemical class. As discussed below, selection of proper bearing material and heat treatment can significantly improve the bearing life.

The hardness of the bearing from Test-28 had reduced from 59 R<sub>c</sub> to 55 R<sub>c</sub>, whereas the bearing from Test-8 had maintained its original hardness of 61 R<sub>c</sub>. It was observed that a different vendor supplied the bearings for Test-8 pump and for the tests that failed prematurely. Both vendors had used AISI 52100 bearing steel but the heat treatment was different. While the bearings from both the vendors were within the Vickers' specified 58-63 R<sub>c</sub>, the different heat treatment had led to the different initial hardness. Long term operation under partial/boundary lubrication conditions in the CTFE tests resulted in the reduced hardness and hence lower bearing life for the bearing that started with 59 R<sub>c</sub> hardness. Bearings supplied by both vendors performed equally well in the hydrocarbon-based fluids, but were not optimized for the CTFE. Higher bearing hardness (61-63 R<sub>c</sub>) would be desirable for longer bearing life.

For Test-29, the main bearing (AISI 52100) was replaced with an M-50 (AMS 6491) bearing. M-50 bearings are used in high performance gas turbine engines and other critical applications where long life is desired. This pump test ran for a total of 930 hours. After 263 hours, the case drain temperature increased sharply. Disassembly revealed a broken piston shoe. The bronze fragments of the shoe were found in the pump housing and in the bearing, but the bearing was still in good condition. Similar shoe failure had been previously experienced in a pump test (Test 21) with a silahydrocarbon-based fluid. All of the nine pistons, the shoe retaining plate, the piston bearing plate and the carbon seal were replaced. The pump was again inspected after 500 and 764 total hours. The case drain flow (see Figure 14) and the coolant flow steadily increased indicating progressive wear of the pump parts. Additional coolant flow was needed to remove the excessive heat generated by the internal friction of the pump. The test was continued until 930 hours. Throughout the test, there was no indication of the bearing problems, such as excessive pump noise or the instrument

signal noise mentioned earlier. Disassembly at the end of the test showed wear on all critical surfaces, but the bearing was in good shape and rotated freely.

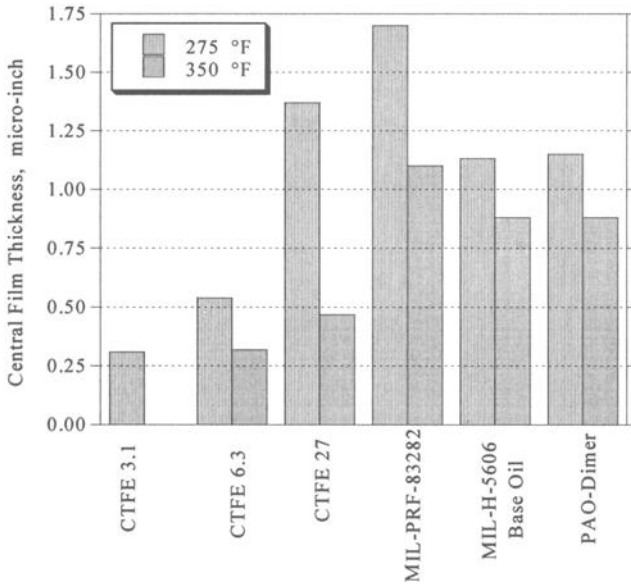


Figure 13. Calculated Elastohydrodynamic Lubrication Film Thickness in Pump Bearing

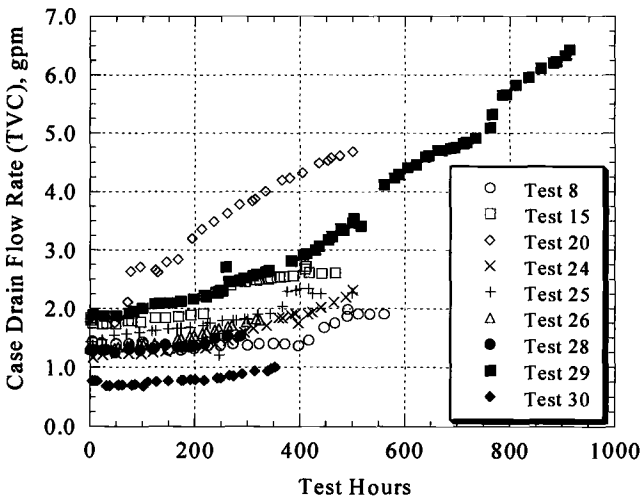


Figure 14. Case Drain Flow for Pump Tests with CTFE Nonflammable Hydraulic Fluids

### *Fluid Analyses*

Fluid samples were taken during each pump test at regular intervals, and were analyzed for viscosity, acid number, water content and lubricity. Inductively coupled plasma emission spectrometry was used to analyze the dissolved metals. In MIL-H-5606, silahydrocarbon and PAO based fluids, no significant metals were observed in the fluid. In the CTFE tests, the concentration of iron and zinc increased initially and leveled off as the tests progressed. While some CTFE formulations contained a zinc-based additive, the others did not. Zinc was observed in all the CTFE pump test samples and is thought to be coming from the bronze plated surfaces. No direct correlation could be drawn between the metal content and pump wear.

### **Conclusions**

1. Heat treatment of AISI-52100 bearings significantly influenced the bearing/pump life.
2. Use of an M-50 (AMS 6491) bearing in place of an AISI-52100 doubled the pump life in a pump test conducted with chlorotrifluoroethylene-based nonflammable hydraulic fluids.
3. Higher case drain temperature and signal-noise on the pump outlet pressure and the case-drain flow were better indicators of failure than an increase in case-drain flow.
4. The hydraulic fluids containing viscosity-index-improvers suffered significant viscosity loss during the pump tests. The reduction in viscosity resulted in a corresponding increase in case-drain flow. The reduced viscosity of these fluids did not affect the pump performance/life.
5. In these pump tests, higher viscosity fluids did not necessarily perform better than the lower viscosity fluids. Longer pump life was determined by better boundary lubrication performance of the fluid/pump combination.

### **References**

- [1] Gschwender, L. J., Snyder, C. E., Jr. and Sharma, S. K., "Pump Evaluation of Hydrogenated Polyalphaolefin Candidates for a -54°C to 135°C Fire-Resistant Air Force Aircraft Hydraulic Fluid," *Lubrication Engineering*, 1988, 44, 4, 324-329.
- [2] Gschwender, L. J., Snyder, C. E., Jr. and Sharma, S. K., "Development of a -54°C to 175°C High Temperature Nonflammable Hydraulic Fluid for Air Force Systems," *Lubrication Engineering*, 1993 49, 8, 621-630.
- [3] Sharma, S. K. and Forster, N. H., and Gschwender, L. J., "Effect of Viscosity Index Improvers on the Elastohydrodynamic Lubrication Characteristics of a Chlorotrifluoroethylene and a Polyalphaolefin Fluid," *Tribology Transactions*, 36, 3, 555-564.

J. Xiao,<sup>1</sup> H. Liang,<sup>1</sup> R. Crisenberry,<sup>2</sup> and M. Cook<sup>3</sup>

## A New Device for Traction Measurement on Ice

---

**Reference:** Xiao, J., Liang, H., Crisenberry, R., and Cook, M., “A New Device for Traction Measurement on Ice,” *Bench Testing of Industrial Fluid Lubrication and Wear Properties Used in Machinery Applications, ASTM STP 1404*, G. E. Totten, L. D. Wedeven, J. R. Dickey, and M. Anderson, Eds., American Society for Testing and Materials, West Conshohocken, PA, 2001.

**Abstract:** Friction on ice in driving, running, and walking situations is important for winter activities in Alaska. In order to simulate the friction, we designed a traction-measuring device fitting to low-temperature applications. By using a hydraulic system we apply a load ranging from less than one pound to as high as five hundred pounds. The static friction can be measured by moving the ice block against any materials desired. Results showed that the ice surface changes according to applied load, sliding speed, and temperature. This device is capable of providing insight of tribological behavior of ice and snow against materials such as automobile tires and shoe materials, etc.

**Keywords:** ice friction, asperity contact, surface layer, tribological testing

### Introduction

Ice is unique among all common substances insofar as its friction is concerned. People who are interested in ice friction include skiers, sleigh driver, hockey players, motorists, pedestrians. Some of them need the friction as low as possible; for example, the slipperiness makes it possible to enjoy winter sports and move heavy cargo by using sleds. On the contrary, some people are concerned with how to increase the friction in winter, especially in Alaska. Injuries are common when pedestrians walk on ice and are involved in accidents because of slippery conditions.

There is a long history of measurement of friction between ice, snow, and various materials. Most tests were concerned with the effects of ski material, load, speed, and

---

<sup>1</sup> University of Alaska, Fairbanks, AK.

<sup>2</sup> Crisenberry Engineering Inc. AK.

<sup>3</sup> Polar Environmental Technology Inc. AK.

temperature on the friction force in recreational skiing. Interest in snow and ice friction also comes from a variety of subjects of practical importance, including automobile tires, icebreaker propulsion, and off-road vehicles. Kinetic friction has been studied the most because of the application of that information to skiing. However, static friction is of more interest in applications such as automotive traction, [1, 2] and human walking traction. The available experimental results are useful for investigating the important processes but do not provide information about the coefficient of static and kinetic friction under low speed.

In this work, we studied interactions between polymeric materials and ice surface at low speed, simulating human walking conditions. We investigated the static frictional behavior of the mentioned materials. In doing so, we developed a new method by which to measure the static friction coefficient between ice and a traction material. A low friction measurement device was designed and constructed. Material evaluation in the cold climate was resolved and frictional behavior was successfully tested. Contact mechanics and the tribological behavior of ice against polymer were discussed.

## Background

Our design considered contact mechanics of two surfaces. The classic laws of dry friction is mathematically expressed as:  $F = \mu N$ . In this equation, the  $F$  is the friction force,  $N$  is the normal load, and  $\mu$  is the coefficient of friction. Whenever two surfaces are pressed together, only a fraction of the surfaces make contact. This is demonstrated in Figure 1. The ideal contact area is therefore defined by the boundaries of their macroscopic interface. In contrast, the real area, in which two solid surfaces are connected locally, is defined as the contacting asperities that transmit the interfacial force between two surfaces. Furthermore, for the real contact area there is difference between the static contact and sliding contact. Figure 2 shows the difference of these two.

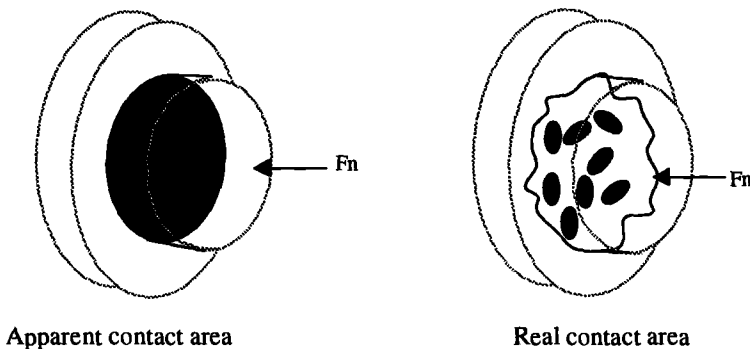


Figure 1 - Comparison of Apparent Contact and Real Contact Areas.

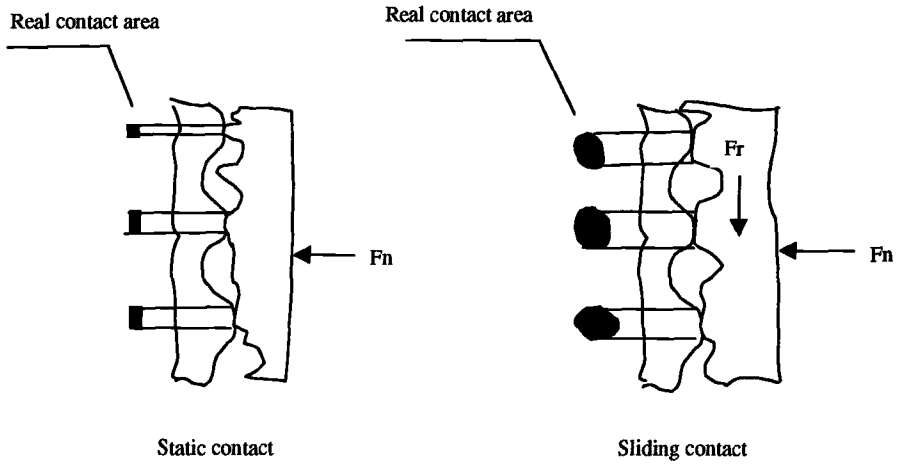


Figure 2 - Comparison of Static Contact and Sliding Contact.

*The elastic and plastic deformation in micrometer scale*

When two homogeneous and isotropic elastic bodies of arbitrary shape are pressed together, a contact area is formed. A simple deviation of its size can be evaluated by using Landau and Lifshitz's method [3,4]. Assuming two contacting spheres have radius  $R$  and  $R'$  respectively, the contact areas, where  $\Delta A = \pi r_0^2$ , is a circular region with radius

$$r_0 = (RR' / R + R')^{1/3} (\kappa F)^{1/3} \tag{1}$$

where  $\kappa = 3/4 (1 - \nu^2/E + 1 - \nu'^2/E')$  with  $E$  and  $\nu$  the elastic modulus and Poisson number, respectively. The distance  $h$  by which the two spheres approach each other is given by

$$h = (R + R' / RR')^{1/3} (\kappa F)^{2/3} \tag{2}$$

The pressure distribution in the contact area has the form

$$P(x, y) = P_0 \sqrt{3/2} [1 - (r/r_0)^2]^{1/2} \tag{3}$$

where  $P_0 = F / \pi r_0^2$  is the average pressure and  $r = (x^2 + y^2)^{1/2}$  is the distance from the center of the circular contact area.

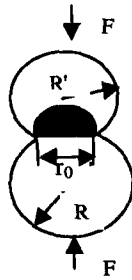


Figure 3 - *Elastic Deformation and Pressure Distribution in the Contact Area Between Two Elastic Solids.*

As discussed before, the real contact area is usually much smaller than that of an apparent one. The ratio may be as low as  $10^{-4}$  [5]. It depends on the contact force and yield stress of the softer material involved. Initially, as two materials begin to be pressed, a single contact area occurs, where the perpendicular pressure becomes so high as to induce the local plastic deformation. When two materials are further pressed, the real contact area is increased so that the load  $L$  is balanced by the contact pressure integrated over contact area. We expect to see this changing process during the friction measurement in our system.

### Experimental Apparatus and Procedures

Sample materials used are traction pads<sup>1</sup>, polycarbonate sheets<sup>2</sup>, as well as ice sheets made in the lab.

The ice sheets were prepared in a coldroom at UAF. They were grown in an aluminum box with a size of 30.5x25.4x3.8 cm (12"x10"x1.5") at  $-6.7^{\circ}\text{C}$  ( $20^{\circ}\text{F}$ ). The top layer of the ice sheets was scraped evenly. After two or three scraping passes, the surface of previous layer was polished. Water was then sprayed on the ice surface. A new layer was grown at the temperature at which the test was conducted.

The traction pads were in size of 9.5x9.5 cm (3.75x3.75 inch). An aluminum guiding block was attached. A rotary cutter was used to cut the mats. The aluminum block was designed to have relieves in order to avoid touching the studs on the pad samples. During cutting, the aluminum guiding block was climbed on the mat. This is important in order to make sample mats with consistent and accurate size and shape. The pad size is within  $9.5 \pm 0.025$  cm ( $3.75 \pm .010$  inches) in square. The polycarbonate pads were cut also into 9.5x9.5 cm (3.75" x 3.75") square piece. Their top and bottom edges were blunted to avoid generation of shear force. The properties of the polycarbonate material are shown in Table 1.

<sup>1</sup> Provided by Polar Engineering, Inc.

<sup>2</sup> Provided by Micromasurement Group.

Table 1 - *Typical properties of polycarbonates*

Tensile strength mPa (psi)	Coe. of thermal exp. $10^{-5}$ m/m/°C ( $10^{-5}$ in./in.°F)	Hardness Rockwell (M)	Thermal conductivity kJ-cm/hr-m <sup>2</sup> -°C (Btu-in/hr-ft <sup>2</sup> -°F)	Coefficient of friction (self)
62-71.6 (9000-10500)	3.7-3.9 (6.6-7.0)	62-70	21.6 (1.35)	0.52

An experimental device was constructed to test the coefficient of static friction. It includes a sample holder, driving system, friction measurement, data acquisition system, and ice sheet. The device is shown in Figure 4. The static measurements were taken in a cold room corresponding to a number of parametric settings of load, slider material, the surface condition, and ambient temperature.

The test is designed so that only one variable is examined at a time. A set of readings corresponding to various settings of one single parameter is taken during each single experiment. In order to obtain an accurate reading, each test is repeated three times.

The moving force for the ice sheet is manually supplied by using a jack. The sliding speed is around 2 cm/sec. A load cell is assembled between the jack and the ice sheet frame to test friction force. In order to obtain a good alignment between the load cell, the centerline of the ice sheet frame, and the centerline of the jack, a hole was made at the center of ice sheet.

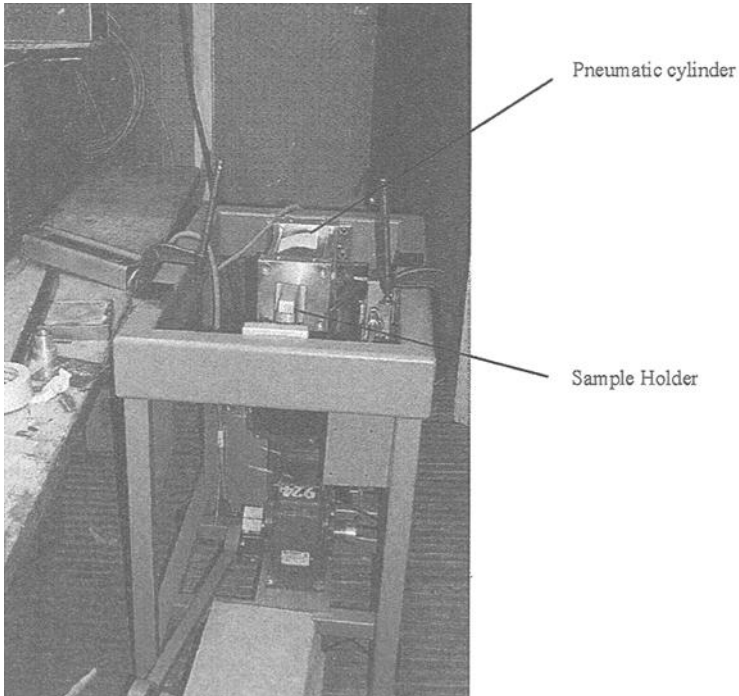
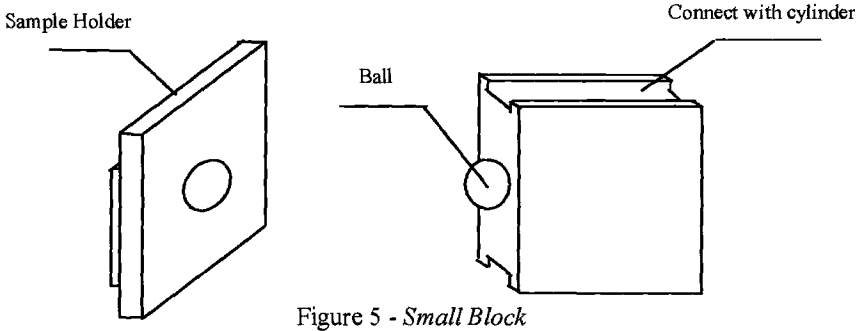


Figure 4 - *Overview of Test Machine.*



Normal load is applied to the contact surface between the ice and sample holder by a double-acting pneumatic cylinder with a 20cm (8") stroke under a 1.7 Mpa (250Psi) maximum pressure. A small block with a ball in one end, as shown in Figure 5, is made to connect the pneumatic cylinder with the sample holder. The ball is used to make a thorough contact, avoiding the shear force and keeping the acting force in the centerline. The normal force is set by adjusting the air pressure and is measured by the load cell.

Experiments were conducted to investigate the temperature and load dependence of friction. The ice surfaces were polished before each test. A series of calibration procedures were performed at the beginning of each test. The oscilloscope and load cell were calibrated as well as the normal force was preset. The pneumatic cylinder was activated by a three-way switch that contains functions of advancing, retracting the ram, and idling. The propulsion force is vertically applied on the centerline of the ice sheet frame. The oscilloscope records the friction force and displays a curve of friction force as shown in Figure 6. The y-axis is the friction force increasing toward down direction, while the x-axis is time. On the curve, the lowest point corresponds to the moment that the ice sheet starts to move. At this point we distinguish the static friction from sliding friction force.

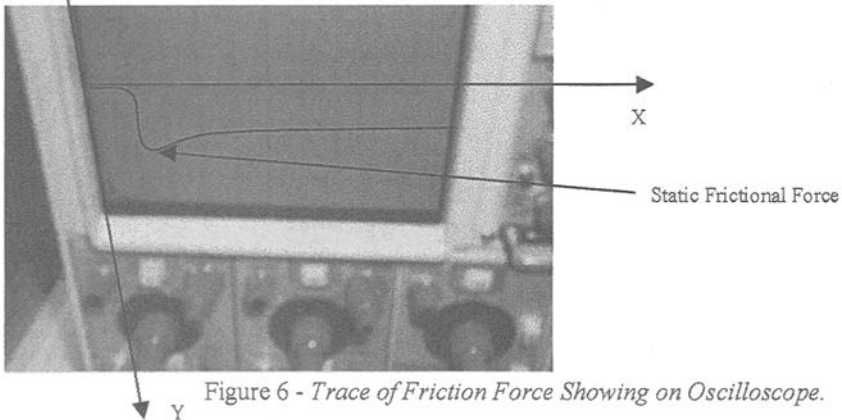


Figure 6 - Trace of Friction Force Showing on Oscilloscope.

**Experimental Result and Discussion**

*Traction Pad Test*

These test series were set to evaluate the frictional properties of a newly developed traction pad. We evaluated the effects of temperature, applied load, pad surface condition, and materials on friction. The coefficient of static friction related to the material and pad surface properties is shown in Figure 7. In this figure, there are seven samples tested at two different temperatures. The data showing in the white columns was tested at  $-29^{\circ}\text{C}$  ( $-20^{\circ}\text{F}$ ) and in the black columns at  $-1.1^{\circ}\text{C}$  ( $30^{\circ}\text{F}$ ). The S/N number indicated sample number without any specific meaning. Results show that the addition of studs on a smooth surface will increase static friction dramatically. These effects show more on high temperature. The deeper the studs penetrate, the more plowing force is generated. Therefore, friction measured with studs is generally higher. The results also tell the difference between the sample with sand inlaid on the surface and the others without. The sample S/N 83 contains sand. Although there were only five studs added to the pad surface, the friction was apparently higher compared with S/N 49 and S/N 26. The S/N 49 and S/N 26 have five and eight studs, respectively. The samples with thirteen studs provide similar friction as that with five studs containing sand. It is clear that pads containing studs and sand inlaid provides higher traction due to increased asperity contact.

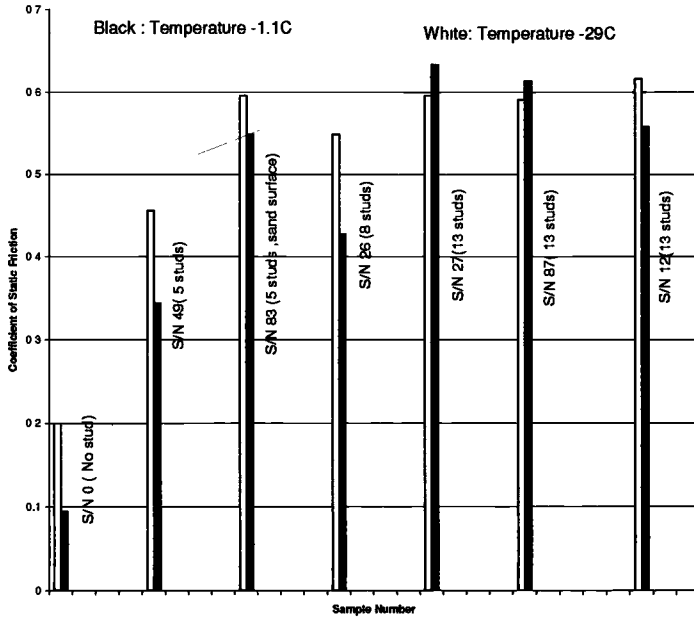


Figure 7 - Coefficient of Static Friction versus Sample Number.

*Polycarbonate Test Series*

In these tests, the effects of load, ice surface condition, and ambient temperature on static friction were further investigated. The load was set in the range from 43.5 kg to 209 kg. The polycarbonate samples were in a 9.5 cm (3.75") square and the temperatures were set at  $-29^{\circ}\text{C}$  ( $-20^{\circ}\text{F}$ ),  $-23.3^{\circ}\text{C}$  ( $-10^{\circ}\text{F}$ ),  $-17.8^{\circ}\text{C}$  ( $0^{\circ}\text{F}$ ),  $-12.2^{\circ}\text{C}$  ( $10^{\circ}\text{F}$ ),  $-6.7^{\circ}\text{C}$  ( $20^{\circ}\text{F}$ ), and  $-1.1^{\circ}\text{C}$  ( $30^{\circ}\text{F}$ ) respectively. The results are presented in Figures 8-10.

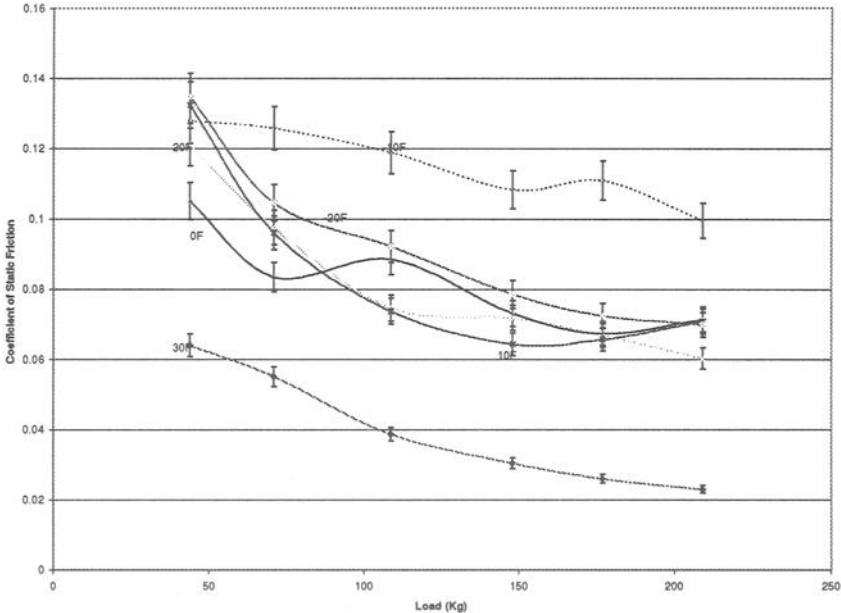


Figure 8 - Effect of Load on Coefficient of Static Friction

Figure 8 shows the coefficient of static force as a function of applied load. At all load levels, the coefficient decreases with load. This might indicate that the contact has gone beyond the asperity level. As discussed earlier, if an asperity contact is present, the frictional force is approximately directly proportional to the load due to the real contact area being in a linear function of the load. [6] Only when the whole area is contacted, the friction becomes independent of contact area. This work correlates well with Conant's et. al. [7] conclusion. They found that the kinetic friction coefficient decreased with an increase in the loading pressure and this seemed to be less true for static friction. Wilkinson, Jr. [8] reported that when a tire was in contact with ice, the coefficient of friction decreased with load and pressure. When a ski was sliding on snow, as reported by Bowden and Hughes [9], the coefficient of friction decreased when the load exceeded about 50 kg.

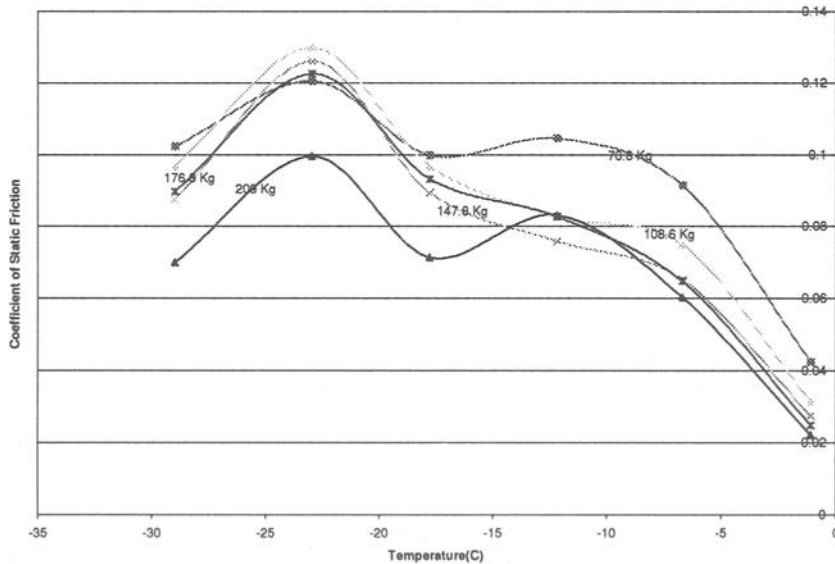


Figure 9 - Effect of Temperature on Coefficient of Static Friction

The next question is why the friction decreases with load when two surfaces are thoroughly contacted. There are two possibilities according to previous study. One is due to the melting of ice under pressure [10,11]. The other is due to the existence of a surface layer. The layer was first documented as “liquid-like” layer by Faraday [12]. Many researchers have reported the existence of a surface layer on ice. This layer has different physical properties from those of the bulk ice. Surface properties of this layer are strongly temperature dependent. Clifford [13], using Nuclear Magnetic Resonance (NMR) measurements on ice, observed a very narrow line ( $\sim 0.2$  G) that he attributed to some of liquid remaining in ice down to temperature of at least  $-12^{\circ}\text{C}$  ( $18.2^{\circ}\text{F}$ ). Kvlividze et al. [14] demonstrated that this line is distinct from the NMR lines corresponding to protons in water and bulk ice and is caused by the liquid-like layer on the ice surface. The surface layers seem to consist of several layers, each possessing specific physical properties, different from that of the bulk [15]. Barer et al. estimated the liquid-like layer thickness at various temperatures ranging from 10 to  $50\text{\AA}$  when temperatures ranged from  $-12$  to  $-2^{\circ}\text{C}$  ( $18.2$  to  $28.4^{\circ}\text{F}$ ) [16]. The existence of a surface layer is obvious. However, how the layer affects the frictional behavior of ice is not known.

Compared to other solids, ice is more sensitive to temperatures. The temperature affects frictional resistance mainly through its influence on the properties of the solid asperities and the thin film on ice. It is reasonable to expect a thicker surface film at higher temperatures. Under low temperatures, a greater share of the load will be carried by the solid surface asperities and the frictional force is expected to be high. When the temperature increases, the surface becomes softer and the surface film is thicker. The

frictional force will then decrease. In Figure 8, when the temperature is close to  $-1.1^{\circ}\text{C}$  ( $30^{\circ}\text{F}$ ), the coefficient is low. A decrease in temperature appeared to consistently increase the coefficient of static friction. When the temperature is higher than  $-9.4^{\circ}\text{C}$  ( $15^{\circ}\text{F}$ ), the effect of load on the coefficient is more pronounced. When the temperature is below  $-17.8^{\circ}\text{C}$  ( $0^{\circ}\text{F}$ ), the coefficient is independent on load. This might due to the pressure induced melting.

In our tests, we simply compared two different ice surfaces. One of these surfaces was a “new” one on which the surface of the previous layer was polished. After polishing water was sprayed on it and the ice sheet was annealed overnight at the designated test temperature. The other surface was an “old” surface. The “old” surface was the same as that used in previous tests. As shown in Figure 8, when the temperature was below  $-6.7^{\circ}\text{C}$  ( $+20^{\circ}\text{F}$ ), the friction obtained on the new surface was larger than that on the old one. However, when temperature was higher than  $-6.7^{\circ}\text{C}$ , the friction obtained on the old ice surface is higher. This interesting phenomenon might be the result of formation or thickening of the surface layer. The effect of roughness does not show significant effect here because the load-range we used has exceeded the load for any asperity contact. On the “old” ice surface, there is no significant decrease of friction with increasing temperature. However, the change of friction due to temperature is more pronounced for tests undergone on the new surface. The results show that the surface layer can be regenerated through a proper procedure.

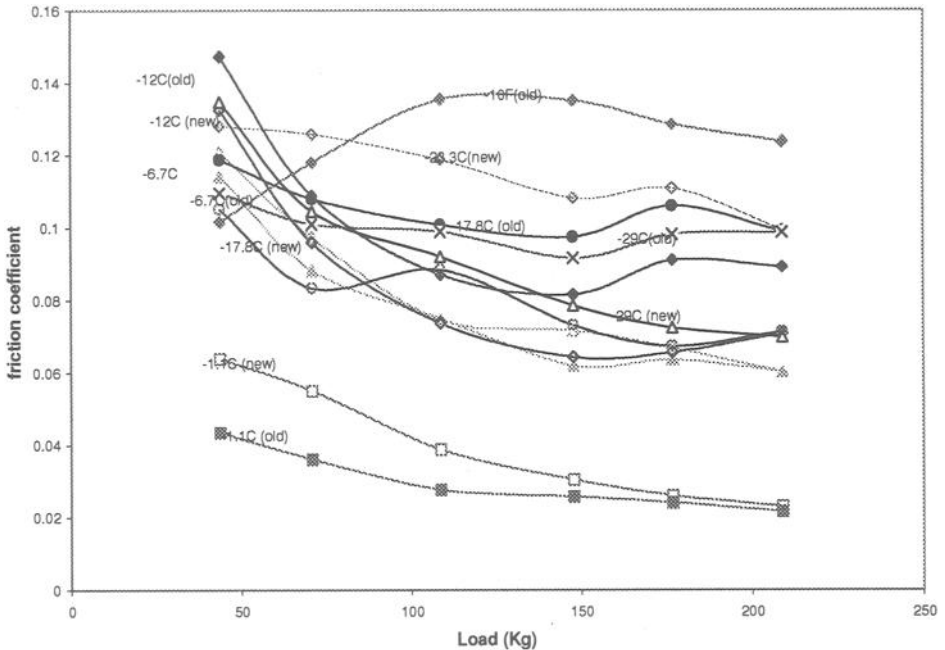


Figure 10 - The Effect of Ice Surface Condition on the Coefficient of Static Friction.

**Conclusion:**

We developed a new device that is capable of measuring static friction of materials on ice and snow surfaces. Results obtained help us understand mechanisms of slow moving subjects, such as a human walking on ice. We conclude the following:

1. The coefficient of static friction decreases with the load increasing from 43.5 kg to 209 kg.
2. A decrease in temperature appeared to consistently increase the coefficient of static friction.
3. The friction was dependent on ice surface conditions. The surface layer shows significant effects on friction.

**Acknowledgment**

This work was partially supported by the Alaska Space Grant Program, the President's Special Fund Project, and the start-up grant of UAF. Support was also received from the Polar Environmental Technology Inc. Authors would like to thank Mr. Eric Johansen who helped to build the machine. Without his help, this work was not possible to accomplish.

**References:**

- [1] S. C. Colbeck, "A Review of the Processes That Control Snow Friction," USA Cold Regions Research and Engineering Laboratory, Monograph 92-2,49 1.
- [2] A. Ahagon, T. Kobayashi, and M. Misawa "Friction on Ice," *Rubber Chemicals and Technology*, 61(1):14-35.
- [3] L.D.Laudau and E.M.Lifeshitz, "Theory of Elasticity," Pergamon, New York, 1975.
- [4] B.N.J. Persson, "Sliding Friction, Physical Principles, and Application," Springer-Verlag Berlin Heidelberg, pp. 45-46, 1998.
- [5] K-H. Zum Gahr, "Microstructure and Wear of Materials," Elsevier, New York, 1987.
- [6] University of Minnesota "Friction on Snow and Ice," Institute of Technology, Mechanical Engineering Department. Also SIPPE Report, TR17. Contact USA Cold Regions Research and Engineering laboratory. 286 PP. 50.
- [7] F. S. Conant, J.L. Dum, and C. M.Cox, "Friction Properties of Tread-type Compounds on Ice," *Ind.Eng.Chem.* Vol.41No.1,pp.120-6, 1949.

- [8] C. S. Wilkinson, Jr., "Studying of the Factors Affecting the Friction of Tread Compounds on Ice," *India Rubber world*, Vol.128, No.4, pp.475-81, 1953.
- [9] F. P. Bowden and T.P. Hughes, "Mechanism of sliding on ice and snow," *Proceedings of the Royal Society of London, Series A* , 172A: 280-298, 1939.
- [10] O. Reynoldss, "On the slipperiness of ice," *Memorandum of the proceedings of the Manchester Literature and Philosophical Society*, 43(5): 1-7.
- [11] F. P. Bowden, "Friction of Non-Metallic Solids," *Journal of the Institute of Petroleum*, 40:89-101.
- [12] M. Faraday, "On regulation, and on the conservation of force," *Philosophical magazine*, 8: 1425-1426, 1859.
- [13] J. Clifford, "Proton magnetic resonance data on ice." *Chemical Communications*,17:889-881, 1967.
- [14] V. I. Kvlividze, V.F. Kiselev, and L.A.Ushakova, "The existence of quasi-liquid films on the surface of ice," *Doklady Akademii Nauk USSR*, 191(5): 1088-1090, 1970.
- [15] V. F. Petrenko "The surface of Ice," *CRREL Special Report 94-22,Hanover NH Aug.* pp 26-27, 1994.

## **SESSION IV: Analysis**

Mathias Woydt<sup>1</sup>

## **Influence of Test Parameters on Tribological Results – Synthesis from Round Robin Tests**

---

**Reference:** Woydt, M., “**Influence of Test Parameters on Tribological Results – Synthesis from Round Robin Tests,**” *Bench Testing of Industrial Fluid Lubrication and Wear Properties Used in Machinery Applications, ASTM STP 1404*, G. E. Totten, L. D. Wedeven, J. R. Dickey, and M. Anderson, Eds., American Society for Testing and Materials, West Conshohocken, PA, 2001.

**Abstract:** A series of cooperative interlaboratory tests (round robins) was conducted in 1997, 1998 and 1999 by the DIN 51834 Working Group on Tribological Tests in Translatory Oscillation Apparatus. The statistical analysis of these test results shows the influence of cleaning solvent, machine model and evaluation criteria on the tribological properties of the lubricants tested. Coefficients of friction and wear results are ranked according to the effects of ten different cleaning solvents, where isopropanol gave the lowest values and isoparaffin solvents the highest. The effect of machine model on coefficients of friction varied from about 0.2 % to 0.9 % of the average. Wear results were not affected. The tests also showed that the seizure criteria and methods of measuring wear required for in the test procedure do not provide a suitable measure of the tribological properties of some lubricants.

**Keywords:** tribology tests, wear, friction, lubrication

### **Introduction**

Industry seeks to use test systems that enable a qualitative or even semi-quantitative correlation between cheap model tests and expensive and time-consuming component or product testing. There is a strong demand today for test procedures that can rapidly screen potential lubricants and materials before system-level life tests are performed.

Tribometers serve to characterize friction and wear behavior of materials and coatings or/and interaction with lubricants, greases, base fluids, additives and gases. They represent the basis for tribology-oriented development of materials and lubricants or for quality assurance. They also serve to check the conformity of a product with a specification.

---

<sup>1</sup>Federal Institute for Materials Research and Testing (BAM),  
D-12200 Berlin (Germany)

The principal advantage of using ASTM, ISO, DIN or other standard test methods is that they have been carefully evaluated by experts and their procedures have been carefully documented. Their repeatability not only depends on the design quality of the test equipment, but also on the knowledge about the influence of test parameters and/or operating conditions. In other words: a test procedure can only be as good as the knowledge about the influence of test parameters and/or operating conditions is advanced.

This is the key question, because the trust in and transferability of test results depend also on the repeatability and reproducibility of the model test procedure.

Roundrobin tests are necessary to prove regularly (usually every two years) for certified labs, that machine and operator produce credible results. Since 1996, the working group for DIN 51834, part 1, which was issued April 1997, has decided to organize and run one round robin test every year in order to be able to show and quantify in the future systematic and other errors. This paper summarizes the findings from the RR tests of 1997, 1998 and 1999 as well as the discussions within this working group, which may be transferable to other tribology test procedures.

## Test Procedure

### *Standardization*

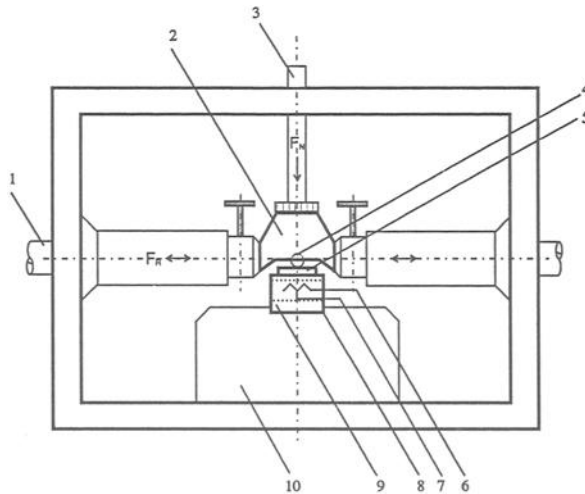
The results presented in this paper were elaborated using standardized test equipment under linear-oscillating motion. According to the policy of Deutsche Institut für Normung (DIN), DIN 51834 [1], part 1, issued April 1997, describes only the technical recommendations for the equipment. Since May 1999 DIN 51834, part 1 and part 2 are available from DIN as official translations into English. DIN 51834 [2], part 2, describes the test procedure itself. The precision statements in part 2 are based on a round robin test performed 1988 with three oils. The test principle was developed in 1968. After more than 30 years of experience with more than 200 test machines worldwide, a number of test procedures have been developed and standardized (see Table 1). These standards are additionally transferred from the ASTM methodology into DIN and vice versa.

Table 1 - *Standard Test Procedures Referring to the High-Frequency, Linear-Oscillating Test Machine*

Type of Lubricant	DIN	ASTM
Oils, fluids	51834, part 2 (white print) ⇒	D6425-99
	51834, part 3 (white print in press)	
	51834, part 4 (under preparation)	
Greases	51834, as future part 7 ⇐	D5706-97
	51834, as future part 8 ⇐	D5707-97
Needle and sinker oils	E 62193, part 1 (yellow print, as draft)	
Solid bonded films	E 65593 (yellow print, as draft)	
Test apparatus	51834, part 1 (white print)	

### Test Equipment

In the basic test configuration, an upper test specimen is rubbed against a lower specimen (see Figure 1). Few milligrams of lubricants or grease may be placed into the tribo-contact. After lubricant has been placed on the test specimen and these have been installed in the test chamber, the normal force is applied mechanically to the upper specimen in a direction normal to the direction of motion at a given test frequency and stroke.



- 1 Drive rods
- 2 Specimen holder (top) (20 different adapters and holders available)
- 3 Loading rods
- 4 Specimen (top)
- 5 Specimen (bottom)
- 6 Temperature sensor
- 7 Heating
- 8 Specimen holder (bottom)
- 9 Piezo measuring element (calibrated according to ISO 9000)
- 10 Receiving block

Figure 1: Schematic view of the SRV<sup>®</sup> Test Arrangement and the Test Chamber

The friction force is measured continuously by means of a piezoelectric load cell under the lower specimen holder, which is attached to a rigid test block. The wear scar and track dimensions are determined after a given test duration by optical microscopy or stylus profilometry.

The test block and the holder can be heated to +295°C (optionally up to +900°C) and cooled to control the temperature of the lower specimen.

DIN 51834, part 2, requests a ball as upper specimen and a disk as lower specimen, both made from 100Cr6H (DIN 1.3505), equivalent to AISI 52100 (UNS G52986) with HRC  $62 \pm 1$ . The lower specimen is a lapped disc with a diameter of 24 mm and a height of 7.85 mm. Its roughness is  $0.45 \text{ mm} < R_z < 0.65 \text{ mm}$ . The upper specimen is a polished ball with a diameter of 10 mm and a roughness of C.L.A.  $< 0.025 \text{ }\mu\text{m}$ .

In addition to part 2, DIN 51834 [3], part 3, describes a procedure using all kinds of materials and coatings. In other words, using DIN 51834, part 3, with AISI 52100 specimen means to test in accordance with DIN 51834, part 2. Other test geometries can be a horizontal cylinder, for Hertzian line contact, or an upright cylinder or ring for area contact.

The characteristic feature of fretting wear compared with other types of wear lies in the intensive interaction between the surfaces, transfer of debris, mode of vibration and wear.

### Influence of Test Parameters

The influence of only those test parameters will be discussed which are assumed to determine the test results, such as cleaning procedure, model of test machine and test pieces. The relative humidity has a friction and wear determining influence for oscillating [4] contacts under unlubricated conditions, but was considered to have only a minor influence under lubricated conditions.

### Round Robin Tests

The round robin tests performed in 1997 with 19 participants, 1998 with 22 participants and 1999 with 36 participants used formulated or only base oils or oils with a low EP capacity in order to show specific properties of the test procedure. The test kits with samples, test oils and a disk in order to save results were sent to the participants in March. The time available for running the round robin tests always was 3 months, from 1st April to 1st June. 80% of the participants returned the results on disk.

Table 2. *Compilation of the Test Oils Used for Round Robin Tests*

Test oil	Viscosity @40 C [mm <sup>2</sup> /s]	Viscosity @100 C [mm <sup>2</sup> /s]	FZG A/8,3/90
CEC RL175/3 (Nov. 1995)	169.3	15.8	
Polyalkyleneglycol 50-100B	139.0	27.0	
Paraffinic ISO VG 220, Additivated	202.5	17.6	>12
SHC 500 (VG46)	46.0	8.5	>12
Synthetic Ester (blue angel) Kajo-Bio-HEES-S (VG46)	49.5	9.7	12

The results of the '97 and '98 round robin tests have been published in [5, 6] after the approval of the results by the working group in September. The participants received a certificate with the results of their own lab and the test data of all other participants in anonymous form. Table 2 compiles the basic properties of the oils used.

The polyalkyleneglycol was butanol initiated with an ethylene-/propyleneoxide ratio of 50:50. The German environmental label "blue angel No. 79" Kajo-Bio-HEES-S was attributed to this hydraulic oil because it is biodegradable and contains eco-friendly additives. The "SHC 500" is a PAO-based synthetic anti-wear hydraulic oil. The polyalkyleneglycol was tested as base oil. The "CEC RL175-3" is a mineral based reference test oil for Timken- and 4-ball-testers with an EP-package.

*Round Robin Test Results*

The collection of the data on disk and the import into a database facilitated the statistical analysis and the identification of clusters as a function of parameters. The analysis of the RR97 and RR98 was performed according to DIN ISO 5725 and DIN EN ISO 4259. RR99 was additionally evaluated by an ASTM D2 statistical program. The significant results from these three round robin tests will be summarized in the following.

*Cleaning Procedure*

A survey of tribological test procedures revealed the use of a variety of different cleaning solvents. DIN 51834-2 requires single boiling spirit (sbp) according to DIN 51361-2-A (80°C to 110°C boiling range) and ASTM Test Method for Measuring Friction and Wear properties of Lubricating Grease Using a High-Frequency, Linear-Oscillation (SRV) Test machine (D5707) and ASTM Test Method for Determining Extreme Pressure Properties of Lubricating Grease Using a High-Frequency, Linear-Oscillation (SRV) Test machine (D5706) stipulate to use a mixture of equal volumes of n-heptane, toluene and isopropanol.

Table 3: *Ranking of Wear Scar Diameter and COF by Using Different Cleaning Solvents*

<b>Test oils CEC RL 175/3 and PAG 50-100B</b>
COF smaller <Isopropanol/Toluene/Hexane<Acetone<single boiling point spirit < Petrolether <Isohexane <Isoparaffin < COF greater
Wear scar smaller < Isopropanol/Toluene/Hexane, Petrolether< Single boiling point spirit< Isoparaffin, Isohexane < Wear scar greater
<b>Test oils ISO VG 40 and ISO VG 220 (additivated paraffinic oils)</b>
COF smaller < Isopropanol/Toluene/Hexane< Single boiling point spirit, Petrolether <Aceton < Isohexane, Isoparaffin < COF greater
Wear scar diameter smaller < Single boiling point spirit, Isopropanol/Toluene/Hexane <Isohexan < Aceton < Wear scar greater

Ultrasonic cleaning was reported by 85% of the participants. The participants in the RR tests used more than 10 different cleaning solvents. The cleaning solvent must influence the test results because the steel samples are protected against corrosion. In consequence,

the remaining layer of the rust inhibitor depends on the cleaning effect of the solvent. Table 3 compiles the ranking of results by cleaning solvents observed as clusters in the RR97 and RR98. As it can be seen, the type of cleaning solvent rank the friction and wear data.

#### *Model of Test Equipment*

In the last few years, the performance of the test machine was continuously improved. Three machine generations have been developed which vary with regard to the electronics (data acquisition, control unit) and design (maximum stroke, normal force). The maximum load for the SRV I is 1,200 N, the SRV II 1,400 N and for the SRV III 2,000 N. The question was: does the model (SRV I, SRV II, SRV III and ICC) influence the tribological results?

Table 4: *Correlation between the model and the mean of the COF of different models in the RR98*

Interfacial media	Number of COF-end	Mean of COF-end	Model of Tribometer
Test oil A	4	0.1110	ICC
Test oil B	4	0.1352	ICC
Test oil A	2	0.1360	SRV 0
Test oil B	2	0.1535	SRV 0
Test oil A	18	0.1149	SRV I
Test oil B	18	0.1424	SRV I
Test oil A	8	0.1145	SRV II
Test oil B	8	0.1387	SRV II
Test oil A	14	0.1232	SRV III
Test oil B	14	0.1500	SRV III

Table 5: *Correlation between the model and the mean wear scar diameter of different models in the RR98*

Interfacial media	Number of $W_K$	Mean of $W_K$	Model of Tribometer
Test oil A	4	0.59350	ICC
Test oil B	4	0.70000	ICC
Test oil A	2	0.70000	SRV 0
Test oil B	2	0.72500	SRV 0
Test oil A	18	0.54809	SRV I
Test oil B	18	0.72668	SRV I
Test oil A	8	0.50812	SRV II
Test oil B	8	0.64125	SRV II
Test oil A	14	0.55278	SRV III
Test oil B	14	0.70014	SRV III

Tables 4 and 5 rank for two test oils the different types of machines to the coefficient of friction and wear scar diameter. On the basis of a COF= 0.1, the model SRVIII report COFs which are 0.7% to 0.9% higher than those of SRVI/II-models. SRVI models report COFs which are 0.18% to 0.36% higher than those of SRVII machines.

No clusters were observed between the models with respect to wear scar diameters. A similar ranking was found in the RR97 and RR99.

*Wear Scar Diameter*

With 0.478 mm ( $P_H = 1,665$  MPa), the value of the optically visible average wear scar diameter for the ball tested with Mobil SHC is slightly above the average Hertzian diameter of 0.427 mm using  $F_N = 300$  N (corresponding to an initial average Hertzian pressure of  $P_0 = 2,092$  MPa). All participants stated for this oil a wear scar diameter as wear amount, because they saw a colored scar in the optical microscope.

Table 6: Comparison between the values of wear scar diameter and wear volume on one ball

Wear quantity ball	MOBIL I SHC 500 VG 46	KAJO-BIO-HEES-S VG 46
Scar diameter [mm]	0.478000	0.79100 (times 1,65)
Wear volume from equations in DIN 51834, part 3 [mm <sup>3</sup> ]	0.000164	0.00122 (times 7,4)
Wear volume from stylus profilometry [mm <sup>3</sup> ]	~0.000035	~0.0008 (times 22,8)

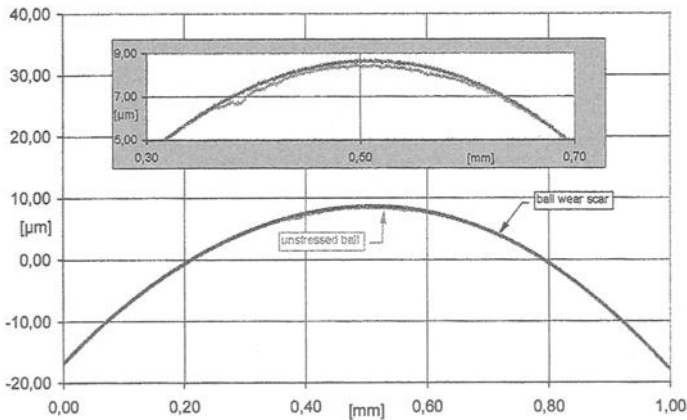


Figure 2: Stylus profilometry across the center of the ball wear scar (stylus TK300)

Figure 2 shows only a tiny difference in the stylus traces of the unstressed surface and the wear scar. In order to rank and better discriminate between different fluids, Table 6 illuminates the importance of the use of the wear volume and the difference in using an equation and stylus profilometry [3, 7].

The equation in DIN 51834, part 3, assumes that wear occurs on both samples and the wear volume of the ball can be calculated from the planimetric wear [ $\mu\text{m}^2$ ] of the track perpendicular to the sliding direction. Testing the MOBIL hydraulic oil, some wear on the track (flat sample) was detectable by means of stylus profilometry, but in this particular case, the ball grooved into the disk, so the equations can't be applied as shown in Table 6. The wear volume on this ball is the difference between the trace in Figure 2 of the unstressed surface and the wear scar.

### *Seizure Criteria*

The RR99 showed for the saturated synthetic ester hydraulic oil in the testing period 5-10 minutes to 15-20 minutes several sharp rises (peaks) in COF. After this period of, say running-in, the COF (see Figure 3) decreased continuously and behaved smoothly. The optical inspection of the scar and track didn't reveal any evidence of adhesive transfer. According to the section "9.2.2" in DIN 51834-2, ~20% of the participants stopped the test and stated "adhesive failure".

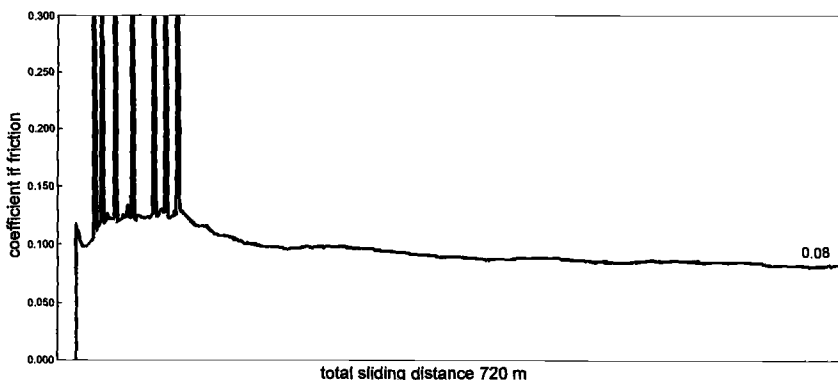


Figure 3: *Typical trace of COF versus sliding distance of the saturated, synthetic ester during RR99 ( $T= 50^{\circ}\text{C}$ ,  $F_N= 300\text{N}$ ,  $\Delta x= 1\text{ mm}$ ,  $v= 50\text{ Hz}$ ,  $t= 120\text{ min}$ )*

Similar frictional behavior was observed for the ester based biodegradable, low additive hydraulic/transmission lubricant [8]. The development of peaks depends on the Hertzian pressure. Peaks appear at a Hertzian pressure above 1.5 GPa. This ester tested in the RR99 meets the technical specifications of construction equipment manufacturers, but would be rated "non-working" using the seizure criteria in DIN 51834-2.

The extreme pressure characteristics using D5706 [9] are evaluated by changes in friction characteristics, whereas EP lubricants, while often (but not always) providing

friction modification, are used primarily to control wear or surface damage. The seizure criteria of DIN 51834-2 are also based on the changes in the friction characteristics. It would seem that a test for EP characteristics of a lubricant should include the evaluation of both friction and wear (and/or surface damage) of the test pieces at a defined Hertzian pressure, which should be reported with the tribological results (see also Chapter seizure).

The coefficient of friction of self-mated AISI 52100 (100Cr6H) couples lies between 0.5 and 0.9 at room temperature and under dry conditions (without adhesive failure, but strong tribooxidation) [10].

### **Discussions Within the Working Group**

The actual versions of DIN 51834 are valid until April 2002. Based on three round-robin tests and some round robin tests performed by companies owning five to seven test machines, a discussion for DIN 51834, part 2, about the procedure and the following modifications has begun with the aim to approve them before the end of year 2000.

#### *Wear Volume*

The wear volume will replace the wear scar diameter, but the wear scar diameter is still valid. This was already introduced into DIN 51834, part 3. If the wear scar diameter is smaller than 1.2 times the average Hertzian contact diameter, then the wear loss has to be proven with profilometry and the wear volume has to be calculated from the stylus trace, because the wear scar is close to the Hertzian diameter. A measurable (optically visible) wear scar diameter may or may not indicate wear on the surface of the ball and the wear track (see chapter wear scar diameter).

#### *Seizure*

The COF value of  $f > 0.35$  will be cancelled. Any peak over  $\Delta 0.2$  is an undesired event for lubricated contacts. The seizure criteria for lubricated contacts will be a sharp rise of  $\Delta 0.2$  over 30 seconds or the proof of adhesive transfer in SEM or light-optical microscopic pictures. Additionally, in DIN 51834, part 3, the geometric pressure at test end will be reported.

#### *Temperature*

Especially the automotive industry pronounced the wish to test at higher temperature. Tests at a constant temperature of 90°C and 135°C will be in addition to the test at 50°C.

#### *Load*

The constant test load can be chosen from any load in 100 N steps. This flexibility is to enable to determine the tribological quantities of friction and wear at an appropriate load where no seizure occurs. The round robin tests performed with greases by US

customers (97-98) revealed that a normal force of  $F_N = 1,200$  N is not enough for some EP-greases to observe seizure. The normal force required in DIN 51834, part 1, "General principles..." will be increased from 1,200 N to 1,600 N.

### *Oil Volume*

According to systematic research of some customers, the oil volume will be increased to 0.3 ml.

### *Coefficient of Friction*

The coefficient of friction value will be indicated to the third decimal point.

### *Topography of Specimens*

The surface of the lapped flat samples will be defined as follows:  $0.035 \mu\text{m} < R_a$  (C.L.A.)  $< 0.05 \mu\text{m}$ ,  $0.02 \mu\text{m} < R_{pk} < 0.035 \mu\text{m}$ ,  $0.05 \mu\text{m} < R_{vk} < 0.074 \mu\text{m}$  and  $0.5 \mu\text{m} < R_z < 0.65 \mu\text{m}$ . The topography needs to be precisely specified in order to facilitate the manufacture of specimens which conform with the requirements of the standard.

### *Stroke*

The stroke will be checked periodically by subtracting the wear scar diameter of the ball from the wear track length which must be identical with the selected stroke.

### *Flat Samples*

The RR showed that the results of customers who had machined their own test specimens in accordance with DIN 51834-2 lie within the statistical limits. Surface analysis of the specimens showed that stragglers and outliers were correlated with the presence of lapping grits in the grooves of the roughness valleys. For the future, the surfaces of test specimen free from other lapping grits are required.

### *Report*

The tribological quantities determined have to refer to the operating conditions as follows: DIN51834-2/normal force/temperature or for example DIN51834-2/600/90.

### **Conclusions**

Round robin tests represent a versatile instrument to identify and quantify systematic and other errors of the test procedure and are an excellent training for users. They increase the knowledge on the influence of test parameters and/or operation conditions on the tribological quantities and are necessary to prove regularly that machine and operator produce credible results in order to respond to the demand for a highly reproducible and repeatable test equipment and procedure. The round robin data displayed the ranking of

the COF by cleaning solvents and that a measurable (optically visible) wear scar diameter may or may not indicate wear on the surface of the ball and the wear track. The wear volume determined by stylus profilometry represents the safest way to report wear. For the future, seizure criteria need a clear definition. These seizure criteria have to reflect the tribological performance in products.

## References

---

- [1] DIN 51834-1 General principles for the tribological testing of lubricants using a linear-oscillation test machines, April 1997, Beuth Verlag, D-10772 Berlin
- [2] DIN 51834-2 Determination of friction and wear characteristics for lubricating oils using a linear-oscillation test machine, April 1997, Beuth Verlag, D-10772 Berlin
- [3] DIN 51834-3 Testing of lubricants – tribological test in translatory oscillation apparatus- Part 3: Determination of tribological behavior of materials in co-operation with lubricants, white print in press, Beuth Verlag, D-10772 Berlin
- [4] Klaffke, D., “On the Influence of Some Test Parameters on the Results of Oscillating Sliding Tests”, Tribotest Journal 6-1, 1999, p. 29-49
- [5] Woydt, M., „Ergebnisse des Ringversuches zur DIN 51834“, Tribologie&Schmierungstechnik, 44. Jg, Heft 6, 1997, p. 284
- [6] Woydt, M., „Einfluß der Reinigungsmedien auf die Prüfung tribologischer Kenngrößen“, Tribologie&Schmierungstechnik, 46. Jg, Heft 2, 1999, p. 36
- [7] Kalin, M. and J. Vižintin, “Use of Equations for Wear Volume Determination in Fretting Experiments”, WEAR, Vol. 237, 2000. P. 39-48
- [8] Vižintin, J. and A. Arnsek, “Scuffing Load Capacity of Rapeseed-Based Oils”, Lubrication Engineering, August 1999, p. 11-19
- [9] ASTM D5706-97 “Determining Extreme Pressure Properties of Lubricating Greases Using a High-Frequency, Linear-Oscillating (SRV) Test Machine”, ASTM, 100 Barr Harbor Drive, West Conshohocken, PA 19428, USA
- [10] Klaffke, D., „On the Repeatability of Friction and Wear Results and On the Influence of Humidity in Oscillating Sliding Tests of Steel-Steel Pairings“, WEAR, vol. 189, 1995, p. 117-121

Shinji Tanaka,<sup>1</sup> Tsunamitsu Nakahara,<sup>1</sup> Keiji Kyogoku,<sup>1</sup> and Satoshi Momozono<sup>1</sup>

## Identification of Boundary Friction Coefficient Under Mixed Lubrication in Block-on-Ring Friction Tester with Aid of Partial EHL Analysis

---

**Reference:** Tanaka, S., Nakahara, T., Kyogoku, K., and Momozono, S., “Identification of Boundary Friction Coefficient Under Mixed Lubrication in Block-on-Ring Friction Tester with Aid of Partial EHL Analysis,” *Bench Testing of Industrial Fluid Lubrication and Wear Properties Used in Machinery Applications, ASTM STP 1404*, G. E. Totten, L. D. Wedeven, J. R. Dickey, and M. Anderson, Eds., American Society for Testing and Materials, West Conshohocken, PA, 2001.

**Abstract:** This paper describes an estimation method of the boundary friction coefficient of sliding parts under mixed lubrication condition. The boundary friction coefficients in a mixed lubrication regime have been identified by comparing the measured frictional characteristics with the calculated results obtained from the mixed lubrication analysis solving simultaneously the elastohydrodynamic lubrication equations and the contact ones. A block-on-ring friction tester set in a pressure vessel has been developed which is able to measure frictional characteristics in various lubrication conditions and many kinds of atmosphere. The test has been carried out in a refrigerant atmosphere.

**Keywords:** mixed lubrication, boundary friction, surface roughness, refrigerant, refrigeration oil, block-on-ring friction tester

Generally, many evaluations for lubricants and sliding materials by using a standard test machine in a laboratory are carried out in boundary lubrication regime [1-5]. However, there is a difference between a laboratory test result and an actual machine test result because the boundary lubrication state in most of actual machines happens in a moment [6]. Therefore, it is important to estimate the boundary friction coefficient between sliding parts under mixed lubrication condition.

By the way, it is considered that the boundary friction coefficient in a mild mixed lubrication regime does not always agree with the friction coefficient in a severe boundary lubrication regime. Therefore, the boundary friction coefficient must be

---

<sup>1</sup>Research Associate, Professor, Associate Professor and Research Associate, respectively, Department of Mechanical and Intelligent Systems Engineering, Tokyo Institute of Technology, 2-12-1, O-okayama, Meguro-ku, Tokyo 152-8552, Japan.

estimated under the mixed lubrication condition.

It is necessary for getting the boundary friction coefficient under the mixed lubrication condition to separate the boundary lubrication part and the hydrodynamic lubrication part. To divide the two parts, a method of identification has been used by comparing the measured frictional characteristics (Stribeck curve) with the calculated results obtained from the mixed lubrication analysis solving simultaneously the elastohydrodynamic lubrication equations and the contact ones [7].

In order to accurately identify the boundary friction coefficient in various mixed lubrication condition and many kinds of atmosphere [8], a block-on-ring friction tester set in a pressure vessel based on ASTM Test Method for Calibration and Operation of the Falex Block-on-Ring Friction and Wear Testing Machine (D2714) has been developed, which is able to measure frictional characteristics in such a wide range of sliding speed as covers from the boundary lubrication to hydrodynamic lubrication condition.

This paper shows some results of the identification from the measurements have been carried out under the lubrication with refrigerating machine oil dissolving hydrochlorofluorocarbon (HCFC) or hydrofluorocarbon (HFC) refrigerant such as the inside of refrigerant compressor.

**Method of Identifying Boundary Friction Coefficient**

To identify the boundary friction coefficient in mixed lubrication regime, it is assumed that the friction coefficient  $\mu_b$  that minimizes the following performance function  $f(\mu_b, k_c)$  is the boundary friction coefficient in mixed lubrication regime.

$$f(\mu_b, k_c) = \mu_{ci}(\mu_b, k_c) - \mu_{mi} \tag{1}$$

$$\min \left\{ \sum_{i=1}^N (|f(\mu_b, k_c)| \times S_i) \right\} \tag{2}$$

where

- $N$  = sampling number
- $S_i$  = bearing characteristic number (=  $\eta V/W$ )
- $V$  = sliding velocity
- $W$  = load per unit of width
- $\eta$  = viscosity
- $\mu_b$  = identified boundary friction coefficient
- $\mu_{ci}$  = friction coefficient calculated by partial EHL analysis
- $\mu_{mi}$  = measured friction coefficient
- $k_c$  = contact constant that relates to surface density and mean radius of curvature of asperities using in the Patir and Cheng's formula (Equation (3)) [9] approximately derived from Greenwood and Tripp's theory (Equation (4)) [10]

$$P_c = 4.4086 \times 10^{-5} k_c E \left(4 - \frac{h}{\sigma}\right)^{6.804} \quad (3)$$

$$P_c = k_c E F_{5/2} \left(\frac{h}{\sigma}\right) \quad (4)$$

$$\frac{1}{E} = \frac{1}{2} \left( \frac{1 - \nu_1^2}{E_1} + \frac{1 - \nu_2^2}{E_2} \right) \quad (5)$$

where

$h$  = film thickness

$E$  = equivalent Young's modulus of test block and test ring

$E_1$  = Young's modulus of test block

$E_2$  = Young's modulus of test ring

$F_{5/2}(\frac{h}{\sigma})$  = integral of Gaussian distribution [9]

$P_c$  = contact pressure between test block and test ring

$\sigma$  = composite rms roughness between test block and test ring

$\nu_1$  = Poisson's ratio of test block

$\nu_2$  = Poisson's ratio of test ring

Bearing characteristic number  $S$ , is the weight for the purpose of fitting the calculated friction coefficients to the measured ones between the hydrodynamic lubrication regime and the mixed one. The data of  $\mu_{mi}$  were transformed the experimental equation by the method of least squares, and the value of the experimental equation is substituted for  $\mu_{mi}$  of Equation (1).

## Experimental Method

The schematic of a block-on-ring friction tester set in a pressure vessel is shown in Fig. 1. This tester can test in various liquids or gaseous atmosphere because the test area is placed in the vessel. The applicable pressure range of the vessel is from 0.7 Pa(abs.) to 5.1 MPa(abs.) and the pressure in the vessel is adjusted with a pressure regulator. The temperature of a sample oil is controlled with the silicone rubber heater which is attached to outside of the vessel and the temperature controlled water which circulates through the vessel, and measured with a platinum resistance thermometer. A test block is attached to two rods for measuring friction force and for being loaded against a test ring through a spring tied to the rod with a wire. Each rod is sealed with a bellows seal to avoid any friction force except the one between a test block and a test ring. The friction force between the block and ring is measured with a load cell outside of the vessel. The load cell transduces friction forces to the voltage, whose data are taken in a personal computer. The sampling frequency varies from 25 Hz to 25 kHz with rotational speed of the shaft. A test ring is placed on the shaft, which is rotated by the DC servo motor which has a wide speed control range of 2 000:1 with keeping small speed fluctuation to covers from hydrodynamic to boundary lubrication condition.

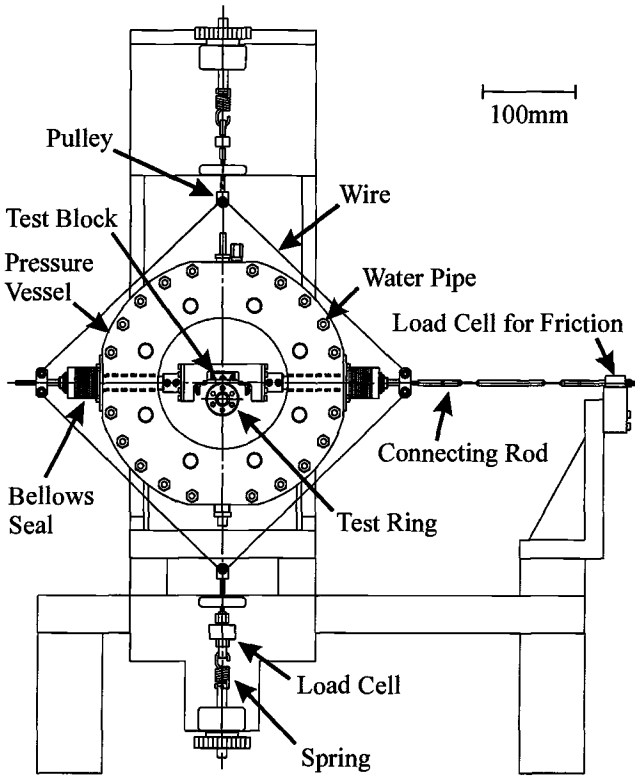


Figure 1- Block-on-Ring Friction Tester Set in Pressure Vessel

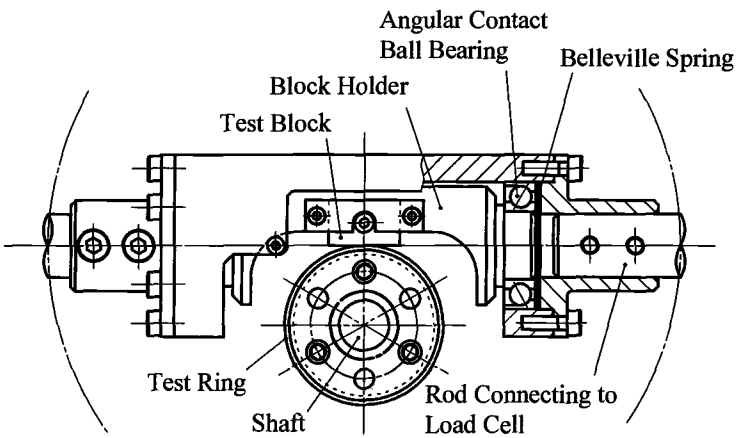


Figure 2- Enlarged View of Sliding Test Area

An enlarged view of the sliding test area is shown in Fig. 2. In order to avoid the misalignment of the mating surfaces between the block and the ring, the block is placed on the shaft of block holder which is supported with angular contact ball bearings so that the block enables to rotate around the pivot of the rod for measuring friction force. Furthermore, there is no torque due to the friction at the contact surface between the block and the ring because the contact surface is on the center line of the rod. Therefore, this friction tester has the ability to measure the friction force of specimens precisely.

Figure 3 shows a test block and ring. These test specimens are the same shape as the ones of ASTM Test Method for Ranking Resistance of Materials to Sliding Wear Using Block-on-Ring Wear Test (G77). The mechanical properties of the block and ring is shown in Table 1. The block and the ring are made from high speed steel (JIS SKH51; quenching) and NiCrMo cast iron or gray cast iron (JIS FC250) respectively, which correspond to the vane and the rolling piston in a refrigerating/air-conditioning rotary compressor. Besides, in order to compare the actual Falex block-on-ring testing machine, typical materials (SKH51/NiCrMo steel (JIS SNCM420)) for the Falex testing machine are also used for the test block and ring.

The combinations of refrigerant and refrigerating machine oil are HCFC22/naphthenic mineral oil (NMO) and HFC134a/polyalkylene glycol (PAG) or polyol ester (POE). Table 2 shows the properties of oils. To examine the effect of additive on the boundary friction coefficient under mixed lubrication condition, phosphorus containing extreme pressure additive (triphenyl phosphate (TPP;  $(C_6H_5)_3PO_4$ ) or tricresyl

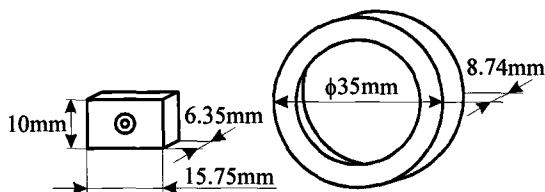


Figure 3- Test Block and Test Ring

Table 1- Mechanical Properties of Specimens

	Material	Young's Modulus (GPa)	Poisson's Ratio	Hardness HRC
Test Block	High Speed Tool Steel (JIS SKH51; Quenching)	222	0.28	60~66
	High Speed Tool Steel (JIS SKH51)	222	0.28	19.7
Test Ring	NiCrMo Cast Iron	118	0.25	47~53
	Gray Cast Iron (JIS FC250)	92	0.25	22.8
	NiCrMo Steel (JIS SNCM420)	204	0.30	31~40

Table 2- Properties of Oils

Oil	Kinematic viscosity ( $\times 10^{-6}$ m <sup>2</sup> /s)		Density@15°C (kg/m <sup>3</sup> )
	40°C	100°C	
Naphthenic mineral oil (NMO)	55.5	5.9	922
Polyalkylene glycol (PAG)	50.5	9.9	917
Polyol ester (POE)	56.0	6.7	980

Table 3- Standard Experimental Condition

Refrigerant	HFC-134a
Refrigerant Pressure	0.1 MPa (abs.)
Refrigerant Concentration	2.8 mass%
Oil	POE (non additive)
Oil Temperature	40 °C
Load	30 N
Sliding Velocity	$7.3 \times 10^{-4} \sim 3.6$ m/s
Block / Ring	High Speed Tool Steel (JIS SKH51; Quenching) / NiCrMo Cast Iron
Surface Roughness of Block and Ring	Ra 0.05 $\mu$ m

phosphate (TCP;  $(\text{CH}_3\text{C}_6\text{H}_4)_3\text{PO}_4$ ) [11] added to POE.

Table 3 shows the standard experimental condition in this study. The refrigerant pressure, the oil temperature and the load between the block and the ring were kept constant, and the sliding velocity between the block and the ring was changed. Furthermore, to minimize the influence of the viscosity of oil decreasing by the refrigerant dissolving, the tests were carried out in low refrigerant gas pressure.

## Experimental Results and Discussion

Figures 4 and 5 show the results of experiment and identifying boundary friction coefficient  $\mu_b$  and contact constant  $k_c$  in mixed lubrication regime in the standard experimental condition. In this case, the results that  $\mu_b = 0.124$  and  $k_c = 0.00066$  were

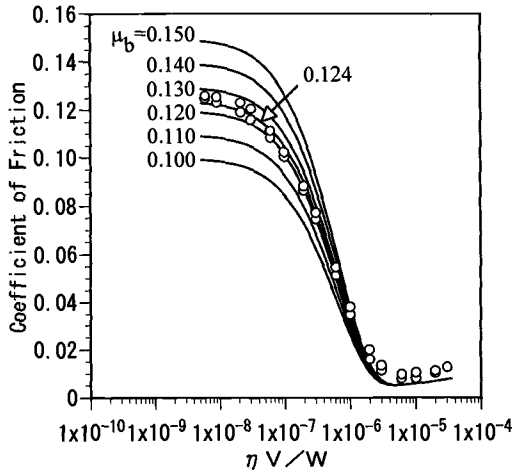


Figure 4- Identification of  $\mu_b$

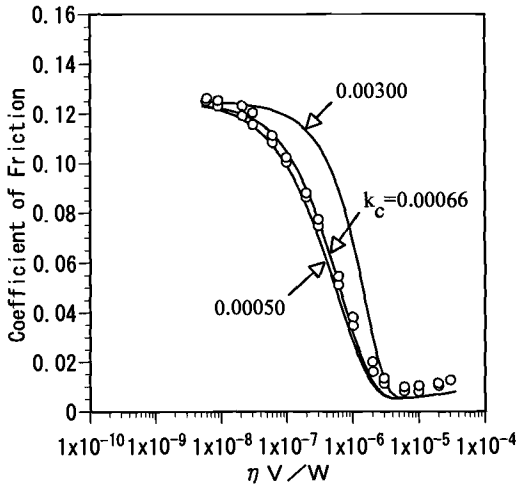


Figure 5- Identification of  $k_c$

obtained. In this test condition, the identified boundary friction coefficient in mixed lubrication regime agreed with the friction coefficient in boundary lubrication regime.

Figure 6 shows the effect of materials of specimens on the identified boundary friction coefficient  $\mu_b$  and contact constant  $k_c$  in mixed lubrication regime. The frictional characteristic of SKH51(quenching)/NiCrMo cast iron was the same as SKH51/SNCM420, but SKH51(quenching)/FC250 indicated higher friction coefficient than the others. By identifying of boundary friction coefficient  $\mu_b$  and contact constant  $k_c$  of SKH51(quenching)/FC250 in mixed lubrication regime, it was obtained  $\mu_b = 0.135$  and  $k_c = 0.00130$ .

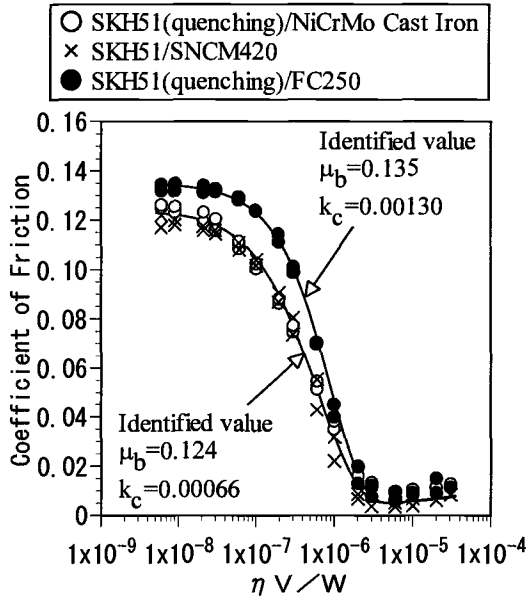


Figure 6- Effect of Materials

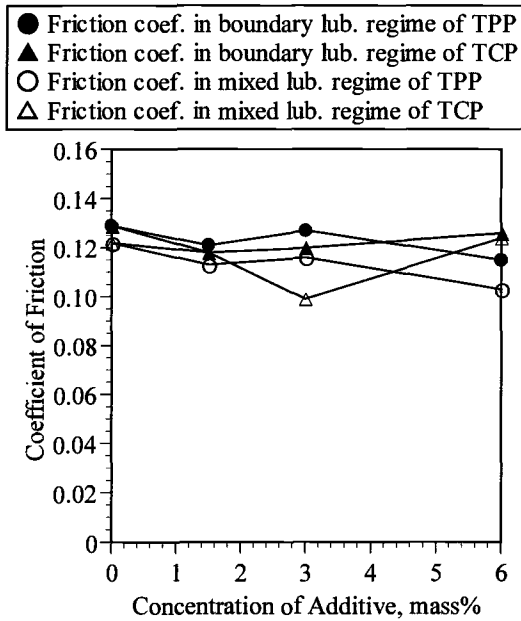


Figure 7- Effect of Additive

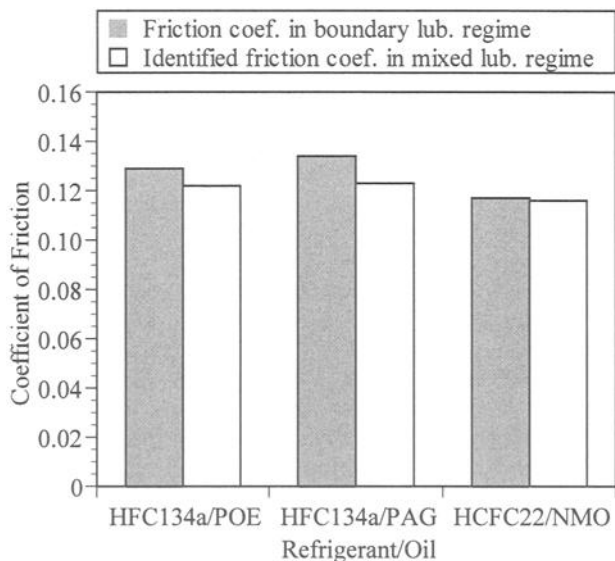


Figure 8- *Effect of Combination of Refrigerant and Oil*

Figure 7 shows the effects of the kind and concentration of additive on the identified boundary friction coefficient  $\mu_b$  in mixed lubrication regime and the friction coefficient in boundary lubrication regime. This figure illustrates that identified boundary friction coefficient in mixed lubrication regime decreases with an increase in quantity of TPP, but TCP shows a minimum boundary friction coefficient in 3.0 mass%. Besides, the results show two cases; one is that the identified boundary friction coefficient in mixed lubrication regime coincides with the friction coefficient in boundary lubrication regime and the other is that the identified boundary friction coefficient is lower than the friction coefficient in boundary lubrication regime.

Figure 8 shows the effect of the combination of refrigerant and oil on the identified boundary friction coefficient in mixed lubrication regime and the friction coefficient in boundary lubrication regime. Both friction coefficients of HCFC22/NMO are the lowest of all combinations and agree with each other. The identified boundary friction coefficients in mixed lubrication regime in cases of HFC134a/POE and HFC134a/PAG are lower than the friction coefficient in boundary lubrication regime.

The fact that both kinds of boundary friction coefficient coincide with each other in some cases indicates that the analysis model is appropriated for the identification. The disagreement in both kinds of boundary friction implies that the boundary friction coefficient is not constant.

### Concluding Remarks

An identification method of the boundary friction coefficient of sliding parts under

the mixed lubrication condition has been presented. The boundary friction coefficients in a mixed lubrication regime have been identified by comparison between the frictional characteristics measured with a developed block-on-ring friction tester, which is able to measure frictional characteristics precisely in wide lubrication conditions and many kinds of atmosphere, and the calculated results obtained from the mixed lubrication analysis that solved simultaneously the elastohydrodynamic lubrication equations and the contact ones.

The results imply that the boundary friction under the mixed lubrication condition does not always coincide with the friction in the boundary lubrication regime. Therefore, it is necessary for evaluating the lubricating performance of lubricants.

## References

- [1] Patterson, D. J., Hill, S. H. and Tung, S. C., "Bench Wear Testing of Engine Power Cylinder Components," *Lubrication Engineering*, Vol. 49, No. 2, 1993, pp. 89-95.
- [2] Cabrera, C. R., Franco, H. J. and Torres, N., "Study of Wear Mechanisms and Characteristics of Coating Films on the FALEX Block-on-Ring Tester Using SEM and EDAX," *SAE Special Publications*, No. 936, 1993, pp. 191-212.
- [3] Chunhong, Z., Junxiu, D., Shizhu, W. and Yuansheng, J., "Investigation of Matching Characteristics of Important Frictional Materials with Lubricant Antiwear Additives," *Wear*, Vol. 152, No. 2, 1992, pp. 317-325.
- [4] Grigorescu, I. C., Soto, R. R., Gonzalez, J. J. and De, V. Y., "Tribological Behaviour of Sprayed Coatings for Shaft Restoration," *Surface & Coatings Technology*, Vol. 45, No. 1-3, 1991, pp. 263-272.
- [5] Xia, H., "Study on the Antiwear Behaviour of S-P-Type Gear Oil Additives in Four-Ball and Falex Machines," *Wear*, Vol. 112, No. 3-4, 1986, pp. 355-361.
- [6] Tanaka, S., Kyogoku, K., Nakahara, T. and Kawahara, K., "Lubrication Characteristics of Refrigerating / Air Conditioning Rotary Compressor (Part 2) : Experimental Verification of Mixed Lubrication Analysis of Vane Tip," *Japanese Journal of Tribology*, Vol. 45, No. 7, 2000, pp. 554-561.
- [7] Tanaka, S., Kyogoku, K. and Nakahara, T., "Lubrication Characteristics of Refrigerating / Air Conditioning Rotary Compressor : Mixed Lubrication Analysis on Vane Tip," *Japanese Journal of Tribology*, Vol. 41, No. 3, 1996, pp. 253-267.
- [8] Tanaka, S., Momozono, S., Kyogoku, K. and Nakahara, T., "Estimation of Coefficient of Boundary Friction Under Mixed Lubrication in Refrigerant Atmosphere," *Journal of Japanese Society of Tribologists (in Japanese)*, Vol. 44, No. 5, 1999, pp. 358-365.

[9] Patir, N. and Cheng, H. S., "Effect of Surface Roughness Orientation on The Central Film Thickness in E.H.D. Contacts," *Proceedings of the 5th Leeds-Lyon Symposium on Tribology*, 1978, pp. 15-21.

[10] Greenwood, J. A. and Tripp, J. H., "The Contact of Two Nominally Flat Rough Surfaces," *Proceedings of the Institution of Mechanical Engineers*, Vol. 185, 1970-71, pp. 625-633.

[11] Lide, D. R., *Handbook of Chemistry and Physics*, CRC Press, 76th Edition, 1995-1996.

B.-O. Åhrström<sup>1</sup>

## Investigation of Frictional Properties of Lubricants at Transient EHD-Conditions

---

**Reference:** Åhrström, B.-O., “Investigation of Frictional Properties of Lubricants at Transient EHD-Conditions,” *Bench Testing of Industrial Fluid Lubrication and Wear Properties Used in Machinery Applications, ASTM STP 1404*, G. E. Totten, L. D. Wedeven, J. R. Dickey, and M. Anderson, Eds., American Society for Testing and Materials, West Conshohocken, PA, 2001.

**Abstract:** In assessment of lubricant properties and in various contact applications, it is of importance to know the frictional qualities. Under quasi-static conditions, normal and transverse forces are measured using force transducers, but the task is more difficult when loads are high and transient as they often are in elastohydrodynamic conjunctions. The experimental method presented in this paper is based on analysis of propagating waves in a beam, due to an impact on its end surface, using FFT analysis. Since the impact is oblique, both non-dispersive compression waves and dispersive flexural waves are generated. The normal force originating from the axial wave is measured using strain gauges, while the transverse force is derived from the FFT's of two lateral acceleration histories using Timoshenko dynamic beam theory. The relation between normal and tangential force histories displays the frictional properties at the impact as a function of time; i.e., variations in frictional properties during loading and unloading (typically 200-400  $\mu$ s in ball bearings and gears) can be observed. A variety of lubricants has been studied up to a Hertzian pressure of 2.5 GPa, and the method and results are presented.

**Keywords:** transient, impact, fourier, FFT, friction, density, dilatation, pressure, tribology, EHD, EHL, lubricant, oil, ball, bar, wave, beam

---

<sup>1</sup>M.Sc., Department of Mechanical Engineering, Division of Machine Elements, Luleå University of Technology, SE-971 87 Luleå, Sweden.

## Introduction

In the field of lubrication and friction the interaction between two surfaces separated by a thin film of lubricant is studied. The aim of the research is to increase efficiency and reduce damage in machine elements such as bearings and gears. As computers and computer codes become more sophisticated, simulations of more complex physical and mechanical processes are being conducted. Reliable results demand detailed knowledge of the simulated event regarding material behavior as well as the physical and mechanical processes involved. Knowledge of material parameters is often lacking, making the results of such calculations less confident. In many contact applications elasto-hydro-dynamic (EHD) lubrication is at hand, which is characterized by moving- and elastically deformed surfaces, high contact pressures, lubricant compression and high shear rates. Hence, accurate quantification of lubricant properties in such conjunctions is difficult due to the prevailing conditions. Investigation of transient EHD-lubrication involves experiments in which frictional properties evaluated from simultaneous normal and transverse forces are studied under impact conditions. From the results of such experiments quantitative information regarding lubricant properties can be gained and used in computer simulations.

Several authors have reported experiments on frictional properties of lubricants under different conditions regarding pressure and shear rate and with different methods. Reference [1] used a spinning ball apparatus to investigate friction under slowly varying shear rates, reference [2] used inclined plate impact and reference [3] used high-pressure viscosimetry. In none of these methods the loading times and other conditions are the same as those prevailing in practical EHD situations. Reference [4] used the impact of a spinning ball to investigate friction under transient conditions. References [5, 6] developed a test method utilizing a steel ball impinging a flat lubricated surface. In these investigations the time-scale is representative for practical EHD situations, but the methods are not capable of recording the time histories of the forces during the impact. The present work presents an improved version of the method in reference [7], which is based on the principle of a steel ball impacting a flat surface allowing the force histories in the contact to be measured during the impact. The method uses the theory of axial and flexural wave propagation in a straight beam for evaluation of normal and transverse transient forces at the flat end of the beam. The transverse force is obtained from two measured accelerations using spectral analysis. See for example reference [8].

## Theoretical Background

Simultaneous normal and transverse transient forces, due to an oblique impact on the end plane of a long rod, are considered. The transverse force  $T_0$  generated by the impinging body is a friction force parallel to the  $z$  coordinate axis. The normal force  $N_0$  is a compressive force oriented parallel to the rod's axis which is the  $x$  coordinate. An off-center impact does not affect neither the transverse nor the normal force, but will generate a bending moment at the end plane oriented in the  $y$  direction and with a magnitude of  $M_0 = N_0 \cdot e$ , see Figure 1. The bending moment and the transverse force

generate a dispersive flexural wave in the  $x$ - $z$  plane described by the center line deflection of the rod  $w(x,t)$ . Second order Timoshenko beam theory is used for evaluation purposes of the flexural wave, implying that both rotational inertia and shear deformation are accounted for. The normal force is assumed to generate a plane 1-D axial wave although it is more or less a point force.

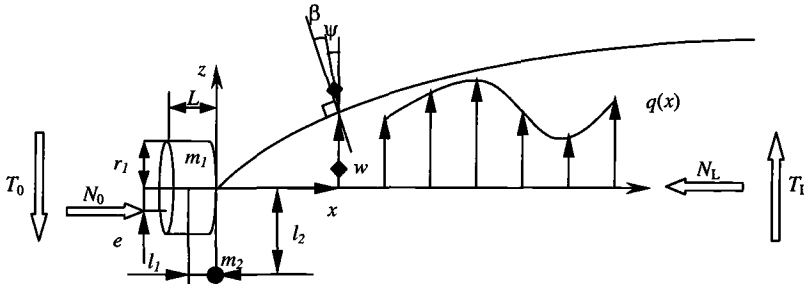


Figure 1. Geometrical properties of a rod subjected to external loads i.e. traction- and normal forces and a distributed load. The cylindrical body represents a rigid body of tungsten carbide to support the high pressures generated by the impinging steel ball, while the point mass ( $m_2$ ) represents the mass of an accelerometer.

The axial wave is ideally non-dispersive and therefore axial strain,  $\epsilon$ , measured at a position along the rod represents the normal impact force,  $N_0$ , through the equation

$$N_0(t) = AE\epsilon(t + t_0) \tag{1}$$

where  $A$  is the cross-sectional area of the rod,  $E$  is Young's modulus and  $t_0$  is the travel time for the wave between the end and the cross-section where strain is measured. On the contrary to the non-dispersive axial wave, the dispersive flexural wave is more complex to handle numerically. The equation of motion in the transverse direction for a Timoshenko beam, reference [9], is

$$EIw'''' + \rho A\ddot{w} - \rho l \left( 1 + \frac{E}{kG} \right) \dot{w}'' + \frac{\rho^2 I}{kG} \ddot{w} = q + \frac{\rho l}{kGA} \ddot{q} - \frac{EI}{kGA} q'' \tag{2}$$

where  $( )'$  and  $( \dot{\ } )$  denote differentiation with respect to the  $x$  coordinate and time, respectively. Young's modulus  $E$ , area moment of inertia  $I$ , density  $\rho$ , cross-sectional area  $A$  and the geometrically related correction term  $k$  (as described by reference [10]) are all constant along the beam. Equation (2) represents a dispersive mechanical system, and a Fourier-decomposition of the time dependent quantity  $w(x,t)$  is introduced. A general harmonic wave solution of the form  $w_h(x,t) = Be^{i(\alpha x + \omega t)}$  inserted in equation (2) yields the characteristic equation for the case where there is no distributed load, that is  $q(x,t) \equiv 0$ ,

$$ElkG\kappa^4 - (\rho IkG\omega^2 + \rho IE\omega^2)\kappa^2 + \rho^2 I\omega^4 - \rho AkG\omega^2 = 0 \quad (3)$$

where  $\omega$  is the angular frequency.

Since equation (3) is of fourth degree, it yields four solutions to the wave number  $\kappa$  of which only two are physically acceptable for an initially quiescent semi-infinite rod impacted at its end. The final expression for a harmonic component of the transverse displacement is:

$$w(x,t) = \hat{w}(x,\omega)e^{i\omega t} = \left[ B_1 e^{i\kappa_1 x} + B_2 e^{i\kappa_2 x} \right] e^{i\omega t} = \left[ B_1 e^{i \left( \frac{1}{\sqrt{2ElkG}} \sqrt{\rho I \omega^2 (kG+E) + \omega \sqrt{\rho^2 I^2 \omega^2 (kG+E)^2 - 4ElkG(\rho^2 I \omega^2 - \rho AkG)}} \right) x} + B_2 e^{i \left( \frac{1}{\sqrt{2ElkG}} \sqrt{\rho I \omega^2 (kG+E) - \omega \sqrt{\rho^2 I^2 \omega^2 (kG+E)^2 - 4ElkG(\rho^2 I \omega^2 - \rho AkG)}} \right) x} \right] e^{i\omega t} \quad (4)$$

The first term in equation (4), having a real wave number, represents a harmonic wave travelling in the positive  $x$  direction. The second term, having an imaginary wave number, represents a non-propagating vibration or a so-called evanescent solution. The term within the bracket is the Fourier transform of the transverse displacement, and  $B_1(\omega)$  and  $B_2(\omega)$  are complex constants. Utilizing the relations between displacement, bending moment and shear force and completing with compensation for external masses, yields the following expressions:

$$\hat{T}_0 = \frac{\rho I \omega^2}{ikG} \left( \frac{(kG\kappa_1^2 - \rho\omega^2)}{\kappa_1} B_1 + \frac{(kG\kappa_2^2 - \rho\omega^2)}{\kappa_2} B_2 \right) - \frac{EI}{ikG} \left( (kG\kappa_1^2 - \rho\omega^2) B_1 \kappa_1 + (kG\kappa_2^2 - \rho\omega^2) B_2 \kappa_2 \right) + (m_1 + m_2) \dot{w}_0 \quad (5)$$

$$\hat{M}_0 = EI \left[ (B_1 \kappa_1^2 + B_2 \kappa_2^2) - \frac{\rho}{kG} \omega^2 (B_1 + B_2) \right] + m_1 l_1 \omega^2 (B_1 + B_2) + \omega^2 \left( m_1 l_1^2 + m_2 l_2^2 + m_1 \left( \frac{r_1^2}{4} + \frac{L^2}{12} \right) \right) \left( \frac{(kG\kappa_1^2 - \rho\omega^2)}{(ikG\kappa_1)} B_1 + \frac{(kG\kappa_2^2 - \rho\omega^2)}{(ikG\kappa_2)} B_2 \right) - \hat{T}_0 L \quad (6)$$

If the moment, due to off-axis impact, would be negligible, that is  $M_0 \equiv 0$ , the complex constants  $B_1(\omega)$  and  $B_2(\omega)$  could be determined through equation (6). The outcome would be that only one measured quantity would be needed in order to evaluate the transverse force. Since zero moment can not be guaranteed, another approach is considered. In order to determine the constants  $B_1(\omega)$  and  $B_2(\omega)$  in equations (5) and (6), two frequency related quantities have to be measured. The two acceleration histories enable the determination through the expressions:

$$\hat{a}_1(x = x_1) = -\omega^2 \hat{w}(x_1, \omega) = -B_1 \omega^2 e^{i\kappa_1 x_1} - B_2 \omega^2 e^{i\kappa_2 x_1} \tag{7}$$

$$\hat{a}_2(x = x_2) = -\omega^2 \hat{w}(x_2, \omega) = -B_1 \omega^2 e^{i\kappa_1 x_2} - B_2 \omega^2 e^{i\kappa_2 x_2} \tag{8}$$

Since position  $x_1$  conveniently equals zero, given from the experimental setup, the expressions in equation (5) and (6), eliminating  $B_1$  and  $B_2$  becomes:

$$\hat{T}_0 = \frac{(\rho I + m_1 l_1)}{ikG} \left( \frac{(kG\kappa_1^2 - \rho\omega^2)(\hat{a}_2 - \hat{a}_1 n)}{\kappa_1(n-m)} - \frac{(kG\kappa_2^2 - \rho\omega^2)(\hat{a}_2 - \hat{a}_1 m)}{\kappa_2(n-m)} \right) - (m_1 + m_2) \hat{a}_1 - \frac{EI}{ikG\omega^2} \left( (kG\kappa_1^2 - \rho\omega^2) \frac{(\hat{a}_2 - \hat{a}_1 n)}{(n-m)} \kappa_1 - (kG\kappa_2^2 - \rho\omega^2) \frac{(\hat{a}_2 - \hat{a}_1 m)}{(n-m)} \kappa_2 \right) \tag{9}$$

$$\begin{aligned} \hat{M}_0 = & \frac{EI}{\omega^2} \left[ \left( \frac{(\hat{a}_2 - \hat{a}_1 n)}{(n-m)} \kappa_1^2 - \frac{(\hat{a}_2 - \hat{a}_1 m)}{(n-m)} \kappa_2^2 \right) + \frac{\rho\omega^2}{kG} \hat{a}_1 \right] - \\ & m_1 l_1 \hat{a}_1 + \frac{1}{ikG} \left( m_1 \left( l_1^2 + \frac{r_1^2}{4} + \frac{L^2}{12} \right) + m_2 l_2^2 \right) \cdot \\ & \left( \frac{(kG\kappa_1^2 - \rho\omega^2)(\hat{a}_2 - \hat{a}_1 n)}{\kappa_1(n-m)} - \frac{(kG\kappa_2^2 - \rho\omega^2)(\hat{a}_2 - \hat{a}_1 m)}{\kappa_2(n-m)} \right) - \\ & \frac{(\rho I + m_1 l_1)L}{ikG} \left( \frac{(kG\kappa_1^2 - \rho\omega^2)(\hat{a}_2 - \hat{a}_1 n)}{\kappa_1(n-m)} - \frac{(kG\kappa_2^2 - \rho\omega^2)(\hat{a}_2 - \hat{a}_1 m)}{\kappa_2(n-m)} \right) + \\ & \frac{EIL}{ikG\omega^2} \left( (kG\kappa_1^2 - \rho\omega^2) \frac{(\hat{a}_2 - \hat{a}_1 n)}{(n-m)} \kappa_1 - (kG\kappa_2^2 - \rho\omega^2) \frac{(\hat{a}_2 - \hat{a}_1 m)}{(n-m)} \kappa_2 \right) + \\ & (m_1 + m_2) \hat{a}_1 L \end{aligned} \tag{10}$$

where  $m = e^{i\kappa_1 x_2}$  and  $n = e^{i\kappa_2 x_2}$ . The time function  $T_0(t)$  is found by inverse Fourier transformation of expression (9), yielding the desired time history of the transverse force  $T(t)$ . It should also be pointed out that in principle also other quantities related to flexural deformation than acceleration (velocity, displacement or strain) could be used for evaluation of transverse force. Acceleration is however best suited for FFT analysis since it is of transient character and falls to zero immediately after the event.

**Experiments**

In order to carry out the experiments, an apparatus has to be designed that satisfies the criteria for a Timoshenko beam and is instrumented for compression- and flexural wave measurements simultaneously. The apparatus has to produce an oblique impact, be easy to clean and apply lubricant onto.

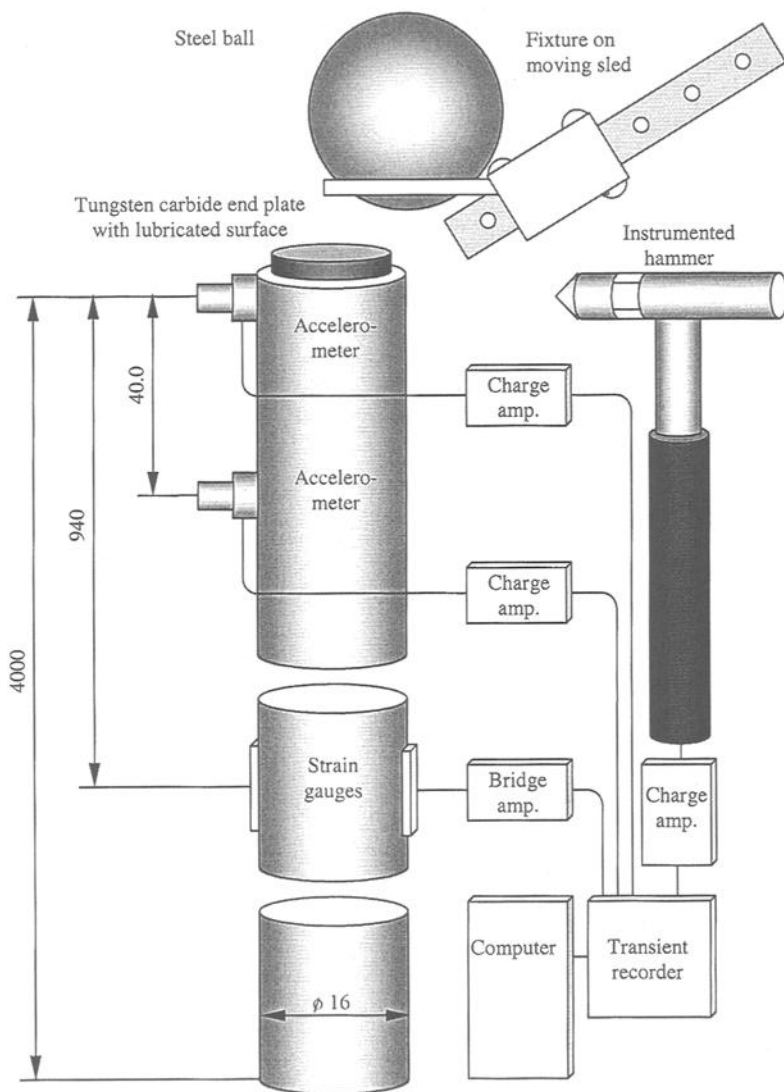


Figure 2. Experimental setup for calibration.

### Setup

In Figure 2 the experimental setup is shown. A cylindrical steel rod (SIS 1650) with diameter 16 mm and length 4 m is standing vertically with its upper end surface free. A tungsten carbide end plate, with high compressive strength, is centered and soldered onto it. A 50 mm steel ball supported and controlled by a fixture on a moving sled is sent to impact the end plane from an oblique angle. At impact the steel ball strikes the tungsten carbide plate, releases from the sled and bounces off the end surface.

Normal- and transverse forces from an off-center impact on the free end generate compressional- and flexural waves in the rod. Both the transverse force and the bending moment contribute to the flexural wave if the impact is not in the center of the cross-section. At a position 940 mm from the end plane a strain gauge pair of piezo-resistive type is mounted, and coupled to a Whetstone-bridge for bending moment suppression, measuring the axial strain history. After amplification (Measurement Group 2210 signal conditioning amplifier) the signal is recorded and utilized to calculate the normal force history  $N_0(t)$  according to equation (1). The distance from the end plane is justified since it is long enough to increase time measurement accuracy, but short enough to avoid perturbations from the reflecting wave. Lateral accelerations ( $z$  direction) are measured by two identical accelerometers (B&K 4393) at two different positions along the beam. The upper accelerometer is positioned as close to the end-plane as possible, creating a reference datum, and the other is positioned 40 mm directly under. Two identical charge amplifiers (B&K 2635) are used to amplify the accelerometer signals, and a digital oscilloscope (YOKOGAWA DL4100) records data. The sample rate used is ten samples per microsecond, and the record length is 10,000 samples. The software utilized for evaluation purpose is Matlab 5.2 including a 10,000 point FFT and inverse FFT. The transverse force is calculated according to equation (9).

### Calibration

A factory calibrated impact hammer (B&K 8202) with a piezo-electric force transducer (B&K 8200) is used for evaluation procedure verification. The sensitivity of the hammer is 0.95 pC/N according to the calibration chart. The signal from the hammer is amplified (B&K 2635) and recorded. A transverse impact diametrically opposite the accelerometer and as close to the upper end plane as possible is suitable for verification of the evaluation model, equation (9). The two measured acceleration histories from such a transverse impact are shown in Figure 3 and it is noted that there is a difference in histories due to the dispersive nature of the flexural wave and the distance between the accelerometers.

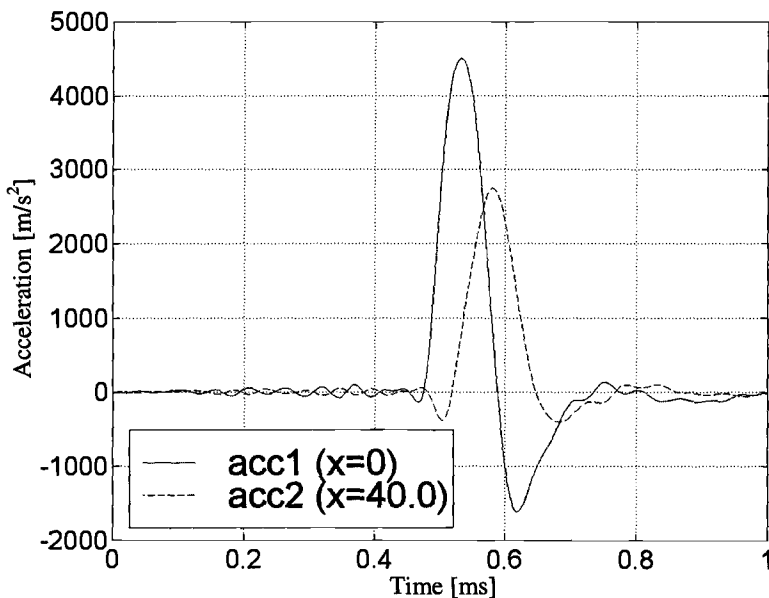


Figure 3. Measured acceleration signals from transverse force calibration.

In Figure 4 the measured and evaluated transverse forces are displayed. The shape of the curves indicates good correspondence between theory and practice. The shape of the curves at the end (after the impact) emanates from the dynamic behavior of the instrumented hammer. Even then, the theory describes the actual event adequately even though that part of the impact event is not important.

Concerning the normal force, the wave propagation is of a totally different nature. Since the compression wave is non-dispersive, the output of the strain gauges is directly proportional to the normal force making the evaluation easy (Figure 5). Due to the wave propagation velocity of the compression wave and the distance to the strain gauge pair, the measured response is delayed 179 microseconds ( $t_0$ ). By striking the end plate with the calibration hammer in the normal  $x$  direction and measuring the time between the load peaks, the delay is determined.

Tests have been done to assure full film lubrication for all pressures and oils. By applying a 100 mV potential difference between the ball and the rod, and measuring any potential equalization due to asperity contact, it has been confirmed that full film lubrication prevails during the impact. If the lubricating film is not fully developed, generated heat lowers the strength of the asperities in contact decreasing the friction coefficient.

The bending moment originating from an off-center impact is calculated through equation (6), but of no importance to the evaluation of the friction coefficient, since only the normal- and transversal forces are required. Hence no efforts have been made to justify the accuracy of the evaluation algorithm for the calculated end moment.

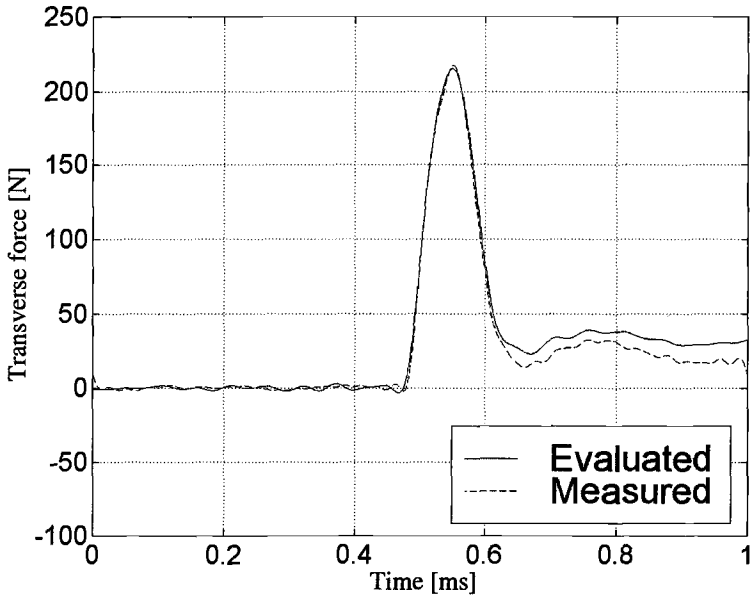


Figure 4. Measured and evaluated transverse force history from calibration.

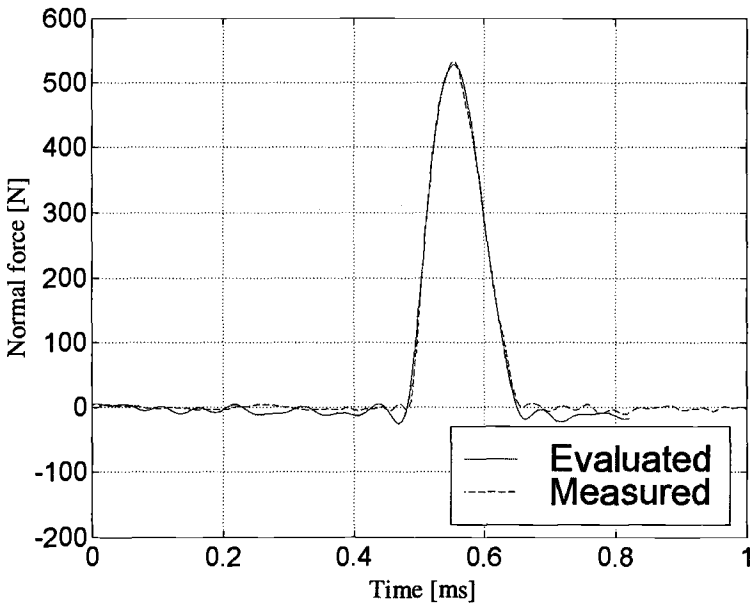


Figure 5. Measured and evaluated normal force history from calibration.

*Experimental Procedure*

Experiments regarding lubricant friction during relevant EHL conditions have been performed. The following lubricants were tested at Hertzian pressures 1.4, 2.0 and 2.5 GPa: Naphthenic mineral oil, Paraffinic mineral oil, Polyglycol, Polyalphaolefin and Rape seed oil. Properties of the tested lubricants are presented in Table 1.

Table 1. *Lubricant properties at atmospheric pressures.*

Lubricant	Density at 15°C $\rho$ [kg/m <sup>3</sup> ]	Dynamic viscosity at 40°C $\eta_0$ [mPas]	Viscosity index VI
NAM	920	154	3
PAM	887	154	95
PG	1002	136	198
PAO	832	37	136
RSO	921	34	215

The ball and end plate were thoroughly cleaned, and a thin layer of the lubricant specimen was applied to the latter. The steel ball was released from a designated height, corresponding to the desired pressure, and sent to impact the end plate from an oblique angle. An actual measurement for a Polyglycol at 2.5 GPa can be seen in Figure 6.

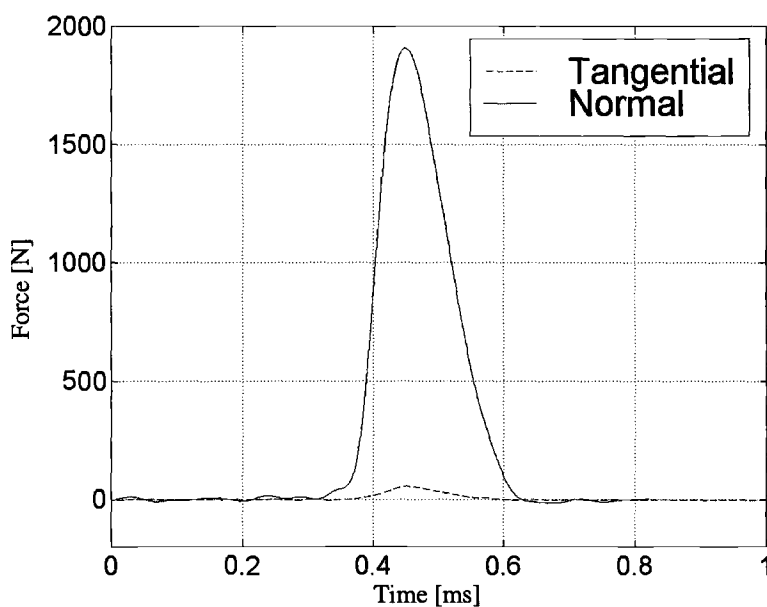


Figure 6. *Measured transverse- and normal force histories for a Polyglycol at 2.5 GPa.*

The contact time is about 250  $\mu\text{s}$  and the magnitudes of the forces are what would be expected for a lubricated conjunction subjected to 2.5 GPa pressure at full film lubrication.

**Result and Discussion**

In Figure 7a-c the friction coefficients (defined as the quotient between transverse- and normal force) for the different lubricants at the designated pressures are displayed. It can be seen that the relation between transverse- and normal force depends on the lubricant, and that the frictional properties of the lubricants seem to vary during the impact. The relations shown in Figure 7a-c are results from several friction experiments with different lubricants and at different pressures. The forms of the curves indicate that friction conditions change during the loading and unloading sequence. A maximum is obtained when the normal force peaks, and after that the friction coefficient decreases by approximately 5-15%. A possible explanation is that due to the high pressure, the lubricants transition into an amorphous solid-like state. The increase in pressure elevates the resistance to shear stress within the lubricant, hence friction coefficient increases. The exception is the measurement in Figure 7a, which is currently the minimum reliable limit for the apparatus.

An error analysis has been executed in order to determine the sensitivity of erroneous measurement of the time shift in the axial wave. A relatively big error, 3  $\mu\text{s}$ , does not have any significant impact on the slope of the evaluated friction coefficient.

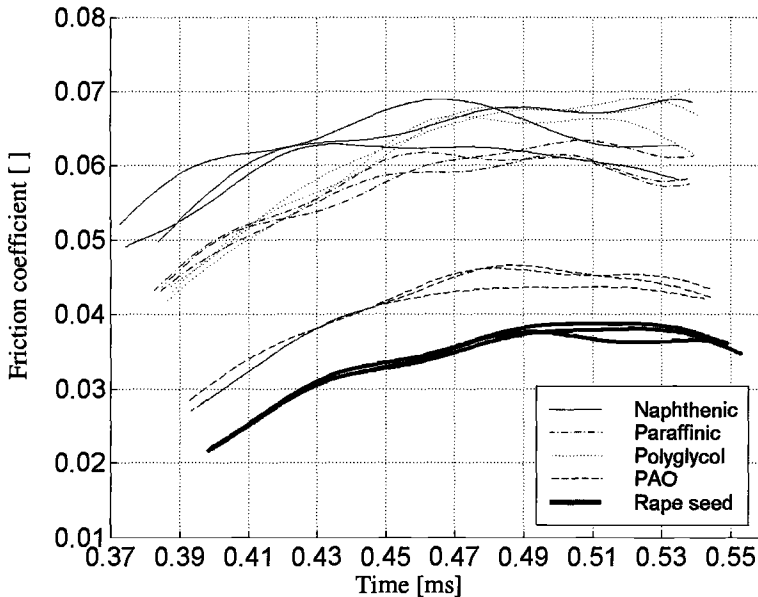


Figure 7a. Friction coefficient as function of time for a Hertzian pressure of 1.4 GPa.

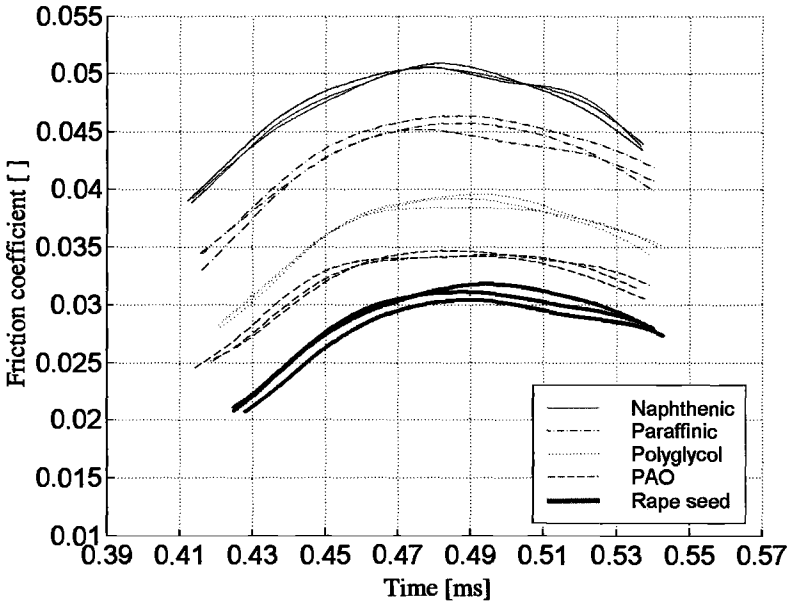


Figure 7b. Friction coefficient as function of time for a Hertzian pressure of 2.0 GPa.

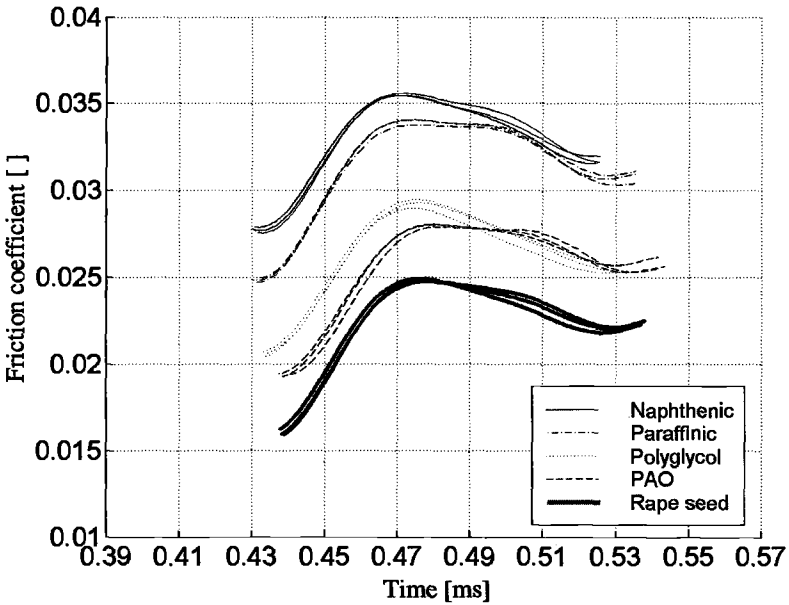


Figure 7c. Friction coefficient as function of time for a Hertzian pressure of 2.5 GPa.

The relation between the different molecular structure of the oils and the friction coefficient is interesting. Long straight molecules like PAO, esters and polyglycols are relatively flexible and deform easily when subjected to pressure. The molecules in a well-refined mineral oil like the naphthenic or the paraffinic oils have less possibilities to adopt different kinds of configurations, and the oil is therefore expected to have a stiffer behavior. A general tendency of decreasing friction coefficient with increasing pressure is observed. This tendency has earlier been detected by reference [11], but no interpretation has been attempted. A physical explanation of this phenomenon requires detailed studies of governing parameters in an EHD conjunction. Further work will be performed in this area.

## Conclusion

Theoretical background and experimental verification are presented for a method that allows simultaneous measurement of transverse and normal forces due to impact on the flat end of a straight beam. Also, the end moment due to off-axis impact can be calculated, but that is only of secondary interest. The method is based on the relation between transverse accelerations of points along the beam, and the generating quantities at the impacted end.

The transverse equation of motion according to Timoshenko's dynamic beam theory has been used in the analysis. Accordingly, shear deformation and rotational inertia of the beam are considered, and it is believed that rotational inertia is of importance because of the high-frequency components generated by an impact. Also, the inertia of the upper accelerometer and tungsten carbide end plate is accounted for in the evaluation model. This effect is considered important due to the high accelerations that arise.

Since the intention is to use the method for friction investigations, it is important that the included forces can be measured accurately. It is observed from Figure 4 and Figure 5 that the calculated transverse and the measured normal forces agree well with the corresponding measured calibration hammer force histories. The accelerometers used are to some degree sensitive to acceleration in the perpendicular direction, causing disturbances from the axial acceleration to superpose the transverse measurement. According to the manufacturer, the maximum transverse sensitivity is 1.8%. The natural frequency of the accelerometers is a limiting parameter and should be as high as possible.

From the result of this investigation it is concluded that: (i) the suggested method is capable of simultaneous measurement of normal and transverse forces during an impact event, (ii) the achieved accuracy is good and (iii) transient friction phenomena can be studied with this method during relevant EHD pressures.

## Acknowledgments

Economic support from Carl Tryggers Stiftelse and the Swedish Research Council for Engineering Sciences as well as constructive discussions with Professor Erik Höglund, Associate Professor K-G Sundin at Luleå University of Technology and Dr. Tomas Norrby and Dr. Åke Byheden at Statoil Lubricants are highly appreciated. Mr. Hans Wikström's competent help in constructing test equipment is greatly valued.

## References

1. Bowden, F. P. and Freitag, E. H., "The Friction of Solids at Very High Speeds I. Metal on Metal; II. Metal on Diamond", *Proceedings of the Royal Society of London* A248, 1958, pp. 350.
2. Ramesh, K. T. and Clifton, R. J., "A Pressure-Shear Plate Impact Experiment for Studying the Rheology of Lubricants at High Pressures and High Shearing Rates", *Journal of Tribology* 109, 1987, pp. 215-222.
3. Bair, S. and Winer, W. O., "The High Shear Stress Rheology of Liquid Lubricants at Pressures of 2 to 200 MPa", *Journal of Tribology*, 112, 1990, pp. 246-252.
4. Bowden, F. P. and Persson, P.-A., "Deformation, Heating and Melting of Solids in High-Speed Friction", *Proceedings of the Royal Society of London* A60, 1961, pp. 433.
5. Jacobson, B. O., "A High Pressure-Short Time Shear Strength Analyzer for Lubricants", *Journal of Tribology* 107, 1985, pp. 220-223.
6. Höglund, E., "The Relationship Between Lubricant Shear Strength and Chemical Composition of the Base Oil", *Wear* 130, 1989, pp. 213-224.
7. Sundin, K.G. and Åhrström, B.-O., "Method for Investigation of Frictional Properties at Impact Loading", *Journal of Sound and Vibration*, 222(4), 1999, pp. 669-677.
8. Doyle, J. F., "Wave Propagation in Structures", *New York: Springer-Verlag*, 1997.
9. Timoshenko, S., "Vibration Problems in Engineering", *Van Nostrand: New York*, 1955.
10. Shames, U. H. and Dym, C. L., "Energy and Finite Element Methods in Structural Mechanics", *Taylor & Francis ISBN 0-89116-505-3*, 1985.
11. Workel, M. F., Doctoral thesis: "Lubricant Behaviour During Impact Under High Pressure and Shear Rate", *The University of Leeds, School of Mechanical Engineering*, 1999.

B. J. Roylance,<sup>1</sup> T. P. Sperring,<sup>1</sup> and T. G. Barraclough<sup>2</sup>

## **Bench Test Determinations of Wear Modes to Classify Morphological Attributes of Wear Debris**

---

**Reference:** Roylance, B. J., Sperring, T. P., and Barraclough, T. G., “**Bench Test Determinations of Wear Modes to Classify Morphological Attributes of Wear Debris,**” *Bench Testing of Industrial Fluid Lubrication and Wear Properties Used in Machinery Applications, ASTM STP 1404*, G. E. Totten, L. D. Wedeven, J. R. Dickey, and M. Anderson, Eds., American Society for Testing and Materials, West Conshohocken, PA, 2001.

**Abstract:** Wear particles represent a crucial source of additional information in performing fundamental wear studies. It has also found important application in monitoring the deterioration of critical components in industrial machinery due to wear, notably in militarily-related machinery functions such as engines and gear transmission units. In this paper, a summary account is given of the way in which specific test machines have recently been utilized to produce wear debris under controlled test conditions. In particular, the morphological features of wear debris are described in relation to wear characteristics obtained from using three test machines: four-ball, pin-on-disc, and gear test machine, respectively. The results of subsequent microscope analysis and classification of the debris morphology are described in relation to the corresponding wear modes experienced in the test. The implications for application of a new software-based, wear debris classifier are reviewed and discussed in relation to present-day methods employed in the maintenance of military engines and gear transmission systems.

**Keywords:** wear debris, morphology, ferrography, test machines, bench testing

### **Introduction**

The capture and subsequent analysis of wear debris as a means of determining non-intrusively the wear-state of critical “rubbing” components such as bearings and gears has been carried out over the past four decades as part of experimental research investigations and industrially based maintenance programs. The methods used to carry out the sampling/capture process at the machine and perform the subsequent analysis are well-documented [1-3]. From determinations of the quantity, size, shape and composition of the debris a “snapshot” of the wear condition and status at a given instant of time is obtained which can be related to the extent and rate of wear, its severity and often, the source of the wear. To establish the mode of wear usually requires that particles be

---

<sup>1</sup> Department of Mechanical Engineering, University of Wales Swansea, Wales, UK.

<sup>2</sup> Spectroinc, 160 Ayer Road, Littleton, MA, 01460.

analyzed morphologically to determine, in particular, their shape characteristics. This is a time-consuming and, generally, highly subjective activity, requiring the acquisition of basic skills in, e.g., using an optical microscope to identify the particle type and specifying the wear process involved. The development and widespread deployment of wear particle atlases and associated shape descriptor terminology by expert analysts [4-6] have proved to be very beneficial for first-time analysts during the initial induction period. Nevertheless, the need remains to develop systematic methods for performing analysis based on morphological classification related to the acquisition of wear debris generated under predetermined, known wear types and conditions.

A series of investigations was recently undertaken at the authors' laboratory with the express aim of developing a generic-type wear particle atlas and wear classification system. Experiments were performed under controlled laboratory conditions using well-established and utilized types of test machines to generate different known wear conditions. In this paper, three of the machines employed in the investigation are described in relation to the test methods used and the associated data. The results of wear debris analysis are summarized against the background of the subsequent development of a classifier system intended for the application in monitoring wear-related deterioration of operating machinery.

### **Tribological Considerations**

The incidence of wear debris generally arises as a direct consequence of interactions occurring between surfaces in rubbing contact in a state of relative motion. To produce debris in a controlled environment requires that the following condition be pre-specified. *Geometry and motion of the interacting components at their point(s) of "contact".*

*Nature and type of lubrication involved.*

*Load – speed condition.*

*Hardness values and surface roughness.*

In a controlled laboratory environment, the kind of measurements made while a test is in progress will typically include:

- *Friction*
- *Temperature – lubricant and solid*
- *Film thickness and/or quality*
- *Wear depth*

Useful information that may be inferred from the test data include:

- *Regime of lubrication – in terms of boundary, mixed or hydro/elasto-hydro lubrication*
- *Contact stress condition and degree of "plasticity" due to loading*

Post-test analysis may include:

- *Wear surface analysis*

- *Hardness and roughness measurements*
- Metallurgical examination of sub-surface structure
- *Lubricant and wear debris analysis*

Note: Items listed above in “*italics*” were implemented in the current investigation, though not all were employed at the same time for every test.

The over-riding consideration when conducting the present tests was to specify the operating regime with particular reference to:

- Geometry and motion
- Friction characteristics
- Regime of lubrication

The primary goal of the post-test analysis was to confirm the wear type and condition and correlate the behavior with the wear debris characteristics.

The general repeatability of the wear – wear debris behavior was another important factor. Tests were repeated several times to ensure credibility of the inferred data, in regard to the type of wear and associated debris. Morphological analysis of debris was undertaken independently by at least two analysts, to ensure integrity of the results.

### **Utilization of Bench Test Methods**

#### *Wear Mode vs. Test Machine*

Table 1 shows how the three test machines were utilized to generate different wear modes and produce ferrous free metal debris in the form of wear particles. The effect of operating under different lubrication and wear regimes on the morphology of the particles was achieved by varying the load, speed and lubrication conditions. Note that the wear debris classification descriptors are based on the universally recognized ferrography method [7].

In order to understand the morphological information a wear particle yields it is important to infer the operating conditions at the contact, and to determine the wear condition along the lines described previously. Likewise, the methods employed to achieve debris retention, capture and processing are to be accomplished with an acceptable level of overall capture efficiency.

#### *Four-ball Machine*

The four-ball machine is normally utilized to perform lubricant tests according to internationally recognized standard test procedures. In the UK, the designated standards are stipulated according to the Institute of Petroleum (IP) as follows: scuffing tests (sliding) - IP239; pitting fatigue (rolling) – IP300.

Figure 1 shows schematically the four-ball configurations for sliding (a) and rolling (b), respectively.

Table 1 - *Wear Mode vs Test Machine Capability*

Test Machine	Four-ball		Pin-on-disc	Gear test Machine	Wear mode
	Sliding	Rolling			
Ferrous free metal debris					
Rubbing	+	+	+	+	Mild abrasion
Sliding	+		+	+	Severe abrasion
Severe sliding	+		+	+	Scuffing (adhesion)
Cutting			+		Severe abrasion
Fatigue (chunky)		+			Pitting fatigue
Fatigue (laminar)				+	Low cycle fatigue

### Experimental Apparatus and Test Procedures

For sliding operation, the three lower balls are clamped in place and the upper fourth ball is rotated against them. For rolling contact, the lower three balls are free to rotate on their own axes and around the 'race' cup under the driving action of the rotating upper ball.

In the current investigation, sliding tests were carried out, each for one minute, using applied loads in the range 36 kg to 150 kg, depending on oil type. As load was increased incrementally with each successive test, non-additive, lower grade oils caused the upper ball to weld to the lower balls and the test was immediately discontinued. Wear was determined in accordance with IP 239 procedures in that the average wear scar diameter was determined from two measurements at right angles to each other, (using an optical microscope) on each of the lower balls (six measurements in all). For the rolling contact mode tests, the running time to the formation of a pit in the upper ball was the sole criterion. Running times per test varied between a few minutes to about three hours. The applied load was in the range 400 – 800 kg. Friction force on the lower balls was recorded for all of the sliding tests by using a calibrated spring in conjunction with a capacitance proximity probe. This information was then relayed to a logging computer through a data acquisition unit. Lubrication was achieved by means of a simple oil bath – the cup, which holds approximately 7mls of oil. A few tests were also conducted using a specially modified gravity fed drip feed system. The oil bath temperature rise was monitored recorded using a T-type thermocouple embedded in the base of the cup. For the oil bath tests, wear particle collection was very carefully undertaken immediately following completion of each test using a special washing procedure to ensure that as much of the debris as possible was extracted and stored in a clinically clean sample bottle which was then sealed and labelled. Previous tests carried out to establish the best method to use for sample collection indicated that a minimum capture efficiency of 70%

was possible, rising to 90%. Samples of wear particles generated were thus obtained that reflected the contrasting behaviour of sliding and rolling motion in the same machine using the same materials and lubricants.

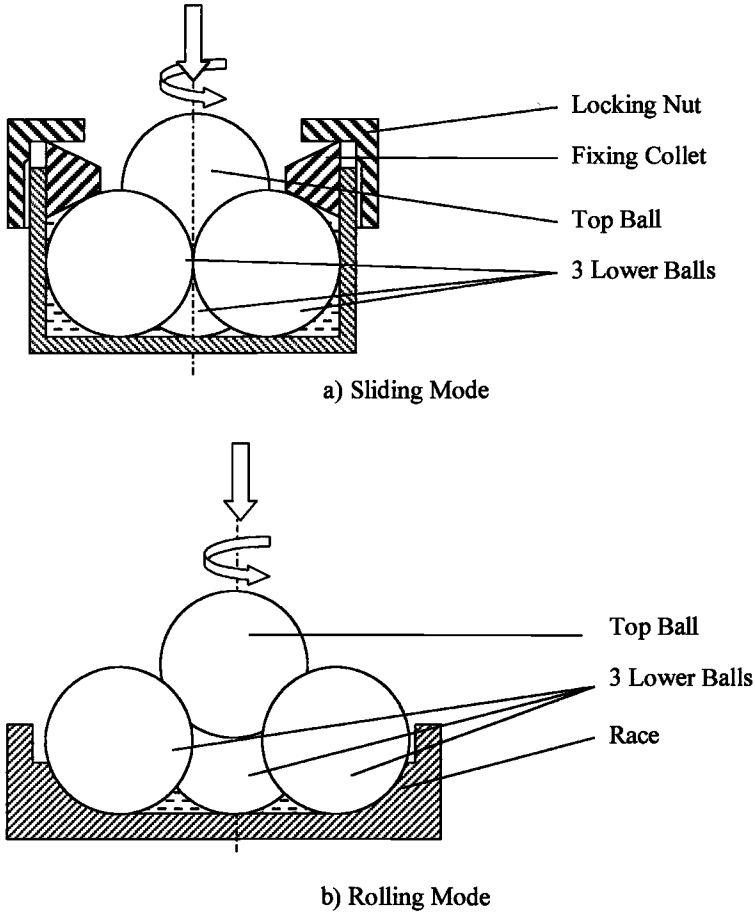
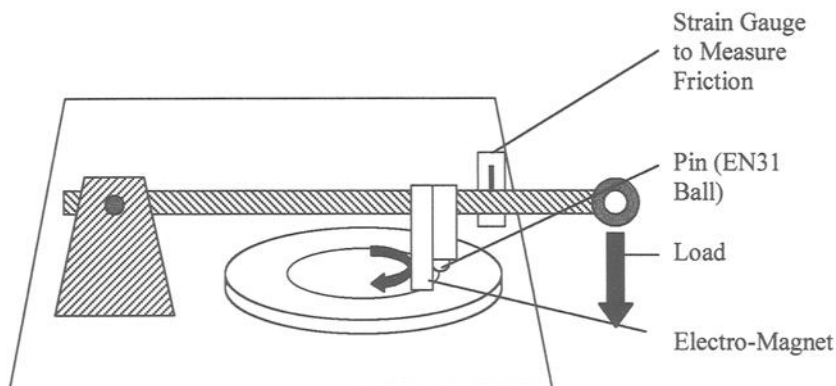


Figure 1 - Four ball test configurations for sliding and rolling contact.

*Pin-on-disc Machine*Figure 2 - *Pin-on-disc Machine*

such as EN8 (080M40, Ra 0.46  $\mu\text{m}$ , VHN 197). Figure 2 shows the pin-on-disc machine in this configuration. Alternatively, a roller was used as the pin, loaded either on its side to give a line contact, or on its end to give a conformal type contact. Another advantage of using the pin-on-disc machine is that it offers a wide range of surface speeds – from 0.1 m/s to 10 m/s. The applied loads ranged from 2 to 40 kg. Collection of the debris was carried out using two methods. During a test, an electromagnet was placed directly behind the pin such that it lifted the debris from the surface as it was generated. At the conclusion to a test, the disc surface was carefully cleaned and all the residue oil, together with the cleaning fluid, was collected in a bottle.

*IAE Gear Machine*

Gear tests were carried out using the IAE gear test machine (Figure 3) which is more conventionally utilized as a lubricant testing device in accordance with standard test procedures as prescribed by IP 166/77. The apparatus comprises a pair of test spur gears, which have a high involute in order that the primary failure mode is scuffing. The gear teeth are loaded by means of a torque applied to the drive shaft. Oil is delivered via a spray nozzle directly above the mesh point, at a temperature between 60 and 120 °C and a flow rate from 17 to 34 L/hr, depending on the test being carried out.

A summary of the characteristics for each test machine is presented in Table 2.

**Test Matrices**

The following test matrices were run for each machine (Tables 3 – 6). The relevance of the operating conditions to those typical of specific practical applications is represented

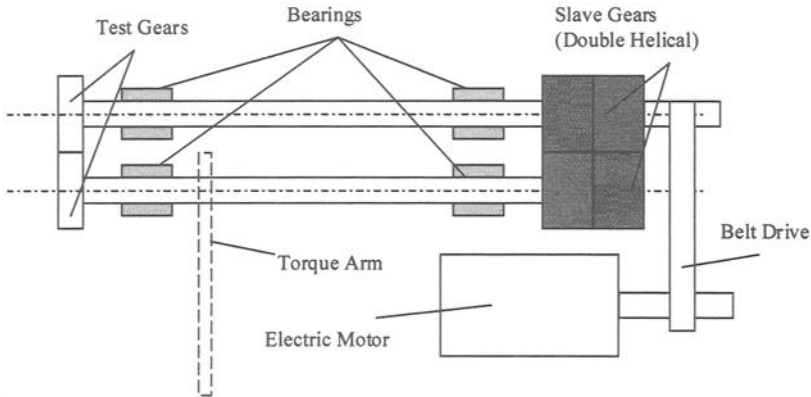


Figure 3 - IAE Gear Machine

Table 2 - Test Machine Characteristics

Test conditions	Test machine		
	Four-ball Machine	Pin-on-disc Machine	IAE Gear Machine
<b>Motion</b>			
Sliding	+	+	
Rolling	+		
Sliding/rolling			+
<b>Geometry</b>			
Point	+	+	+
Line		+	
Conformal		+	
<b>Nominal pressure (MN/m<sup>2</sup>)</b>	150 – 600	700 – 2100	350 – 1400
<b>Sliding velocity (m/s)</b>	0.25 – 1	1 – 10	2 – 12
<b>Materials tested</b>			
534A99	+	+	+
665M17		+	
080M40		+	
<b>Lubricants tested</b>			
SAE10	+	+	
Mobile Jet II	+	+	+
ETO 25	+		+

in Table 7, which is based on a recent survey of various types of machinery utilised by the US Navy.

#### *Four-ball Machine*

Tables 3 and 4 summarize, respectively, the loading conditions for the four-ball machine incurring sliding and pitting fatigue wear modes.

Table 3 - *Test Matrix: Four-ball Machine, Sliding Wear*

Load, kg	Surface speed, mm/s			
	250	500	750	1000
36-90	ABC	ABC	ABC	ABC
100-120	BC	BC	BC	BC
130-150	C	C	C	C
A - SAE 10, B - Mobile Jet II, C - ETO 25				

Table 4 - *Test Matrix: Four-ball Machine, Rolling Pitting Fatigue*

Load, kg	Surface speed, mm/s			
	250	500	750	1000
400	ABC	ABC	ABC	ABC
600	ABC	ABC	ABC	ABC
800	ABC	ABC	ABC	ABC
A - SAE 10, B - Mobile Jet II, C - ETO 25				

#### *Pin-on-disc Machine*

Details of the Pin-on-disc machine loads and speed are shown in Table 5.

Table 5 - *Test Matrix: Pin-on-disc Machine*

Load, kg	Surface speed, m/s			
	1	3	5	10
10	ABC	ABC	ABC	ABC
20	ABC	ABC	ABC	ABC
40	ABC	ABC	ABC	ABC
A - SAE 10, B - Mobile Jet II, C - ETO 25				

#### *IAE Gear Machine*

Test details are presented in Table 6.

Table 6 - Test Matrix, IAE Gear Machine

Applied Load, Nm	Rotational speed, rpm		
	2000	4000	6000
0 – 203.4	BC	BC	BC
0 – 305.1	BC	BC	BC
0 – 406.7	BC	BC	BC
	B – Mobile Jet II, C – ETO 25		

Table 7 - Range of Operating Conditions for Shipboard and Airborne Applications

Test Machine	Load range MN/m <sup>2</sup>	Speed range	Application
Four-ball machine	150 – 600	0.25 – 1.00 m/s	Ship main reduction and aux. Gearboxes, pump compressor bearings, helicopter transmission output module and blade bearing
Pin-on-disc machine	700 – 2100	0.1 – 10 m/s	Shaft support bearings, ship service turbine gearbox, engine accessory gearbox, helicopter mast bearing, transmission input module and engine nose box
Gear test machine	350 – 1400	1000 – 6000 rpm	Ship propulsion, helicopter main gearbox, helicopter IGB and tail rotor gearbox

## Methods of Morphological Analysis

### *Wear Particle Imaging Procedures*

In addition to the friction data recorded from each wear test, images of the various wear debris categories are stored in electronic format. This is achieved by connecting an Olympus BX microscope, via a three chip colour CCD camera (JVC KY-F55B), to a PC fitted with a frame grabber card. High quality images are obtained using this hardware configuration, especially when used in conjunction with Synoptics 'AutoMontage' software, which is explained in more detail in the next section.

*AutoMontage*<sup>®</sup>

Optical microscope images have a very limited depth of field, especially when using high magnification lenses. To overcome this problem a software driven procedure is used which takes a series of images through several different focal planes and merges them into a single in-focus image. The procedure used to capture the images is semi-automatic in the form of a computer controlled stage which moves the sample through a pre-defined number of steps from the top-most in-focus feature to the bottom-most feature. In most cases, images in both transmitted and reflected light are used for different types of analysis. Silhouette images work well when examining the overall shape of a particle, whereas any surface feature analysis requires a reflected light image.

### *Surface Measurement*

In order to examine the surfaces of the disc from the pin-on-disc machine, white light interferometry was used. Precise information of the surface was obtained with respect to height to within 0.1  $\mu\text{m}$ . From this, surface roughness values and the wear state were determined and the wear track was examined in detail.

### *Wear Particle Atlas and Classification*

Traditionally, when an analyst defines a particle with regard to its type and possible history, the wear particle atlas serves as an encyclopædia containing pictures of typical wear debris. Presently, the atlas is provided on a CD-ROM; browsing through the images is assisted by computer searches. Nevertheless, there remains a requirement to generate images of debris under known conditions which can best be achieved by controlled wear tests.

Machine health is often determined quantitatively by measuring the amount of debris generated using various methods. However, qualitative methods are being favored that take into account more detailed analysis of the particle features. Increasingly, computer-aided classification methods are being utilised to analyse particle shape which, when coupled with size distribution data, results in effective determination of machine health.

## **Results**

### *Four-ball Sliding*

The diameters of the wear scars of the lower three balls were measured to yield three distinct wear states as a function of applied load (Figure 4). Mild wear is typified by very low wear rate, and hence, small wear scars. Transition wear occurs within a very narrow loading band when the wear scar and friction increases rapidly with applied load. Severe wear is identified by much larger wear scars.

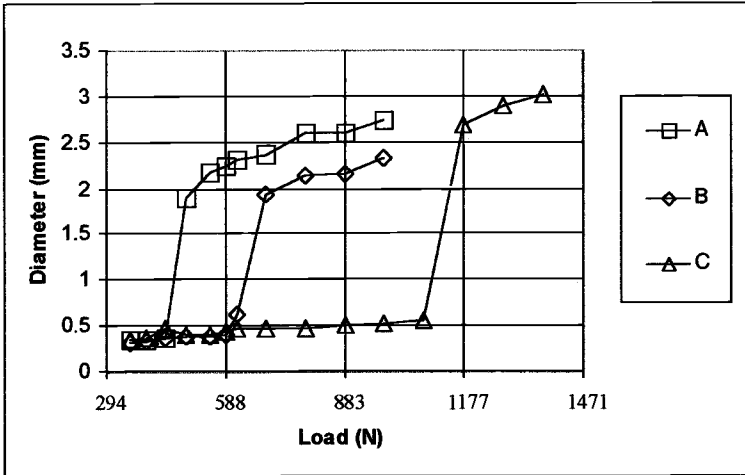


Figure 4 - Wear Scar Diameters for Lubricants A, B and C

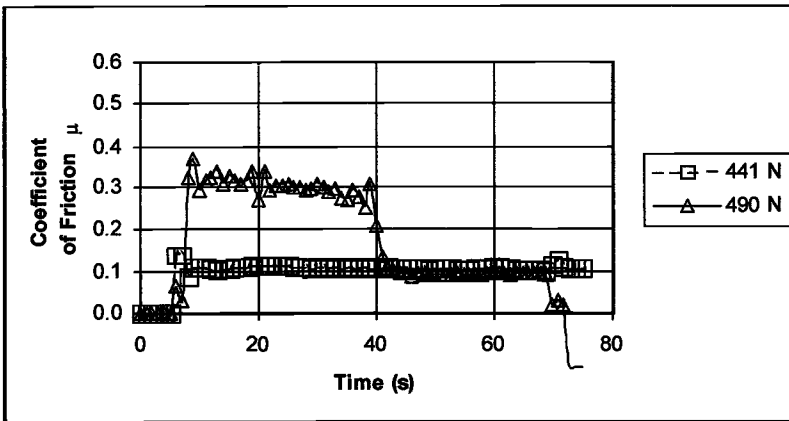


Figure 5 - Friction Traces, Lubricant A

Friction measurements made while the tests were in progress provided useful indications of the lubrication regime, and also repeatability of the tests. Figures 5 and 6 indicate that the friction traces can be divided into two sets: those that exhibit a high coefficient of friction, and those that remain at a constant low friction throughout the duration of the test. It is during the periods of high friction that the large wear scars are

formed, accompanied by an increase in level of the noise and vibration of the balls. Thus, at low friction conditions,  $\mu \leq 0.1$  elasto-hydrodynamic or mixed lubrication conditions prevail. During transition, boundary lubrication conditions predominate and  $\mu$  values exceed 0.3.

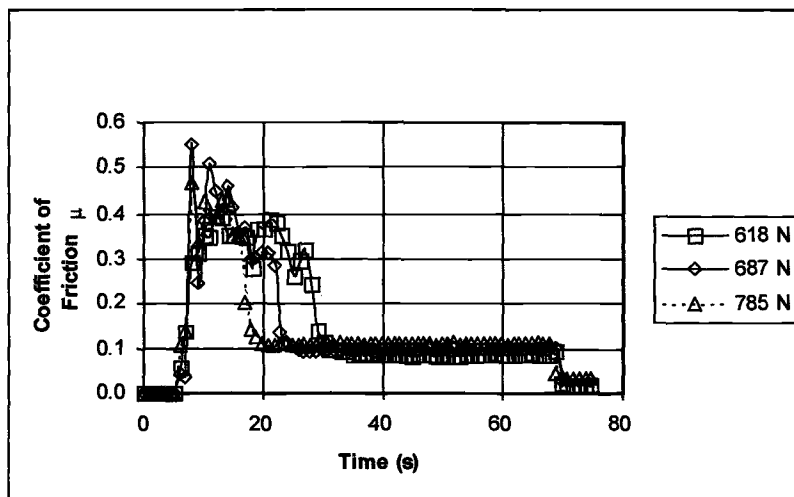


Figure 6 - Friction Traces, Lubricant A

#### *Four-ball Rolling*

After failure, the top balls were examined for pitting damage. Faint tracking marks were evident on the lower balls. When the tests were stopped before pitting occurred, the wear debris present consisted of very small rubbing wear particles,  $< 30 \mu\text{m}$  in linear dimensions. After failure, fatigue particles were found in abundance, identified by evidence of surface cracks and pits. They were generally found to be in the size range 30 to  $500 \mu\text{m}$ .

#### *Pin-on-disc Machine*

As with the sliding four-ball tests the pin-on-disc machine results can be divided into two categories: mild wear and severe wear. This is the case whether the pin and disc are of similar hardnesses or not.

Friction force was measured in each test and Figure 7 shows a typical mild wear situation when compared with one exhibiting severe wear. As with the four-ball machine, the coefficient of friction for the low loading case is below 0.1 which is typical for a lubricated metal sliding on metal, whereas the severe wear has a much higher coefficient of friction (above 0.3) because of the increased metal-to-metal contact. Under these

condition localised welding (adhesive wear) occurs which accounts for the “noisy” signal generated.

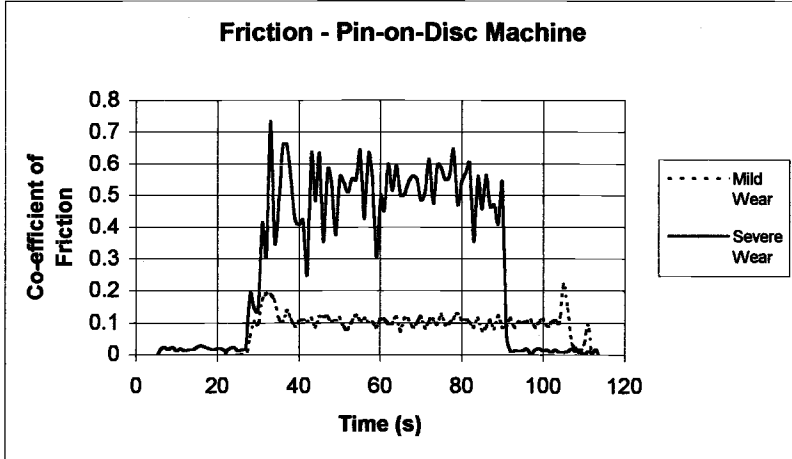


Figure 7 - Friction Trace, Pin-on-Disc Machine

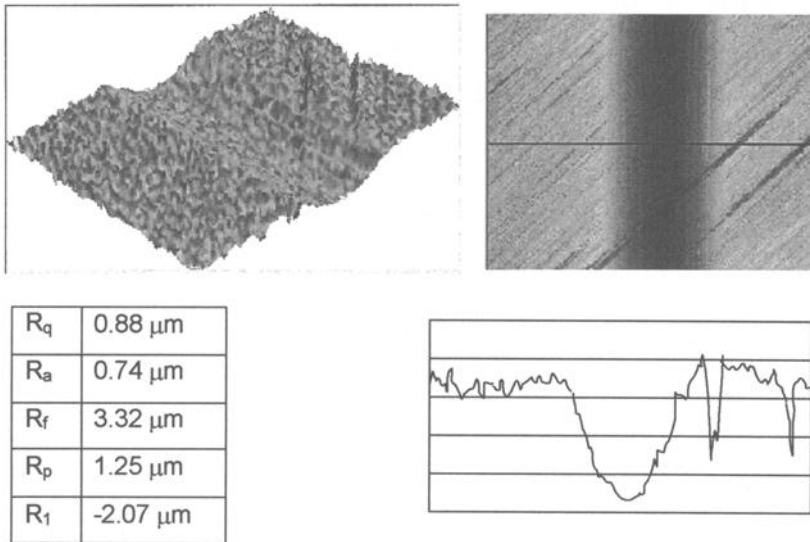


Figure 8 - White Light Interferometry Image of Mild Wear

When using materials whose hardness ratios exceeded 1.3 cutting wear can be generated. This is the case when using a mild steel disc and a bearing steel pin. In this

case the wear was primarily from the disc. When very low loads were applied, very little wear was seen and the wear track on the disc was barely visible. At higher loads, but still within the mild wear regime, a more noticeable wear track was obtained as shown in Figure 8. The pin ploughed material away from the center of the track and pushed it to either side. When the loading was further increased and the experiment entered the severe wear mode, metal transfer occurred resulting in a more uneven wear track (Figure 9).

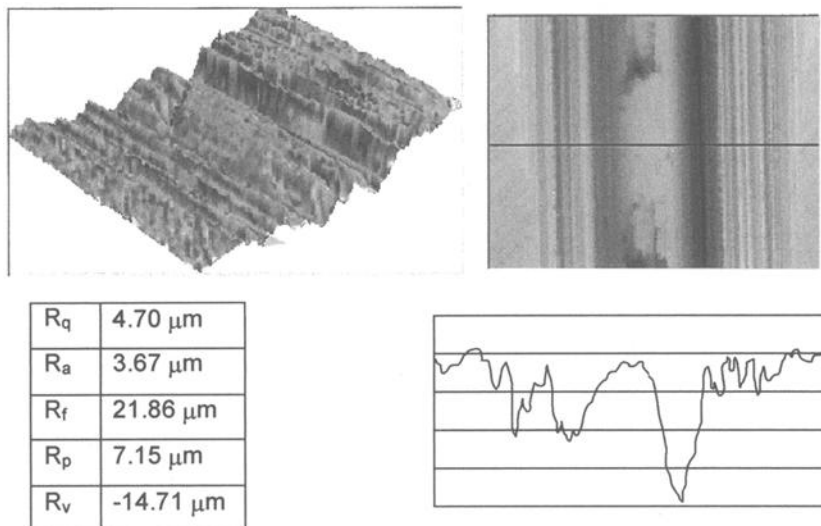


Figure 9 - White Light Interferometry Image of Severe Wear

Table 8 shows the increase in wear cross-sectional area with increasing test duration. The sudden increase to  $1.595 \text{ mm}^2$  indicates the transition from mild wear to severe wear on the disc.

Table 8 - Cross-sectional Area of Wear Tracks

	10 seconds	1 minute	10 minutes	1 hour
Wear track cross-sectional area ( $\text{mm}^2$ )	0.352	0.456	0.656	1.595

When testing with materials of similar hardness under severe wear mode conditions, the ball was worn more than the disc. After the test was completed and the disc surface was examined it was found that the disc had metal deposited on it resulting in a slightly irregular ridge (Figure 10).

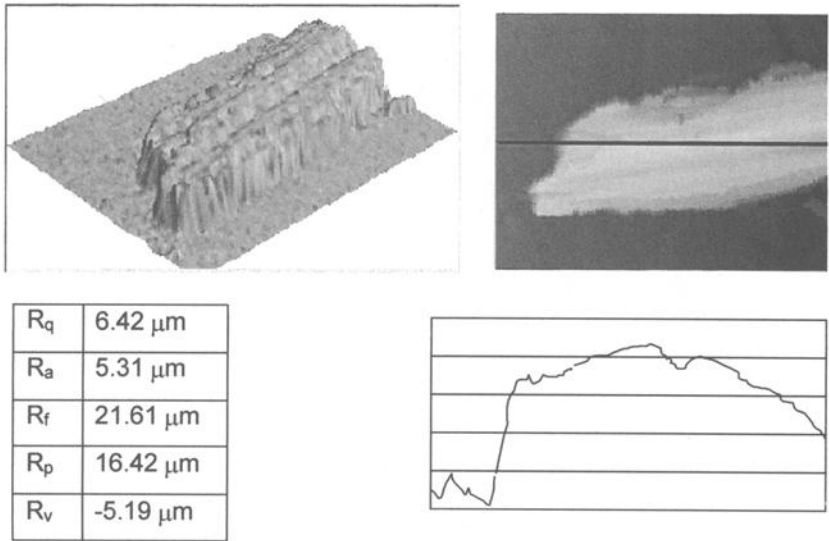


Figure 10 - *White Light Interferometry Image, Disc Surface, Similar Hardness Materials Gear Machine*

Particles were removed from the gear machine at the end of every load increment and the quantity (concentration) of debris present was measured using an inductive device. Since load was increased steadily and all of the wear debris was removed at each load, the abscissa can be considered to replace time and the ordinate as wear rate (Figure 11).

The pattern of failure is generally the same. Initial running-in wear – low steady wear followed by rapid severe wear (scuffing) failure. At approximately 125 Nm, two tests, G1 and G3 show a large increase in wear rate but recover to a lower rate finally failing at almost double this loading. However, the other two tests, G2 and G4 show the same wear increase but then fail quickly. The “recovery” phenomena is thought to be caused by a self healing mechanism of the gears.

**Wear Particle Types**

From analyzing the wear particle types generated it is possible to infer the wear state of a machine. It is important, therefore, to be able to identify the different wear debris types in relation to the wear state that produced them. For this study, four wear types were identified: mild, severe sliding, rolling pitting fatigue and cutting wear.

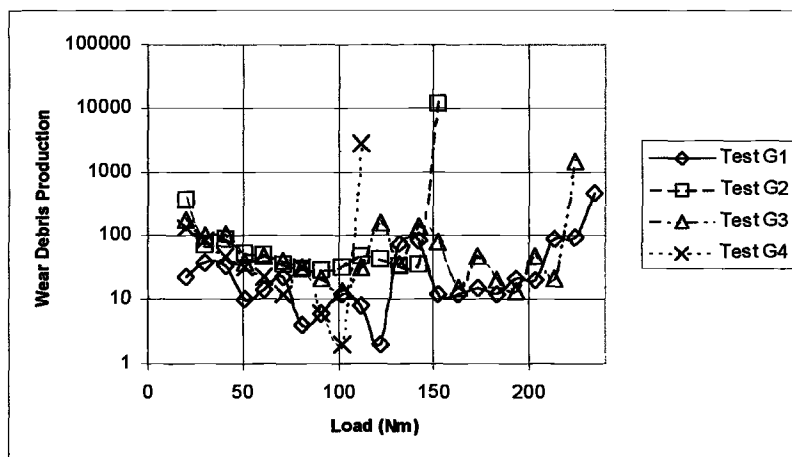


Figure 11 - *Wear Particle Generation from the IAE Gear Machine, 2000 rpm, Mobile Jet II, 60 °C, 25 L/min*

### *Mild Wear*

Mild wear debris was found to occur in all of the tests carried out and comprises small (typically < 50  $\mu\text{m}$ ) particles which exhibit few surface features and have a low aspect ratio (Figure 12). They include both mild sliding and rubbing wear particles which result from the abrasive removal of the asperities of the surfaces of the moving parts.

### *Severe Sliding Wear*

Severe sliding wear is an adhesive wear mechanism in which there is metal-to-metal contact. The asperities of the two opposing surfaces are plastically deformed and weld together leading to transfer from one of the surfaces to the other. The transferred member

### **Wear Particle Types**

From analyzing the wear particle types generated it is possible to infer the wear state of a machine. It is important, therefore, to be able to identify the different wear debris types in relation to the wear state that produced them. For this study, four wear types were identified: mild, severe sliding, rolling pitting fatigue and cutting wear.

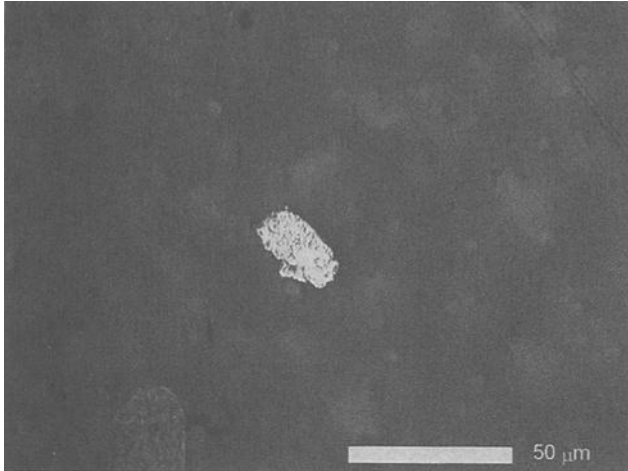
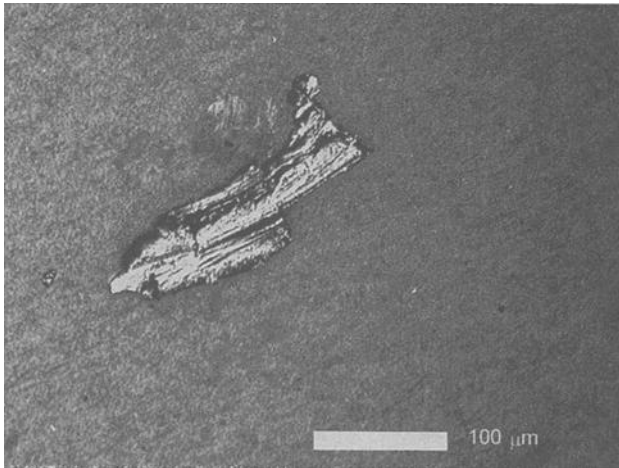


Figure 12 - *Mild Wear Particle*

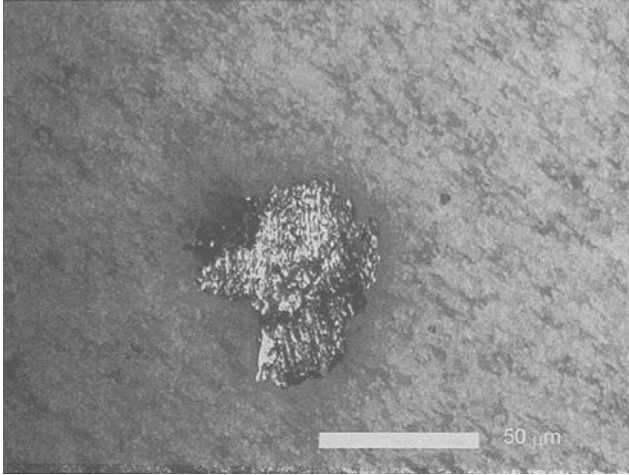
may subsequently break off to form a particle. Alternatively, it may act as a crude cutting tool through severe abrasive action of the opposing surface from which it originally came. Typical severe sliding features are surface striations and often there is temper



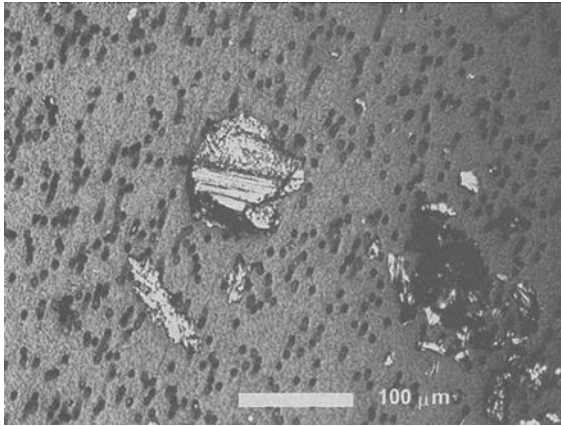
a) Four-ball machine Sliding Wear

coloring which indicates that considerable heating has occurred due to high local friction. Severe sliding wear was found during heavy loading on the sliding four-ball machine

(Figure 13a), pin-on-disc machine (Figure 13b) and the IAE gear machine when it was close to failure (Figure 13c). The particles captured from each type of test were generally similar in size and shape.



b) Pin-on-Disc Machine Sliding Wear



c) IAE Gear Machine Sliding Wear

Figure 13 - Severe Sliding Wear Particles

*Fatigue Wear*

Pitting fatigue failure occurred in rolling contact mode. The representative particle shown in Figure 14 indicates that they have a low aspect ratio and exhibit cracks and pits on the surface. The outline shape of the particle tends to confirm the influence of a rolling action as opposed to the distinct effect of sliding witnessed by the particles shown in the previous figures.

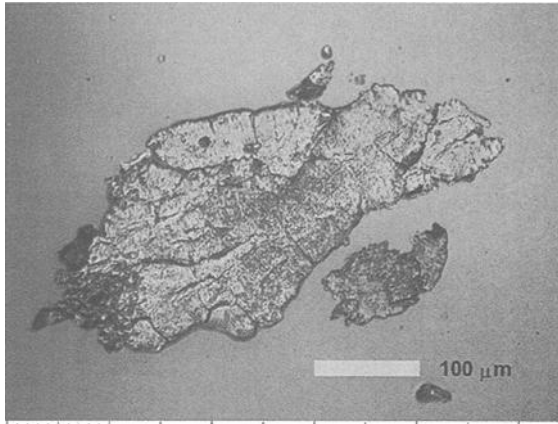


Figure 14 – *Fatigue Particle*

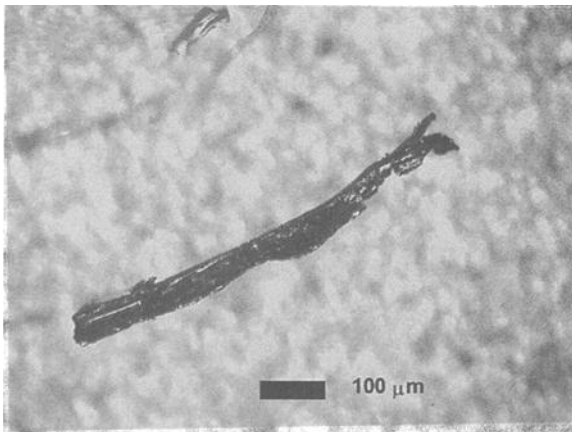


Figure 15 - *Cutting Wear Particle*

### *Cutting Wear*

Cutting wear occurs when a hard surface rubs against a softer surface in such a way as to penetrate the surface in a manner similar to that of a machine tool cutting action. However, this does not mean that cutting wear will not be present when testing with identical materials since localized work hardening can cause one of the materials to gouge the other. Cutting wear therefore is, by definition, curved and elongated which exhibit chatter marks and takes the appearance of lathe swarf when viewed under high magnification (Figure 15).

### **Summary of Main Findings**

The three test machines used in this study produced numerous samples of debris for each of the four wear types described above. In each case the particles displayed some or all of the morphological characteristics typical of each type. Particle type depended on lubrication regime and motion. Load, speed and lubricant each influenced the regime at any one time. Particle size was a function of machine type, loading and speed. In general, higher loads generated larger wear particles.

The surface appearance of the particles gave the clearest indication of particle type. Striations commonly present on the severe sliding wear particles were not present on the mild, fatigue or cutting wear particles. Where crack formations and pitting was evident, the particles were generated in a pitting fatigue test.

Overall shape was good for classifying cutting wear particles (aspect ratio  $>10$ ) but was less distinct for examining the other three types. However, when edge details are included in the analysis, the fissures of fatigue particles can be readily identified.

### **Application**

Many computer programs have been written to help analysts use the information yielded by particle morphology. Computerised wear particle atlases are now commonly utilized for putting particle information in electronic format. However, without an appropriate image selection procedure, the atlases are no better than the traditional printed format. In order to present suitable images to an analyst, it must be possible to input various parameters (either manually or automatically) which are in turn, used to select the correct particles.

Many selection systems have been devised (for example, artificial neural networks, fuzzy logic or Bayesian networks) each with advantages and disadvantages. For this work a Bayesian belief network method was chosen because it offers the facility to compute complex analysis of the interactions between inputs and outputs based on relatively simple mathematics.

### *Development of Bayesian Network Method*

Belief networks (also known as Bayesian networks, Bayes networks and causal probabilistic networks), provide a method to represent relationships between propositions or variables, even if the relationships involve uncertainty, unpredictability or imprecision. They may be learned automatically from data files, created by an expert, or developed by a combination of the two. They capture knowledge in a modular form that can be transported from one situation to another which allows a clear visualization of the relationships involved. In the case of wear particle analysis these uncertain variables are the particle attributes such as shape, in which a single particle can, for example, exhibit both features of a regular or irregular outline shape.

The input classes defined for this particular Bayesian network are summarized in Table 9 alongside the different possibilities within these classes.

Table 9 - *Inputs to Bayesian Belief Network*

Input	Possible Classifications
Shape	Regular, irregular, curved or elongated
Surface	Rough or smooth
Edge	Rough or smooth
Size	Very fine (<50 μm), fine(50-100 μm), very small (100-150 μm), small (150-300 μm), medium (300-600 μm), large (600-1000 μm) or very large (> 1000 μm)
Color	Bright, dark or heated
Cracks	Yes or no
Striations	Yes or no
Pits	Yes or no

Table 10 - *Output from Belief Network*

Inputs	Output
Shape: Regular	Fatigue: 91.12%
Surface: Rough	Mild: 3.23:
Edge: Rough	Severe Sliding: 4.25%
Size: Small (175 mm)	Cutting: 1.4%
Color: Bright	
Cracks: Yes	
Striations: No	
Pits: Yes	

It was important to have a good training set in order to “teach” the network. Using the particles generated throughout the test program, each one was classified according to the attributes in Table 9 and also given a particle type, either, mild, severe sliding, fatigue or cutting wear. The probabilities of all the combinations of inputs were calculated to

provide results in the form of a percentage likelihood of type occurring (see example in Table 10).

### *Systematic Classification of Oil-wetted Particles (Syclops)*

Analysts at Royal Air Force Early Failure Detection Centres (EFDCs) examine ferromagnetic particles collected by a magnetic detector plug (MDP) using an optical microscope. A need now exists for an automatic wear particle classification system so that unknown wear particles can be more easily identified. To create a working model, a graphical user interface (GUI) was developed in order that the belief network could be used for the classifier. Previous experience suggested that employing stylised images for the particle attributes was the best method for obtaining the input data needed by the belief network. The analyst is presented with a computer screen with the eight different attribute sets which the user selects and then brings up a second screen containing the stylized images of the different classifications. Once all eight categories are chosen the information generated by the belief network generates a selection of possible particles from the wear particle atlas that corresponds closely to the users inputs. If there are none that appear to fit any category, an error signal is communicated and asks the analyst to check the inputs.

### **Conclusions**

From the bench tests much information has been gathered, with an emphasis on wear debris. Experiments with similar lubrication regimes and contact type (sliding, rolling, etc.) revealed the wear debris to be similar from each machine when functioning under similar conditions; e.g., sliding contact four-ball debris was similar to that found with the pin-on-disc machine when operating within the same lubrication regime. Lubricant type had very little impact on the wear debris although it influenced the conditions under which EHL failed, leading to metal-to-metal contact.

Utilizing the debris generated from the test program a set of training particles was produced and incorporated in a Bayesian belief network as an integral part of a wear particle classifier.

The bench tests afforded a suitable opportunity to control various types of wear failure. Load, speed, friction and temperature conditions were correlated with friction, wear and wear debris type.

### *Acknowledgments*

The authors would like to acknowledge the US Office of Naval Research and the UK Ministry of Defence for funding this research. The information relating to naval machinery (Table 7) supplied by Mr. Paul Howard of Paul Howard Enterprises is very much appreciated.

**References**

- [1] Davies, A. "Handbook of Condition Monitoring," 1998, Chapman and Hall, London, ISBN 0 421 613204.
- [2] Roylance, B. J. and Hunt, T. M. "Wear Debris Analysis," 1999, Coxmoor Publishing Co. Oxford, ISBN 1 90189 2026.
- [3] Reda, A. A., Bowen E. R., and Westcott V. C. "Characteristics of Particles Generated at the Interface Between Sliding Steel Surfaces," *Wear*, 1975, Vol. 34, pp. 261-273.
- [4] Bowen, E. R. and Westcott, V. C. "Wear Particle Atlas. Final Report to Naval Engineering Center," Lakehurst NJ Contract No 56-74-C-182" 1976.
- [5] Anderson, D. P. "Wear Particle Atlas, Revised Report NAEC-92.163 Naval-Army Engineering Center," 1982.
- [6] Ding, J. G. "A Computerise Wear Particle Atlas for Ferrogram and Filtergram Analysis,". Proceedings JOAP International Conference on Condition Monitoring (G. R. Humphrey and R. W. Martin, eds.,) 1998, pp. 125-131.
- [7] Seiffart, W. W and Westcott V. C. "A Method for the Study of Wear Particles in Lubricating Oil," *Wear* 1972, Vol. 21, pp. 27-42.

Katherine M. Helmetag<sup>1</sup>

## A New Look at an Old Idea: The Torque Curve Revisited

---

**Reference:** Helmetag, K. M., “A New Look at an Old Idea: The Torque Curve Revisited,” *Bench Testing of Industrial Fluid Lubrication and Wear Properties Used in Machinery Applications, ASTM STP 1404*, G. E. Totten, L. D. Wedeven, J. R. Dickey, and M. Anderson, Eds., American Society for Testing and Materials, West Conshohocken, PA, 2001.

**Abstract:** Current lubricant testing methods for the pin and vee block machine produce only two data points, the torque at the final failure load, and the final failure load. Lubricant designers have had trouble correlating these single point data with field results. To obtain correlation of bench testing with field performance, it is imperative to examine all of the data produced during the course of the Extreme Pressure test, and appropriate plots of the data. An improved correlation of the laboratory test to industrial machinery performance has been found when plots of torque versus load are compared for lubricants under development. There are certain features in the torque versus load curve which can provide additional information and further improve correlation of bench test results to field data. An example metalworking process will be described.

**Keywords:** pin and vee block, lubrication, extreme pressure, testing

### Introduction

The lubrication engineer has a difficult job—to design a friction-reducing material for a process that often cannot be easily simulated at the bench scale. To assist in this task, many lubrication testing machines have been developed over the years. This work will focus on the pin and vee block (Falex) tester (Figure 1), which has been in use for over 70 years and is one of the most common bench testing rigs for lubricants. The metalworking process that will be examined is cold heading of steel.

Several methods are described by the ASTM and Institute of Petroleum (IP) for testing of lubricants using the pin and vee block tester. The methods include ASTM Test Methods for Measurement of Extreme Pressure Properties of Fluid Lubricants (Falex Pin and Vee Block Methods) (D 3233) and ASTM Test Method for Evaluating Thin Film Lubricants in a Drain and Dry Mode using a Pin and Vee Block Test Machine (D 5620). The IP method is Extreme Pressure, Anti-Wear, Friction, and Corrosion Protection Properties of Fluid Lubricants: Falex Machine (IP 241).

---

<sup>1</sup> Chemist, Metal Forming Group, Houghton International, 930 Madison Avenue, Valley Forge, PA 19482.

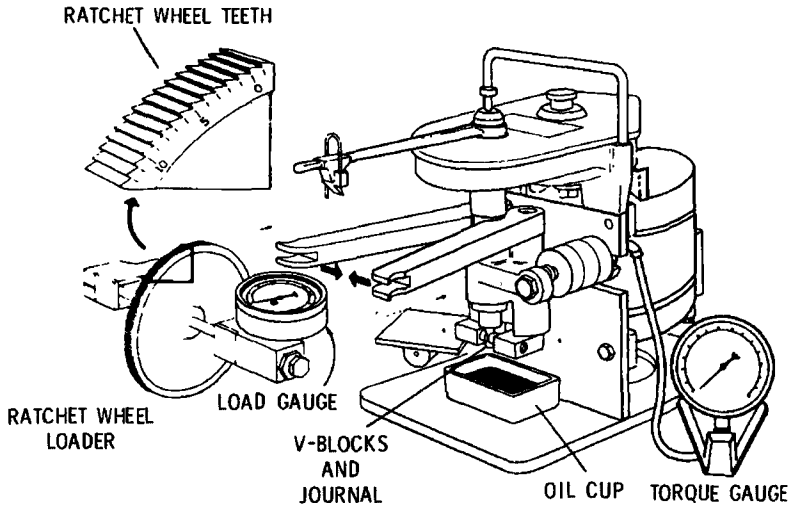


Figure 1 - *The Falex pin and vee block tester*

These methods are used to describe the Extreme-Pressure (EP) performance character of the lubricants under test. The data generated by these methods is largely the final failure load and the torque at final failure. Method B of Method D3233 is the most common method employed in lubricant development. The method is known as a step-load method, in which the load is increased in steps. The correlation of this method with the field is not well established for many metalworking operations.

This lack of correlation can be explained in the following manner: the behavior of the lubricant throughout the test is only observed with the intention of noting the failure point, and is ignored in the interpretation of the test results. It is this data which can provide the information required to differentiate lubricants and identify any unique performance characteristics which will detail field performance. In particular, the presence of slope anomalies in the curve can indicate changes in the lubrication function which are independent of the final failure load.

This type of data interpretation is not new, having been proposed in 1968 by Faville, et al[1]. The complexity of this type of analysis would seem to explain its limited use by tribologists and lubrication engineers today.

### **The Problem**

A manufacturer of fasteners produced a variety of parts by cold heading processes. Most parts were cold headed with a chlorinated, sulfurized heading oil applied after the wire was sheared into slugs. The reduction of chlorinated oils was a priority as

part of an environmental program and the manufacturer was obliged to identify a non-chlorinated replacement for the heading oil in use at the plant.

A brief description of the cold heading process is warranted here. Cold heading is a cold forming process closely related to cold forging in which the material is deformed along a primary axis, with compressive strain exceeding the radial or peripheral strain by a significant amount[2]. The process includes both forward and backward extrusions and involves considerable metal movement. A great deal of heat is generated by the internal friction of the moving metal and is sufficient to insure the activation of most EP additives.

Several oils were selected for this study and tested in the most difficult operation, formation of a forward and backward extruded part that was at the minimum limit of metal flow for a successful cold head. The process was six stages and the heading oil was applied at two locations. The lubricants were bench tested using the pin and vee block device and Method B of D3233. There was no correlation of bench and field data, and further lubricant development was halted. The lubricant manufacturer was forced to examine the bench testing practice with regard to better correlation with the field prior to continuing product development.

## Experiments

The D3233 method was examined, and some modifications were made. Method A of D3233 was selected for the basis. The run-in stage of the test was reduced to 90 seconds at 200 pounds of direct load. The load ramp then commenced from the run-in load. The torque and load were recorded continuously by a computer equipped with data acquisition tools, such that a chart of the torque versus load data could be easily plotted. This plot is the critical output of the test method. The entire testing rig as used was supplied by Falex Corporation (Sugar Grove, IL). A block diagram of the data acquisition setup is shown in Figure 2.

The metal working oils selected for this work were cold heading oils that had been tested in the field. Each oil contained a different additive package, having one or more EP elements in it. Table 1 describes the oils in terms of additive content and viscosity. Each oil is currently used in manufacturing to produce cold headed parts.

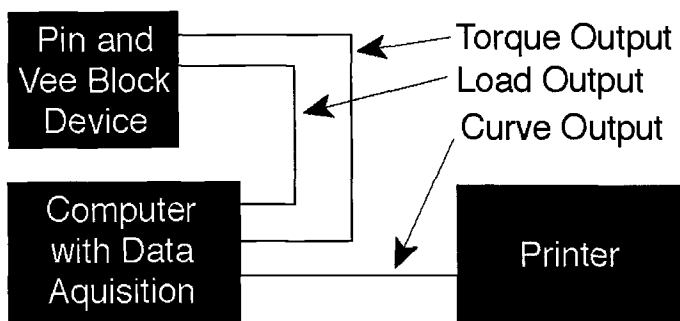


Figure 2 – Block diagram of computerized testing setup

Table 1 - *Oils used in this study.*

Sample	Additive Content	Viscosity, cSt @ 39°C
OSOC	Organic Sulfur, Organic Chlorine	135
OS	Organic Sulfur	281
ISP	Inorganic Sulfur / Phosphorus	86
OSPOS	Organic Sulfur / Phosphorus, Organic Sulfur	106

## Results

The oils tested gave predictable results with Method B of D3233, with the results shown in Table 2.

Table 2 - *Method A and Method B of D3233 test results*

Sample	Method A	Method A	Method B	Method B
	Load	Torque	Load	Torque
OSOC	2200	78	2600	72
OS	1500	92	1700	95
ISP	2650	44	2700	52
OSPOS	3000	48	3000	47

The improved method showed many differences that could not be predicted from Method B of D3233. Figures 3 through 6 show the torque versus load curves for each oil.

## Discussion

It must be noted that lack of bench to field correlation is not an unknown problem in tribology. In fact, this lack of correlation has led to the proliferation of testing rigs and journal geometries that can be found in the market place today. In fact, many testing rigs attempt to duplicate field operations so closely that they are limited to one particular operation or fluid for validity. The appeal of a device such as the pin and vee block tester is that test methods for it can be modified to produce relevant data for many types of operations. Such is the case with the problem at hand.

The manufacturer was cold heading the steel parts with a heading oil that is represented by sample OSOC. The product had excellent performance and it was vital to replace it with a non-chlorinated product having similar or better performance. It was determined that the pin and vee block rig was most suitable for testing the lubricants, and Method D3233 was selected since it was the standard method for testing the EP function of lubricants.

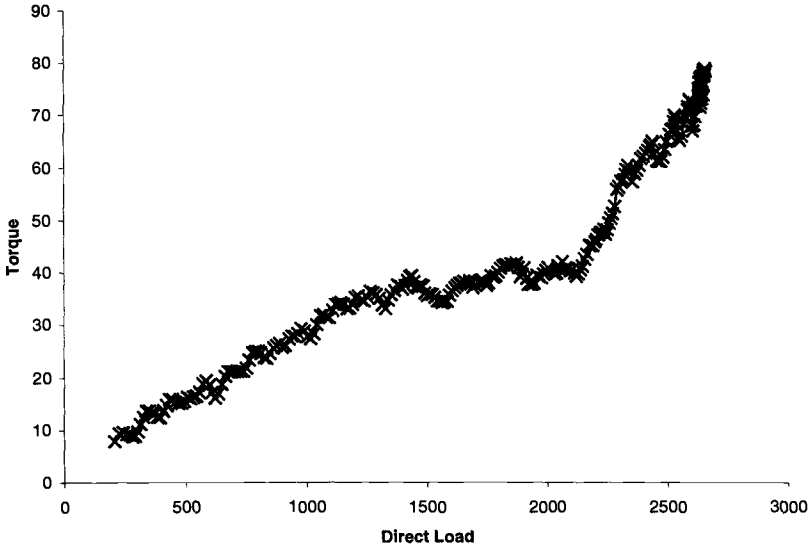


Figure 3 - Torque versus Load for Sample OSOC

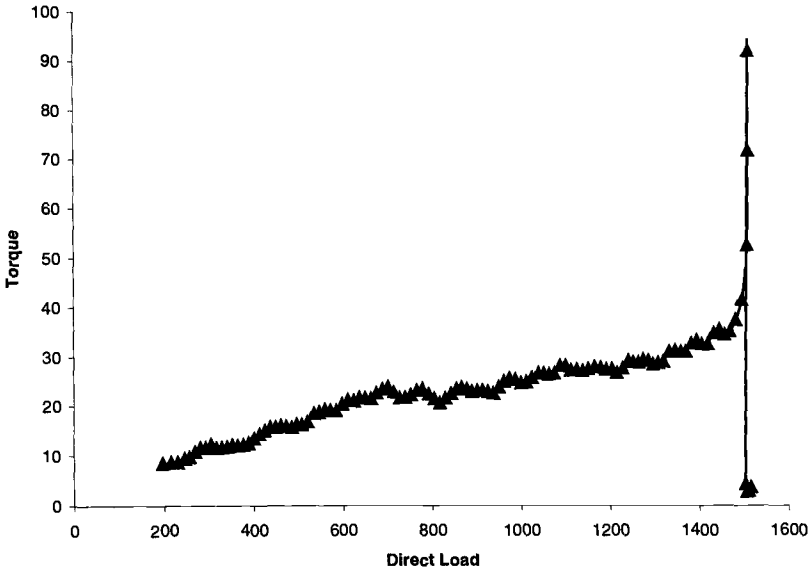


Figure 4 - Torque v. Load for Sample OS

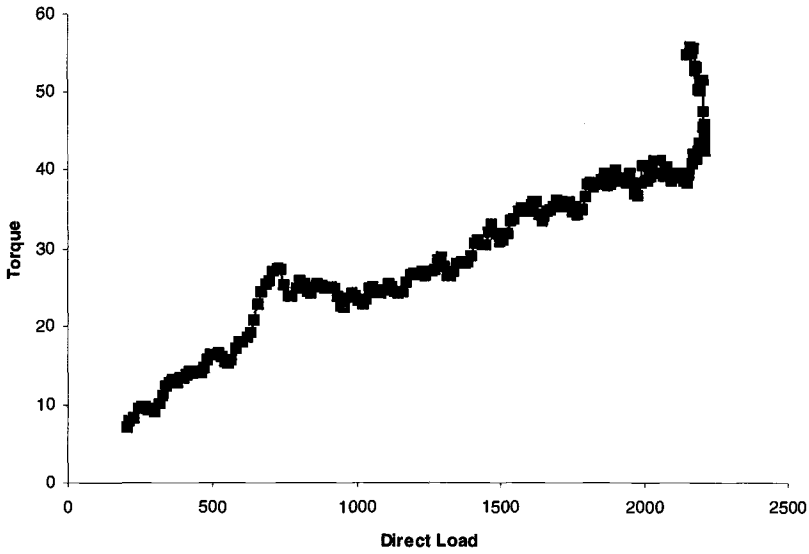


Figure 5 - Torque versus Load for Sample ISP

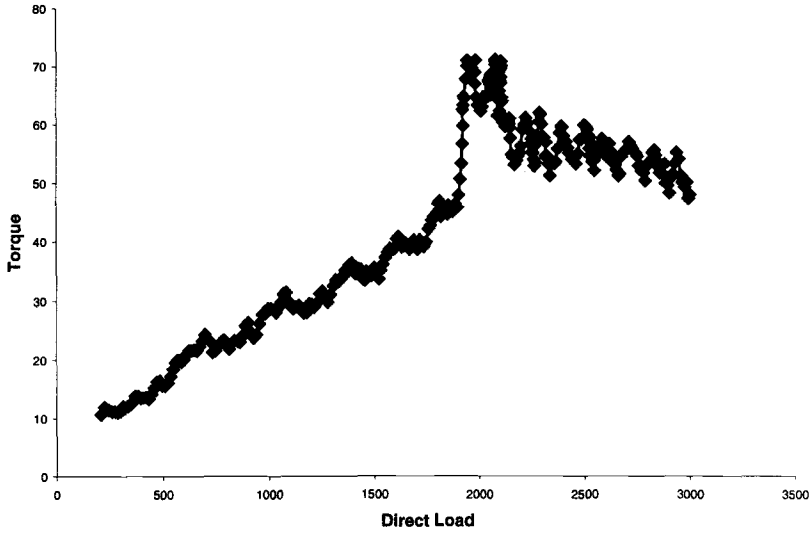


Figure 6 - Torque versus Load for Sample OSPOS

The data from both Method B and Method A of Method D3233 (Table 2) produce similar results for the lubricants in question, ranking them in the following order:

OSPOS, OSOC, ISP, OS, with OSPOS having the best performance and OS having the worst performance. Based on this data, sample OSPOS was recommended for trial in the difficult operation.

Unfortunately, the Method D3233 data conflicted highly with the field results shown in Table 3. Field results were in terms of tooling lifetime, a very important issue for manufacturers. The cost of tooling is second only to the cost of the stock when consumables are considered. Extended tooling lifetimes are crucial to profitable operations in a metal working shop.

Table 3 - Tooling Lifetimes for Oils

Sample	Parts per Punch	% Good Parts
OSOC	250 000	98
ISP	220 000	95
OSPOS	50 000	50

Since torque data represent one half of the output of the D3233 method, it is obvious that the values are significant to lubricant performance. There were several attempts made to differentiate the lubricants based on the data obtained from Method D3233, but it was not until the entire output of the test was examined that a pattern became clear.

The plot of torque versus load for each of the heading oils was examined and some unique features became obvious for each material. Figure 7 shows the overlay plot of the torque versus load curves for the oils tested.

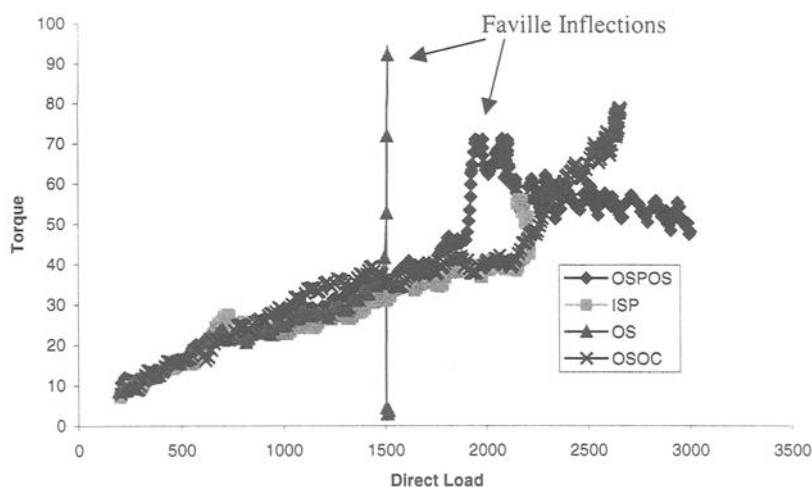


Figure 7 - Overlay plot of Torque versus Load data.

The overlay plot of torque versus load data brought several interesting features to light. Each of the curves has a distinct shape, with a given slope and torque at each load value. The different values of torque that each lubricant shows at a given load are indicative of the differences in the lubricants. The overall quality of the lubrication provided by the lubricating oil throughout the load range can be described as the lubrication function. To this function, some mathematical concepts can be applied to extract relevant data. Changes in the slope of a curve generally indicate changes in the underlying function. Therefore, it can be presumed that a change in the slope of the torque versus load curve would indicate a change in the lubrication function of the lubricant. This would indicate a difference in performance. Changes in slope are called inflections. The phenomenon of "torque pop-up" was briefly described in reference 1 as a potential method of comparing lubricants. In deference to the authors, this will be referred to as a "Faville inflection."

Oil OSOC had a relatively flat torque versus load curve, with an inflection at 2300 pounds of direct load. The position of the Faville inflection was examined as a possible means of distinguishing the oils. Oil OS gave an inflection at 1500 pounds of direct load. Oil ISP gave a slight inflection at 700 pounds of direct load and an inflection at 2200 pounds of direct load. The last oil, OSPOS, showed an inflection at 2000 pounds of direct load.

Based on the comparison of the load at the incidence of these inflections, a much closer relationship between bench results and field performance can be drawn. The overall shape of the curves for oils OSOC and ISP are similar, and so is performance. It should be noted that the Faville inflection for oil OSPOS occurs at a direct load 200 pounds below that for oil ISP. This correlates well with the field performance, and it would seem that low torque values though this region are descriptive of the lubrication function required by the process in question.

The testing rig employed for this method was equipped with a modern computerized data acquisition system. Additional testing was done on a traditional, non-computer equipped pin and vee block testing rig and it was determined that torque readings should be taken at 100 pound increments to improve precision over readings at 250 pound increments. While this does increase the amount of data generated by the method, it improves precision significantly and insures that the onset of the Faville inflection will be identified accurately.

Additional testing was done using ASTM Test Method for Measurement of Extreme-Pressure Properties of Lubricating Grease (Four-Ball Method) (D 2596). The load wear index for each oil was calculated. Anecdotal correlation between the load wear index and the onset of the Faville inflection was observed for the oils. The actual degree of correlation was not identified, and more work is required to determine if this correlation is truly valid.

## **Conclusion**

The current methods described for the pin and vee block testing rig are not sufficient to fully describe lubricant performance. This has resulted in an increase in the amount of testing required to fully understand lubricant performance and to correlate bench testing to field results. With a slight modification in testing procedure and a

dramatic modification to data analysis, vastly improved bench-field correlation can be found.

Table 4 - *Load Wear Index and Faville Inflection Load*

Sample	Load Wear Index	Faville Inflection Load
ISP	156	2 200
OSOC	156.2	2 300
OSPOS	75.5	2 000

The new method and analysis technique are simple to perform and can be executed with existing equipment. This method can be implemented immediately by the bench tester, without additional expenditure of capital—an important aspect for smaller laboratories. While computerized instrumentation and data acquisition tools do improve precision, they do not preclude accuracy.

The new method benefits from the experience of a field-savvy tribologist. As more and more torque versus load curves are plotted, the tribologist will begin to notice particular features that can be assigned to process requirements and lubricant additives.

Future work on this topic will include a rigorous examination of the relationship between the onset of the Faville inflection and the load wear index from the four-ball device.

## References

- [1] Faville, F. A. and Faville, W. A., "Falex Procedures for Evaluating Lubricants," *Lubrication Engineering*, Volume 24, Issue 8, 1968, pp 349-358.
- [2] Russel, J. V., "Steels for Cold Forming," *Source Book on Cold Forming*, ASM, pp 104-110, 1975, originally published 1962, *Metals Engineering Quarterly*.

M. Z. Huq<sup>1</sup> and J.-P. Celis<sup>1</sup>

## Evaluation of Fretting Wear Under Oscillating Normal Force

---

**Reference:** Huq, M. Z. and Celis, J.-P., “Evaluation of Fretting Wear Under Oscillating Normal Force,” *Bench Testing of Industrial Fluid Lubrication and Wear Properties Used in Machinery Applications, ASTM STP 1404*, G. E. Totten, L. D. Wedeven, J. R. Dickey, and M. Anderson, Eds., American Society for Testing and Materials, West Conshohocken, PA, 2001.

**Abstract:** In this paper a novel fretting mode II wear test is presented. This test consists of an oscillating normal force superimposed on a constant force. The oscillating force can be applied over a range of frequencies. The principles of this fretting mode II test and the type of damage induced in this particular test and contact motion are discussed. The influence of the main fretting mode II parameters (force amplitude, test duration, etc.) on the materials degradation in the contact has been analyzed. Experimental data were obtained for different materials combinations, e.g., bulk WC-Co oscillating against alumina, hard coatings such as physical vapor deposited (PVD) (Ti,Al)N and PVD TiN oscillating against alumina and silicon nitride counterbodies, and a soft tin coating oscillating against a self mated one. The mode II fretting test results indicate that wear takes place in the slip region. Cracking and spalling out in the slip region are both observed in some instances. The critical normal force at which fatigue failure occurs, was determined for bulk ceramics and ceramic coatings. The evolution of the electrical contact resistance in the case of self-mated soft tin coatings tested under fretting mode II conditions is also reported.

**Keywords:** fretting mode II, slip zone, wear, fatigue, ceramics, coatings

### Introduction

Fretting is an interfacial material degradation process occurring when surfaces of contacting solid bodies are subjected to small-amplitude oscillatory relative motions [1]. The fretting damage results from a simultaneous or subsequential occurrence of two or more different wear processes, such as adhesion, oxidation, fatigue and/or abrasion [2,3].

---

<sup>1</sup> Research Assistant and Full Professor, respectively, Dept. of Metallurgy and Materials Engineering, Katholieke Universiteit Leuven, de croylaan 2, B-3001 Leuven, Belgium.

The practical importance of this material degradation process attracts widespread concern in industry. Fretting is the modern plague of industrial machinery [4,5] and occurs in a number of applications such as aircraft components (splines, cables, bearings, hinges, seals, actuating devices, rocket propulsion fuel tanks, etc.) [6], nuclear power plants [7], automobiles, electrical contacts, and surgical implants [8]. Such contact vibrations are often induced by cyclic accelerations, cyclic stresses, acoustic noises, or by thermal cycling. The damage induced on materials surfaces in vibrating contacts is determined by the variables of the fretting process. This work was undertaken in order to clarify the effect of several operational parameters on the fretting mode II degradation mechanism. This in turn facilitates the selection of appropriate countermeasures against fretting.

Fretting mode II is a degradation mechanism happening when an oscillating normal load causes a varying in the contact area between an upper and lower limit [9]. Under fretting mode II, slip occurs in a contact zone delineated by the minimum and maximum contact area. The fretting mode II can be encountered in ball bearing applications, jet engine industry, electrical contacts, and power plants. In bearings, a rolling element experiences a certain amount of microslip at the ball-race interface during operation that can result in a surface damage. For hard materials, e.g., ceramics and ceramic coatings, the damage associated with microslip can cause a microfracture that can lead to a sudden bearing failure due to the relatively low toughness of ceramics or ceramic coatings. An understanding of the resistance of materials to fretting fatigue is essential for the evaluation of the lifetime of components. To date however, only a few studies have attempted to examine the fretting mode I fatigue life of ceramics [10,11] and impact fatigue of ceramic coatings [12]. Recently the authors have developed an oscillating normal load fretting tests [9] allowing the investigation of the fretting wear and fatigue properties of bulk materials and coatings under dynamic loading. The test rig also allows investigation of the influence of wear on electrical contact resistance.

The aim of this study on fretting mode II tests was to determine the effect of the slip amplitude, the maximum applied force and the number of fretting cycles on the degradation of bulk ceramics, hard ceramic coatings and soft coatings. In particular, the existence of a critical normal force below which no surface damage occurs, was investigated for the systems alumina against WC-Co and silicon nitride against (Ti,Al)N coatings. The electrical contact resistance for soft tin vs. tin coatings was determined at different force amplitudes.

## Experimental Method

### *Principles of Fretting Mode II Testing*

The contact vibration under fretting mode II requires a periodically varying applied normal force in the contact. In the case of a ball-on-flat contact geometry such an oscillating normal force results in a periodic variation of the circular contact boundary, between a minimum,  $a_{\min}$  and a maximum,  $a_{\max}$ , contact radius. In order to acquire a periodic variation of contact boundary, an experimental fretting mode II set-up was developed at the Dept. of Metallurgy and Materials Engineering, KU Leuven. Details

about the fretting mode II test rig are described elsewhere [9]. The test apparatus consists of a ball held stationary against a flat test specimen fixed on a lever arm. The lever transfers the downward force of a dead weight placed on one end into an upward force at the other end, thereby pressing the sample upward against the counterbody. A pre-selected static load,  $P$ , is applied on the plate (lever arm). Subsequently, a sinusoidal cyclic force with a constant amplitude,  $\Delta P$ , is applied to the specimen at a given frequency (Figure 1). The force amplitude is given by:

$$\Delta P = P_{\max} - P_{\min} \tag{1}$$

with  $P_{\max}$  the maximum compressional normal force, and  $P_{\min}$  the minimum compressional normal force. At  $P_{\min}$  a minimum contact area is obtained which is known as the locked region.  $\Delta P$  causes a varying contact zone between  $a_{\min}$  and  $a_{\max}$ . That zone is known as the slip region.

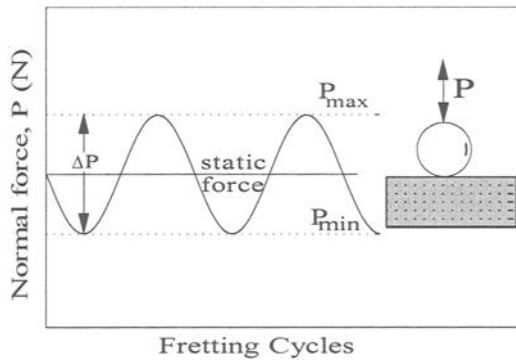


Figure 1 - Principle of the loading in a ball-on-flat fretting mode II contact.

*Wear Scar Analysis*

The case of a ball pressed against a large flat specimen is presented in Figure 2. The ball is subjected to a normal force,  $P$ , that determines the radius of contact,  $a$ . The maximum contact pressure or normal stress can be calculated from the Hertz equations [13]. The Hertzian contact pressure,  $p$ , varies radially over the circular contact area according to:

$$p(r) = p_{\max} \sqrt{1 - (r/a)^2} \tag{2}$$

$$p_{\max} = \frac{3P}{2\pi a^2} \tag{3}$$

with  $r$  the distance from the center of the contact circle, and  $p_{\max}$  the central peak contact pressure. The pressure distribution in the circular contact region is represented by a hemisphere with a maximum value  $p_{\max}$  at the centre and a zero value at the circumference. The shear stress distribution over that circular contact area is according to Hertz [13]:

$$\tau = \frac{\tau_0}{\sqrt{1 - (r/a)^2}} \quad (4)$$

with  $\tau_0$  the contact shear stress in the center of the contact region. The shear stress rises to infinity at the edge of the contact region and is at minimum at the center of the contact circle. The contact radius,  $a$ , can be analytically determined for combinations of bulk materials according to the Hertz theory [13] and for coatings by using the model of Daio et al. [14] where indenter, coating and substrate materials properties are considered. Details about this can be found in Ref. [9].

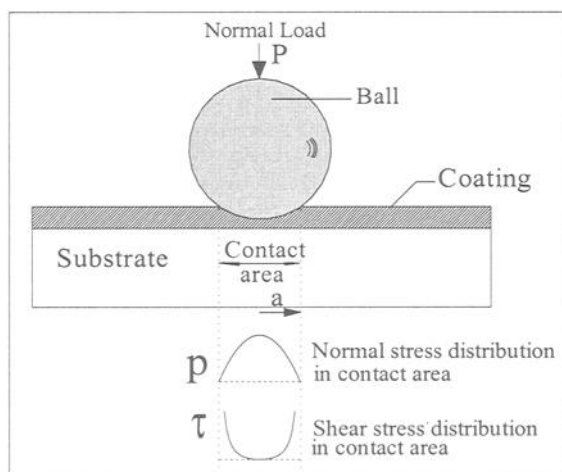


Figure 2 - Ball-on-flat configuration, showing distribution of normal and shear stresses in the contact.

The in-phase operation of the vibrator unit produces an oscillating variation of the normal force applied on the contact. This is illustrated in Figure 3 for the case of an alumina ball pressed against a high speed steel flat. Wear damage does not occur in the central region with radius  $a_{\min}$ , defined as the locked region. Microslip and surface damage are confined to the region with outer,  $a_{\max}$ , and inner,  $a_{\min}$ , radii, called the displacement stroke or slip region. This wear pattern results from the distribution of stresses induced by the oscillation of the normal load. As mentioned above, the maximum pressure in a ball-on-flat contact configuration works at the center and reaches to a zero value at the circumference, while the shear stress rises to infinity at the edge of the contact region and is at minimum at the centre of the contact. So a higher surface shear

stress is active in the slip region. This shear stress is primarily due to a Young's modulus and poisson's ratio mismatch between both contacting surfaces during the sinusoidal varying normal force. The magnitude of the slip depends on the static normal force applied to the contact and the amplitude of the normal force oscillation as shown in Figure 3. It is obvious that the displacement stroke induced at a given force amplitude is largest at a low static force. The minimum radial displacement stroke that can be achieved experimentally is limited by the accuracy of the normal force actuator.

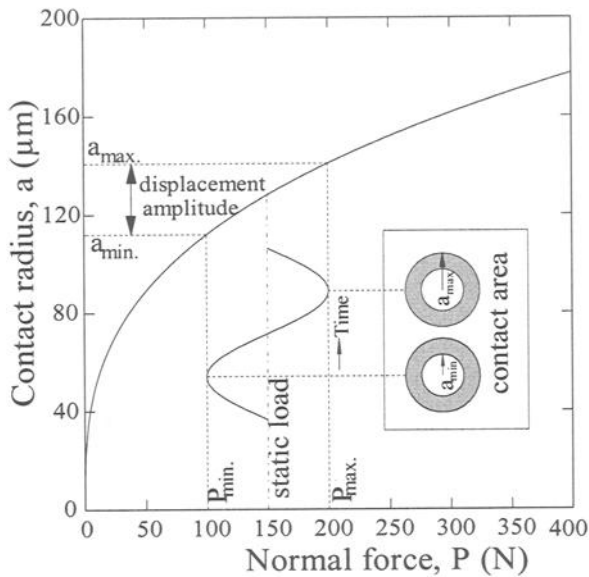


Figure 3 - Calculated variation of the Hertzian contact radius ( $a$ ) with normal force ( $P$ ) during fretting mode II tests. Calculation was done for an alumina ball ( $\varnothing 5$  mm) loaded on a flat high speed steel.

#### Materials and Experimental Conditions

The flat specimens used in this study were hard WC-3%Co bulk material, hard PVD (Ti,Al)N coating (thickness:  $2.1 \mu\text{m}$ ), hard PVD TiN coating (thickness:  $5 \mu\text{m}$ ), and soft tin coating (thickness:  $2 \mu\text{m}$ ). Details about the synthesis and the properties of these materials can be found in References [9,15,16]. The balls were either high density alumina (Ceratech, The Netherlands) or silicon nitride (Cerametel, Luxemburg). The balls are  $\varnothing 5$  mm grade 5 balls. In the case of tin coated samples, a cross cylinder contact geometry was used. The surface roughness,  $R_a$ , of all samples was at the start of the tests below  $0.6 \mu\text{m}$ . Tests were performed at different  $\Delta P$ -values and a constant frequency of 35 Hz for different number of cycles in ambient air of 50% RH and  $22^\circ\text{C}$ . One test was carried out with a TiN-Si<sub>3</sub>N<sub>4</sub> pair of material immersed in distilled water. The force amplitude was monitored during the fretting mode II tests via an oscilloscope. The on-

line monitoring of the electrical contact resistance was done by using a four point method. The contacting surfaces were cleaned with acetone and ethanol prior to fretting tests. After fretting tests, the specimens were examined by scanning electron microscopy (SEM), and the wear tracks were measured by laser stylus profilometry (Rodenstock RM 600). Wear tracks were analyzed by energy dispersive spectroscopy (EDS).

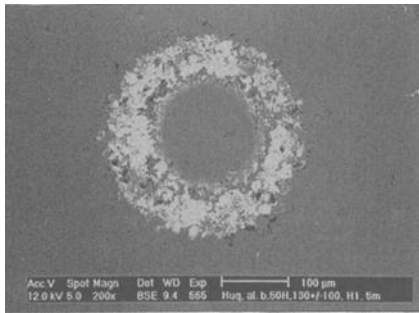
The issue of fretting fatigue damage in mode II fretting is of particular concern. To check whether a microscopic fatigue spalling or cracking occurs at the surfaces of the first bodies, the test specimens were removed from the machine after different predetermined test durations, and the contact areas were examined by Normaski optical microscopy and SEM. Each test was done at a new contact area. A spalling or cracking dimension of about 20  $\mu\text{m}$  was considered as a typical terminal fatigue point. Fatigue curves were obtained in this way for both bulk and coated materials.

## Results and Discussion

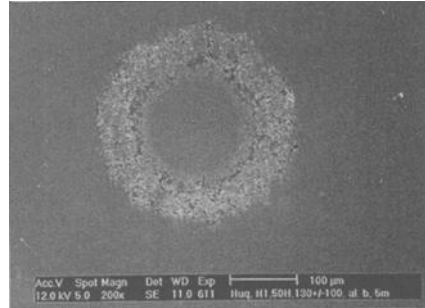
### *Fretting Mode II Behavior of Hard Bulk Materials*

*WC-Co vs. Alumina* – The fretting mode II surface damages on an alumina ball tested against a WC-Co flat are presented in Figure 4. The fretting test was performed at a static normal force of 130 N and a superimposed sinusoidal oscillation with an amplitude,  $\Delta P$ , of 200 N, at a frequency of 35 Hz. The test was run for  $5 \times 10^6$  fretting cycles. A locked unworn region at the center surrounded by a worn slip region is clearly visible on both counterbodies (Figures 4a and 4b). The locked region corresponds to the contact zone at the minimum normal force. The radius of the locked region agrees closely with the Hertzian contact radius at the minimum normal force of 30 N [16]. Microanalyzes were performed on fretting mode II tests wear tracks in order to determine eventual material transfer between the first bodies. Transfer of elements did not take place in the locked region of the counterbodies. Cross-sectional depth profiles on the WC-Co flat sample (Figure 5) reveals that no permanent deformation of the flat occurred in the locked region on loading with the alumina ball. The contact area in the locked zone remains unaffected with increasing numbers of fretting cycles. Profilometric measurements on the alumina ball can not be performed because of the limits of profilometer used to measure curved surfaces of  $\varnothing 5$  mm.

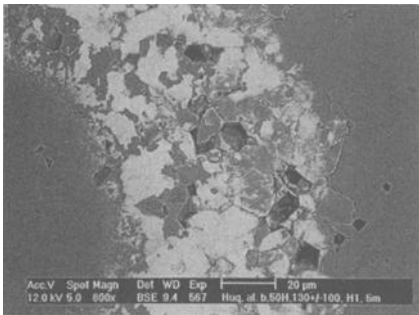
The damage in the slip region on alumina is shown in details in Figure 4c. It reveals the presence of wear debris, the spalling of alumina grains and the presence of cracks along grain boundaries. The presence of a cone cracking was not noticed either at low or at high normal forces. The absence of a cone cracking on the alumina surface indicates that the maximum tensile stress in the contact was not high enough to induce cone cracking. The wearing of the WC-Co flat sample in the slip region is shown in Figure 4d. High magnification SEM observation revealed a spalling out of WC-Co in that slip region. Cracking was not detected on the WC-Co surface. This has to be linked to the higher fracture toughness of WC-Co in comparison to alumina, although both alumina and WC-Co have almost a similar hardness [16]. Microanalyzes in the fretting mode II wear tracks revealed the presence of W, Co, and C in the slip region on the alumina ball.



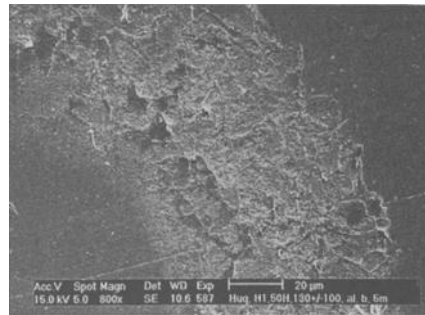
(a) alumina: overview of wear scar



(b) WC-Co: overview of wear scar



(c) alumina: slip zone



(d) WC-Co: slip zone

Figure 4 – SEM micrographs of the wear scars on alumina and WC-Co, after fretting mode II tests performed with an alumina ball against a WC-Co flat specimen. Test parameters:  $P$ : 130N,  $\Delta P$ : 200 N, 35 Hz, cycles:  $5 \times 10^6$ , air of 50% RH, 25 °C.

This suggests that transfer of flat material to the ball did occur. Microanalyzes on the flat surface in the slip region confirm the oxidation of WC-Co and the presence of alumina. This finding is in agreement with reports of Mohrbacher et al. [17] and Campbell [18] mentioning that disordered  $WO_3$  forms during the bidirectional fretting wear of WC-Co against alumina. The presence of a transfer layer and the evidence of the detachment of WC-Co from the flat specimen can be deduced from the cross-sectional wear track profiles shown in Figure 5. It is apparent from these profiles that at increasing number of fretting cycles the damage progressively accumulates. The size of the outer contact zone, i.e., the contact radius at maximum load, increases slightly with increasing numbers of fretting cycles. That is due to debris accumulation and an extrusion of debris from the initial contact zone. The lateral contact radius at maximum force does thus not agree any more at increasing numbers of fretting mode II cycles with the initial Hertzian contact radius.

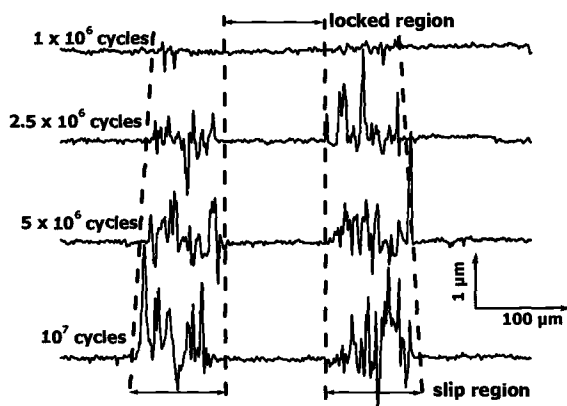


Figure 5 – Cross section depth profiles of wear scars on a WC-Co flat loaded against alumina balls for different numbers of fretting mode II cycles. Test parameters are:  $P$ : 130 N,  $\Delta P$ : 200 N, frequency: 35 Hz, ambient air of 50% RH.

*Fretting Fatigue of Alumina* – Figure 4 alluded to the existence of cracking and spalling. The threshold load for cracking or spalling was determined according to the procedure explained above. Such threshold conditions are plotted on a maximum normal force ( $P_{max}$ ) vs. number of cycles "design map". Figure 6 shows such a fretting fatigue design map for alumina. Failures as cracking and spalling were distinguished by optical Normaski microscopy and SEM. The solid symbols in the 'map' indicate tests where for a given normal force terminal spalling and/or cracking was noticed at the surface of alumina ball. The solid curve in the figure is a best fitting delineating occurrence and non-occurrence of spalling and/or cracking. Figure 6 then indicates the zone of safe operation, under fretting mode II conditions. For a differential force-displacement response, stresses are generated at the grain boundary and result in grain boundaries fracture [19]. Many studies on crack propagation of ceramics [20-23] have revealed that repeated Hertzian contact loading causes a severe mechanical fatigue. In severe cases, microcracks at grain boundaries can coalesce into a fragmentation zone, resulting in the detachment of grains from the ceramic surface. Such a grain boundary microfracture results in an abrupt material degradation after an incubation period [24,25]. But, what are the basic elements working behind a premature microcracking? In polycrystals, grain boundary stress concentrations from shear, in combination with pre-existing thermal anisotropy stresses, can lead to premature grain boundary microcracking [26-28]. Again, previous wear studies with translating or rotating spherical indenters provide a precedent for this mechanism [25]. In the present case of a ball-on-flat fretting mode II contact, the maximum surface shear stress is operative in the slip region (Figure 2). Grains whose boundaries have been damaged during the fretting cycles are subsequently pulled out by the shear stress working in the slip region.

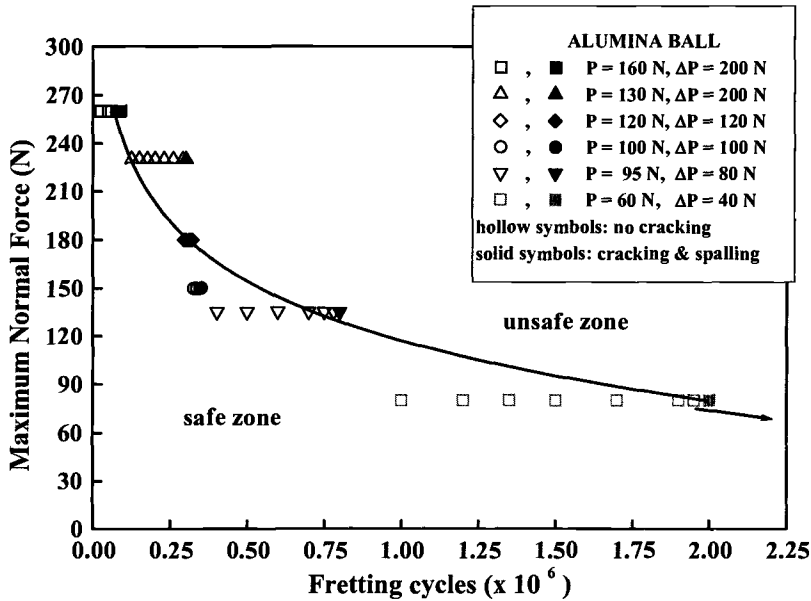
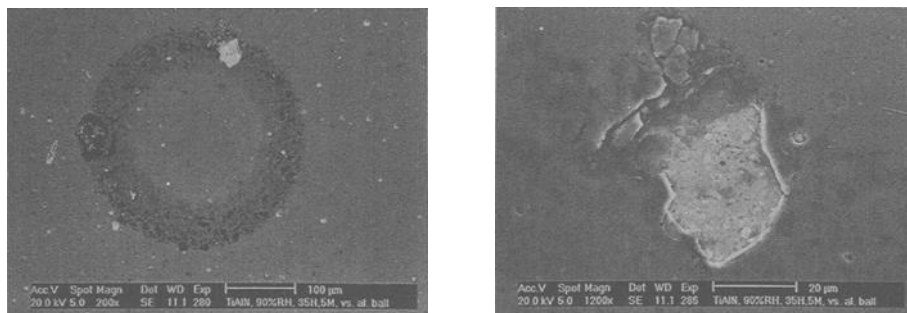


Figure 6 – Design map showing maximum contact force vs. number of fretting cycles for the onset of fatigue cracking in an alumina ball (Ø5 mm), for fretting mode II tests performed against WC-Co flat.

*Fretting Mode II Behavior of (Ti,Al)N and TiN Coatings*

*Fretting Fatigue of (Ti,Al)N Coatings* – Fretting mode II test was performed on a (Ti,Al)N coated HSS flat surface pressed against an alumina ball at a static normal force of 160 N. The normal force was oscillated at an amplitude, ΔP, of 200 N and a frequency of 35 Hz for 10<sup>7</sup> cycles. Figure 7 shows the wear scar on the (Ti,Al)N coating. An unworn region at the centre surrounded by a worn region can easily be noticed. The outer dimension of the locked zone agrees with the Diao and the Hertzian contact radius for a minimum normal force of 60 N [9]. At low normal loads both models give quite similar results. The surface finish in the locked region on both first bodies, remains unchanged. Microanalyzes confirm that transfer of material did not take place in the locked region on both first bodies. Wear of the coating is evident in the slip region where the presence of debris is also noticed. An EDS analysis revealed that the wear track contains oxides of elements present in the coating as well as alumina particles. Fretting wear tests performed under mode I revealed previously the oxidation of (Ti,Al)N coatings into Al<sub>2</sub>O<sub>3</sub>.TiO<sub>2</sub> when tested against alumina balls [15,29]. Moreover this investigation on (Ti,Al)N thin coatings, revealed micro-cracks and spalling off in the slip region (Figure 7). Details of the white area in the slip zone of Figure 7a shown in Figure 7b reveals spalling of the coatings and as a consequence substrate material is exposed. Spalling of



(a) overview of wear scar

(b) microcracks and spalling in slip zone

Figure 7 – Wear scars on a (Ti,Al)N coated flat specimen after fretting mode II tests performed against an alumina ball. Test parameters are:  $P$ : 160 N,  $\Delta P$ : 200 N, frequency: 35 Hz, fretting cycles:  $10^7$ , ambient air of 50% RH.

the coatings in the slip region happens due to a cohesive-adhesive failure of the coating caused by the build up of shear stresses which arises from the cyclic loading as described earlier. Failure of the coatings was not noticed in the outer periphery of the contact area. This can be explained by the fact that tensile stress at the maximum load ( $P_{max}$ ) is not high enough to initiate cone cracking. A severe spalling damage was noticed in the slip region on the alumina balls for reasons discussed in previous section.

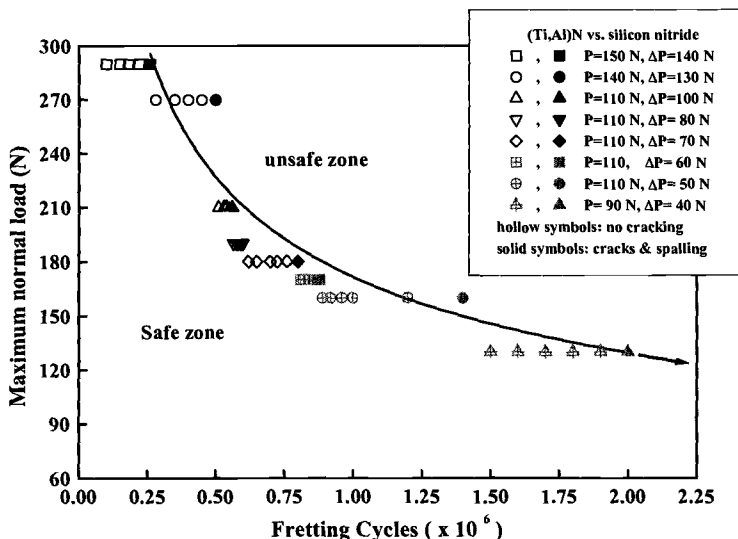
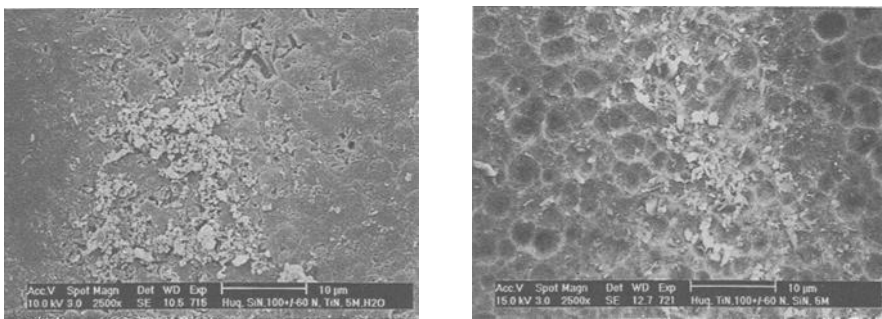


Figure 8 – Design map, maximum contact force vs. number of cycles for the onset of fatigue cracking in (Ti,Al)N coatings, tested against silicon nitride ball ( $\varnothing$  5 mm).

When (Ti,Al)N coatings were tested against a silicon nitride ball at  $P = 140\text{N}$ ,  $\Delta P = 130\text{N}$ , at a frequency of 35 Hz for a test duration of  $10^6$  cycles, it was found that wear, cracks and spalling of the coating took place in the slip zone. At increasing number of fretting cycles, the propagation of cracks took place and more spalling of the coatings was noticed in the slip zone. Failure of (Ti,Al)N was not noticed in the locked region, nor in the outer periphery of the contact area. Spalling of silicon nitride in the slip zone was not noticed at the loads and the number of cycles used in this investigation.

In view of the preceding results, a large series of fretting mode II tests were performed with a (Ti,Al)N coating loaded on a silicon nitride ball. The threshold conditions for (Ti,Al)N coating are plotted on a maximum normal force ( $P_{\text{max}}$ ) vs. number of cycles "design map" in Figure 8. The solid symbols in the 'map' indicate test conditions where a terminal spalling and/or cracking was noticed on the surface of the (Ti,Al)N coating. Cracking and spalling of the coatings in the slip zone occurred due to a cohesive-adhesive failure of the coating induced by the build up of shear stresses. Due to successive shear stresses in the slip region, cracks initiate at preexisting defects. In (Ti,Al)N coatings, such defects can be pores and macros [29].

*Fretting Fatigue of TiN Coating* – TiN coatings were tested against alumina and silicon nitride in order to compare the fretting mode II behavior of TiN with the one of (Ti,Al)N coatings. The tests were run in air under the same sets of test parameters as used for (Ti,Al)N coatings. Neither cracking nor spalling was observed on the surface of TiN for tests performed against alumina or silicon nitride, but oxidation at the surface of the coatings was noticed. Moreover, a severe spalling of alumina and a more limited spalling of silicon nitride took place. Tests on TiN coatings pressed against silicon nitride both immersed in water were also performed. Again, neither cracking nor spalling of TiN was noticed. On the contrary, silicon nitride does not wear even after  $0.5 \times 10^7$  cycles in air



(a) Silicon Nitride: slip zone

(b) TiN: slip zone

Figure 9 – Wear scars on  $\text{Si}_3\text{N}_4$  and TiN after fretting mode II tests done on TiN coated flat loaded on a  $\text{Si}_3\text{N}_4$  ball. Test parameters:  $P: 100\text{N}$ ,  $\Delta P: 120\text{N}$ , frequency: 35 Hz, fretting cycles:  $0.5 \times 10^7$ , water.

whereas in water there was a severe damage after  $0.5 \times 10^7$  cycles. Spalling of silicon nitride took place by preference in the slip zone and the debris were transferred to the TiN coating (see Fig. 9). High magnification SEM observations revealed intergranular cracks on silicon nitride and a grain pull out was noticed along longer cracks. These results are in accordance with the results of Kishimoto et al. [30], who stated that water enhances cyclic fatigue by stress corrosion that causes microfracture and wear at bridging sites.

A comparison of the fretting mode II tests reveal that TiN is lesser damage sensitive than (Ti,Al)N. (Ti,Al)N coatings have a lower elasticity modulus compared to TiN coatings [29]. This may explain the better fatigue resistance of TiN coatings in comparison to (Ti,Al)N coatings under fretting mode II tests. Another element could be the presence of surface defects (pores and macros).

#### *Fretting Mode II Behavior of Soft Tin Coating*

Tin coatings are extensively used as top layers on electrical contacts that are subjected to vibrations, for example, in automotive parts. Besides wear, the electrical contact resistance is an important functional property in such applications. Therefore the electrical contact resistance was investigated in fretting mode II tests performed on self-mated tin coatings loaded at a static normal force of 3.0 N, on which a load amplitude,  $\Delta P$ , of 5 N oscillated at 30 Hz is superimposed. Both first bodies exhibited after the fretting mode II tests an identical wear pattern, namely an undamaged central region and an outer worn slip region (Figure 10). The wear debris were extruded towards the outer

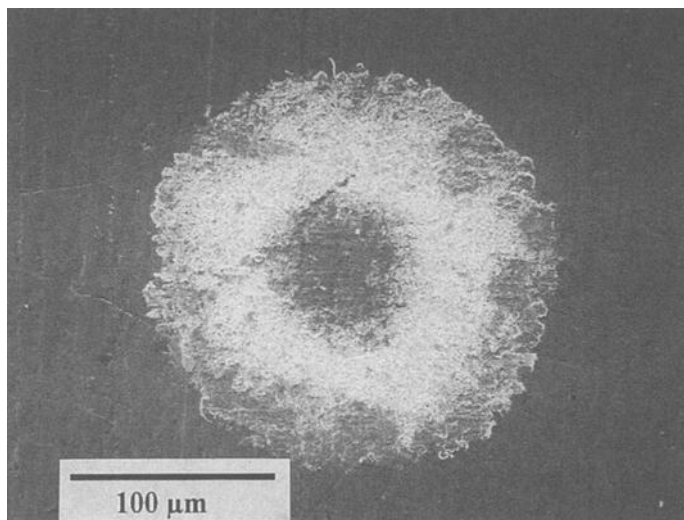


Figure 10 – *Wear scar on a tin coated specimen after a fretting test against self mated specimen at  $P$ : 3 N,  $\Delta P$ : 5 N, frequency: 30 Hz, fretting cycles:  $8.0 \times 10^6$ .*

periphery. An EDS spot analysis of the wear scar revealed the presence of oxygen in the slip region, whereas the spectra did not reveal the presence of oxygen in the locked region. Oxidation in the slip region occurs as a result of the periodic exposure of the contact area to air. The oxides detected are SnO or SnO<sub>2</sub>. According to literature, tin can indeed form oxides in air at low temperature (~150 °C) [31]. Since the central part of the wear track remains permanently in contact with the counterbody, that region does not oxidize during fretting mode II test under the selected test parameters. The evolution of the electrical contact resistance during the fretting mode II test is displayed in Figure 11. The electrical resistance remains constant at a low value of about 1 mΩ throughout the whole test period. That low electrical contact resistance is achieved through the central part of the contact area that always remains in contact. The wearing that takes place in the slip region does not badly influence the electrical resistance.

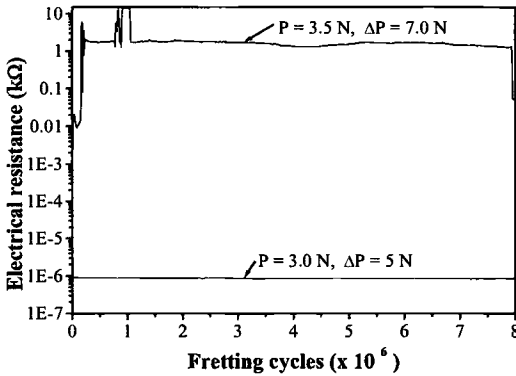


Figure 11 – Electrical contact resistance vs. number of cycles for fretting mode II tests performed on self mated tin coated specimens for test duration of  $8 \times 10^6$  fretting cycles.

Self-mated tin coatings were also tested under fretting mode II but at a minimum normal force ( $P_{min}$ ) at 0 N. Under such fretting mode II test conditions, a disconnection between first bodies can take place. A static normal force of 3.5 N was applied and varied between 0 N and 7.0 N at 30 Hz. The evolution of the electrical contact resistance during the test is displayed in Figure 11. At the initial stage of the test a very low electrical contact resistance of about 4 mΩ was recorded. That stage of low contact resistance was followed by a stage showing some instability for a number of fretting cycles. Finally, the resistance stabilized at a high value of 1.5 kΩ for the rest of the test in contrast to the very low electrical contact resistance of a few mΩ noticed when a permanent locked area is achieved. The instability in the contact resistance noticed after a limited number of fretting cycles is probably due to the breaking of the tin oxides present initially on the surface of the coatings. At a minimum load of 0 N, the locked region disappears was confirmed by EDS spot analyzes. These analyzes revealed indeed the presence of oxygen and coating elements all over the contact area. Since the whole contact area was sequentially exposed to air, oxidation occurred over the whole contact

area. Fragmentation of that oxide layer, results in the formation of abrasive debris causing a subsequently wear and a high electrical contact resistance.

### Conclusion

Material degradation in fretting mode II tests occurs on both ceramics as well as on hard and soft coatings. The study reveals that a surface damage occurs in the slip region on both first bodies, whereas the surface finish in the locked region remains unchanged. Tribochemical changes in the slip region happen due to the periodical exposure of the slip region to the environment.

This investigation demonstrates that alumina and hard (Ti,Al)N coatings are prone to fatigue cracking under fretting mode II testing. Design maps indicating the conditions of safe operation were determined for alumina and hard (Ti,Al)N coatings under fretting mode II. In both cases, an increase of the maximum contact force causes a decrease of the fatigue resistance. (Ti,Al)N has a better fatigue resistance under fretting mode II compared to bulk alumina. Remarkable was the finding that TiN coatings do not suffer from fatigue cracking at normal loads where (Ti,Al)N and alumina fail by contact fatigue. Although WC-Co is prone to fretting wear and spalling, it shows a good fatigue resistance under the tests conditions selected. Silicon nitride has a better fretting fatigue resistance in dry air, but its fatigue resistance lowers in water. Fatigue cracks were not detected on the surface of soft tin coatings. Electrical contact measurements showed that, notwithstanding wear occurs in the slip region, the electrical contact resistance under fretting mode II remains very low and constant, for test conditions where a locked contact region is achieved.

### Acknowledgment

Part of this work have been financed by the European Commission (Brite Project EUPIII BRPR-CT97-0380 and EUELECON BRPR-CT97-0429) and the Belgian Government (contact IUAP P4/33 and ABOS). One of the author (M. Z. Huq) thanks the KU Leuven for the granted bursary.

### References

- [1] Brown, S. R., "Materials Evaluation Under Fretting Conditions," *ASTM Special Technical Publication 780*, Warminster, PA, 1981, pp. 1-2.
- [2] Waterhouse, R. B., *ASM Handbook*, ASM international, Vol. 18, 1992, pp. 242-306.
- [3] Begelinger, A. and De Gee, A. W. J. in *AGARD Conference Proceedings*, No. 161, National Technical Information Service, Springfield, Va., 1974, pp. 9.1-9.7.
- [4] Waterhouse, R. B., *Fretting Fatigue*, Elsevier Applied Science, London 1981.

- [5] Waterhouse, R. B., *Fretting Corrosion*, Pergamon, Oxford, 1972.
- [6] Kennedy, P., Peterson, M. B. and Stallings, L., "An Evaluation of Fretting at Small Slip Amplitudes," *Materials Evaluation under Fretting Conditions, ASTM STP 780*, Warminster, PA, 1981, pp. 30-48.
- [7] Ko, P. L., "Experimental Studies of Tube Frettings in Steam Generators and Heat Exchangers," *Journal of Pressure Vessel Technology*, Vol. 101, 1979, pp. 125-133.
- [8] Sandstrom, P. W., Sridharan, K. and Conard, J. R., "A Machine for Fretting Wear Testing of Plasma Surface Modified Materials," *Wear*, Vol. 166, 1993, pp. 163-168.
- [9] Huq, M. Z., Butaye, C., Celis, J.-P., "An Innovative System for Fretting Wear Testing Under Oscillating Normal Force," *Journal of Materials Research*, Vol. 15, No. 7, 2000, pp. 1-9.
- [10] Jahanmir, S., *Friction and wear of ceramics*, Marcel Dekker, Inc., New York, 1994.
- [11] Suresh, S., *Fatigue of Materials*, Cambridge university Press, 1998.
- [12] Bouzakis, K. D., Vidakis, N., Leyendecker, T., Lemmer, O., Fuss, H.G., Erkens, G., "Determination of the Fatigue Behavior of Thin Hard Coatings using the Impact Test and a FEM Simulation," *Surface and Coatings Technology*, Vol. 86-87, 1996, pp. 549-556.
- [13] Timoshenko, S. and Goodier, J.N., *Theory of Elasticity*, McGraw-Hill Book Company, Inc., New York, N. Y., 1951.
- [14] Diao, D. F., Kato, K., and Hokkirigawa, K., "Fracture Mechanics of Ceramic Coatings in Indentation," *ASME Journal of Tribology*, Vol. 116, 1994, pp. 860-865.
- [15] Huq, M.Z. Celis, J.-P., "Fretting Wear of Mutilayered (Ti,Al)N/TiN Coatings in Air of Different Relative Humidity," *Wear*, Vol. 225-229, 1999, pp. 53-64.
- [16] Huq, M.Z., Celis, J.-P., "Fretting Fatigue Under Oscillating Normal Loading of Alumina Against WC-Co," submitted to *Journal of American Ceramic Society*, 2000.
- [17] Mohrbacher, H., Blanpain, B., Celis, J.-P., and Roos, J. R., "Raman Spectroscopy on Defective Wear Debris Generated by Contact Vibrations," *Journal of Materials Science Letter*, Vol. 14, 1995, pp. 279-281.
- [18] Campbell, P., "Tribological Behaviour of Advanced Ceramics and Cermets," Ph.D. Thesis, Katholieke Universiteit Leuven, Belgium, 1996.
- [19] S. Suresh, *Fatigue of Materials*, Cambridge University Press, Cambridge, Great Britain, 1991.
- [20] Ewart, L. and Sursh, S., "Dynamic Fatigue Crack Growth in Polycrystalline Alumina Under Cyclic Compression," *Journal Materials Science Letter*, Vol. 5, 1986, pp. 774-778.
- [21] Kishimoto, H., Ueno, A., and Kawamoto, "Crack Propagation Behavior of Sintered Si<sub>3</sub>N<sub>4</sub> Under Static and Cyclic Load," *Journal of Society Materials Science Japan*, Vol. 36, 1987, pp. 1122-27.
- [22] Kishimoto, H., "Cyclic Fatigue in Ceramics," *JSME International Journal*, Ser. 1. 34, 1991, pp. 393-403.
- [23] Guiberteau, F, Pature, N. P., Cai, H., and Lawn, B. R., "Indentation Fatigue: A

- Simple Cyclic Hertzian Test for Measuring Damage Accumulation in Polycrystalline Ceramics," *Philosophical Magazine A*, Vol. 68 (5), 1993, pp. 1003-1016.
- [24] Ajayi, O. O., and Ludema, K. C., "Surface Damage of Structural Ceramics: Implications for Wear Modeling," *Wear*, Vol. 124, 1988, pp. 237-245.
- [25] Cho, S. J., Hockey, B. J., Lawn, B. R., Bennison, S. J., "Grain Size and R-Curve Effects in the Abrasive Wear of Alumina," *Journal of American Ceramic Society*, Vol. 72, 1989, pp. 1249-52.
- [26] Hockey, B. J., "Plastic Deformation of Aluminium Oxide by Indentation and Abrasion," *Journal of American Ceramic Society*, Vol. 54, 1971, pp. 223-231.
- [27] Cannon, R. M., *Advances in Ceramics Structure and Properties of MgO and Al<sub>2</sub>O<sub>3</sub> Ceramics*, edited by W. D. Kingery (Columbus, Ohio: The American Ceramic Society), 1984, pp. 818-825.
- [28] Chan, H. M., Lawn, B. R., "Indentation Deformation and Fracture of Sapphire," *Journal of American Ceramic Society*, Vol. 71, 1988, pp. 29-35.
- [29] Huq, M. Z., Celis, J.-P., "Oscillating Sliding Wear of Monolayer and Multilayer Ceramic Coatings in Air," *Surface and Coatings Technology*, Vol. 113, 1999, pp. 242-250.
- [30] Kishimoto, H., Ueno, A., Fujiwara, Y., Konodo, T., Kominato, I., "Influence of Water Vapor on Crack Propagation Behaviour of Sintered Silicon Nitride Under Cyclic Load," *JSME International Journal, Series A*, Vol. 39(3), 1996, pp. 435-440.
- [31] Themlin, J. M., Chtaïb, M., Henrard, L., Lambin, Ph., Darville, J., Gilles, J. M., "Characterization of Tin Oxides by X-Ray-Photoemission Spectroscopy," *Physical Review B*, Vol. 46, 1992, pp. 2640-45.

Michael Anderson<sup>1</sup>

## The Use of Tribological Aspect Numbers in Bench Test Selection – A Review Update

---

**Reference:** Anderson, M., “The Use of Tribological Aspect Numbers in Bench Test Selection – A Review Update,” *Bench Testing of Industrial Fluid Lubrication and Wear Properties Used in Machinery Applications, ASTM STP 1404*, G. E. Totten, L. D. Wedeven, J. R. Dickey, and M. Anderson, Eds., American Society for Testing and Materials, West Conshohocken, PA, 2001.

**Abstract:** This paper will review the use of tribological aspect numbers when selecting a bench test to simulate a field application. “Realizing Bench Test Solutions to Field Tribology Problems by Utilizing Tribological Aspect Numbers” [1] first published in 1993 is an analytical method for selecting bench tests that best simulate field conditions or wear problems. Scientists, product developers, lubrication formulators, and material engineers and scientists can use this approach to select the most applicable bench test. The bench test selected can then be used to evaluate materials under laboratory conditions that can simulate field conditions and environments.

Bench testing is the simplest form of testing, isolating one particular set of tribological conditions. It is generally the first step in the testing program, preceding more complex, multi-variable, component tests. The tribological aspect number (TAN) was developed to identify and code a particular tribological condition. This identification or coding simplifies the process of matching the field condition to a bench test. Today, more individual bench tests are available to the tribologist. This review paper will describe the TAN approach, update the list of bench tests and their corresponding TAN and give several specific situations. This paper will also investigate the test parameter options and acceleration of test procedures required to produce test results in a reasonable time period.

**Keywords:** bench test, simulation, TAN, tribological aspect number, test geometry, tribology, wear test selection

### Introduction

Testing is necessary to develop performance properties of materials and lubricants used in a variety of field applications. The three major types of tests are bench, component and field. Bench tests isolate a singular tribological condition. Component tests typically contain several tribological conditions, increasing the complexity of the test and, therefore, increasing the variability of test results. Field tests, usually performed on complete production systems, outside a laboratory environment, are very complex with little ability for the designers to control key operating conditions. Therefore,

---

<sup>1</sup> Vice President, Falex Corporation, 1020 Airpark Drive, Sugar Grove, IL 60554

repeatability of field tests is generally less than that associated with bench or component tests.

Selecting the test that will give results that correlate with the field has always challenged the test designer. The tribological aspect number (TAN) [1] was developed to assist the test designer in making the transition from the field problem to the bench test. The TAN approach helps to reduce or eliminate many of the compromises previously employed due to lack of information, availability of bench test equipment and the economic necessity of accelerating the test. Previously, test designers had to rely on standardized tests, experience or other recommendations in order to develop a test method for evaluating materials. Use of the TAN to identify tribological conditions simplifies the bench test selection process by using the four digits that comprise the TAN code. This paper includes a detailed review and discussion of the step-by-step approach to identify the TAN, update the table of comparative tests and offer examples of tests developed using the TAN approach.

### **Tribological Aspect Number (TAN) Approach**

It must be understood that every bench test gives the researcher results under the conditions of the test that is being run. Whether that test data is applicable is secondary. Therefore it is imperative that the bench test selected accurately and completely represent the field condition or wear problem. A tribological condition must be described in terms of a system. If any of the test conditions are changed or not properly selected, there is the potential for developing laboratory test data that will not compare with the results obtained in the field.

Also important is the fact that most tribological problems occur within one mechanism of a more complex system or component. Therefore, for the TAN to be properly applied in component or complex systems, the tribological make-up of the wear problem must be isolated and its specific TAN identified.

There are countless methods for selecting a specific bench test including experience, standardized tests, or limitations in available equipment. The TAN approach uses a 4-digit number. Each digit identifies a specific condition as will be discussed. This 4-digit number characterizes the tribological condition in such a way as to easily reference bench tests having been previously identified with the same TAN procedure.

### **First Step – Identifying the Tribological Aspect Number (TAN)**

The procedure for identifying the TAN begins with understanding the field condition or wear problem and then identifying the 4 individual tribological conditions described in the TAN approach. The resulting 4-digit Tribological Aspect Number, *ABCD*, characterizes the tribological condition. The four individual aspects are as follows:

- A. Contact velocity or motion characteristic.
- B. Contact area or geometry characteristic.
- C. Contact pressure or load characteristic.
- D. Entry angle characteristic.

The “Tribological Aspect Number Guide,” [3] is a tool used to assist in the

identification of TAN codes. Each individual digit of the TAN will be discussed in the following paragraphs.

#### *A. Contact Velocity (Motion) Characteristic (Fig. 1)*

The first digit identifies the velocity characteristic [*1*] of the tribological system. The term motion should also be considered in this description. For it is really the motion between the surface of one material and the contacting surfaces of other materials that is actually being characterized. Although it is theoretically correct to refer to the motion as contact velocity, it is probably better understood to refer to this characteristic as motion. A clarification of the 4 motion selections is required. It should be noted and understood that a characterization of *1* represents pure sliding. Further, a characterization of *3* (roll/slide) could represent either pure rolling or combination rolling/sliding. But what is not clear is the fact that with cyclic motion, an identification of *2*, defined as reversing or reciprocating, there exists the possibility for pure sliding, pure rolling or combination rolling under this motion. Future consideration should be given to an additional category, call it *5*, for cyclic, reversing or reciprocating motion having some degree of rolling and allowing a characterization number of *2* for cyclic, reversing or reciprocating motion with pure sliding. Finally, fretting, identified as *4*, is its own unique type of motion characterized by high speed, very low amplitude reciprocation or vibration. TAN [*1*] allows for the following conditions for contact velocity:

1. Unidirectional and continuous in pure sliding motion
2. Cyclic
3. Rolling or combination rolling/sliding
4. Fretting (high speed, low amplitude motion)

#### *B. Contact Area (Geometry) Characteristic*

The contact areas (digit 2) for TAN [*1*] as listed in Figure 2 are complete. The only comment to be made would be to classify the contact area as the contact geometry. Further a discussion is needed on what is meant by the term “open” in *7* and *8* under this characteristic. The term “open” refers to one of the contacting pieces as always being in contact with an untouched surface. Such application could involve a spiraling or continuous lateral movement of one of the contacting surfaces. It can also be pointed out that when contacting surfaces maintain their Hertzian contacts, i.e. “point to point” or “line to line” there generally involves some degree of rolling motion. Therefore the options for contact geometry, with examples, are as follows:

1. Point to Point: Ball Bearing Assemblies
2. Line to Line: Roller Bearing Assemblies
3. Point to Area: Pin on Disk
4. Line to Area: Pump Rotor Vane
5. Area to Same Area: Thrust Washers, Disk pads
6. Smaller Area to Larger Area: Truncated Washers or pads
7. Open; Fixed Contact Geometry: roll forming

8. Open; Variable Contact Geometry: Metalworking Applications such as Cutting, Stamping, Drawing

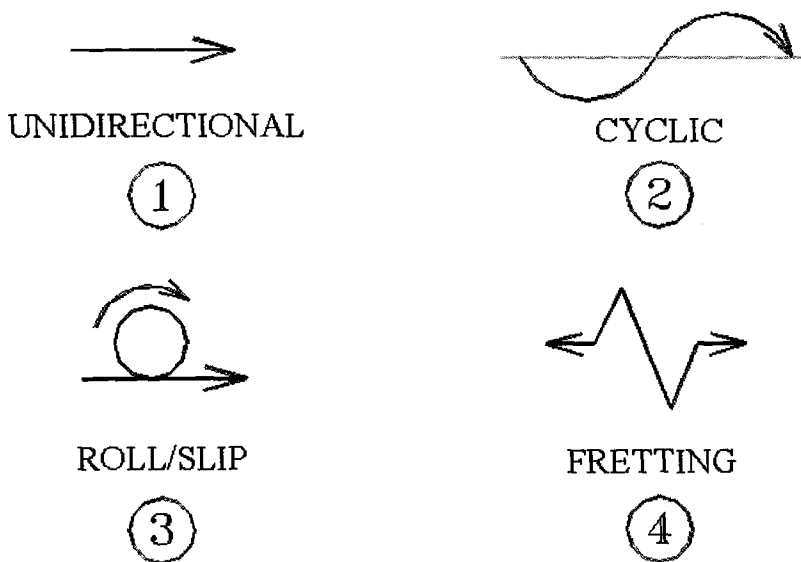


Figure 1 – Contact Velocity Characteristic (Motion)

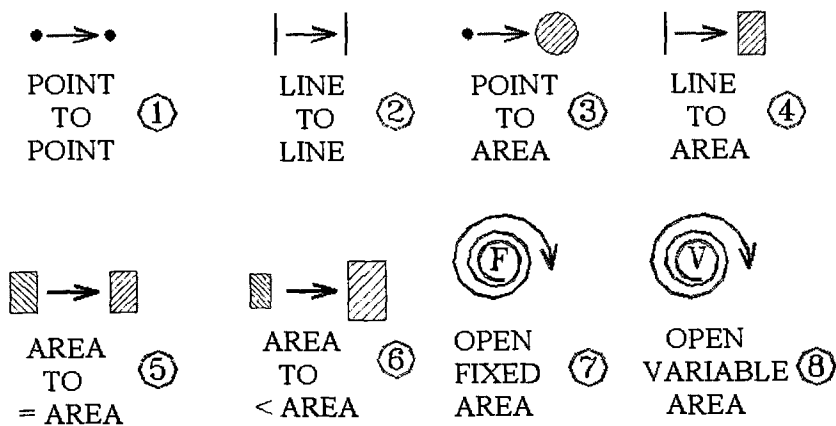


Figure 2 – Contact Area Characteristic

C. Contact Pressure

This characteristic can also be described in terms of load as well as contact pressure. Load is the parameter that it applied in bench tests. Pressure is defined as the load divided by the contact area. Depending on the contact geometry (digit 2), contact pressure could possibly decrease. Therefore, when identifying contact pressure, one should consider the directionality of the pressure or the applied load. The three identifications [1] for the contact pressure or load characteristic are as follows:

1. Unidirectional
2. High Frequency (could possibly be impact wear if the surfaces separate.)
3. Cyclic

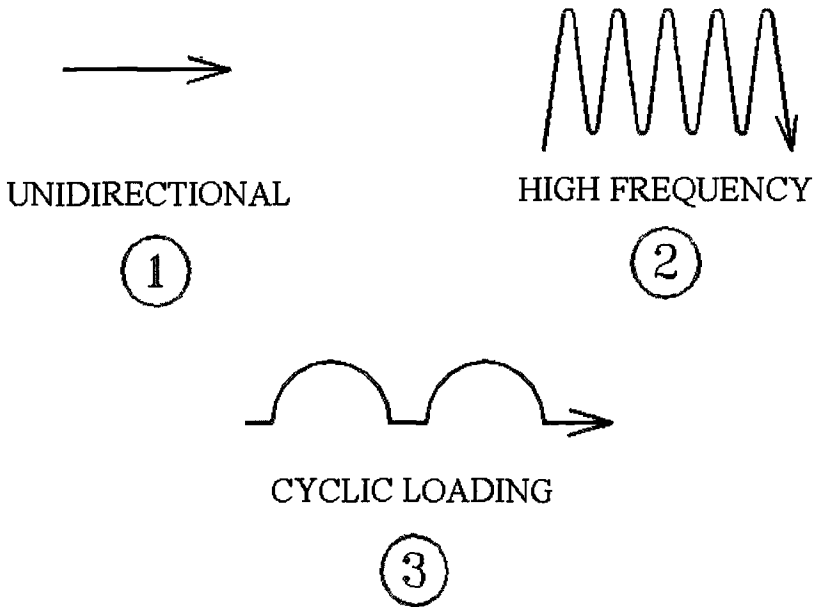


Figure 3 – Contact Pressure Characteristic (Load)

D. Entry Angle

The entry angle is a very important and often overlooked. It can be described as a design enhancement or deficiency. In many instances this characteristic can easily be changed by a modification in the test specimen geometry. In the paper there are 9 identifications for entry angle. This characteristic could easily be described in 4 or 5 identifications. A rating of 0 for this characteristic depicts a contact that is contiguous; that is, there is no possibility of introducing a fluid lubricant into the contact area. Systems that have a rating of 0 for entry angle are generally candidates for solid bonded

film lubricants, plastics, ceramics or other materials that are considered self lubricating. A rating of 1 indicates a very steep angle and would result in a significant degree of “plowing” or “wedging” the lubricant away from entering the contact area. A characteristic of 8 or 9 indicates a very small entry angle which at the same time is very efficient at allowing the lubricant to enter the contact zone. 9 is typical of ball or roller bearings, while 8 is typical of a curved surface sliding on a flat and generating a wear scar or bearing surface. While from 1 to 8, the angle continues to diminish allowing greater efficiency of lubricant entry, this region could be described in terms of perhaps one or two identifying conditions. These could be large angle and small angle. The complete range of entry angles is listed in Figure 4.

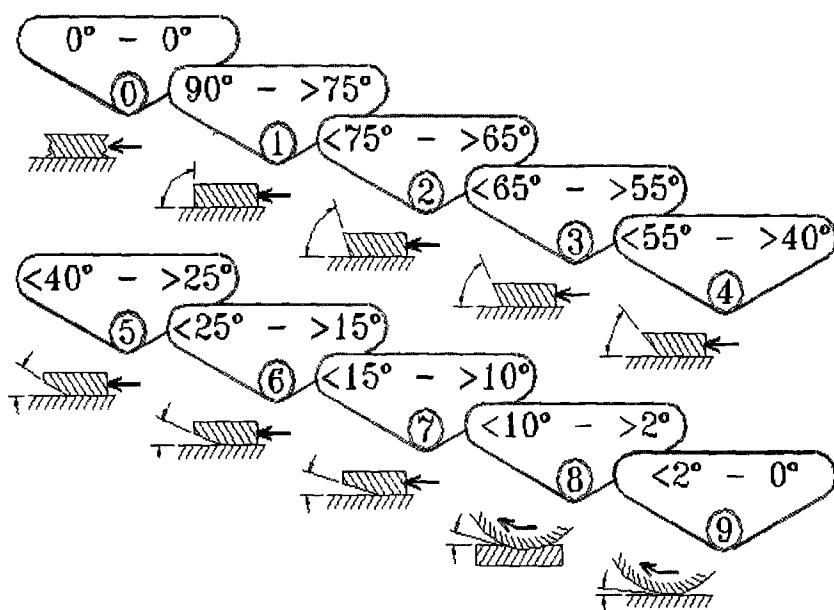


Figure 4 – Entry Angle Characteristic

### Second Step – Selecting the Bench Test

After the TAN has been identified, the next step is to select the bench test having the identical TAN code. This is an ideal situation and not always possible. Often times, there does not exist a test machine with a matching TAN or the test designer can only use a test machine that is available. In such cases, the user must consider test procedure compromises to overcome the deficiencies of using a test machine having a non-matching TAN.

It is important to note that many bench tests can perform several TAN codes through the use of adapters or modifications to the test device. The Four Ball Wear Test Machine

is an example offering the possibility of TAN codes of 1317, 3119, 1318, and 1511 [1]. Other examples of test machines having multiple TAN test configurations are as follows:

- 1) Block-on-Ring Test Machine [4]
  - Block-on-Ring: 1418, 2418
  - Ball-on-Ring: 1318, 2318
  - Canted Cylinder: 1318, 2318
  - Conforming Block-on-Ring: 1519, 2519
- 2) Linear Reciprocating Test Rig [5]
  - Ball-on-Plate: 2319
  - Piston Ring Test: 241\*, 242\*
  - Flat-on-Flat: 251\*
  - Pin-on-Plate: 2319

\* Specimen design of leading edge geometry defines digit in entry angle (fourth digit).
- 3) Pin-and-Vee Block Test Machine [4]
  - Pin-and Vee Block: 1418
  - Conforming Pin and Vee Block: 1519
- 4) Tapping Torque Test Machine [4]
  - Thread Tapping: 1718, 1719
  - Drawing: 1919
  - Roll Reduction Test: 3819
  - Roll Forming: 3619
  - Reaming: 1719
  - Drilling: 1711
- 5) Multi-Specimen Test Machine[4]
  - Numerous [2]

Alternatively, there may be several different test machines that can perform the same TAN. Therefore, it is important to concentrate on the test setup specific for the TAN and not just on the test machine.

Table 1 contains an updated list of tests with matching TAN codes. The entry angle was originally listed in a separate column [*J*] but was eliminated in this table. The entry angle is typically dependent on the design of the leading edge.

### **Third Step – Establishing the Test Conditions**

After the bench test has been identified, the test designer has to take into consideration the conditions under which the test will run, that is, the selection of test parameters. In the TAN [*J*], a separation is identified for the test conditions of speed, load, material, and use of test fluids with those of the test temperature and duration. All of these test conditions are variable to the test results and should be considered together, except for time or duration which will be discussed in detail in the Fourth Step. The previously mentioned test conditions should reflect the field condition as closely as possible. A more descriptive listing of test parameters follows:

Table 1 – Tribological Aspect Numbers (TAN) with Test Configuration Description

TAN	DESCRIPTION	TAN	DESCRIPTION
1219	SHEAR STABILITY	1518	CONFORM BLOCK-ON-RING
1317	4 BALL TEST CROSSED CYLINDER CROSSED PIN	1519	PIN AND CONFORM BLOCKS SPLIT JOURNAL CONFORM BLOCK ON RING JOURNAL BEARING
1318	BALL ON DISK BALL ON RING PIN ON DISK PIN ON RING BALL ON 3 DISK 3 PIN ON DISK 3 BALL ON DISK	1530	FACE CLUTCH
1319	BALL ON CYLINDER	2119	OSC. ROLLING 4 BALL OSC. ROLL/SLIDE
1417	TIMING BELT TEST	2317	OSC. 4 BALL
1418	BLOCK ON RING TIMKEN O RING TEST PIN AND VEE BLOCK	2318	OSC. 3 PIN ON DISK OSC. BALL ON 3 DISK OSC. BALL ON RING OSC. PIN ON RING OSC. PIN ON DISK OSC. 3 BALL ON DISK
1419	VANE ON DISK	2417	OSC. TIMING BELT
1428	CYCLIC STRESS	2418	OSC. BLOCK ON RING OSC. O RING TEST
1510	STICK SLIP THRUST WASHER FACE SEAL FRICTION POWDER TEST	2419	OSC. VANE ON DISK OSC. CYLINDER ON FLAT/DISK
1511	SLOTTED WASHER FLAT PIN ON DISK 3 FLAT PIN ON DISK 3 PAD ON DISK BALL ON 3 SEATS	2424- 2426	PISTON RING WEAR TEST
1512- 1517	SLOTTED WASHER FLAT PIN ON DISK 3 FLAT PIN ON DISK 3 PAD ON DISK	2510	OSC. THRUST WASHER OSC. FACE SEAL
		2511	OSC. BALL ON 3 SEATS OSC. SLOTTED WASHER OSC. FLAT PIN ON DISK OSC. 3 FLAT PIN ON DISK OSC. 3 PAD ON DISK

Table 1 – Tribological Aspect Numbers (TAN) with Test Configuration Description (continued)

TAN	DESCRIPTION	TAN	DESCRIPTION
2512-2517	OSC. SLOTTED WASHER OSC. FLAT PIN ON DISK OSC. 3 FLAT ON DISK OSC. 3 PAD ON DISK	3228	FOUR SQUARE GEAR TEST FZG
2518	OSC. CONFORM BLOCK ON RING	4119	BALL BEARING FRETTING FRETTING CORROSION GREASE
2519	OSC. JOURNAL BEARING OSC. SPLIT JOURNAL OSC. PIN AND CONFORM BLOCK	4219	ROLLER BEARING FRETTING TEST
3119	3 BALL MICROFILM ROTATING BALL ON DISK TWO CROWNED ROLLER ROLLING 4 BALL BALL BEARING ASSEMBLY	4318	RECIP. BALL ON FLAT
3219	HYPOLID WALKING CAM GEAR CAM RING ON 2 CYLINDERS TWO ROLLERS (FLAT) ROLLER BEARING ASSEMBLY	4419	RECIP. CYLINDER ON FLAT
		4511-4517	RECIP. SLOTTED WASHER RECIP. FLAT PIN ON DISK RECIP. 3 FLAT PIN ON DISK RECIP. 3 PAD ON DISK

- a) Load – force applied between two moving objects independent to contact and typically perpendicular to the motion.
- b) Pressure – the force that is occurring over the area of contact.
- c) Speed – unit of distance over a period of time or the magnitude of motion expressed in rotations per time interval in rotary applications, linear distance per time interval, or cycles per time interval in reciprocating applications.
- d) Temperature – thermal condition of the test system. Depending on the test design, control of the temperature can be to the individual, contacting test pieces or to the test fluid if present. Also notable is that the temperature at the area of contact may be higher than the bulk, surrounding materials. Precise temperature measurement at the area of contact can be difficult to measure and/or control.
- e) Materials – contacting substances should be selected consistent with those occurring in the field. Special care should be taken to match not only the material, but surface

structure, surface finish, surface and case hardness, and other material properties that exist in the contacting surfaces in the field.

- f) Lubricant or test fluid – fluid material used to remove or control heat at the area of contact or to reduce/or control friction or wear.

#### **Fourth Step – Test Duration**

The duration of a given test will effect the measurable amount of wear that will occur under the previously mentioned test conditions. There are two considerations for determining the duration:

- Preset test duration – test results are compared after all tests are run at the same test conditions for the same duration. Observed test results could be wear rate, total wear, friction force or torque, coefficient of friction and/or temperature effects. The test duration is set to minimize the time for economic reasons but must be long enough to obtain statistically meaningful data [1] and to avoid introducing more aggressive and non-representative wear mechanisms as described [1]. When wear rates are low, longer test duration will be required to effect measurable wear.
- Time to failure – all tests are run under identical test conditions until a measured variable is exceeded or a predetermined point of failure occurs. Test results are reported in time to failure.

The test designer can select test duration to be similar to that, which occurs in the field condition. Sometimes this is not practical and acceleration of the test results is required in order to obtain data in a reasonable time period. This is often accomplished by challenging the test system through the selection of slightly more aggressive test variables. The test designer is cautioned not to overly challenge the test variables as more aggressive wear mechanisms or degradation to the contacting surfaces can result that are not occurring in field. In such cases, test results can have little or no correlation with field results. Conditions can result that can negate the intent of the acceleration and are listed and well detailed [1]. Consequently, the test designer must evaluate the test mechanism failure in the lab during and at the end of the test and verify that it is consistent with the failure mechanism that is occurring in the field.

#### **Simulation versus Ranking**

The goal of the TAN approach is a direct simulation of field conditions of a tribological system. If the test and test conditions are chosen to exactly match those in the field, the surfaces in contact should respond the same in the test as in the field. Therefore, direct correlation with the field results should take place. Should an exact match not be possible, the test designer will have to select a bench test that matches as closely as possible the field condition TAN. Then the test designer will have to select test parameters that will demonstrate differences in a specific test result, such as wear or friction, under the conditions of his modified TAN test system. This is referred to as ranking. Ranking is an effective way of comparing products to identify a particular property and is most practical when employing standardized tests for use in specification

work. The difference between TAN identification from field to bench test is illustrated in Figure 5 [1].

1. IDENTIFY FIELD PROBLEM

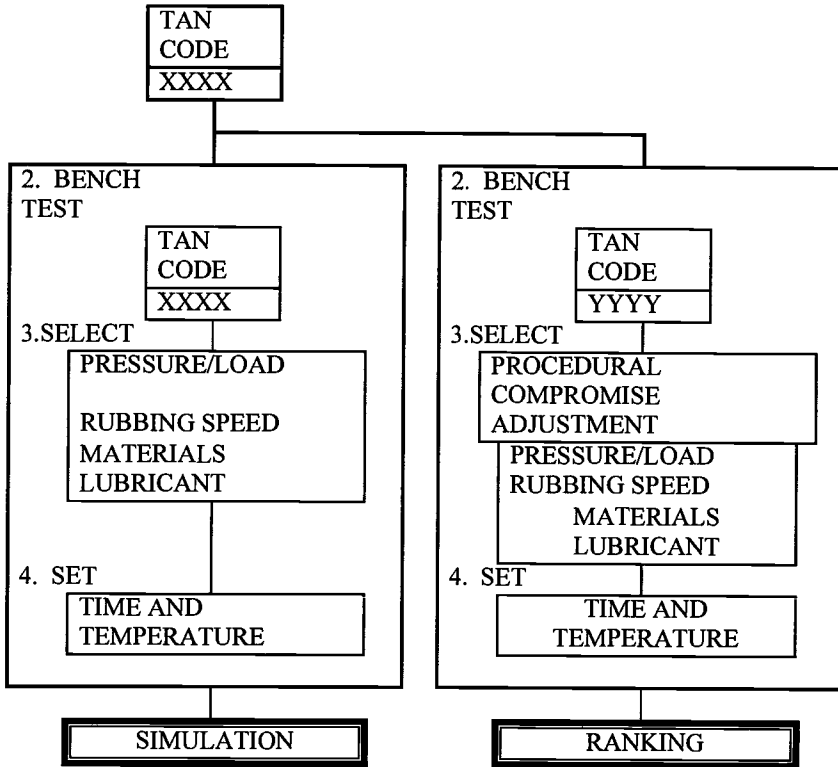


Figure 5 – Procedural Steps – Field Problems to Bench Test Solution

**Specific Development of Tests Using the TAN Approach**

The TAN approach has been used many times when transitioning from the field to the laboratory. The researcher should consider multiple tests to satisfy statistical significance and should not rely on a single test value.

Several examples of bench test selection are described as follows:

- 1) *Disk Brake Material Comparison for Wear Life and Friction* – The TAN for a disk brake system would have a 1 (unidirectional and continuous) for the contact velocity/motion, 5 (area to equal area) for contact area, 1 (unidirectional) for contact pressure/load, 1 (90°->75°) for the entry angle. Therefore the TAN is 1511 and matches nicely with the 3 Pad on Disk test [2], which has an identical TAN. It is possible to consider that the contact pressure should be 3 (cyclic loading). This

would be easy enough to modify in the test setup for load and would be germane for endurance wear testing. For measuring friction or coefficient of friction under discreet times, the TAN of 1511 is accurate. Other considerations for test design: use dry (non-fluid) atmosphere; select speed and load values; and make test pieces from actual materials: pads from disk pads, disk from rotor; finish test pieces consistent with actual parts.

- 2) *Piston Ring Wear Evaluation* - A piston ring against the cylinder wall would have a TAN of 2 (cyclic) for contact velocity; 4 (line to area) for contact area; 2 (high frequency) for contact pressure/load; 4-6 ( $>15^\circ$ - $<55^\circ$ , depending on design). Therefore piston rings have a TAN of 2424, 2425 or 2426. Two tests are available that meet this TAN. Linear reciprocating ring on liner, which has a TAN of 2424. The high frequency load is effected through the loading system and the entry angle is determined by the design of the piston ring as actual pieces of piston rings are used. Additionally, the Piston Ring Adapter for the Multi-Specimen [2] test which has a TAN of 2414. High frequency loading is not possible to attain with this test machine, but sliding tests under maximum load can effect meaningful wear test comparisons. Again because actual piston rings are used, the design of the part actually dictates the entry angle.
- 3) *Friction of Powders and Cosmetic Pastes* - Measuring friction properties of bulk particulate or pastes containing particles in systems moving under load. The TAN for this system would be a 1 (unidirectional and continuous) for contact velocity; 5 (area to equal area) for contact area; 1 (unidirectional) for contact pressure; and 0 (contiguous) for entry angle. The TAN for this field condition is 1510 and would best be represented by the Powder Friction Test run on the Multi-Specimen test machine [2]. Special considerations include the summation of finite contact areas over area yielding an overall test condition of area to equal area. Continuous and constant movement over the particles acts as a contiguous entry angle, for purposes of measuring friction.
- 4) *Face Clutch Test* - Face clutches would have a TAN of 1 (unidirectional and continuous) for contact velocity; 5 (area to equal area) for contact area; 3 (cyclic loading) for contact pressure/load; and 0 (contiguous) for the entry angle. Therefore the TAN is 1530. The thrust washer [2] test having a TAN of 1510 with a procedural compromise of cycling the pressure/load to simulate contact with the face clutch plate allows for a test having TAN 1530. Design of the field service frictional face clutch would dictate precise entry angle (if any) or contact area. Often times, actual field parts can be incorporated into test designs.

## Conclusion

The TAN approach accurately identifies the tribological condition using an analytical procedure with emphasis on an applications approach. Exact simulation is possible by matching the field TAN with the bench test TAN and judiciously selecting test parameters. This approach should give correlation with the field condition. Acceleration is possible and desirable provided the acceleration does not introduce any extraneous conditions having adverse affects on the existing wear mechanisms. Ranking tests can be developed when the TAN for the bench test does not exactly match the identified TAN

for the field condition. Ranking tests are effective when evaluating materials for their performance of a particular property for comparative purposes.

Therefore, the TAN remains an excellent guide for the identification of the tribological condition in the field and offers the ability to select a bench test having a similar tribological condition. This review paper is not intended to alter the original design of the TAN concept but to elucidate its use and practicality when selecting bench tests.

### References

- [1] Voitik, R. M., "Realizing Bench Test Solutions to Field Tribology Problems by Utilizing Tribological Aspect Numbers," *Tribology: Wear Test Selection for Design and Application*, American Society for Testing and Materials STP 1199, A.W. Ruff and Raymond Bayer, Eds., ASTM, Philadelphia, 1993.
- [2] Voitik, R. M., *Solving Problems with Adapters for the Falex Multi-Specimen Test Machine*, Falex Corporation, 1020 Airpark Drive, Sugar Grove, IL 60554, 1995.
- [3] Viotik, R. M., *Tribological Aspect Guide*, Falex Corporation, 1020 Airpark Drive, Sugar Grove, IL 60554, 1993.
- [4] *Falex Condensed Catalog*, Falex Corporation, 1020 Airpark Drive, Sugar Grove, IL 60554, 1998.
- [5] *Catalog of Tribology Test Equipment*, Plint and Partners, Old Station Park, Compton, Berkshire, United Kingdom, RG20-6NB, 1997.

Tsuyoshi Kawazoe<sup>1</sup> and Akira Ura<sup>1</sup>

## Corrosive Wear Testing of Metals in Seawater

---

**Reference:** Kawazoe, T. and Ura, A., “Corrosive Wear Testing of Metals in Seawater,” *Bench Testing of Industrial Fluid Lubrication and Wear Properties Used in Machinery Applications, ASTM STP 1404*, G. E. Totten, L. D. Wedeven, J. R. Dickey, and M. Anderson, Eds., American Society for Testing and Materials, West Conshohocken, PA, 2001.

**Abstract:** The objective of this study is to evaluate the corrosive wear resistance and to clarify the damage behavior of materials used for sliding parts in seawater. Sliding wear tests of six different metals including carbon steel, stainless steel and copper base alloys rubbed against  $Al_2O_3$  and a bearing steel were carried out in 3% NaCl solution using a reciprocating ball-on-disk test rig equipped with an electrochemical potentiostat. The obtained results indicate that the corrosive wear resistance should be evaluated by synthetically considering many factors: electrochemical potentials, material properties, and corrosion characteristics of the contacting materials, including corrosive products.

**Keywords:** tribology, corrosive wear, tribocorrosion, sliding wear, marine corrosion,

### 1. Introduction

Machine parts sliding in seawater incur corrosive wear that causes degradation of the performance and the life of marine machinery. The corrosive wear consists of corrosion, mechanical wear and surface damage due to the interaction between them, whereby corrosion products are repeatedly formed and eliminated corrosion products on the new surfaces exposed by sliding. Several authors have investigated whether corrosive wear depends not only on material properties but also on circumstances and operating conditions; for example, does corrosion accelerate or suppress wear? [1,2,3].

This study was conducted with the aim of evaluating the corrosive wear resistance and clarifying the damage behavior of metals most commonly used for seawater. Six metals (S25C, SUJ2, SUS304, Cu, A1BC3, BC2+0.5%Ni) rubbed against  $Al_2O_3$  and SUJ2 in artificial seawater were investigated using a ball-on-disk type wear test machine and a potentiostat. The obtained results show that sliding wear behavior in seawater is mainly affected by the material properties (hardness and adhesion), the potential difference of the contacting materials, and surface protective and lubricating capabilities of the corrosive products.

---

<sup>1</sup>Associate professor and professor, respectively, Mechanical System Engineering Department, Nagasaki University, 1-14 Bunkyo-machi, Nagasaki, Japan, 852-8521

**2. Experimental Method**

Corrosive wear tests were carried out in accordance with the ASTM G5-71, (ASTM Annual Book of Standard,1971) " Potentiostatic and Potentiodynamic Method,"using a reciprocating ball-on-disk type test rig equipped with an electrochemical potentiostat (Fig.1). A disk of  $\phi 30 \times t 5.5$  mm was rubbed against a ball of  $\phi 19.05$  mm immersed in 3% NaCl solution. The potentiostat was connected to a reference electrode (SCE-Hg/Hg<sub>2</sub>Cl<sub>2</sub> KCl) and a counter electrode(Pt). The solution volume was 200 cc. The normal load was applied by a weight and the friction force was measured using a piezoelectric force transducer. Reciprocating disk motion was provided by a electric motor with a cam and gears.

Materials properties are given in Table 1. Surface roughness of the disk was under  $0.05 \mu m$  Ra, produced by buffing. Table 2 shows the experimental conditions: 30N(max. Hertzian contact pressure contact pressure = 0.95GPa for SUJ2/SUJ2) was adopted as the normal load. The experimental potentials were classified into three kinds of potentials, that is, electrode potential (ELP), cathodic potential (CAP=ELP+500mV) and corrosion potential (COP=ELP+500mv). Wear volume was derived from the section profile of corrosive wear track measured by a profilometer. The surfaces of the test specimen were observed with a scanning electron microscope and chemically analyzed using X-ray photoemission spectroscopy and energy dispersive analysis of X-ray.

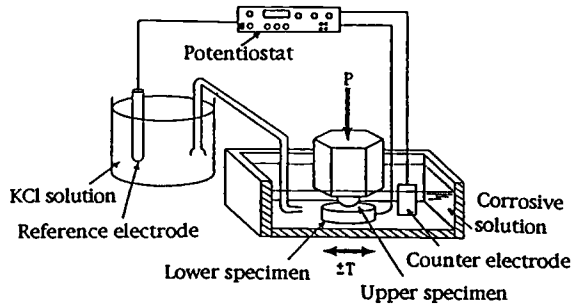


Figure 1 – Schematic of test apparatus.

Table 1 – Properties of test materials

---	Material	Hardness (Hv)	Electrode Potential (mVvs.SCE)
Ball	Al <sub>2</sub> O <sub>3</sub>	1750	-----
	SUJ2	823	-490
Disk	S25C	120	-500
	SUJ2	821	-490
	SUS304	256	-100
	Cu	135	-120
	AIBC3	181	-190
	BC2+ 0.5%Ni	156	-140

Table 2 – Experimental conditions

Normal Load(N)	30
Sliding Velocity (mm/s)	13.3
Sliding distance(m)	40 (2000cycles)
Sliding amp.(mm)	10
Temperature(°C)	25 ± 3
Potentials	CAP,ELP,COP

### 3. Results and Discussion

#### 3.1 Wear

Figure 2 shows the specific wear rate of the disks sliding against  $Al_2O_3$  under three experimental potentials. The specific wear rate ( $W_s$ ) is given by the following equation.

$$W_s = \frac{V}{PL} \tag{1}$$

where  $V$  is wear volume,  $P$  is the normal load and  $L$  is the sliding distance.

The wear of  $Al_2O_3$  was very little because of its high isolation resistance and high hardness. In relation to the potentials, the specific wear rate of all disks increases in the order of increasing corrosion, that is,  $W_s$  at cathodic (CAP) < electrode (ELP) < corrosion potential (COP). It is found that corrosion has a significant effect on the sliding wear in seawater. At the electrode potential where many sliding parts are in the most use for seawater, AIBC3, BC2+0.5%Ni and SUJ2 show low specific wear rate, due to their inherent hardness and corrosion resistance. The cathodic potential has a favorable effect on corrosive wear resistance of all disks. The typical section profiles of the wear tracks sliding against  $Al_2O_3$  are illustrated in Figure 3. AIBC3 and BC2+0.5%Ni show mild wear tracks with smooth surfaces in Figure 3(a) and 3(b). By contraries, S25C has many micro-ditches on the contact surface due to corrosion even at the electrode potential in Figure 3(c), but has higher wear resistance at the cathodic potential in Figure 3(d).

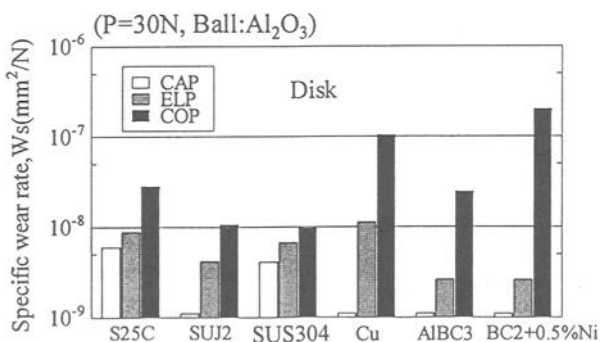


Figure 2 – Specific wear rate sliding against  $Al_2O_3$ .

Figure 4 shows the specific wear rate of the disks and the balls sliding against SUJ2. In contrast to the case of sliding against  $Al_2O_3$ , the corrosion potential (COP) does not always produce the maximum specific wear rate because the SUJ2 material of the ball itself is corroded by seawater. Focusing on the electrode potential, BC2+0.5%Ni and SUJ2 have an excellent corrosive wear resistance, but AIBC3 and Cu exhibit much higher wear rate than the other materials. The same is approximately true for the specific wear rate at the cathodic potential, where the ferrous materials are more effective in reducing sliding wear as compared to the copper base materials.

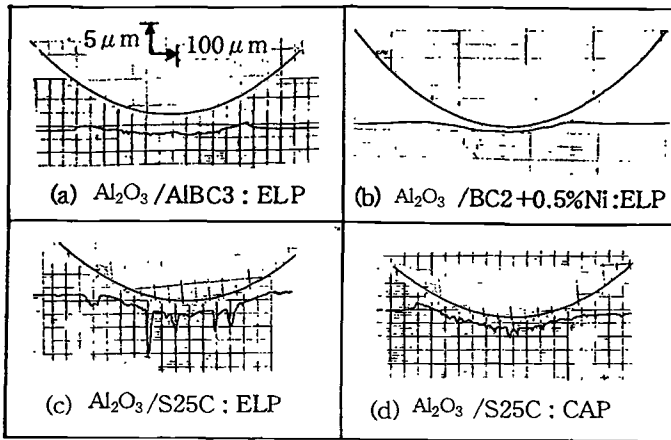


Figure 3 – Section profiles of wear tracks sliding against  $Al_2O_3$ .

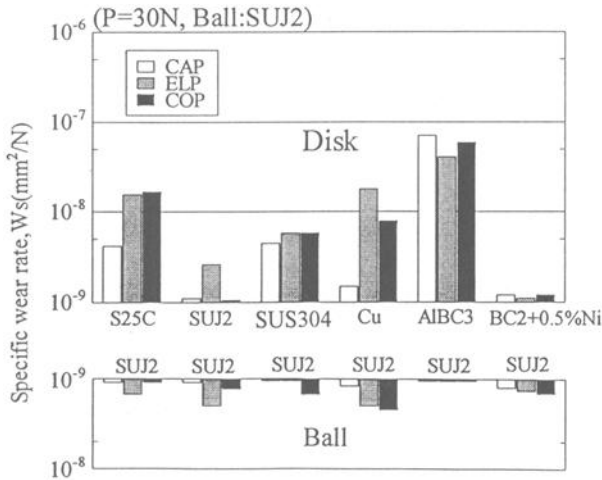


Figure 4 – Specific wear rate sliding against SUJ2.

Figure 5 illustrates the typical section profiles of wear tracks sliding against SUJ2. Since Cu tends to adhere strongly to metals, the wear proceeds through transfer and back transfer of the debris between Cu and SUJ2, and detachment from the surface as shown in Figure 5(a). This phenomenon of strong adhesion is also supported from the measurement of a highly fluctuating frictional coefficient( $\mu$ ) from 0.14 to 0.28 as shown in Figure 8. BC2+0.5%Ni shows almost smooth profile and the lowest corrosive wear rate (Fig. 5(b)). This result is thought to be caused by high corrosion resistance, small adhesive force and lubrication with sea water ( $\mu=0.08\sim 0.14$ ). Thus, BC2+0.5%Ni is in practical use for stern tube bearings supporting marine propeller shafts. AlBC3 presents a large wear track like a circular arc, but the counter specimen of SUJ2 keeps its spherical shape almost without corrosion and wear at the electrode and the cathodic potentials (Fig. 5(c), (e)).

The wear of AlBC3 is accelerated by abrasive wear resulting from many micro-cutting scars on the worn part, observed by SEM as shown in Figure 6. A higher content of Fe element rather than Cu element on the micro-cutting scars was detected by EDX analysis, accordingly it is thought that hard Fe-base  $\kappa$  phase of AlBC3 or hard SUJ2 itself have an effect on the abrasive wear. AlBC3 has been applied to a shaft sleeve lubricated by seawater in a marine machinery part, it is however reported that wear particles from AlBC3 bring about an excessive wear [4]. In case of SUJ2/SUS304, a relatively small wear occurs on SUS304 disk as a result of a competition between breakdown and reformation of  $Cr_2O_3$  surface film due to sliding (Fig.5(d)). Figure 5(f) shows the section profile of SUJ2/SUJ2 at the cathodic potential. Both the ball and disk have no damage in spite of similar metals. This is because of their high hardness, lubrication with seawater and the fact that there is no difference of contacting potential between them.

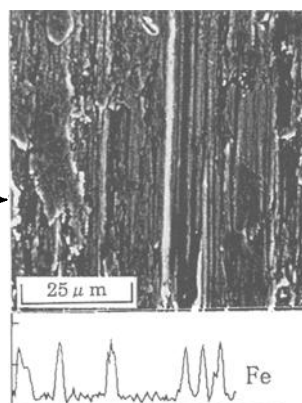
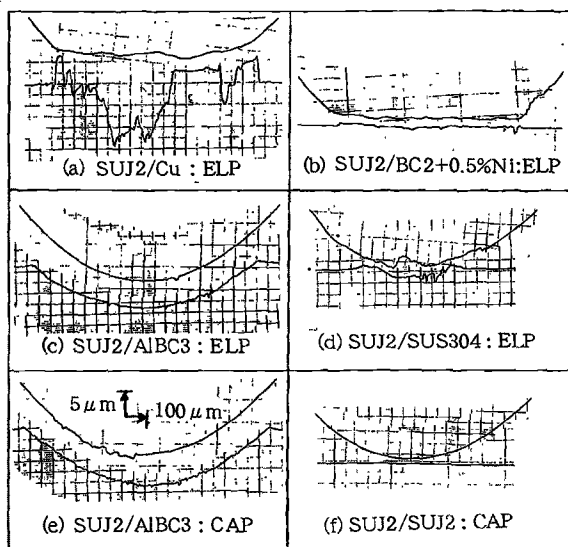


Figure 6 – SEM image & EDX analysis of AlBC3 sliding against SUJ2 at CAP (→Scanning line).

Figure 5 – Section profiles of wear tracks sliding against SUJ2.

3.2 Friction

The effect of the experimental potentials on sliding friction in seawater was examined. Figure 7(a),(b) and 8 show changes of coefficient of friction with the potentials which continuously vary in the order of cathodic, electrode and corrosion potentials. The coefficient of friction during sliding against  $Al_2O_3$  tends to decrease with increase of the potential except for the disk of S25C. Especially Cu and Cu base materials exhibit the above tendency. Considering that the  $Al_2O_3$  ball is electrically isolated and has a low chemical reactivity compared to metals, the corrosion and material properties of the disk itself significantly influences the friction. Accordingly, the analysis of the wear and non-wear tracks by XPS was conducted in order to investigate the relation between friction and corrosion products at the corrosion potential. A lot of  $Cu_2O$  was detected on the wear tracks of the copper materials as shown in Table 3.  $Cu_2O$  film is generally presented as a granular oxide of low cohesive force to the substrate [5]. It is therefore considered that  $Cu_2O$  plays the role of a lubricant and decreases friction. The wear track of S25C includes  $Fe_3O_4$  as a main product and a small amount of  $FeOOH$ . In these products, Mizutani [6] reports that  $FeOOH$  has a tendency to increase friction. Table 3 also shows  $Al_2O_3$  on all the wear tracks which may be transferred from the ball.

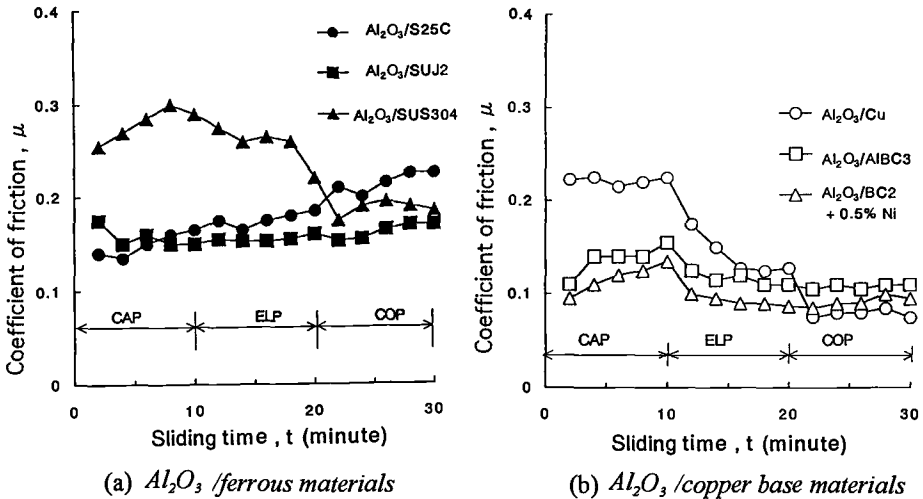


Figure 7 – Coefficient of friction vs. potential(Ball:  $Al_2O_3$ ).

Table 3 - Surface analysis at corrosion potential

Disk	Wear track	Disk	Wear track
S25C	$Fe_3O_4$ , $FeOOH$ , $Al_2O_3$	Cu	$Cu_2O$ , $Al_2O_3$
SUJ2	$Cr_2O_3$ , $Al_2O_3$	AIBC3	$Cu_2O$ , $Al_2O_3$
SUS304	$Cr_2O_3$ , $Al_2O_3$	BC2+0.5%Ni	$Cu_2O$ , $Al_2O_3$

On the other hand, the coefficient of friction during sliding against the ball of SUJ2 is hardly affected by the potentials (Fig. 8). It can be understood that the friction is mainly controlled by SUJ2 which is corroded preferentially rather than the disks of noble metals such as Cu and SUS304. At the same corrosion potential, the coefficient of friction of SUJ2/S25C appreciably decreases as indicated in Figure 8 (symbol(\*)), although  $Al_2O_3$ /S25C somewhat increases in comparison with those of CAP and ELP as mentioned above. It is presumed that this phenomenon is caused by introduction of seawater into the contact: the surface irregularity (Fig. 9) enhanced by corrosion promotes the introduction of seawater resulting in reduction of friction.

Figure 10 shows changes of coefficient of friction with the different ball materials. The coefficient of friction during sliding against SUJ2 is apparently higher than that against  $Al_2O_3$  because of high adhesive force due to metal to metal contact. Resulting from the above-mentioned, the followings should be considered as factors affecting sliding friction in seawater; lubricating capability of corrosion products, introduction of seawater into contact surfaces, adhesive force at contacting materials and increase of contact area with progress of wear.

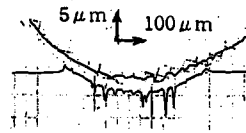
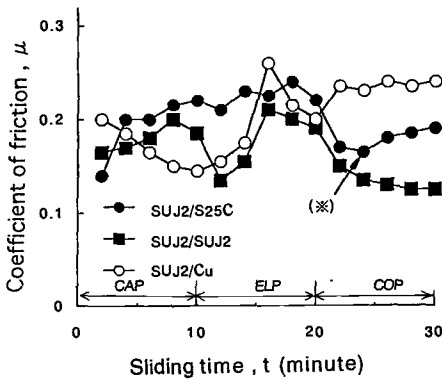


Figure 9 – Section profiles of wear track(SUJ2/S25C).

Figure 8 – Coefficient of friction vs. potential(Ball:SUJ2).

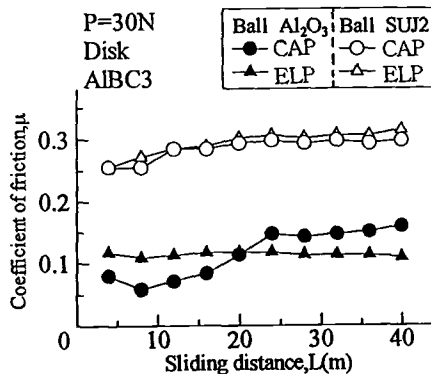


Figure 10 – Typical example of coefficient of friction vs. ball materials. (Disk: AIBC3)

### 3.3 Analysis of Corrosive Wear Depth

Corrosive wear consists of corrosion, mechanical wear and surface damage due to interaction between them. If the ratio of the three factors to the total damage can be analyzed, it serves as an aid to reduce the corrosive wear by focusing on the main factor. Thus these ratios were examined at the corrosion potential, using the damage depth on the disks, measured by a profilometer.

Figure 11 illustrates the example of section profile of disk at the corrosion potential. Relative to a non-corroded region (sealed and coated by adhesive tapes) as a datum surface, the total depth of corrosive wear is described by the following expression.

$$H_t = H_{pc} + H_{mw} + H_{in} \tag{2}$$

where

$H_{pc}$  = depth due to pure corrosion

$H_{mw}$  = depth due to mechanical wear

$H_{in}$  = depth due to an interaction between corrosion and mechanical wear

Here, it may be assumed that  $H_{mw}$  is equal to the depth of damage at the cathodic potential because of difficulty to measure it at the corrosion potential.

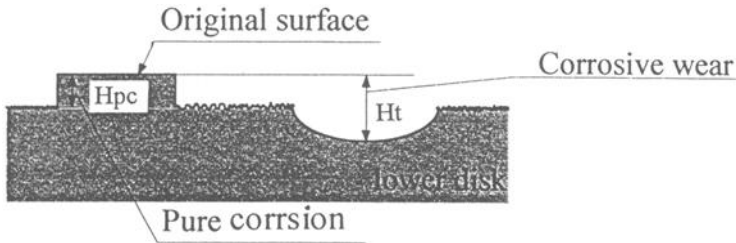


Figure 11— Example of section profile of disk at corrosion potential.

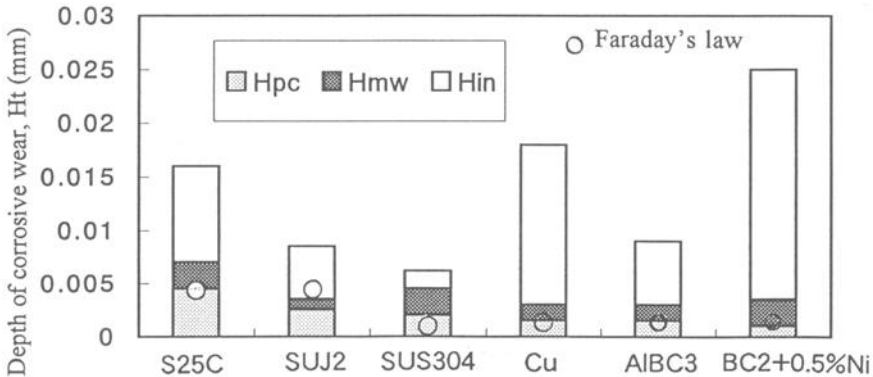


Figure 12 — Classification of corrosive wear depth of disk (Ball:  $Al_2O_3$ ).

Figure 12 shows the depth of corrosive wear of disks sliding against  $\text{Al}_2\text{O}_3$ . The depths of pure corrosion almost agree with the value calculated by Faraday's law [7]. S25C and SUJ2 (the ferrous materials) indicate 30 to 40% as the ratio of pure corrosion to the total depth of damage, which implies a greater effect of their corrosion on the total damage. On the contrary, the copper base materials (being electrochemically noble) show shallow depths due to pure corrosion but a high ratio of the interaction to the total damage. This is thought to be mainly caused by removal of corrosion products such as  $\text{Cu}_2\text{O}$  film from the contact scratched by hard  $\text{Al}_2\text{O}_3$ ; newly activated surfaces are exposed on the copper base materials by sliding friction, where the corrosion products are formed and removed repeatedly resulting from weak cohesive force between the products and the substrate. Especially  $\text{Al}_2\text{O}_3/\text{BC2}+0.5\%\text{Ni}$  including Zn element of high corrosion rate indicates the typical example.

For the disks sliding against SUJ2, the total depth of damage is mainly occupied by mechanical wear because that SUJ2 of the ball protects the disks (except for S25C) from corrosion as a sacrificial anode and increases adhesive forces to the disks.

#### 4. Conclusions

Wear tests of six different metals, including ferrous and copper base materials sliding against  $\text{Al}_2\text{O}_3$  and SUJ2, were conducted using an electrochemical test method in artificial seawater. The obtained results show the following:

- (1) The specific wear rate ( $W_s$ ) of all disks sliding against  $\text{Al}_2\text{O}_3$  increases in the order of increasing corrosion, that is,  $W_s$  at CAP < ELP < COP. For sliding against SUJ2, however, COP does not always give the maximum  $W_s$  because SUJ2 itself is corroded by seawater.
- (2) SUJ2 (of the ferrous materials) and BC2+0.5%Ni (of the copper materials) show higher corrosive wear resistance than the others at the electrode potential regardless of the ball materials, which depend mainly on their high corrosion resistance and low adhesive force.
- (3) The main factors influencing sliding friction in seawater are lubricating capability of the corrosion products, adhesive force between the contacting surfaces, introduction of seawater into the contact, and increase of contact area with progress of wear.
- (4) Classifying the total depth of corrosive wear into pure corrosion, mechanical wear and interaction between them, the ratios obtained depends on the material properties and the corrosion characteristics of the contacting materials.

#### References

- [1] Mishler, S., Debaud, S. and Londolf, D., "The Tribocorrosion of Passive Metals," *Proc of Material Solution on Wear of Engineering Materials*, Indianapolis, 1997, pp. 157-164.
- [2] Iwai, Y., Ito, H., et al., "Wear Behavior of Carbon Steels and Stainless Steels in NaCl or  $\text{Na}_2\text{SO}_4$  Solution," *Transactions of the Japan Society of Mechanical Engineers*, C-62-601, 1996, pp. 248-255.
- [3] Kawazoe, T., Ura, A., and Nakashima, A., "On The Tribocorrosion of Metals," *Proc. of Japanese Society of Tribologists*, Tokyo - D31, 1999, pp. 291-292.

- [4] Nagahata, Y., et al., "Sliding Wear of Copper Base Alloys," *Journal of the Marine Engineering Society in Japan*, 2-6, 1967, pp. 53-59.
- [5] Uhlig, H., Okamoto, G., et al., "Corrosion and Corrosion Control," *Publisher: Sangyo Tosho, ISBN4-7828-3006-8*, 1997, pp. 336.
- [6] Yahagi, Y. and Mizutani, Y., "Corrosive Wear of Carbon and Austenitic Stainless Steels in NaCl Solution," *Wear*, 110, 1986, pp. 401-408.
- [7] Kowaka, M., "Corrosion Damages and Its Protective Methods," *Publisher: Agune, ISBN4-900508-49-7*, 1995, pp. 5.

## **SESSION V: Modeling and Simulation**

Chao Gao,<sup>1</sup> Norm Gitis,<sup>1</sup> Neil Nguyen,<sup>1</sup> and Michael Vinogradov<sup>1</sup>

## **Simulation of Tribological Performance of Coatings for Automotive Piston Ring and Timing Chain in Bench Testing**

---

**Reference:** Gao, C., Gitis, N., Nguyen, N., and Vinogradov, M., “Simulation of Tribological Performance of Coatings for Automotive Piston Ring and Timing Chain in Bench Testing,” *Bench Testing of Industrial Fluid Lubrication and Wear Properties Used in Machinery Applications, ASTM STP 1404*, G. E. Totten, L. D. Wedeven, J. R. Dickey, and M. Anderson, Eds., American Society for Testing and Materials, West Conshohocken, PA, 2001.

**Abstract:** Piston rings with three different coatings were tested on a lubricated cylinder liner for friction force, wear depth, electric contact resistance (ECR) and acoustic emission (AE), using Micro-Tribometer model UMT. UMT was also used to test four types of coatings on timing chain linkage pins to evaluate their scratch resistance with a wedge-shaped micro-blade made of tungsten carbide. Scratch resistance measurements with a diamond stylus of 0.5  $\mu\text{m}$  radius were much less distinctive for the four coatings, as compared to those with the micro-blade. It was found that when the micro-blade broke through the coating on the linkage pins, the AE signal changed more rapidly than the friction force. The friction force could not distinguish tribology performance between Coating 1 and Coating 2, whereas the AE easily differentiated the two coatings. In the testing of piston-ring coatings, it was found that ECR increased with running time during the first half hour or so. It reflected the lubricant buildup at the interface, since the lubricant introduces a much higher electrical resistance. The AE signal was found not always correlated with friction forces, since mechanical interactions contributing to AE are not only along the frictional direction. Good correlation was found for wear depth measured in-situ using UMT and post-test using a Tencor profilometer. Testing repeatability was demonstrated.

**Keywords:** tribology testing, coatings, automotive, friction, wear

### **I. Introduction**

Automotive piston rings and cylinder liners undergo significant repetitive pressures and speeds, challenging their durability and friction properties [1,2]. Similarly, automotive chains must last over years while undergoing various speed and pressure conditions. The durability problems may manifest themselves in increased noise levels, higher friction, power losses, and breakage of chain components, all of which adversely affect engine performance.

---

<sup>1</sup> Center For Tribology, Inc. Campbell, CA 95008

All the apparent signs of the problems usually reflect surface wear that may be due to the variety of wear mechanisms, including multi-cycle fatigue, abrasion, and adhesion. Thus, piston/cylinder and timing chain manufacturers have to employ advanced techniques of surface treatment to ensure high durability of each component at the friction interfaces [3,4]. The correct choice and optimization of those techniques require the most advanced testing methods and equipment. In particular, it is crucial to perform the testing not only with the ideal schematics (like ball-on-disc or stylus-on-disc), but also with the real components, such as chain pins, linkage plates, piston rings, and cylinders.

The tribology tester involved in this paper is called Micro-Tribometer model UMT [5]. It is capable of accommodating a wide range of standard testing modes, as well as, real situation interfaces and test conditions, in addition to measuring a number of parameters relevant to the friction interface. The science of friction, lubrication and wear is tribology. The science of precision repeatable measurements of friction and wear is tribometry. The latest tribological and metrological knowledge have been utilized in the design of UMT. The UMT tester is fully computerized for data acquisition and programming test conditions. This universal and highly precision instrument can accommodate both ideal friction pairs like pin-on-disc, ball-on-disc, 4-balls, pin-on-vee block, ring-on-block, disc-on-disc, and the real industrial assemblies like piston ring on cylinder, screw-in-nut, pin-in-chain, sliding and rolling bearings. It can provide any rotational or linear motions to the parts, in both vertical and horizontal directions, thus simulate their dynamics in the real machines. It measures numerous tribological parameters including:

- friction force, torque and coefficient,
- in-situ wear depth and wear rate,
- contact acoustic emission,
- contact electrical resistance or capacitance.

The force range can be as low as a fraction of mN, or as high as thousands of N. The speed can be as low as a fraction of  $\mu\text{m/s}$ , or as high as 50 m/s. Temperature, humidity, and air pressure at the interface can also be changed. Either a constant or linearly increasing loading force can be applied by an electro-mechanical loading system, via a low-stiffness suspension. Such a loading system is found to be capable of keeping true normal force and having a great advantage in adhesion and scratch resistance study for coatings, as shown in this paper.

Wear depth at the interface was obtained by using a high resolution optical encoder to record the distance of the upper sample traveled during the testing, with a resolution of 20 nm and an accuracy of 50 nm.

High-frequency contact acoustic emission was used in UMT, which provides additional insights into tribological processes. First, it confirms and clarifies friction and wear data, and it relates easily to the wear mechanisms taking place in the interface. Second, being more sensitive than friction to tiny micro-wears, it detects surface degradation and wear earlier. High frequency range is needed for AE sensor, because the mechanical interactions occurred only at contact spots, which can be as small as sub  $\mu\text{m}$ . The frequency of the AE sensor used in our UMT ranges from 200 kHz up to 5 MHz. So low frequency noises from machine vibrations and environment have minimal effect and we do not have to filter these signals. The signal intensity depends mainly on two factors: (a) physical contacts at contact spots (lower speed, more contacts) and (b) contact impact

(lower speed, less impact). Therefore, AE is a complex function of speed, contact material and geometry.

## II. Experimental

### 1. Friction and Wear Test for Piston Rings on A Cylinder Liner

Two sets of experiments were conducted in this paper. The first one was the friction and wear test using UMT for piston rings coated with three different films of  $\mu\text{m}$  thick. Sample ID is labeled as Coating 1, Coating 2 and Coating 3. The testing Procedure for piston-ring and cylinder-liner is as follows:

Piston ring held stationary  
 15 Hz reciprocating of the liner sample  
 25.4 mm (1 inch) stroke (reciprocation distance)  
 One drop of SAE 5W-30 oil (~0.1 ml) at the interface  
 3 to 80N (8Kg) normal load  
 10 minutes of running in and 2 hours of testing time.

Using UMT to Measure  
 Coefficient of Friction  
 Wear Depth  
 Acoustic Emission  
 Contact Electric Resistance  
 Post-test Wear Depth measured by Tencor Profiler

Each tested piston ring was mounted on a two-dimensional load/friction sensor (upper specimen) with a custom holder. The liner sample was mounted horizontally on a reciprocating platform (lower specimen). The piston ring was stationary, while the holder with the liner sample was in a reciprocating motion to simulate the real situation of a cylinder-piston pair. A constant load was applied onto the piston ring by means of an electro-mechanical loading system via a low-stiffness suspension. Vertical load  $F_z$ , friction force  $F_x$ , wear depth  $WD$ , acoustic emission signal  $AE$  and electric resistance  $ECR$  were continuously measured and monitored, as well as recorded in data files. After each test the scar depth on the liner samples were also measured using a Tencor surface profiler. Scar depth on the ring was a difficult task for the Tencor Profiler due to the arch (curvature) on the ring along the circumferential direction. All the tests were performed at ambient temperature of  $23^\circ$  and relative humidity of 60%. Three runs were repeated for the same piston ring on different parts of the liner.

### 2. Scratch Test for Linkage Pins against a Diamond Stylus and A Micro Blade

In this experiment, linkage pins with four various coatings for timing chains are tested against a diamond stylus of about  $1\ \mu\text{m}$ -radius tip and also against a micro blade made of tungsten-carbide with wedge shape of about 0.5 mm wide and of about  $0.5\ \mu\text{m}$  sharp. The 4 coatings are labeled as Sample 1, Sample 2, Sample 3 and Sample 4, respectively.

Two pieces of each pin, a total 8 samples, were tested for scratch resistance using diamond stylus with a 5-micron-radius tip. Two pieces of each pin, a total 8 samples, were tested for scratch resistance, this time using a carbide blade with a flat-edge.

Each tested pin was mounted horizontally on a custom-supporting table (lower specimen). The scratching tools in the form of either a blade or stylus were mounted on a two-dimensional load/friction sensor (upper specimen) with a special holder. The pin was stationary while the holder with a stylus or blade was moved along the length of a pin by a motorized lateral sliding stage with constant speed. A linearly increasing vertical load was applied onto the blade/stylus holder by means of an electro-mechanical loading system via a low-stiffness suspension. Vertical load  $F_z$ , friction force  $F_x$  and acoustic emission signal  $AE$  were continuously measured and monitored, as well as recorded in data files. After each test the scar depth was measured using a Tencor surface profiler.

Testing procedure was as follows: The loading system applied a linearly increasing load from 0.5 mN up to 150 mN on the diamond stylus, and from 0.1 N up to 40 N on the micro-blade within 40 seconds, respectively, while the scratch tool moved against the pin surface at a speed of 0.1 mm/s. All the tests were performed at ambient temperature of 23° and relative humidity of 60%.

### III. Experimental Results and Discussion

#### 1. Friction and Wear Results for Piston Rings on A Cylinder Liner

In Figure 1, typical coefficient of friction (COF), wear depth at the ring-liner interface, acoustic emission (AE) and electric contact resistance (ECR) are shown as a function of testing time for Coating 1 on Liner 1A. At about 30 minutes, there was a valley in COF, while a peak occurred at the same time for AE. Further examinations revealed that a peak in ECR also occurred at that running time and wear rate (slope on the wear depth) became smaller. Similarly obtained data for other two coatings are summarized in Table I with WD, also measured using a Tencor profiler with a tip radius of 0.5  $\mu\text{m}$ .

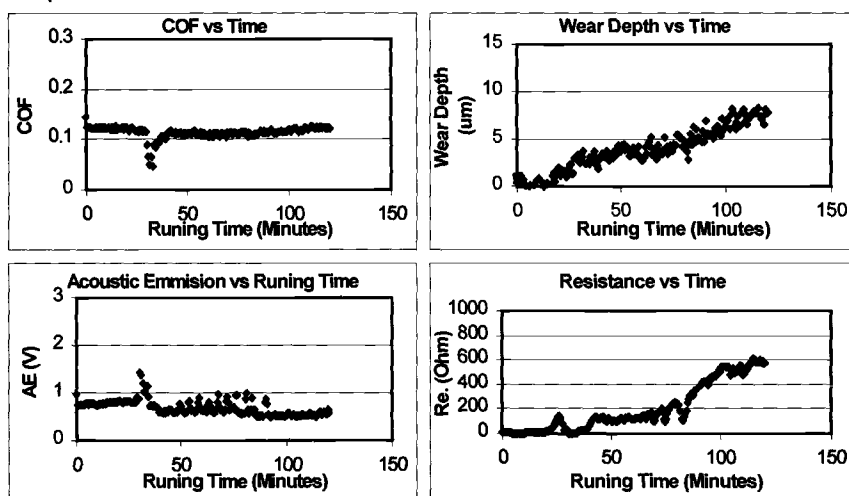


Fig. 1, COF, WD, AE, ECR for Coating 1 on Liner 1A

Table 1, *Summary of Friction and Wear Tests for Piston Rings on A Cylinder Liner. Loading force was set at 80 N and about 0.1 ml of SAE 5W-30 oil was used at the interface. The motion was set for a 25.4 mm stroke at 15Hz. Each coating was tested three times on a liner, at three locations noted as A, B, C.*

Ring Coating	Coating 1			Coating 2			Coating 3		
Cylinder Liner	1A	1B	1C	2A	2B	2C	3A	3B	3C
Friction Coefficient	0.12	0.1	0.1	0.1	0.07	0.1	0.08	0.07	0.1~0.2
Wear Depth (µm) by UMT	8.0	4.0	3.5	5.0	6.0	5.0	5.5	4.5	6.5
Liner Wear Depth (µm) by Tencor	6	3	3	3	2.5	3	3	2	3
Coating Wear Depth (µm) by Tencor	Appears minimum by optical examination. Cannot be reliably measured using Tencor due to the arch (curvature) on the ring along the circumferential direction. May consider Roundmeter from Taylor Hobson, England, for this purpose.								
Acoustic Emission (V)	0.7	0.8	0.9	0.9	0.7	0.6	2.5	1.9	2 - 3
Resistance (Ohm)	600	1000	600	800	800	800	600	1000	1000

It is obvious that AE is much higher for Coating 3 than that for Coating 1 or 2. COF and WD are not much different. Good correlation for WD measurements is found using UMT and Tencor profiler. Notice that WD by UMT, is somewhat larger than that by Tencor profiler. This is not surprising, since some wear depth on the piston ring was expected, noting that UMT measures total WD at the interface.

To further explore the differences in these three coatings on piston rings, the friction and wear experiments were conducted for smaller loads, the same testing conditions for Figure 1 or Table 1. Coefficient of Friction and Acoustic Emission are shown as function of normal loads in Figure 2 and in Figure 3 respectively, for piston ring against a cylinder liner. Testing time for each load was set for 15 minutes. The repeatability was good for both COF and AE. COF decreases with increasing loads, about 5N, and then more or less remains constant. AE increases with increasing loads. From COF, Coating 1 has best performance, whereas from AE, Coating 2 exhibits best performance. More studies are needed to really differentiate between Coating 1 and Coating 2. Measurements for multiple relevant parameters are needed for tribology evaluation of friction pair. Both COF and AE indicate Coating 3 is a bad choice for ring Coating. AE signal was not necessarily correlated with friction forces, since mechanical interactions contributing to AE is not only along the frictional direction.

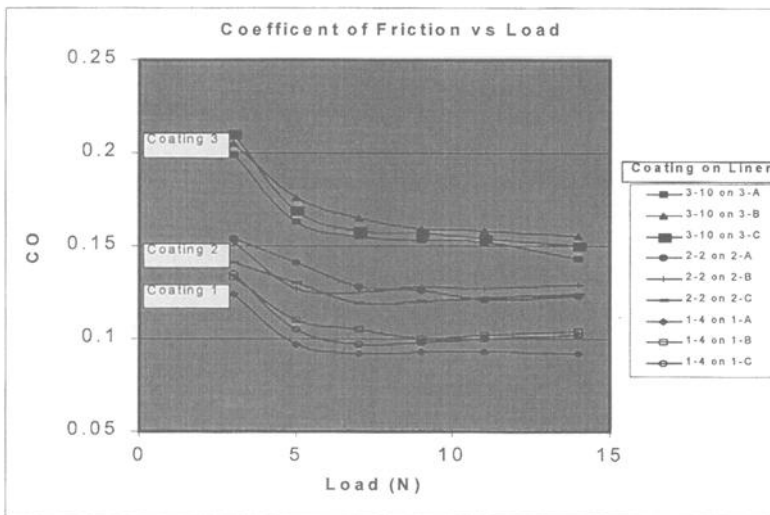


Fig. 2, Coefficient of Friction vs Load for ring coatings against a liner.

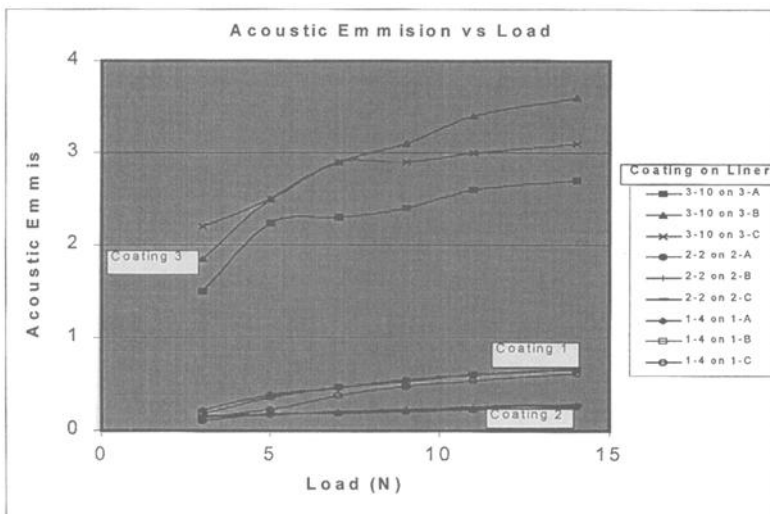


Fig. 3, Acoustic Emission vs. Load for Ring Coatings against a liner.

## 2. Scratch Results for Linkage Pins against a Diamond Stylus and A Micro-Blade

Coefficient of Friction and Acoustic Emission are shown as functions of normal loads in Figure 4 and Figure 5 respectively, for linkage pins against a diamond stylus. The normal loads were linearly increasing from 0.5 mN to 150 mN over a period of 40 seconds

as the stylus moved at a speed of 0.1 mm/s. When normal loads were more than about 150 mN, the stylus broke. There were no significant differences in COF among these four coatings. All increased with normal loads. These increases could be due to the plowing effect since the stylus tip penetrated deeper with increasing loads. There were also no significant differences in AE among these four coatings. All were more or less consistent. This agrees with COF observation since the coatings were not broken by the stylus tip.

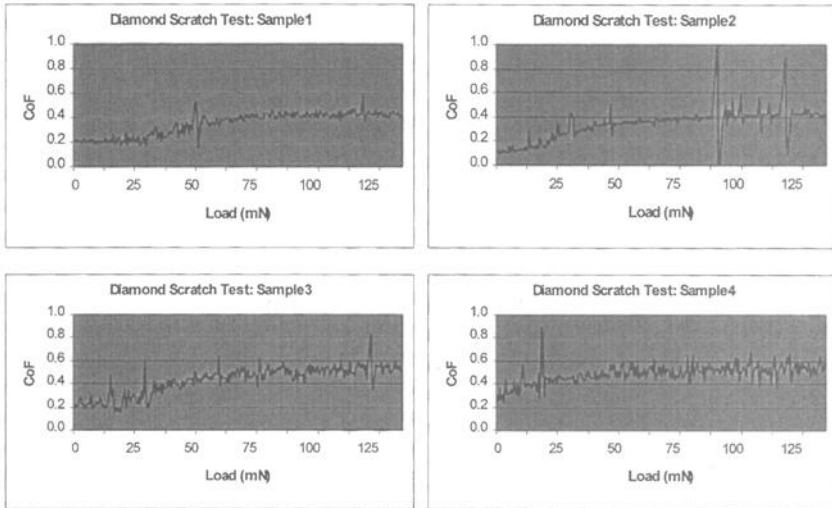


Fig. 4, Coefficient of Friction vs. Load Using Diamond Stylus for Sample 1 – 4

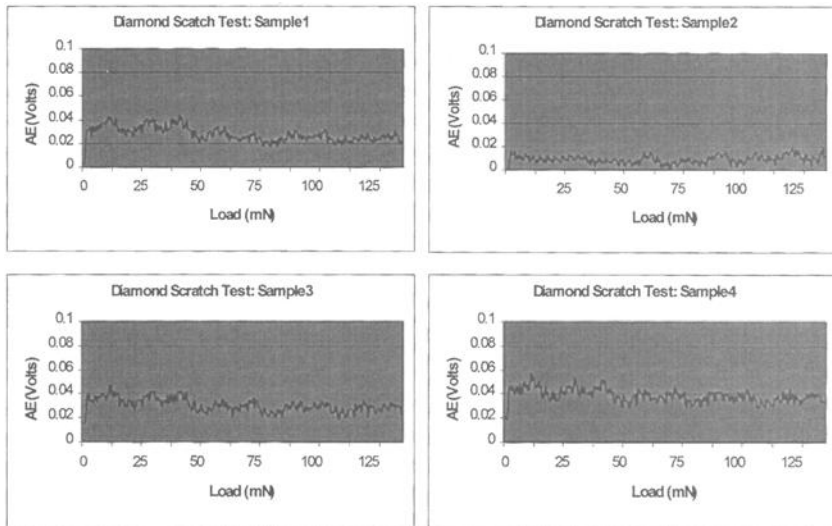


Fig. 5, Acoustic Emission vs. Load Using Diamond Stylus for Sample 1 – 4

Now, turn to micro-blade made of tungsten carbide for scratch tests. In Figure 6 and Figure 7, Coefficient of Friction and Acoustic Emission are plotted as functions of normal loads respectively. This is for linkage pins too, but against a micro-blade instead of a diamond stylus. From the COF, Sample 4 is rated as the worst and Sample 3 as the second worst, but it is more difficult to differentiate Sample 1 from Sample 2. This is no longer the case with AE data available, as shown in Figure 7. Sample 2 is superior over Sample 1, as AE data shows. AE data rates Sample 4 as the worst (in agreement with COF rating), Sample 3 as the second worst (also in agreement with COF rating). Combining both COF and AE data, concludes Sample 4 is the worst coating, Sample 3 the second worst, Sample 2 the best and Sample 1 the second best, in terms of tribology performance.

From the distinctive effectiveness for scratch resistance evaluation of micro-blade over diamond stylus, the sharp stress distribution at the contact spot is a more important parameter as compared to contact pressure in scratch.

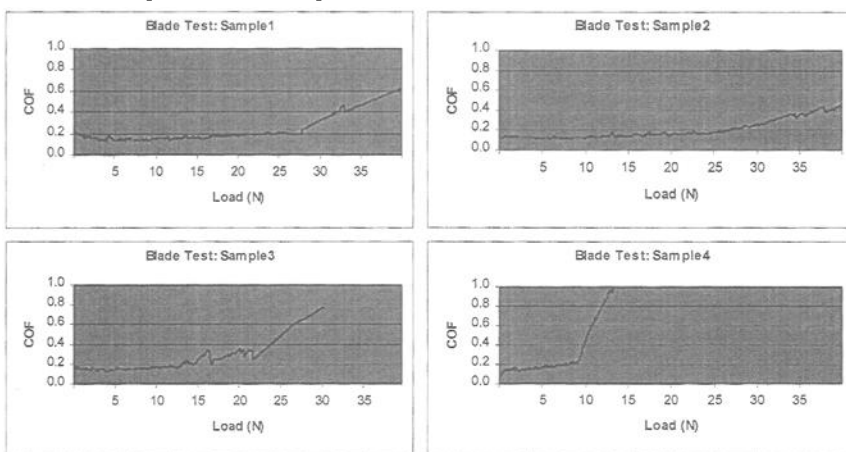


Fig. 6, Coefficient of Friction vs. Load using Blade Test for Samples 1 – 4.

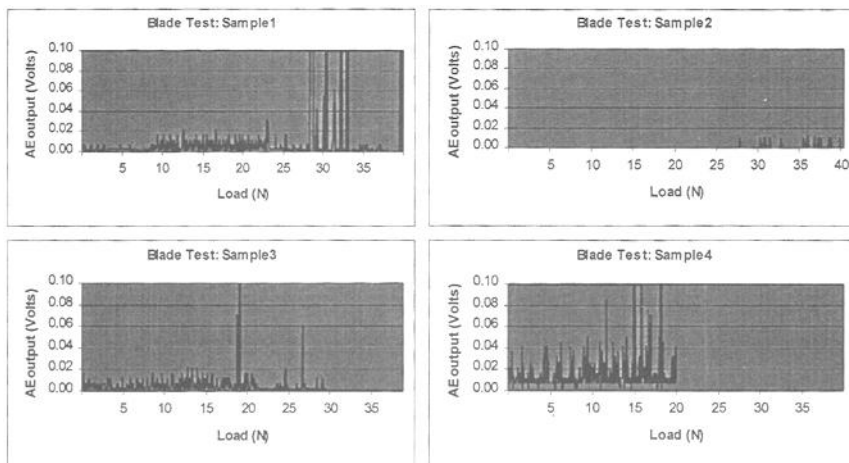


Fig. 7, Acoustic Emission vs. Load using Micro-Blade Test for Samples 1 – 4.

#### IV. Conclusions

From friction, wear, acoustic emission and electric contact resistance data generated using the Micro Tribometer, the following conclusions can be derived:

1. Good data repeatability is found for UMT, as demonstrated in Figures 2 and 3, as well as in Table I. Good correlation in wear measurements between in-situ UMT and post-test Tencor profiler was demonstrated in Table 1.
2. AE was found to be more sensitive than COF. Quite often, COF alone could not differentiate friction pair for designers, as demonstrated in Figures 6 and 7. AE was very useful not only in these cases as a tiebreaker, but also to significantly improve confidence level for conclusions drawn from the COF data.
3. Electric contact resistance was the most sensitive probe at the interface. In the case of piston ring against a cylinder liner, it may provide insights on how lubricant gets into the moving interface.
4. There is reasonable correlation between the measured parameters (COF, WD, AE, ECR) at the friction interfaces. Namely, the signals are complementary and confirmative to each other.
5. In the friction and wear tests for piston ring with three coatings on a cylinder liner, Coating 1 exhibited the best overall tribology performance, whereas Coating 3 exhibited the worst. AE signal from Coating 3 on the liners indicated a high mechanical interaction at the interface, which may cause long-term durability and noise problems.
6. In the scratch tests for timing chain linkage, a diamond stylus was found ineffective for evaluation of scratch resistance for the four coatings, whereas the micro-blade was very effective, with AE capability.

#### References

- [1] Hyde, G.F. Cromwell, J. E. and Barnes, "Piston Ring Coatings for Internal Combustion Engines", SAE Paper 790865.
- [2] Ku, Y-G. and Patterson, D. J., "Piston and Ring Friction by the Fixed Sleeve Method", SAE Paper 880571.
- [3] Plint, M. A. and Allison-Greiner and A. F., "Routing Engine Tests-Can We Reduce Their Number?," *Petroleum Review*, July, 1990, pp 368-370.
- [4] Uras, H. M. and Patterson, D. J., "Oil and Ring Effects on Piston-Ring Assembly Friction by the Instantaneous IMEP Method," 1985, SAE Paper 850440.
- [5] Gitis, N., March, *Lubrication Engineering*, Vol. 54, 1998, No.3.

Lavern D. Wedeven<sup>1</sup> and Eric Hille<sup>2</sup>

## **Tribology Testing for Load Carrying Capacity of Aircraft Propulsion System Lubricating Oils**

---

**Reference:** Wedeven, L. D. and Hille, E., "Tribology Testing for Load Carrying Capacity of Aircraft Propulsion System Lubricating Oils," *Bench Testing of Industrial Fluid Lubrication and Wear Properties Used in Machinery Applications, ASTM STP 1404*, G. E. Totten, L. D. Wedeven, J. R. Dickey, and M. Anderson, Eds., American Society for Testing and Materials, West Conshohocken, PA, 2001.

**Abstract:** A tribology testing capability has been developed to provide a closer link between bench testing and performance in component hardware. The new test capability enables simulation of lubrication and failure mechanisms that control the life and durability of lubricated contacts in machine hardware. The key feature associated with simulation is the independent control of entraining velocity and sliding velocity. The Wedeven Associates, Inc. test machines (WAM) control the motions and forces of a single contact in 3-dimensional space. The machine software links the operator to the machine with tribologically meaningful parameters. The value of this approach is shown by test protocols developed for the evaluation of aircraft propulsion oils. The test protocol simulates the Ryder Gear Test Method, which is based on a scuffing performance criterion. The inclusion of traction (friction) measurements is found to reflect wear and a superficial form of scuffing (micro-scuffing). The test method illustrates the performance of U.S. Navy oils formulated for corrosion inhibition (CI). In addition to additive chemistry, the results show the chemical contribution of the base stock with respect to wear and scuffing resistance.

**Keywords:** aircraft propulsion oils, bench testing, lubrication, scuffing, scuffing performance, traction (friction), tribology, wear

---

<sup>1</sup> President, Wedeven Associates, Inc, 5072 West Chester Pike, Edgmont, PA 19028-0646.

<sup>2</sup> Aerospace Engineer, Naval Air Warfare Center, Bldg 2360, 22229 Elmer Road, Unit 4, Patuxant River, MD 20670.

## WAM Test Technology for Lubricated Contact Simulation

### *Introduction*

Tribology testing is an integral part of problem solving and the development of new lubricants, materials and surface technologies. The effectiveness of tribology testing is directly linked to the rate at which problems are solved and new technologies are developed. Because of this, the selection and capabilities of tribology tests have an enormous economic impact.

Tribology tests generally have two practical purposes: (1) they provide fundamental material property data as well as mechanistic understanding, and (2) they are used to predict performance in service. For any test to have practical value, there must be a clear link between testing and hardware performance. This is by far the greatest challenge. The challenge associated with this task is due to the complexity of a tribological contact system and the mysterious changes in the system created by chemical, material and geometric interactions during operation. An effective linkage between testing and hardware performance can only be obtained with suitable simulation of the mechanistic processes that control performance. In most cases, it is more important to simulate lubrication and failure mechanisms than it is to simulate the mechanical parameters of loads and speeds of component hardware. An important ingredient in test simulation is the pathway to failure. Performance limits of bearings, gears and other component hardware are defined as much by the lubrication and deterioration mechanisms on the way to failure as by the final failure mode itself.

Tribology testing can be made more effective with flexible test machines that invoke and control a wide range of lubrication and failure mechanisms. The objective of this paper is to describe the key features of an effective tribology testing technology [1]. The new technology has been realized through the development of five generations of test machines (WAM1 – WAM5). The technology is illustrated with an example involving the simulation of the Ryder Gear Test Method for the qualification of aircraft propulsion oils.

### *Approach to Tribology Testing and Hardware Simulation*

The contacting bodies in every component can be viewed as a tribological system composed of four structural elements that control its tribological success. Starting from the internal elements of a contact interface, these structural elements are: (1) the hydrodynamic or elastohydrodynamic (EHD) generated film; (2) the boundary lubricating surface films; (3) the near-surface material and (4) the subsurface material. Each of the structural elements performs specific functions during operation. Collectively they embody the durability of the contact. An appropriate test must create these structural elements and invoke the lubrication and failure mechanisms that control performance in component hardware. The creation of these structural elements starts with selection and fabrication of representative test specimens.

The control of lubrication and failure mechanisms is derived from the consideration of three factors. First, the recognition of the powerful role the inlet region has on the generation of an EHD film and its ability to precisely control the overall separation between the surfaces. Second, the recognition that the control of stress and strain within a Hertzian contact is a key element affecting the thermal, chemical and mechanical failure processes. The third item is associated with an ability to independently control the conditions within the inlet and Hertzian regions so that a large range of lubrication and failure phenomena can be simulated. The independent control of the conditions in the inlet and Hertzian regions is accomplished by controlling both the surface velocities of the test specimens as well as the angle between their velocity vectors. Surface separation is controlled by the entraining (or rolling) velocity vector. The entraining velocity is defined as one-half the vector sum of the surface velocities. The strain within the Hertzian region is controlled by the vector difference between the surface velocities. A key feature of the WAM technology described below is the decoupling of the inlet and Hertzian regions. This is accomplished by control of the surface velocities and their directions. This approach allows the entraining velocity in the inlet region to become independent of the sliding velocity in the Hertzian region.

*WAM Test Machine Technology*

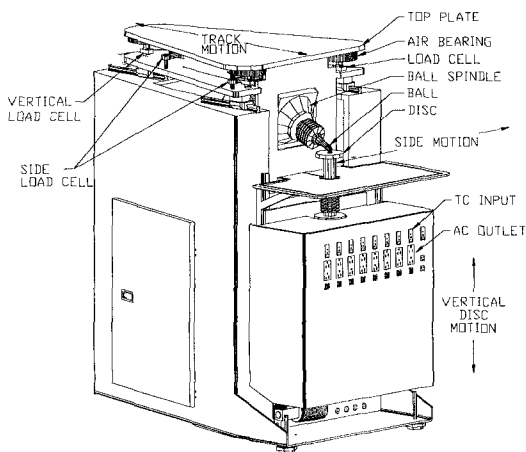


Figure 1 - Isometric drawing of WAM4 tribology test machine

A schematic of the WAM4 test machine is shown in Figure 1. The machine is capable of controlling the entraining velocity, sliding velocity and bulk temperature of the specimens independently. Ball and disc specimens are generally used when the desired materials and finishes are available. Custom designed crowned rollers are used in place of ball specimens when special materials or surface finishes are required.

Both specimens are mounted in motorized spindles. The motors are servo-controlled with drive system electronics that give precision control of rotational position, angular velocity and angular acceleration. The relative position of the specimens can be arranged to change the orientation of the surface velocity vectors of the two specimens at the contact point, as shown in Figure 2. This feature provides independent control of the entraining velocity and sliding velocity. The spindles are said to be aligned when the velocity

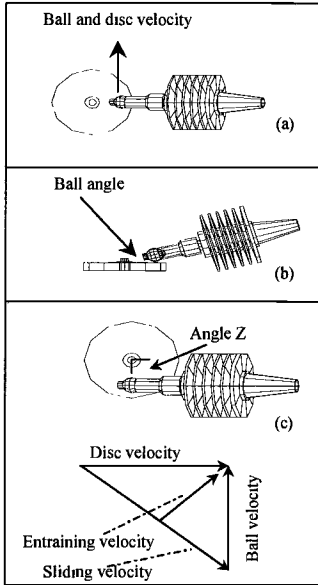


Figure 2 – Ball and disc contact

vector of the ball is collinear with the velocity vector of the disc at the point of contact (see Figure 2a). To obtain pure rolling across the contact interface, the axis of the ball is tilted (see Figure 2b).

The test machine allows the direction of the velocity vectors to be changed by moving away from the aligned position. Figure 2c shows the ball and disc positioned where their surface velocity vectors are perpendicular to each other. The angle  $Z$  between the ball and disc velocity vectors can be continuously varied between 0 and 180°. The entraining velocity and sliding velocity vectors are illustrated in Figure 2c. The entraining velocity is defined as one-half the sum of the ball and disc velocity vectors. The sliding velocity is defined as the vector difference between the ball and disc velocity vectors. The ability to vary surface velocities in direction and magnitude provides a large range of entraining velocities and sliding velocities. The independent control of entraining velocity and sliding velocity allows the formation of EHD film separation between the surfaces to be made independent of the tangential strain within the contact. The decoupling of film thickness from tangential

strain provides the opportunity to control EHD and boundary lubrication mechanisms, along with their failure pathways.

The test machine is capable of independently controlling the bulk temperatures of the test specimens. Specimen temperatures are monitored with trailing thermocouples and controlled with a multi-channel PID temperature controller.

The disc specimen is loaded against the ball with a stepper motor driven actuator. Contact load and friction forces are measured using load cells positioned in three orthogonal directions. The ball spindle is suspended below the top plate, which is supported in the vertical direction by air bearings. Load cells, which are positioned in a horizontal plane, provide friction force measurements in both X and Y directions. Load cells positioned under each air bearing are used to measure the vertical force on the contact.

The machine provides a number of mathematical calculations to translate between the tribological parameters and fundamental machine movements. A host computer translates the user's commands into basic machine functions. The computer has control over the position of the ball in relation to the disc, as well as the rotational speeds of the two specimens. The computer can move the ball spindle in the plane of the disc using a set of stepper motor driven ball screws. Position feedback is received from linear encoders mounted on both axes. This real-time feedback automatically corrects for some of the deflections within the machine due to friction forces. The computer can

move the ball concentric with the disc axis of rotation using circular interpolation. This feature allows the angle between the velocity vectors to be changed during operation. Both hardware and software allow precision control of the contact kinematics.

The WAM software is developed to provide a flexible operator interface and programmable control. The machine is manually operated from a keyboard and mouse. Approximately seventy variables can be monitored or controlled. A basic screen format Figure 3 provides ten boxes to display variable names and values. The variable names and values can be changed at any time. The ten digital boxes provide the major communication link between the operator and the test machine. Up to ten variables can be saved to a file. Test protocols are easily programmed. Because of test protocol complexities and precision requirements, most tests are conducted from automated run files.

Above the buttons on the screen is space for graphical displays of test variables to be plotted during testing. Up to four dependent variables can be plotted simultaneously.

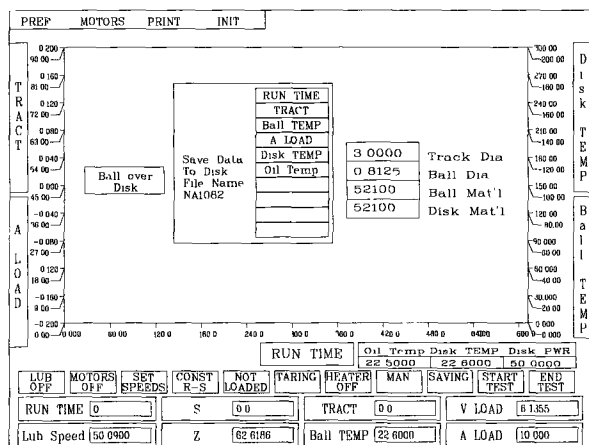


Figure 3 – WAM test fixture computer screen

The axis scales for the dependent and independent variables can be varied and changed at any time during a test. The horizontal axis will scroll to the right and left if the displayed values go out of range. The configuration of the numerical boxes at the bottom of the screen, and the axis scales can be saved to a file for subsequent testing. While the test is running, graphically displayed

values are updated in their selected colors once each period. At the top left of the screen is a set of pop-up menus that are used to change various configurations and to provide miscellaneous house-keeping functions. The machine and software provide a highly flexible testing environment for tribological simulation of component hardware.

### WAM Load Capacity Test Method for Aircraft Propulsion Oils

#### Background

The Ryder Gear Test Method provides a scuffing or load capacity rating for aviation oils. The load capacity rating is derived from a scuffing criteria, which is one of several surface deterioration mechanisms controlling life and durability of bearing and gear hardware. Through its use over many years as a qualification test, the Ryder

Gear Test Method has developed a large database. The database provides a historical record for oil lubricating performance.

Under U.S. Navy sponsorship WAM test machines have provided Ryder-like load capacity data of gas turbine and gearbox oils. These efforts also expand the scope of oil characterization beyond the narrow perspective of a pass/fail or ranking of oils, with scuffing performance the only criteria. To provide a continuity between Ryder Gear load capacity data and future oil characterization methods, a "WAM Economical Load Capacity Screening Test" was developed to rank a wide range of engine and gearbox oils similar to the Ryder Gear Test Method [2]. This test method ranks oils with respect to a scuffing failure event. It also characterizes oils with respect to traction (friction) behavior.

The introduction of high thermal stability (HTS) oils, and particularly corrosion inhibited (CI) oils, has highlighted the need for testing sensitivity for low lubricating performance oils. Low lubricating performance, as evidenced in the Ryder test, reveals itself in the form of a superficial form of scuffing ("micro-scuffing").

The test protocol described below was developed partially under U.S. Navy PO No. N00421-98-M-6001. The test conditions selected highlight the load capacity performance features of low-performing oils that are submitted for qualification under the MIL-PRF-23699 specification. Load capacity tests are conducted with ball and disc specimens, which are operated under conditions similar to the U.S. Navy Ryder Gear Test Method.

### *Objective*

The purpose of this test method is to rank oils according to the Ryder Gear Test Method, with enhanced sensitivity for low lubricating performance. It is important to recognize that the Ryder Gear performance criteria are based upon visual observations of scuffing damage on the Ryder gear teeth. Since some scuffing features found on Ryder gear teeth are superficial, a Ryder-like test method must also invoke the same type of surface deterioration mechanism. Micro-scuffing is a superficial form of scuffing, which is confined to the surface topographical features of the gear teeth. Micro-scuffing is generally associated with surface damage at low load stages where contact stresses are too low to cause "macro-scuffing". Scuffing, or macro-scuffing, is associated with the complete loss of surface integrity. Scuffing involves gross failure of near-surface material, in addition to surface roughness features.

The effectiveness of lubrication over a range of contact temperatures can be determined by monitoring the traction coefficient. While "traction coefficient" and "friction coefficient" have the same definition, we prefer to use "traction" when dealing with contacts that have a combination of rolling and sliding motion. "Friction" is reserved for simple sliding, where the same area of one body is always in continuous contact. When traction (friction) is measured, micro-scuffing is generally detected by a rapid decline in traction coefficient. The decline in traction coefficient is associated with the removal of surface roughness features. While this action actually restores some of the EHD fluid film separation between the surfaces, the rapid removal of surface features by plastic flow and rapid polishing wear reflects a failure of the oil to

provide adequate surface films for boundary lubrication. In contrast, macro-scuffing is associated with a sudden increase in traction coefficient due to massive adhesion and plastic flow of near surface material. A sudden and massive scuffing failure requires high contact stresses in the presence of high sliding velocities.

The observation of traction coefficient during a load capacity test is quite informative. High precision measurements of traction coefficient clearly identify “events” like scuffing and micro-scuffing, as previously discussed. Traction behavior reflects the continual interactive process between oil chemistry and the contacting material pair. Subtle changes in topographical features due to wear are reflected in traction behavior.

This test method is a simulation of Ryder Gear Test ranking. The test conditions are carefully selected to make the results correlate with the Ryder Gear Test. While the Ryder Gear Test operating conditions, in terms of rolling/sliding speeds, temperatures and contact kinematics, are representative of helicopter gearbox hardware, slight operational changes are likely to cause different ranking. This is based on WAM load capacity tests conducted over a range of test conditions, which affect EHD film generation and contact temperature. Load capacity tests over a range of conditions are recommended. The conditions selected here are specific to Ryder ranking using a set of five reference oils supplied by the U.S. Navy. In addition, there is no confirmation that scuffing load capacity performance is in any way connected with other prominent life-limiting performance criteria, expressed as surface distress (wear and micro-pitting). Additional tests for surface distress, or a complete simulation of specific hardware, are recommended to supplement scuffing load capacity results.

#### *Test Approach*

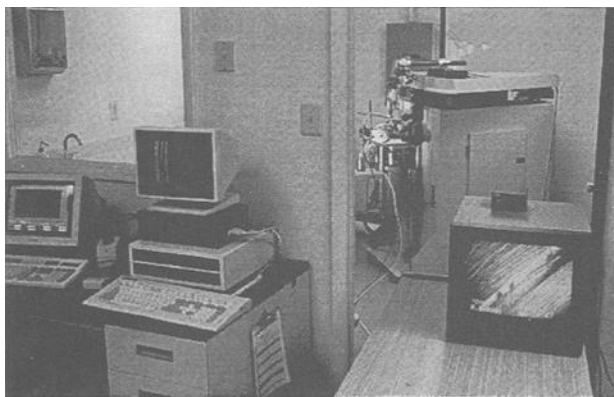


Figure 4 - *WAM Test Facility*

The load capacity test protocol is conducted with a WAM test facility shown in Figure 4. A computerized run file controls load and contact kinematics between the specimens. Specimen temperatures are recorded with trailing thermocouples. The high-speed test protocol uses AISI 9310 ball and disc specimens with tight

specifications for surface finish and hardness. To capture Ryder-like oil performance features, the following test specimen specifications and test conditions have evolved.

Ball	2.0638 cm (13/16in.) dia., AISI 9310, "hard grind" surface roughness, Ra = 0.25 $\mu\text{m}$ (10 $\mu\text{in}$ ), hardness Rc 62.5-63.5.
Disc	10.16 cm (4in.) dia., AISI 9310, surface finish Ra = 0.15 $\mu\text{m}$ (6 $\mu\text{in}$ ), hardness, Rc 62-64.
Ball vel.	$U_b = 7.21 \text{ m/sec}$ (284 in/sec).
Disc vel.	$U_d = 7.21 \text{ m/sec}$ (284 in/sec).
Orientation	Non-collinear velocity vectors (angle between velocity vectors = 75°)
Entraining vel.	5.72 m/sec (225 in/sec).
Sliding vel.	8.78 m/sec (346 in/sec).
Load	Exponential increase from 1.8 kg (4 lbs) to 63.6 kg (140 lbs) in 30 stages.
Test duration	Until scuff, or suspension (30 stages = 30 minutes).
Failure criteria	Scuff defined by loss of surface integrity and sudden increase in traction. Micro-scuff defined by rapid decline in traction coefficient.
Performance	Oil performance is judged by load stages causing micro/macro scuffing event(s) and traction behavior, which reflects wear of surface topography.
Temperature	Specimen temperatures controlled by frictional heating. Surface temperatures increase with load stage from ambient to ~200 °C.
Oil supply	Computer controlled peristaltic pump, approximately 1 drop/sec. Oil flow rate is selected for adequate lubrication without significant cooling.

The entraining velocity ( $U_e$ ) and sliding velocity ( $U_s$ ) are defined below:

$$U_e = 1/2(U_b + U_d)$$

$$U_s = (U_b - U_d)$$

where  $U_b$  = surface velocity vector of the ball at the contact point

$U_d$  = surface velocity vector of the disc at the contact point

The entraining velocity ( $U_e$ ) and sliding velocity ( $U_s$ ) are key parameters that control the degree of surface separation and the rate of surface tangential shear that the oil must accommodate. With the parameters selected, the initiation of a load capacity test is similar to the Ryder Gear Test in that there is generally little or no evidence of surface damage during the first load stage.

The test parameters recorded include the following:

- Ball and disc temperatures
- Traction coefficient
- Ball and disc surface velocities
- Contact load
- Time

Option: video recording of running track on disc specimen

The test method utilizes the following features:

1. Slow application of load to avoid surface damage during test startup

2. Exponential rather than linear increase in load so that a final scuffing event is reached, rather than a transition into a wear mode without scuffing.
3. Prominent surface finishing features to highlight surface film formation and wear protection through the use of traction coefficient behavior.
4. Use of frictional heating to control specimen temperature and to cover a wide range of temperatures.
5. Continuous specimen contact rather than cyclic contact to avoid load/unload damage.
6. Small incremental load stages to increase resolution.
7. Non-collinear velocity vectors to capture Ryder-like sliding velocities and film thickness-to-surface roughness ratio.

The test protocol parameters focus on creating tribological conditions which activate the same type of chemical response as the Ryder gear test. The key parameters controlling these conditions are: (1) entraining velocity to control EHD film thickness; (2) sliding velocity; (3) surface topography and (4) specimen temperatures (including effects of frictional heating). If the ranking of oils by a scuffing event falls in line with the Ryder Gear Test, it is assumed that the key tribological conditions invoked must be similar to the Ryder. The progression of surface features (like abrasive scratches, polishing of grinding ridges and surface film formation) formed prior to a scuffing event also follow the same sequence generated in the Ryder test.

### *Test Procedure*

Prior to each test series, the ball and disc specimens are cleaned in an ultrasonic bath with petroleum ether, followed by acetone. The AISI 9310 "hard grind" ball specimens are processed through the hard grind stage of a ball manufacturing process. The "hard grind" ball specimens tend to have a consistent surface finish ( $R_a = 10\text{--}13\ \mu\text{in}$ ) for good repeatability. The test balls are from a single manufacturing batch consisting of approximately 8,000 balls. The disc specimens are carburized to a hardness of Rc 62-64.

Following machine calibration, checkout tests are conducted with the reference oil, Herco-A. Load capacity tests conducted with Herco-A encounter micro-scuff events. Continued testing beyond a micro-scuff event eventually results in a scuffing event. A scuffing event is not always clearly defined for Herco-A when it is preceded by multiple micro-scuffing events. Work, conducted under Navy PO No. N00421-98-M-6001, has shown that specimen hardness influences both micro-scuff and scuffing events. Disc specimens are heat treated in large batches to maintain consistency.

The test protocol gives an exponential rise in load with load stage. The exponential rise is to partially offset a cube root relationship between load and contact stress. The exponential rise in load also balances an increase in chemical activity with temperature so a scuffing event can be reached before the end of the test protocol. A minimum of four test determinations are made for each test oil.

*Test Protocol Description*

Figure 5 shows a typical load capacity test plot. A test plot includes the contact load, ball and disc temperatures and traction coefficient. Typical traction coefficients during the first few load stages are on the order of 0.03. The test conditions during the first few load stages provide nearly full-film EHD lubrication. Ball and disc temperatures increase with load stage due to frictional heating. As load and temperature increase, the ratio of EHD film thickness to surface roughness decreases. An increasing traction coefficient reflects a greater degree of asperity interaction within the contact. The rate of rise in traction coefficient reflects ability of the oil to form surface films at

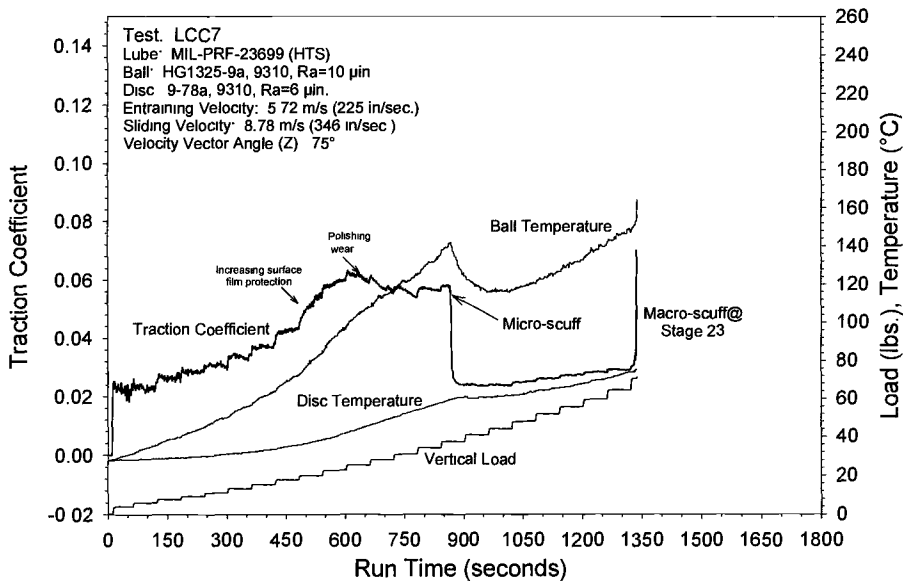


Figure 5 - WAM high speed load capacity test protocol and test plot

asperity sites for wear resistance. A decreasing traction coefficient reflects polishing wear. A sudden drop in traction is associated with a rapid loss of surface topographical features (micro-scuff event). Micro-scuffing events, represented by momentary reductions in traction coefficient, reflect marginal oil chemistry to sustain surface films for protection against local adhesion and wear of surface features. Some oils show multiple micro-scuffing events. Multiple micro-scuffs are characteristic of the non-formulated 4 cSt oil, Herco-A. A macro-scuffing event is easily detected by a sudden increase in traction coefficient.

*Data Processing and Traction Behavior*

Since traction behavior reflects oil chemistry for wear resistance, the traction data for each test is processed to obtain an average traction coefficient for each load stage. The average traction coefficient vs load stage is then plotted to compare the traction behavior of the test oil with other oils as shown in Figure 6. The vertical arrow on the test plot identifies the average load stage at which micro-scuffing or scuffing events occur.

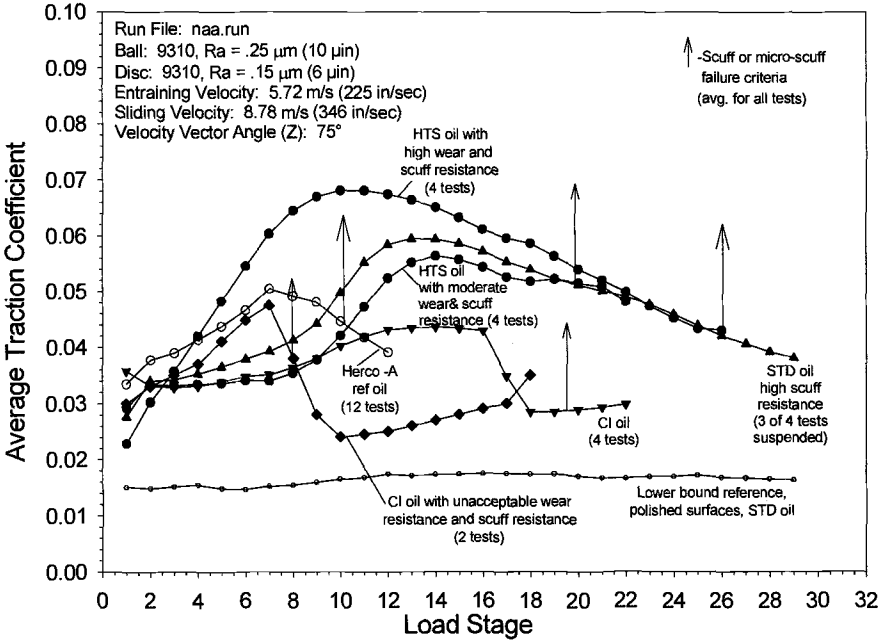


Figure 6 - Scuffing and traction behavior of MIL-PRF-23699 type oils. Average traction coefficient vs. load stage

Figure 6 includes the traction behavior for the reference oil Herco-A. Figure 6 also includes the traction behavior of a test conducted with polished surfaces. The test oil is a standard (STD) MIL-PRF-23699. This test provides a lower bound traction, which is essentially unaffected by surface roughness features and boundary lubrication. The lower bound traction is attributed to the shear behavior (traction) of the bulk oil. Interactions between surface topographical features do not occur until late in the test protocol when the contact temperatures are high and the EHD film is thin. The test oils show different traction and scuffing behavior compared to Herco-A. During the first few load stages, the high traction of Herco-A may be associated with two factors: (1) lower base oil viscosity (4.5 cSt @ 100°C) and EHD films thinner than the 5 cSt test oils and (2) the formation of wear protective, and perhaps high friction, oxides. Once the oxides and organo-metallic films are removed from the surface by wear with Herco-A, there is little boundary lubricating chemistry available to allow

continued running without local adhesion and plastic flow of asperities. Load capacity tests with Herco-A show multiple micro-scuff and scuffing events between load stages 8 and 14. The traction and scuffing behavior of Herco-A is used as a reference for low lubricating ability.

### *Performance Criteria*

From all the load capacity traction data collected over time, there seems to be a strong connection between traction coefficient and wear of surface finishing features. While fluid temperature within the contact also affects traction, the rise and fall of traction coefficient primarily reflects the process associated with how the physical and chemical properties of the oil handle the intimate collisions of surface features within the contact during a load capacity test. Since the WAM High Speed Load Capacity Test protocol covers a large temperature range, we assume that the lubricating ability of the oil, as reflected in traction, is also being tested over a large temperature range. If this is the case, the lubricating ability of the test oils can be differentiated with respect to preservation of surface topographical features, at least to a limited range of temperature or contact severity. Additional testing is required to determine if subtle differences in traction truly reflect variations in chemical activity for wear resistance in practice.

It can be postulated that the desired lubricating attributes of an oil are good wear resistance and scuffing resistance (and surface fatigue resistance) "across-the-board" of temperature and stress. The WAM High Speed Load Capacity Test protocol may be covering at least some of the desired performance features and test conditions. For gear or other surfaces with prominent roughness features, one could argue that some mild polishing wear is desired to topographically condition the surfaces for low asperity stress to prevent early micro-pitting. If this is the case, good performance would be associated with relatively low traction coefficient and high scuffing load stages. Further tribology studies of service hardware are needed to clarify the desired oil attributes and testing conditions. Until this is done, we have to live with a tenuous link between qualification testing and field performance. For now, the traction behavior and scuffing resistance of an oil, as determined with the present set of Ryder-like test conditions, can serve as an initial step toward full characterization and clarification of performance criteria. In the meantime, the data base collection of test oils, along with field experience in the near term, should provide greater confidence in the test method.

### *Evaluation of CI Oil Formulations*

Because of additive competition, corrosion inhibited oils are difficult to formulate. CI additives serve to inhibit corrosive reactions at the surface. Yet various types and concentrations of tricresyl phosphate (TCP) are required to adsorb or react with the surface for wear and scuffing protection. The traction and scuffing performance of three CI oil formulations are shown in Figures 7-9. The fully formulated oils are compared with their base stocks in the same figures. In all cases, the traction coefficients are much lower for the base stocks. The base stocks also have much lower scuffing failures, as is summarized below.

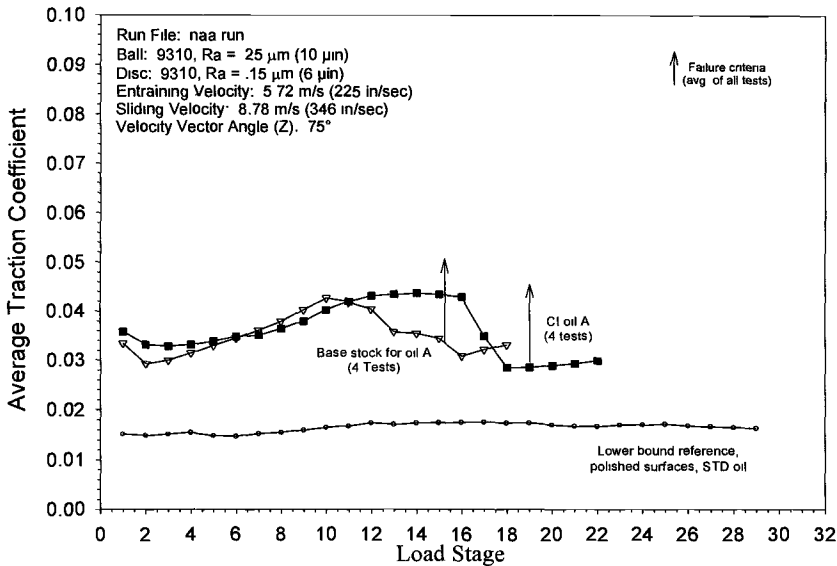


Figure 7 - Scuffing and traction behavior of MIL-PRF-23699 formulated CI oil A and its base stock. Average traction coefficient vs load stage

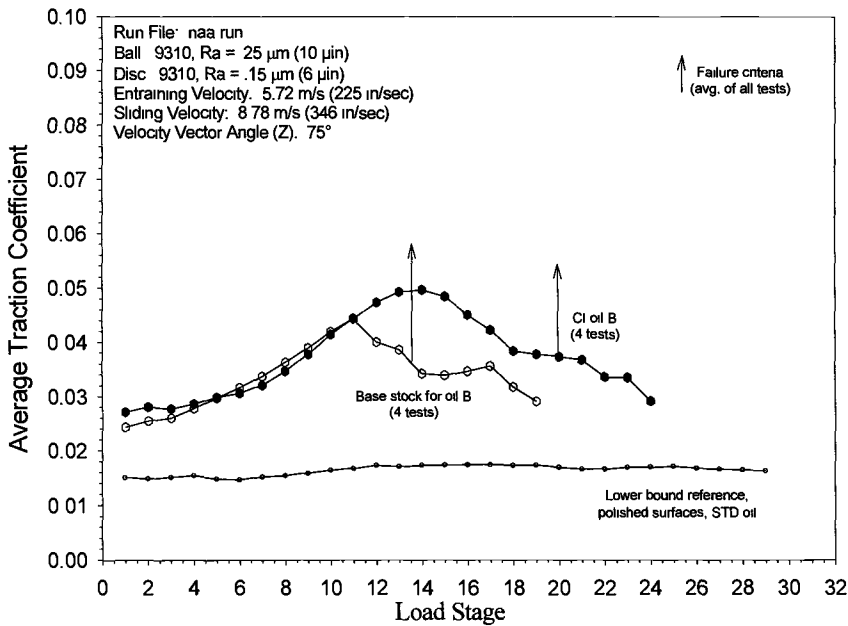


Figure 8 - Scuffing and traction behavior of MIL-PRF-23699 formulated CI oil C and its base stock. Average traction coefficient vs load stage

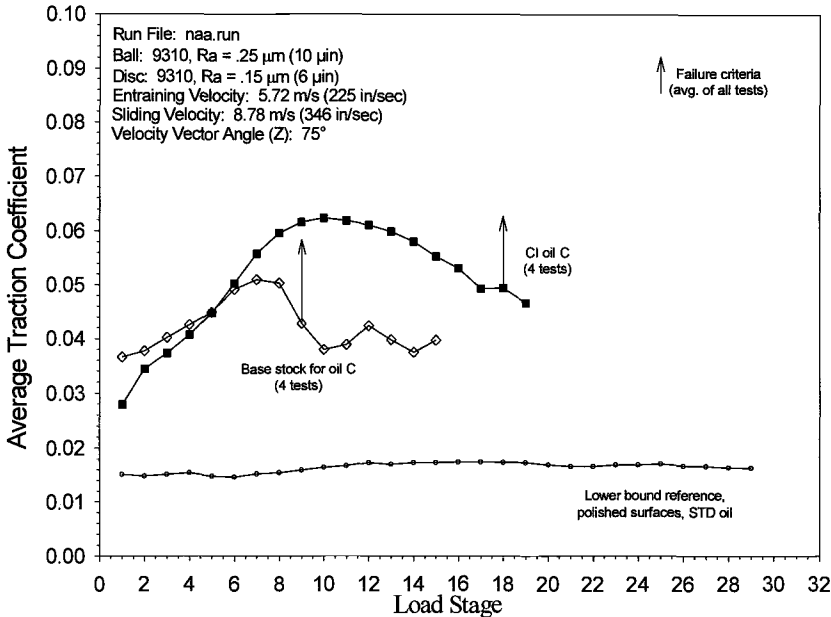


Figure 9 - Scuffing and traction behavior of MIL-PRF-23699 formulated CI oil C and its base stock. Average traction coefficient vs load stage

<u>CI oil or base stock</u>	<u>Scuffing failure stage</u>
Oil A	19.0
Oil A base stock	13.25
Oil B	20.0
Oil B base stock	13.75
Oil C	18.0
Oil C base stock	9.0

The fully formulated oils give a boost in scuffing performance in the range of six to nine load stages. The boost in scuffing performance may be related to TCP concentration. Oil A, which has the lowest TCP concentration, shows the lowest gain in scuffing failure stage compared to its base stock.

The most interesting feature is the correlation between base stock and formulated oil performance, along with the differences among the base stocks. The traction behavior of Oil C base stock shows a much sharper rise in traction coefficient with load stage than the base stocks for Oil A and Oil B. This behavior is also reflected in the fully formulated oils. The use of traction behavior in the test method provides an opportunity to connect chemical attributes for lubrication from both the base stock and additives.

### **Conclusions**

1. A highly flexible testing capability (WAM technology), which provides independent control of entraining velocity and sliding velocity, offers opportunity for simulation of lubrication and failure mechanisms which control performance of service hardware.
2. A simulation of the Ryder Gear Test Method is achieved by using specific entraining and sliding velocity vectors to nvoke equivalent wear and scuffing mechanisms. Oil performance is judged by traction coefficient behavior (wear), micro-scuffing and gross scuffing.
3. The use of traction behavior in the test method provides an opportunity to connect chemical attributes for lubrication from both the base stock and additives.

### *Acknowledgments*

The authors gratefully acknowledge support from the U.S. Naval Air Systems Command, Patuxent River, Maryland.

### **References**

- [1] Wedeven, L. D., "Method and Apparatus for Comprehensive Evaluation of Tribological Materials," United States Patent Number 5,679,883, Oct. 21, 1997.
- [2] "Temporary Methods for Assessing the Load Carrying Capacity of Aircraft Propulsion System Lubricating Oils," SAE AIR4978, Appendix D, February 14, 1997, Ref. No. 97-965.
- [3] U.S. Navy Contract N00140-92-C-BD32, U.S. Navy Purchase Order Numbers N00173-95-P-9981 and N00421-95-M-0037.

**Author Index**

- |                              |                         |
|------------------------------|-------------------------|
| <b>A</b>                     | <b>J</b>                |
| Åhrström, B.-O., 221         | Jonsson, U., 53         |
| Alanou, M. P., 109           |                         |
| Alliston-Greiner, A. F., 140 | <b>K</b>                |
| Anderson, M., 283            | Kawazoe, T., 296        |
|                              | Kelling, N., 153        |
| <b>B</b>                     | Kingsbury, E., 68       |
| Barracough, T. G., 235       | Kyogoku, K., 210        |
| Bishop, R. J., Jr., 33       |                         |
|                              | <b>L</b>                |
| <b>C</b>                     | Larsson, R., 53         |
| Celis, J.-P., 267            | Liang, H., 185          |
| Cook, M., 185                | Lord, J., 53            |
| Crisenberry, R., 185         |                         |
|                              | <b>M</b>                |
| <b>D</b>                     | Marklund, O., 53        |
| Doleschel, A., 15            | Michaelis, K., 15       |
|                              | Mizuhara, K., 3         |
|                              | Momozono, S., 210       |
|                              | Munson, J. W., 81       |
|                              |                         |
| <b>E</b>                     | <b>N</b>                |
| Eriksson, E., 53             | Nakahara, T., 210       |
| Evans, H. P., 109            | Nguyen, N., 309         |
|                              |                         |
| <b>F</b>                     | <b>P</b>                |
| Filzek, J., 97               | Pepper, S., 68          |
|                              | Plint, A. G., 140       |
|                              | Plint, M. A., 140       |
|                              |                         |
| <b>G</b>                     | <b>R</b>                |
| Gao, C., 309                 | Roylance, B. J., 235    |
| Gitis, N., 309               |                         |
| Groche, P., 97               |                         |
| Gschwender, L. J., 168       |                         |
|                              | <b>S</b>                |
| <b>H</b>                     | Sharma, S. K., 168      |
| Helmetag, K. M., 258         | Snidle, R. W., 109      |
| Hertz, P. B., 81             | Snyder, C. E., Jr., 168 |
| Hille, E., 318               | So, H., 125             |
| Hoehn, B.-R., 15             | Sperring, T. P., 235    |
| Hu, C. C., 125               |                         |
| Huq, M. Z., 267              |                         |

## 334 BENCH TESTING OF INDUSTRIAL FLUID LUBRICATION

### T

Tanaka, S., 210  
Tomimoto, M., 3  
Totten, G. E., 33

### U

Ura, A., 296  
Uusitalo, Ö., 53

### V

Vinogradov, M., 309

### W

Wedeven, L. D., 318  
Woydt, M., 153, 199

### X

Xiao, J., 185  
Xie, L., 33

## Subject Index

### A

Acoustic emission, 309  
 Additives, 15  
 Aerospace gears, high speed, 109  
 Aircraft  
   Department of Defense, 168  
   propulsion oils, 318  
 Alumina, 267, 296  
 American Iron and Steel  
   Institute bearing, 168  
 Asperity contact, 185  
 ASTM standards  
   D 2882, 33  
   D 3233, 258  
   D 5620, 258  
 Automotive piston ring and  
   timing chain coatings, 309  
 Automotive tires, 185

### B

Ball, 221  
 Ball and disc apparatus, 53  
 Ball-on-disk, 125, 296  
 Beam, 221  
 Bearings, 235  
   AISI, 168  
   rolling element, 109  
 Biodiesel fuel lubricity, 81  
 Block-on-ring friction tester, 33,  
   210  
 Boundary lubrication, 68, 125

### C

Calcium carboxylate, 125  
 Case-drain temperature, 168  
 Ceramics, 267  
 Chlorotrifluoroethylene, 168  
 Coatings, 267, 309  
 Compression waves, 221  
 Contact configuration, 3  
 Contact, elastohydrodynamic  
   point, 53  
 Contact failure, 140

Contact resistance, electrical,  
   267, 309  
 Contact severity, 68  
 Contact stress  
   Hertzian, 81  
   cyclic, 33  
 Contact tribometer, 68  
 Copper base alloy, 296  
 Corrosion inhibition, 318  
 Corrosive wear, 296  
 Cracking, 267  
 Crankcase lubricant, 140  
 Cylinder liner, 153

### D

Debris, wear, morphological  
   attributes, 235  
 Deep drawing, 97  
 Department of Defense, 168  
 Deutsches Institut für  
   Normung (DIN), 199  
 Diesel injection pumps, 81  
 Disk machines, high speed, 109  
 Dynamic beam theory, 221

### E

EHD conditions, 221  
 EHD lubrication, 140  
 EHL analysis, 210  
 Elastohydrodynamic lubrication,  
   68, 210  
 Elastohydrodynamic point  
   contacts, 53, 140  
 Electrochemical potential, 296  
 Energy pulse, 140  
 Engines, 235  
   tests, 153  
 Evaluation criteria, lubricant,  
   199  
 Extreme pressure test, 258

### F

Falex pin method, 258  
 Ferrography, 235

## 336 BENCH TESTING OF INDUSTRIAL FLUID LUBRICATION

Field correlation with bench testing, 258, 283  
Film, 125, 258  
Film lubrication, solid, 68  
Film parameters, 3  
Film thickness, 53  
Fire resistance hydraulic fluids, 168  
Flexural waves, 221  
Forming process, sheet metal, 97  
Four ball tests, 15, 33, 235  
Fourier transform analysis, 221  
Fretting mode II, 267  
Friction, 15, 97, 153, 318  
    characteristics, 210, 221  
    coefficient, 68, 81, 199, 210  
    force, 309  
    modifier, 125  
    power intensity, 140  
    static, 185

### G

Gears, 15, 109  
    gear transmission units, 235  
    lubricants, 140  
    Ryder Gear Test Method, 318  
Grinding/generating process, 109

### H

Hertzian contact stress, 81  
Hertzian pressure, 221  
Hydraulic pump testing, 3, 168

### I

Ice friction, 185  
Image analysis, 53  
Interferometry, 53  
Isoparaffin solvents, 199  
Isopropanol, 199

### L

Light source, 53  
Liner, cylinder, 153  
Linkage pins, 309

Loading, 33, 221  
    applied, 185  
    carrying capacity, 318  
    torque versus load curve, 258  
    velocities, 3  
Lubrication analysis, 210  
Lubricity additives, 81  
Lubricity number, 81  
Luleå ball and disc apparatus, 53

### O

Oil type, 15

### M

Marine corrosion, 296  
Matveesky's friction power intensity, 140  
Metals  
    forming, sheet, 97  
    metalworking process, 258  
    seawater corrosive wear test, 296  
    steel, 125, 296  
Military-related machinery functions, 235  
    aircraft, 168  
Molybdenum, organic, 125  
M-ROCLE, 81  
Multi-channel method, 53

### O

Oil, 221, 318  
    type, 15  
Oscillation apparatus, translatory, 199

### P

Phosphorus/sulfur, 125  
Physical vapor deposited coating, 267  
Pin and vee block, 258  
Pin-on-disk, 235  
Pin-on-V-Block Falex Wear Test, 33  
Piston rings, 153, 309  
Pitting, 15  
Plint's energy pulse, 140  
Polyalphaolefin, 168

Polytetrafluorethylene, 125  
 Power loss, 15  
 Pressure test, 258  
 Process stability, 97  
 Profilometer, 309  
 Profilometry, stylus, 153  
 Propulsion system, 318  
 Pump, injection, 81  
 Pump tests  
     axial flow piston, 168  
     hydraulic, 3  
     vane, 33

**R**

Refrigerant, 210  
 Refrigeration oil, 210  
 Rolling contact tribometer, 68  
 Rolling element bearings, 109  
 Ryder Gear Test Method, 318

**S**

Scratch resistance, 309  
 Screening tests, laboratory, 168  
 Scuffing, 15, 109, 318  
 Seawater, 296  
 Sheet metal forming, 97  
 Shell four ball tester, 15  
 Shoe materials, tribological  
     behavior, 185  
 Signal noise, 168  
 Silicon nitride, 267  
 Sliding, 109  
 Sliding parts, 210  
 Sliding rate, 15  
 Sliding speed, 125, 185  
 Sliding velocities, 3  
 Sliding wear, 296  
 Slip zone, 267  
 Sodium chloride solution, 296  
 Solvent, cleaning, tribological  
     property influence, 199  
 Spalling, 267  
 Speed, wear test, 33  
 Spiral orbit tribometer, 68  
 Steel, 125, 296

Strain gauges, 221  
 Strip drawing principle, 97  
 Stylus profilometry, 153  
 Sulfur reductions, 81  
 Surface finish, 109  
 Surface layer, 185  
 Surface roughness, 210

**T**

TAN, 283  
 Three-vane-on-ring, 33  
 Timing chain coatings, 309  
 Timoshenko dynamic beam  
     theory, 221  
 Tin coating, 267  
 Tires, automobile, tribological  
     behavior, 185  
 Torque curve, 258  
 Traction coefficient, 68  
 Traction measurement, 185  
 Translatory oscillation  
     apparatus, 199  
 Tribological aspect numbers, 283  
 Tribology tests, 153, 199  
 Tribometer, rolling contact, 68  
 Twin disk simulation, 15

**U**

U.S. Navy, 318

**V**

Viscosity, 15, 168  
     index improvers, 168  
 Volumetric wear, 153

**W**

Water glycol hydraulic fluid, 33  
 Wear test selection, 283  
 Welding, 109